CHARGE TRANSFER PROCESSES AT LIQUID/LIQUID INTERFACES

J.A. Campbell

Degree of Doctor of Philosophy

University of Edinburgh

1991

Declaration

This thesis has been composed by myself and the work is my own, except where indicated by reference

Acknowledgement

I thank Dr H. H. Girault who has supervised this work, and has been unfailingly enthusiastic throughout. Many other people have contributed to this research both by helpful (and sometimes unhelpful) discussion, and by provision of equipment and data, particularly the following members of the Edinburgh Electrochemistry Group: A. Brown, B. Seddon, Y. Shao, A. Stewart, G. Taylor and K. Taylor.

I also thank Callum McHardy for introducing me to the medical microlab computing facility and for typing out a large number of equations twice! I am grateful to my friends and family for putting up with me over the last eighteen months when writing up has made me even more difficult to live with than usual. Penny Campbell and Mary McGeady were especially helpful in allowing me to stay with them for "respite" periods of work. I thank my parents and God most of all. Finally, in the words of Ecclesiastes 12: 11-14;

The words of the wise are like goads, their collected sayings like firmly embedded nails - given by one Shepherd. Be warned, my son, of anything in addition to them.

Of making many books there is no end, and much study wearies the body. Now all has been heard, here is the conclusion of the matter:

Fear God and keep his commandments for this is the whole duty of man. For God will bring every good deed into judgement, including every hidden thing, whether it is good or evil.

ABSTRACT

An approximate analytical expression for the current potential characteristic for charge transfer at a microdisc interface under steady state conditions is given for reversible, quasireversible and irreversible kinetics. The quasireversible expression is proposed as a simple means for analysis of experimental voltammograms thus gaining access to the potential dependent forward rate constant and the charge transfer coefficient, α. It is used to analyse simulated data and the results compared to the simulation parameters.

The mathematics of the linear diffusion of cyclic voltammetry for electron transfer at the Interface between Two Immiscible Electrolyte Solutions (ITIES) is addressed, and the numerical solution of the resulting integral equation is evaluated. The results show how the cyclic voltammograms for reversible electron transfer at the ITIES vary when different ratios of reactants and products are used, and how these differ from the classical reversible cyclic voltammograms.

A microhole formed by eximer laser ablation in a polyester membrane is proposed as a useful support for a micro-ITIES providing symmetrical diffusion characteristics analogous to an inlaid disc electrode. This support (and also regular arrays of microholes) has been used to obtain symmetrical steady state voltammograms for the transfer of the acetylcholine cation from water to 1,2-dichloroethane.

A micro-ITIES supported at the tip of a micropipette has been used to study the transfer of alkali metal ions assisted by crown ethers which gave a lower limit for the pseudo first order interfacial transfer rate constants of 10^{-2} cm s^{-1}, and provided data on the complexation constants of Li^+, Na^+, K^+, Rb^+ and Cs^+ with dibenzo-18-crown-6.

The oxidations of di-n-butylferrocene and ferrocene by hexacyanoferrate III at the ITIES were investigated using both microinterfaces supported at the tip of a micropipette, and large interfaces.

CONTENTS

Common Abbreviations

Roman Alphabet

a_i	activity of species i
A	electrode area
ACh^+	acetylcholine cation
b	subscript - backward, reverse
	superscript - bulk quantity
B15C5	benzo-15-crown-5
C	concentration
D	diffusion coefficient
DBFeC	di-n-butylferrocene
DB18C6	dibenzo-18-crown-6
E	electrical potential
E^o	standard electrode potential
$E^{o'}$	formal electrode potential
$E_{1/2}$	half wave potential
f	subscript -forward
F	Faraday constant
FeC	ferrocene
FeII	hexacyanoferrate II
FeIII	hexacyanoferrate III
G	Gibbs energy
ΔG^o	standard Gibbs energy of a process
i	interfacial current
ITIES	interface between two immiscible electrolyte solutions

k	Boltzman constant
M	unspecified cation
n	number of electrons
O	oxidised form of unspecified species
r	electrode radius
R	Gas constant
	reduced form of unspecified species
T	absolute temperature
TBATPB	tetrabutylammonium tetraphenylborate
TBATPBCl	tetrabutylammonium tetrakis(4-chlorophenyl)borate
z	charge number
Z	frequency factor

Greek Alphabet

α	charge transfer coefficient
	subscript -phase denoted α
	superscript -phase denoted α
β	subscript -phase denoted β
	superscript -phase denoted β
γ	activity coefficient
Γ	surface concentration

δ	diffusion layer thickness
ϕ	Galvani potential
κ	transmission coefficient
μ	chemical potential
ν	linear potential sweep rate heterogeneous reaction rate
σ	superscript -surface

List of Figures

List of Tables

INTRODUCTION

Charge transfer reactions across liquid/liquid interfaces have been recognised to be of fundamental importance in industrial processes such as phase transfer catalysis and hydrometallurgic extraction[1-4]. They also underlie the function of ion selective electrodes[5-7] and are crucially relevant to biological systems where the transfer of both ions and electrons across cell membranes is critical to the whole life cycle[8]. Water/oil/water concentration cells were seen as being analogous to biological semipermeable membranes in 1906[9]. The development of electrochemical methods to study charge transfer reactions at the Interface between Two Immiscible Electrolyte Solutions (ITIES) has stimulated renewed interest in it as a relatively simple model for one half of the cell membrane[10,11]. Because of the ubiquity of these types of interfacial charge transfer a good understanding of their mechanism at a molecular level is desirable, not purely to satisfy academic curiosity, but also for their consequences in everyday life.

The electrochemical study of the ITIES is reckoned to have first begun with Nernst's experiments at a phenol membrane[12]. He observed the transfer of coloured inorganic electrolyte ions when current was passed through a water/phenol/water system containing the electrolytes at partition equilibrium. A good deal of work followed which centred on investigating and defining the various potential differences arising at such interfaces[13-15]. As early as 1939 Verwey and Niessen[16] published a theoretical paper on the electrical double layer at the ITIES. Although subsequent theoretical treatments were concentrated on the double layer at the metal/electrolyte interface, recently interest was revived in the double layer structure at the ITIES and this phenomenon has now been studied widely experimentally[17-19].

1.1 SUMMARY OF EXPERIMENTAL WORK TO DATE

In 1956 Guastalla[20] observed ion transfer through changes in interfacial tension which corresponded to changes in ion concentrations. Gavach and Guastalla later obtained steady state polarisation curves from aqueous

KCl with tetraalkylammonium picrate salts in nitrobenzene[21]. Guastalla also performed slow sweep cyclic voltammetry on a similar system in 1970[22]. With the recognition in the 1970's[23-25] that under certain conditions the ITIES behaves as an ideally polarisable electrode the way was opened for the wholesale transposition of classical electrochemical methodology to the study of charge transfer reactions at liquid/liquid interfaces. Since that time there has been a substantial amount of work done in the area.

The use of Chronopotentiometry at the ITIES was pioneered by Gavach and coworkers[26] who observed diffusion controlled ion transfer. An electrolyte dropping electrode system analogous to the dropping mercury electrode was developed by Koryta et al[25]. They used nitrobenzene dropping into water to study the transfer of tetraethylammonium (TEA^+) at the water/nitrobenzene interface. Initially these authors used two and three electrode systems but, recognising the severe distorting effects of the ohmic solution resistance on their results, a four electrode system similar to those used in electrophysiology was proposed. The limiting currents observed in early experiments at the electrolyte dropping electrode were 20-90% higher than those calculated on the basis of the Ilkovic equation, and the system appeared to have a narrower effective operating range than the original dropping mercury electrode. Subsequently much effort was concentrated on the stationary interface, although the ascending water electrode is now effectively used in Japan and China[27,28,29].

Cyclic voltammetry has become the most widely used technique and was first successfully employed with a four electrode potentiostat in 1977 by Samec, Mareček Koryta and Khalil to study tetramethylammonium transfer from water to nitrobenzene[30]. A standard rate constant for the ion transfer of 5.6×10^{-4} cm s^{-1} was quoted but this was later noted by the same authors to be an artefact due to the uncompensated solution resistance. The difficulties in overcoming solution resistance have proved to be the main barrier to performing satisfactory kinetic studies. The introduction of positive feedback iR compensation enabled Samec Mareček and Weber[31] to report a rate constant, determined by cyclic voltammetric peak shift analysis, of 5.5×10^{-2} cm s^{-1} for caesium ion transfer from water to nitrobenzene, using potential sweep rates of up to 10V s^{-1}.

In 1980, Samec[32] proposed the use of convolution potential sweep voltammetry for the determination of kinetic parameters, citing its advantage over the more common peak shift cyclic voltammetry analysis that *a priori* knowledge of the kinetic law for the reaction is not required but may be inferred by experiment[33]. While this is true, the technique itself is essentially only a more sophisticated data analysis of the peak shift experiment and as such is still subject to the same drawback that uncompensated solution resistance cannot be distinguished from quasireversible kinetics[34]. Convolution analysis was applied to Cs^+ transfer[35] and kinetic results derived were in agreement with those obtained previously[31]. Anion transfer was also studied by the Prague group both polarographically and voltammetrically[36] and found to be diffusion controlled under the conditions used.

Homolka and others have published a considerable amount on alkali and alkaline earth metal transfer facilitated by neutral ligands (or ionophores)[37 - 40]. They produced much useful information on stability constants for ionophores such as nonactin, dibenzo-18-crown-6, -24-crown-8 and -30-crown-10. They have predicted and confirmed the effect of different reaction stoichiometries on potential peak separation[40] and provided some kinetic data[41].

A variety of ion and assisted ion transfer systems have been studied since and kinetic parameters determined, mostly by convolution potential sweep methods[42,43] but also by chronopotentiometry[44]. Other standard electrochemical techniques which have been applied to charge transfer reactions at the ITIES include ac cyclic voltammetry[45,46] and impedance measurements[47,48]. The Prague group and Japanese investigators have used mainly the water/nitrobenzene interface but other workers have used the water/1,2-dichloroethane interface[49-52]. Most recently interest in modelling biological systems has led to the focussing of attention on the effects of adsorbed phospholipid monolayers at the ITIES[53]. This system is one step closer to the biological cell wall than the normal ITIES and approximates to one half of a bilayer lipid membrane (BLM).

Electron transfer between ferrocene and hexacyanoferrate III across the nitrobenzene/water interface[54] was reported by Samec, Mareček and Weber in 1977. They found the half wave potential and peak separation

for this reaction to be dependent on the concentration ratio of the redox couples used[55]. Although not readily explained at the time this now appears consistent with a diffusion controlled process and is discussed in chapter 4 below. Convolution analysis has also been applied to this system[35].

Geblewicz and Schiffrin[56] measured a rate constant of 0.9×10^{-3} cm s^{-1} for electron transfer from lutetium diphthalocyanine in 1,2-dichloroethane to hexacyanoferrate III in water by peak shift analysis. The applicability of this analysis under their experimental conditions is questioned below. Kihara et al[27] have recently studied a variety of different electron transfer systems at the water/nitrobenzene interface by current scan polarography and provided much new data for investigation.

Cunnane Schiffrin, Beltram and others[57] have successfully used ion transfer to control the potential at the ITIES and drive electron transfer between tin diphthalocyanine in 1,2-dichloroethane and hexacyanoferrate III in water. Maeda, Kihara et al[28] have used the same principle in reverse by driving an assisted ion transfer through an electron transfer at the water/nitrobenzene interface. This has very interesting implications for interfacial extraction processes. It enables the selective extraction of an ion without external application of an electrical potential, hence the two liquid layers may be thoroughly and efficiently mixed during extraction. The redox states which drive the reaction may then be regenerated by electrolysis after separation.

1.2 RECENT THEORETICAL WORK

The theory of interfacial thermodynamics and charge transfer reactions has been developing simultaneously with the experimental work. Hung gave detailed consideration to the Galvani potential difference in relation to the distribution equilibrium of ions across the interface and extended this to the case of interactions between components in both phases[58,59]. Girault and Schiffrin[60] and Kakiuchi[61] have applied the Gibbs adsorption isotherm formalism to relate interfacial concentration excesses to charge density and interfacial tension. Samec[62] initially discussed the basic

kinetic equations for the rates of ion and electron transfer across the ITIES on the basis of the theory of chemical reactions in polar media. Together with Kharkats and Gurevich he later adopted the stochastic approach as being more appropriate to ion transfer kinetics[63]. Girault and Schiffrin, on the other hand, have proposed a theory for ion transfer kinetics based on an analogy with the transport processes of diffusion and migration[64]. They have also presented a theory for electron transfer[65] involving a pre-encounter equilibrium model.

Samec[66] considered the properties of the stationary wave of current versus potential for an electron transfer across the ITIES by using a stationary Nernst diffusion layer type treatment applicable to the dropping electrolyte electrode. This led him to the interesting conclusion that the system's behaviour may vary from reversible through quasireversible to irreversible solely by variation of the bulk concentration of any reactant. The appropriateness of this conclusion is discussed in chapter 4. Makrlik later presented the same treatment in a more general form[67].

Most recently Marcus[68,69] has presented theoretical aspects of the kinetics of electron transfer reactions at the liquid/liquid interface. He has considered the reorganisation energies involved and the means of using data acquired at the metal/liquid interface to predict rate constants for electron transfer at the liquid/liquid interface.

1.3 THE CURRENT POSITION

Despite all the above mentioned work the inherent difficulties in measuring the kinetics of interfacial charge transfers still prove a major stumbling block to gaining understanding into their mechanisms. These difficulties subsist in providing that some aspect of the interfacial charge transfer process itself, rather than the mass transport of reactants or the electrical resistance of the solutions, is the rate determining step.

The standard electrochemical means of surmounting mass transport limitations is either by rapid variation of electrode potential (eg fast sweep voltammetry, ac polarography, ac impedance and chronoamperometry) or by enhancing the rate of arrival of reactants (eg rotating disc, wall jet and

micro electrodes). Published investigations by other workers have used only techniques in the first category. There remains however the substantial problem of the low polarity of the organic phase which normally results in a large iR drop requiring to be compensated. The analogue compensation by positive feedback normally employed inevitably introduces a large amount of noise which limits the accuracy of current acquisition. The alternative use of a concentrated supporting electrolyte in the organic phase causes significant ion pairing effects between the transferring ion and the supporting electrolyte counter ion[35] and the use of dilute media is preferable. These difficulties render most of the techniques used so far inherently inaccurate and recently led Samec to conclude that the most reliable method is measurement of the charge transfer resistance by ac impedance. However as seen in ref 46 full semi-circles are difficult to obtain and the accuracy of the measurement is heavily dependent on the soundness of the curve fitting algorithm employed. Furthermore there is some doubt as to whether processes observed at high frequency are genuine charge transfer reactions, involving a change in solvation, or merely oscillation of a charged species about an equilibrium position at the interface. In any case the accuracy of such techniques at liquid/liquid interfaces is limited at short times by the low impedance of the double layer in parallel with the faradaic process.

1.4 THE SCOPE OF THE PRESENT WORK

The objectives of the present work were to develop a kinetic methodology and experimental facilities for the study of charge transfer reactions at the liquid/liquid interface at Edinburgh University. Initially this involved the application of some of the classical methodologies mentioned above to the simple ion transfer case. These did not prove successful and the use of microelectrodes was then investigated. The work presented here concentrates on this area which applies the principle of enhancing diffusion by the use of microelectrodes to overcome mass transport limitations and thus to obtain kinetic data on reactions. This experimental approach was based on work by Taylor and Girault[52] which showed that micro-liquid/liquid interfaces supported at the tip of the micropipette can be used to provide a spherical diffusion pattern similar to

that observed at solid microelectrodes as illustrated in figure 1. There are two main advantages to gain by adopting this approach: (i) Potential sweep rates and hence rates of data acquisition are one or two orders of magnitude slower than those required by the aforementioned methods and hence less sophisticated instrumentation is necessary; (ii) The magnitude of currents observed is small enough that, despite high resistances in the organic phase, the iR drop does not generally require to be compensated.

Charge may cross an interface carried either by an electron or by an ion. The three types of charge transfer reaction considered here are depicted in figure 2. In both the facilitated ion (fig 2b) and electron (fig2c) transfer cases it is proposed that the reactions be made pseudo first order by making the aqueous electroactive species many times more concentrated than the organic species. This enables the diffusion of the aqueous species to be ignored and is the basis on which a kinetic analysis of the current wave observed at a micropipette is founded. The analytical description for the quasireversible steady state wave herein proposed is compared with the numerical simulation of diffusion to a microdisc published by Heinze[70] and with the semi-analytical solution of Bond, Oldham and Zoski[71].

When the diffusion of species on both sides of the interface is considered the situation becomes quite complex, especially with a micropipette where the diffusion regime is asymmetric (fig 1). Diffusion inside the pipette is constrained to an almost linear geometry, but that outside lies somewhere between that observed at a microdisc in an infinite insulating plane and spherical diffusion[72]. A complete consideration of these diffusion problems is beyond the scope of this work, but symmetrical linear diffusion for the electron transfer case is considered (chapter 4) and indicates under what conditions an assumption of pseudo first order kinetics is appropriate.

The simple ion transfer reaction (fig2a) is first order and analogous to a simple redox at the metal/electrolyte interface with both species soluble. However it is experimentally less tractable than the more complex facilitated ion and electron transfer cases as diffusion inside the pipette cannot be ignored. For this reason a cell was developed to give symmetrical spherical diffusion by supporting the liquid/liquid interface

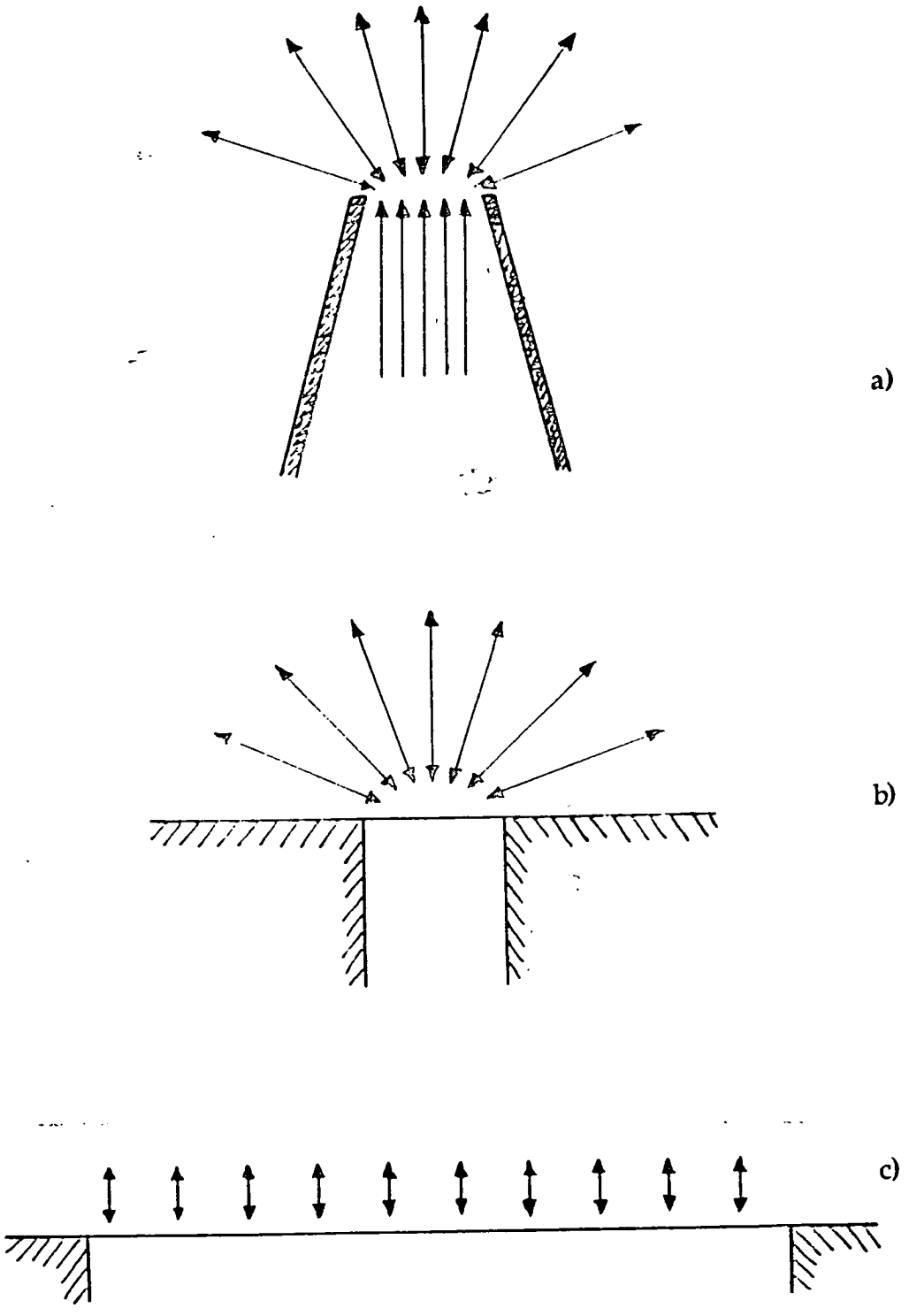

Fig. 1 Diffusion geometries at; a) a micropipette, b) a microdisc, and c) a large planar interface.

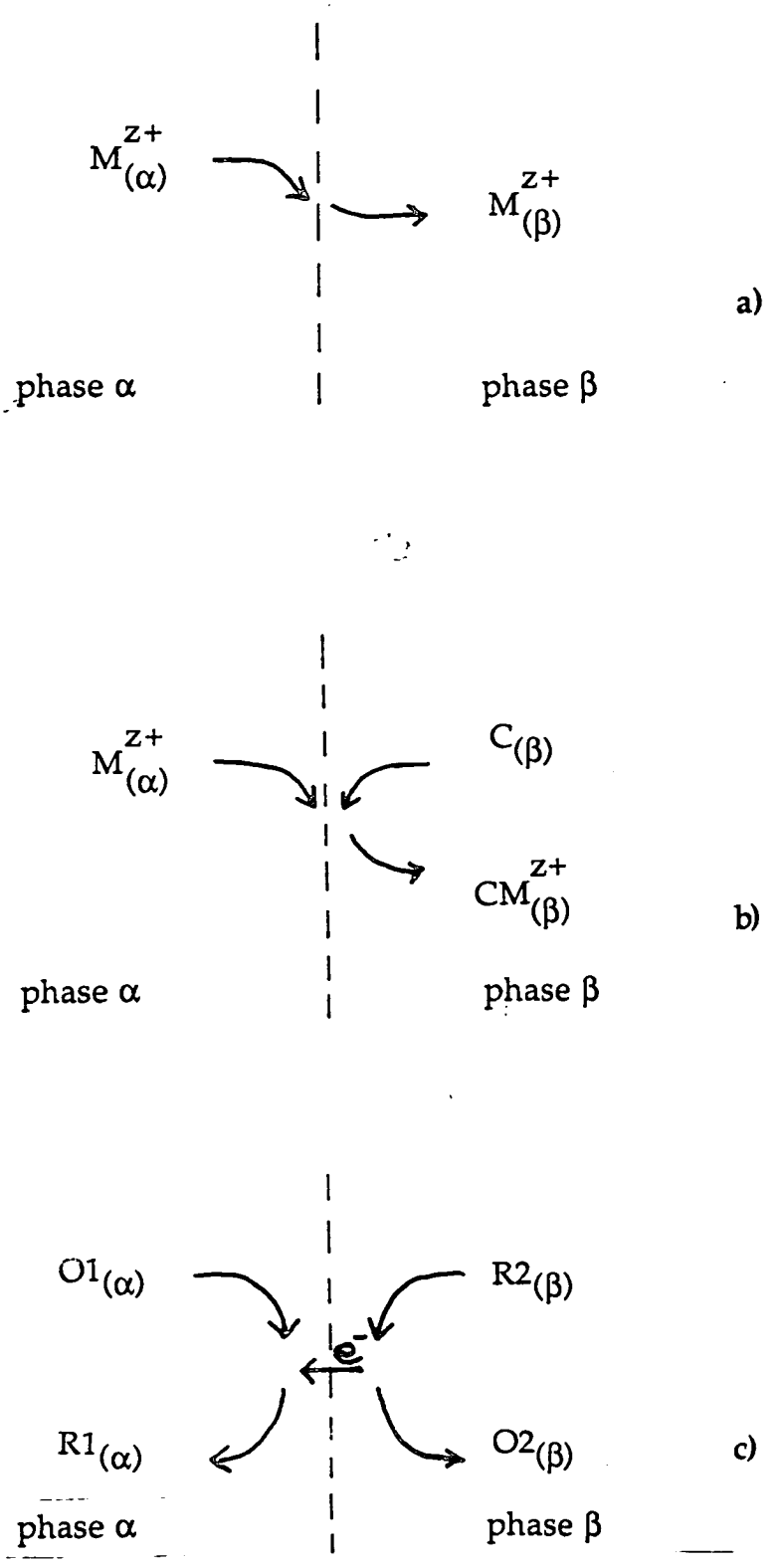

Fig. 2 Charge transfer reactions at the liquid/liquid interface; a) ion transfer, b) assisted ion transfer, and c) electron transfer.

at a microhole in a thin (12 μm) polyester membrane. The application of standard microdisc electrode analysis to this interface is discussed.

EXPERIMENTAL

2.1 BACKGROUND

To perform an electrochemical experiment the minimum number of electrodes required is two, however it is more normal to use three or more electrodes. In the study of the metal/electrolyte interface the electrode at which reactions are being observed is called the working electrode, a counter electrode is used to carry the current produced by the other half cell reaction(s) not under study and a reference electrode is used to monitor the potential difference which drives the chemical reactions at the working electrode. The counter electrode must be large with respect to the working electrode, in order that it does not limit the charge transfer process at the working electrode, and it is usually distant from the working interface or somehow separated from it so that the counter electrode reaction products do not interfere with the working electrode chemistry. The reference electrode is placed in the solution as close as possible to the working interface in order to monitor accurately the interfacial potential difference. Only a very small current is passed through the reference electrode to ensure that its chemical composition and hence potential remains constant through the experiment.

At the ITIES the liquid/liquid interface itself may be regarded as the working electrode (although conduction is not necessarily by electrons). A minimum of two electrodes are necessary between which the electrical potential difference and current can be applied and measured. However as these electrodes perform the dual role of reference and counter electrodes they need to be both large in area versus the interface (to avoid significant chemical change with the passage of current) and very close to the interface (to prevent significant resistive losses). This is generally impracticable and the two electrode configuration at the ITIES is restricted to use with a microinterface where currents and interfacial areas are very small. The standard practice at the ITIES is to use four electrodes, a counter electrode in each phase distant from the interface and a reference electrode in each phase close to the interface. The electronic circuitry is

arranged such that very little current passes through the reference electrodes, which serve only to monitor or control the potential difference across the interface, and the current arising from the charge transfer processes across the interface is carried and measured through the counter electrodes.

2.2 MICROELECTRODE EXPERIMENTS

2.2.1 Instrumentation

Four different types of microelectrode were used, these were micro-ITIES supported at: (1) a glass pipette tip; (2) a single microhole in a thin polyester film; (3) an array of microholes in a thin polyester film and (4) a Platinum microdisc was used to determine the redox behaviour of some species. Where the liquid/liquid interface or working electrode area is less then about 8×10^{-9} m^2 (equivalent to a disc electrode = 50 μm radius) the experimental currents passed are considered small enough for only two electrodes to be necessary. The instrumentation used for the cyclic voltammetry experiments with single microelectrodes thus consisted solely of a potential ramp generator (PPR1 HITEK, England), a laboratory constructed current follower (circuit diagram, figure 3) and an X,Y recorder (Advance Bryans series 60,000). Experiments with microhole arrays where the total interfacial area was of the order of 1×10^{-6} m^2 were performed using a four electrode set up with a zerostat as described in the large scale ITIES section below.

2.2.2 Cell Design and Electrode Construction

For experiments with Platinum microdisc electrodes and micro-ITIES supported at the tip of a glass pipette the electrochemical cell was a glass U tube of internal diameter 4mm as illustrated in figure 4. The microelectrode and U tube were mounted on an optical bench and the position of the electrode or pipette tip was monitored on a television screen using an Olympus zoom microscope and Sony CCD (DXC-102) video camera. This enabled the electrode or micro-ITIES to be positioned extremely close to the organic reference electrode to minimise iR losses.

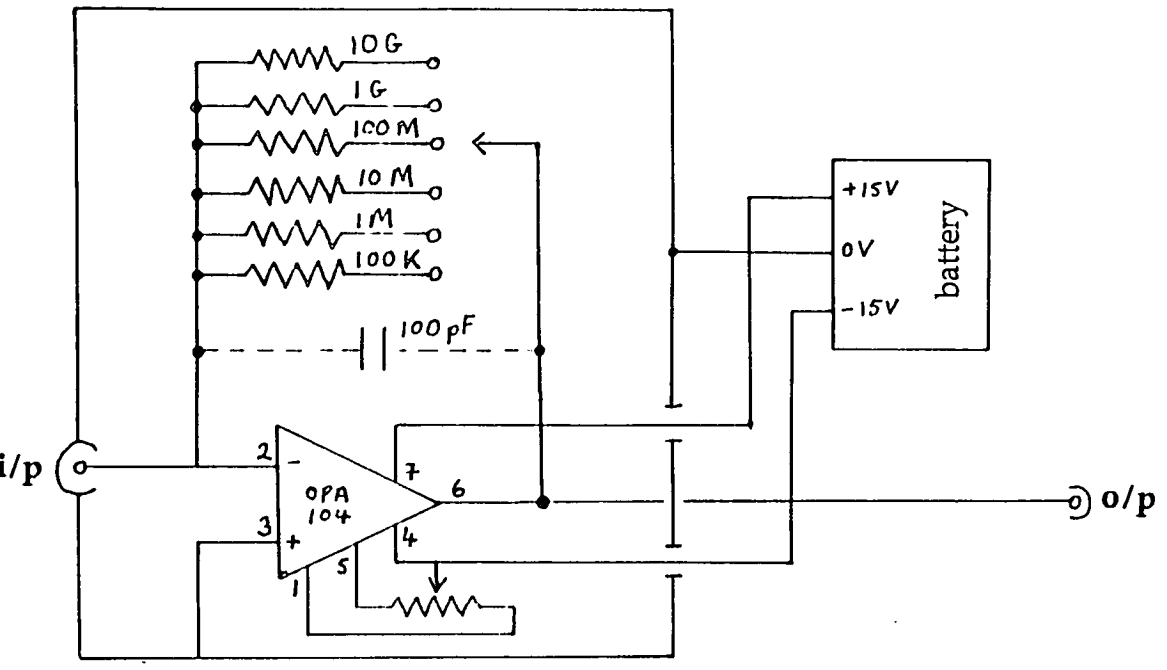

a) Current follower

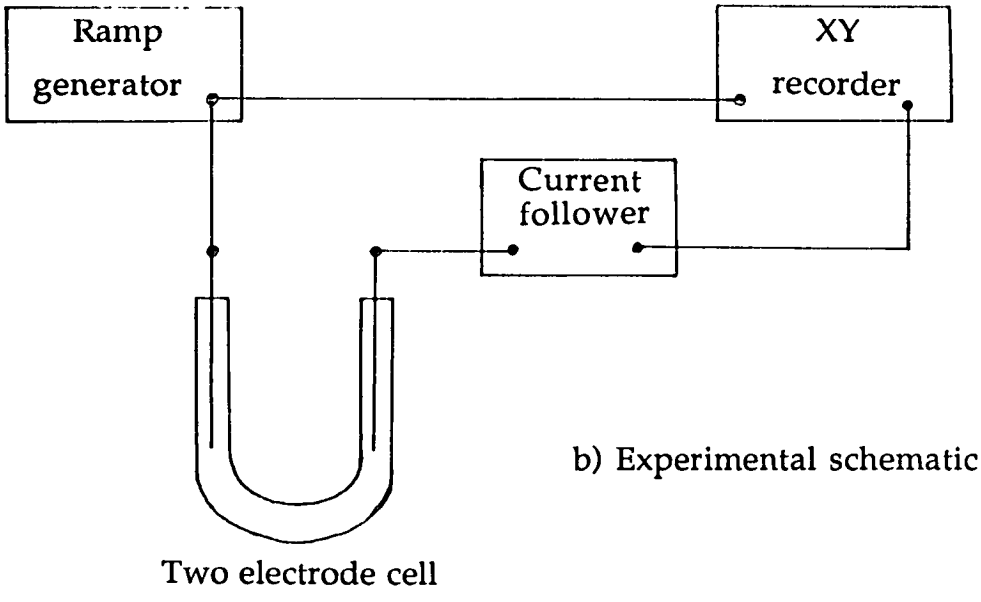

b) Experimental schematic

Fig. 3 a) current follower circuit diagram, b) experimental schematic.

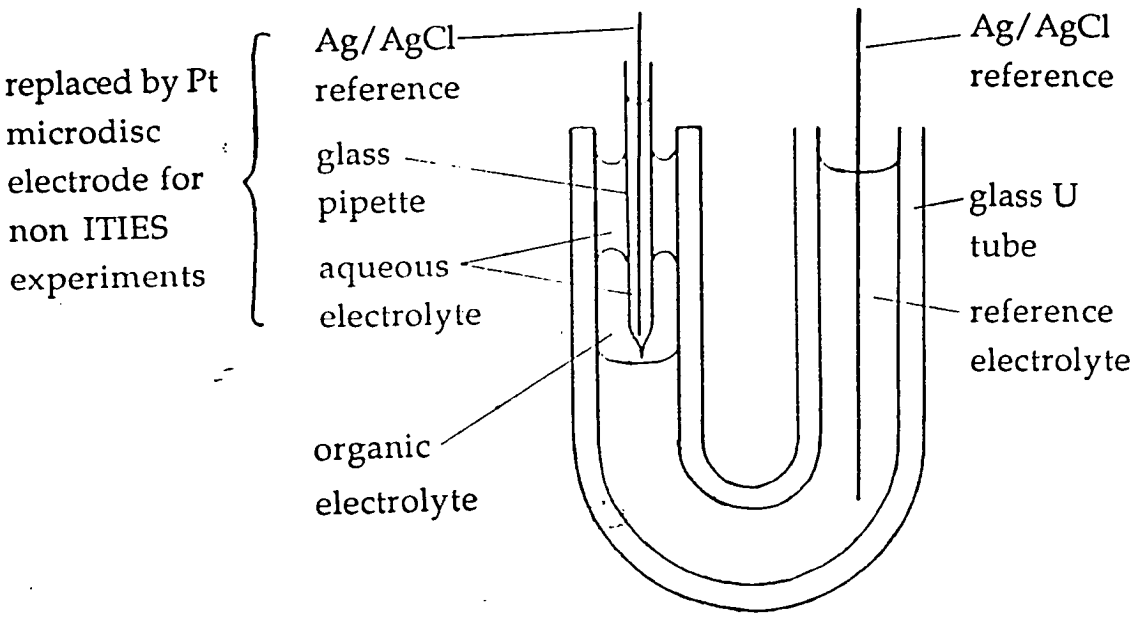

Fig. 4 Two electrode cell for micropipette and platinum microdisc experiments

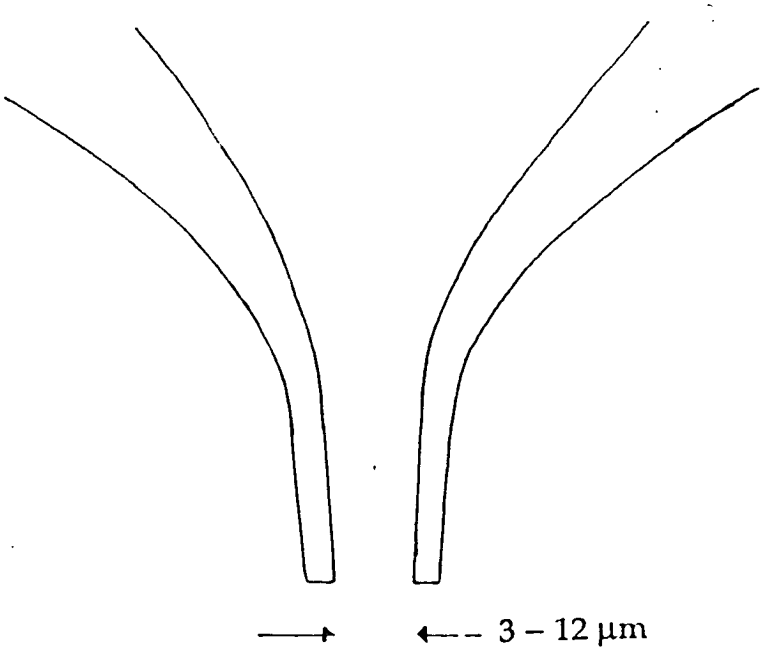

Fig. 5 Section of pulled glass micropipette tip

The Platinum microdiscs were constructed by sealing a bead of soft glass onto Platinum wire (Goodfellow, Cambridge) of 25 μm diameter. The soft glass was then sealed into a piece of glass tubing and a back contact to the platinum made by back filling the tube with solder, inserting a wire and gently heating to melt the solder. The glass of the working face of the electrode was then cut and ground flat and the electrode inspected under a microscope for defects. Electrodes were polished on fine alumina prior to use.

Glass capillaries (Clark Electromedical, Reading) 0.8mm i.d. were pulled twice using a vertical pipette puller (David Kopf Instr., California). The pipette tips thus produced were then carefully broken to give tip openings of 3-12 μm radius in a plane normal to the axis of the capillary (figure 5).

Silver/silver chloride reference electrodes were formed by electrolysis of silver wire (Goodfellow 99.9% Ag) in aqueous solutions of KCl or NaCl.

Single microhole experiments were conducted using the two electrode cell illustrated in figure 6a. Figure 6b shows the four electrode modification of this cell used for the microhole arrays. The micro holes themselves were formed by laser ablation techniques to micrometre precision (Exitech Ltd, Cambridge) in a 12 μm thick polyester membrane. The membrane was treated on one side to render it hydrophilic (Exitech Ltd process, ibid). Single holes of 5, 10, 20 and 50 μm diameter were used. Microhole arrays consisted of 15 μm diameter holes centred 100 μm apart as illustrated in figure 7. A complete array contained a number of the sub arrays shown in figure 7 giving a total of approximately 7600 holes and hence a total interfacial area of 1.3×10^{-6} m^2. Membranes with single holes were mounted on short pieces of glass capillary tubing with silicon rubber solution (Dow Corning) and cured overnight at 30°C. Array membranes were mounted similarly on a piece of glass tubing with a wide flange at the bottom.

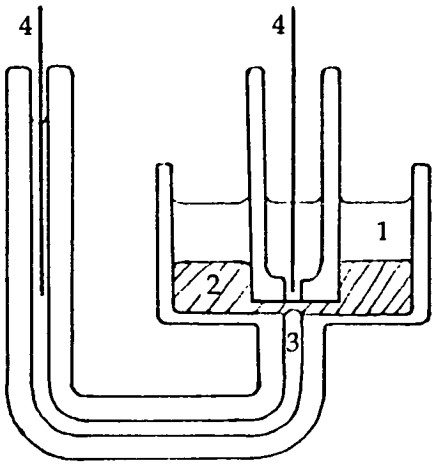

a)

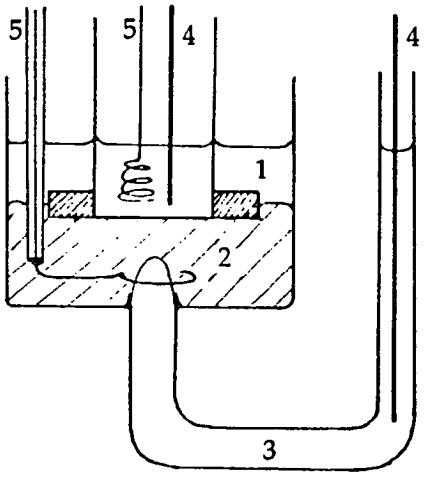

b)

Fig. 6 Microelectrode cells. a) two electrode cell for single microhole, b) four electrode cell for microhole array. (1) aqueous electrolyte, (2) organic electrolyte, (3) organic reference electrolyte, (4) Ag/AgCl reference electrodes, (5) counter electrodes.

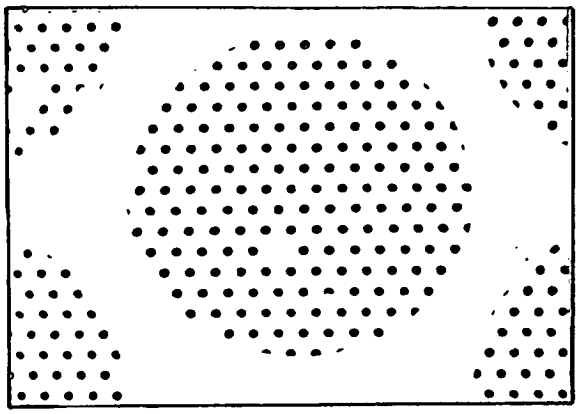

a)

200 μm

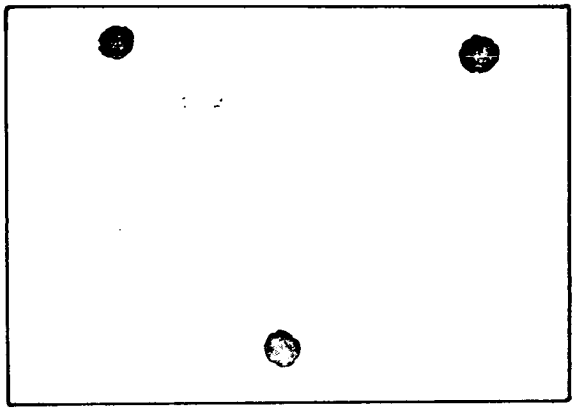

b)

20 μm

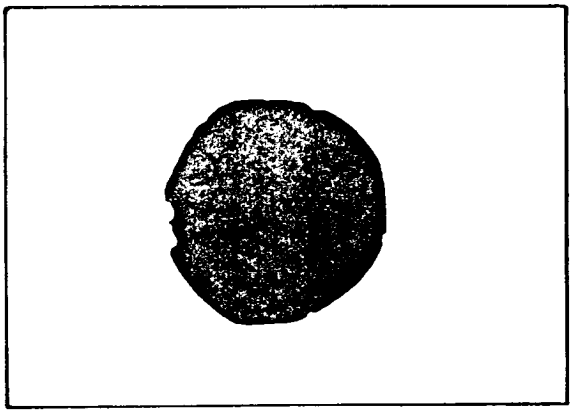

c)

4 μm

Fig. 7 Electron micrographs of a) array of 15 μm diameter holes centred 100 μm apart, b) close up of three 15 μm diameter array holes, and c) close up of a single hole from array.

2.3 LARGE SCALE ITIES

2.3.1 Instrumentation

Electrical potential, or current, across large interfaces was controlled using a three electrode potentiostat (Southampton University) in conjunction with a laboratory constructed zerostat (figure 8). The reference and counter electrode terminals of the potentiostat were connected to the organic phase electrodes and the zerostat terminals to the aqueous phase. The zerostat may be used in one of two modes, either to control the interfacial current and measure the electrical potential difference across the interface using the ΔV facility, or to measure current via i while controlling the potential difference. In the former case a resistor is placed between the reference and working electrode terminals on the potentiostat, the organic and aqueous reference electrodes are connected to the RE1 and RE2 zerostat terminals respectively and an appropriate potential waveform is applied to the potentiostat voltage input. Experiments were more usually performed by application of a controlled potential between the two reference electrodes and measurement of the current between the counter electrodes via i. In this case the aqueous reference and counter electrodes are connected to the zerostat RE2 and CE2 terminals respectively. Feedback iR compensation is adjusted for the zerostat at R1 and the potential added back to the potentiostat input. iR compensation was the maximum possible before resonance occurred in the current output signal. High frequency noise thereby introduced could be removed from the current output by the filter F1. The potential ramp for cyclic voltammetry was delivered from a PPR1 (HITEK) and the current response measured on an X,Y recorder (Advance Bryans, series 60,000). Potential sweep rates in the range 1 mV s^{-1} to 1 V s^{-1} were used.

2.3.2 Cell Design

Three different cells were used and are shown in figure 9a, b and c. Design A enabled the phases to be arranged contrary to the natural orientation of DCE below water (following the density gradient) and hence a flat interface could be achieved by a suitable pressure balance. Cell B (donated by Dr Samec, Prague) was used in preference to cell A when it became available

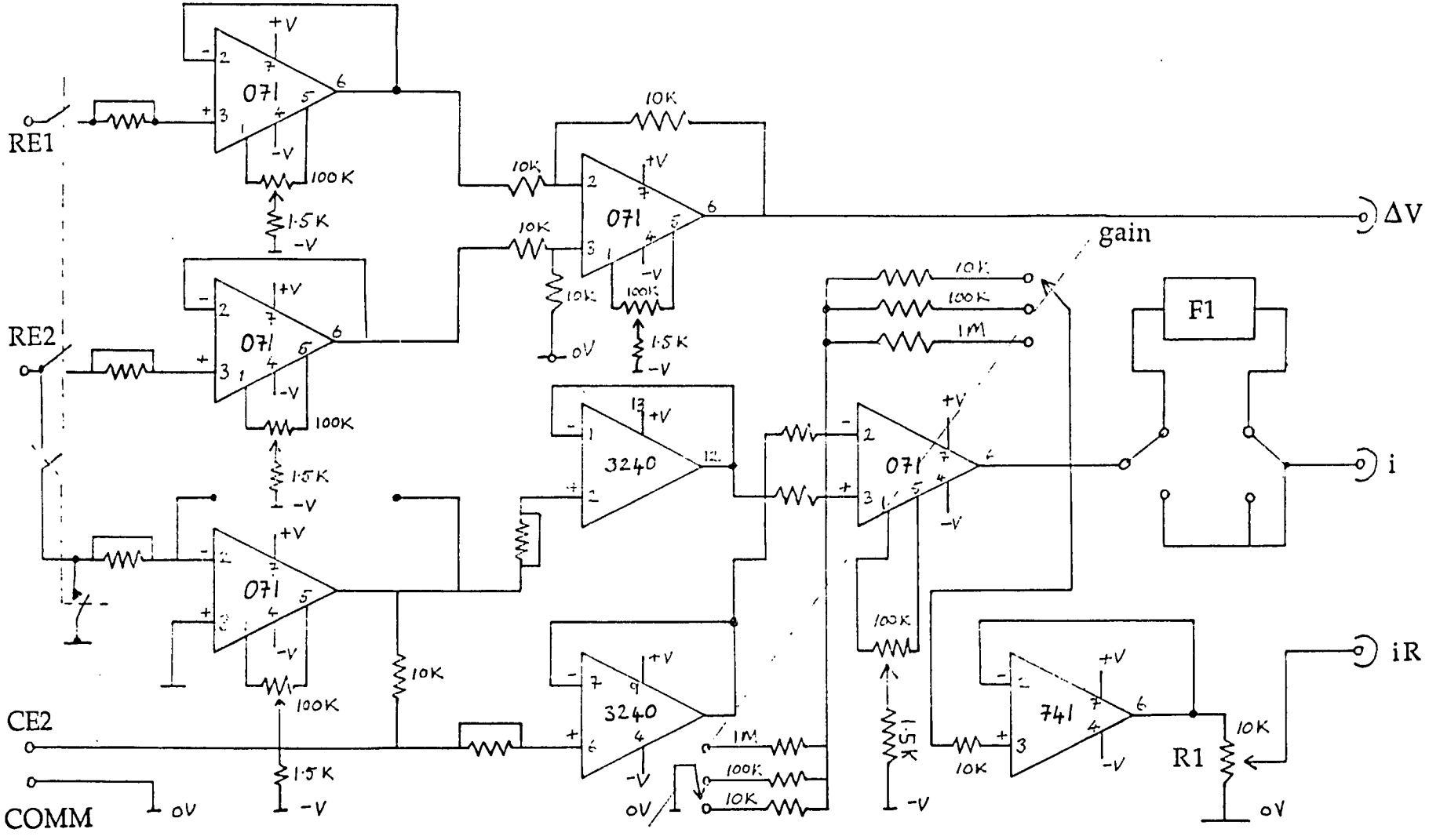

Fig 8 Zerostat circuit diagram including filter F1 and iR compensation resistor R1.

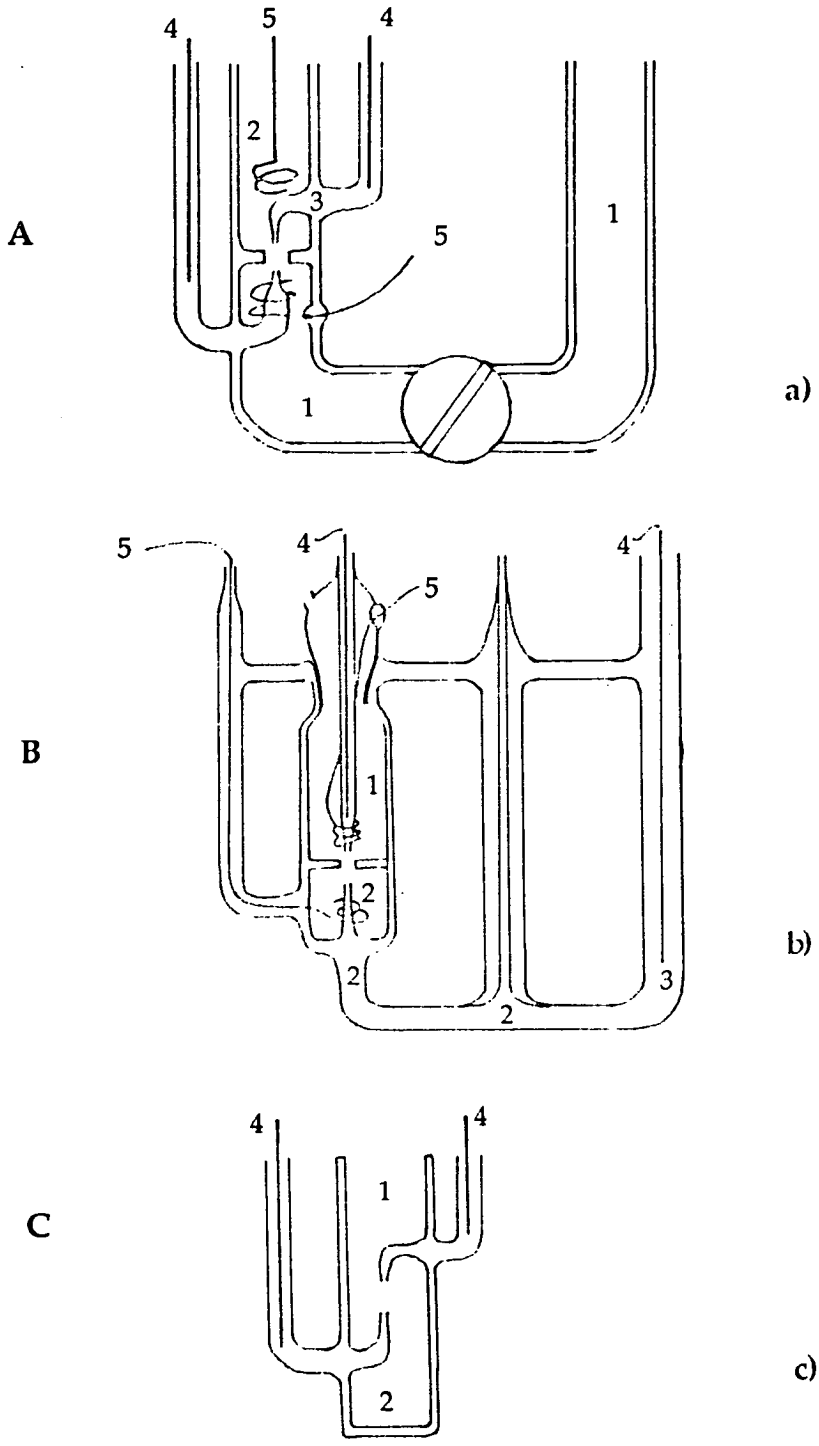

Fig. 9 Large ITIES cell designs. (1) aqueous electrolyte, (2) organic electrolyte, (3) organic reference electrolyte, (4) Ag/AgCl reference electrodes, (5) counter electrodes.

as it was much easier to fill and had better pressure control. The dimensions of cell C are such that the DCE phase must be below the aqueous phase, hence the interface produced is curved, however the simple symmetrical design provides for easier iR compensation and quicker filling than for cells A and B.

2.4 CHEMICALS

All solutions were made up in distiled water or water from a Milli RO15 (Millipore) water purification system.

Dichloroethane (BDH, AnalaR) was used as supplied

The aqueous salts used were as follows:

LiCl	Fluka purum p.a.
NaCl	Fisons A.R. grade
KCl	Fisons A.R. grade
RbCl	Aldrich 99.8 +%
CsCl	Aldrich 99.9%
$MgSO_4$	Fisons SLR
Li_2SO_4	BDH AnalaR
$K_3Fe(CN)_6$	BDH AnalaR
$K_4Fe(CN)_6$	BDH AnalaR

Acetylcholine chloride (AChCl) Fluka 99%

Tetrabutylammonium chloride (TBACl) Fluka purum

Tetrabutylammonium bromide (TBABr) Fluka puriss

Crystal violet chloride (CVCl)

Tetraethylammonium chloride (TEACl) Fluka purum

Potassium tetrakis (4-chlorophenyl) borate (KTPBCl) Lancaster Synthesis

Potassium tetrakis (pentafluorophenyl) borate (KTPBF)

Tetrabutylammonium-tetraphenylborate (TBATPB) was prepared by precipitation from equimolar aqueous solutions of TBABr and NaTPB, then recrystallised from acetone. Tetrabutylammonium-tetrakis(pentafluorophenyl)borate (TBATPBF) was prepared similarly and recrystalised from methanol. Tetrabutylammonium-tetrakis(4-chlorophenyl)borate (TBATPBCl) was synthesised by coprecipitation of equimolar solutions of TBABr and KTPBCl in a methanol/water solvent. The product was recrystallised from methanol. Dibenzo-18-crown-6 (DB18C6) (Aldrich 98%), benzo-15-crown-5 (B15C5) (Aldrich 98%), ferrocene (FeC) (Fluka, purum) and dibutylferrocene (DBFeC) (TCI E.P. Japan) were used as supplied.

THEORY

3.1 THE NATURE OF THE ITIES

Under specified conditions, as mentioned above, the ITIES behaves in a fashion analogous to the metal/electrolyte interface, i.e. it becomes polarisable and charge may only be transferred by peculiar electroactive species. The ideally polarisable ITIES, the nature of the electrical double layer formed at the interface and the origin of various interfacial electrical potential differences, are all summarised below.

3.1.1 Interfacial Potential Differences

The phenomenon of potential differences observed across liquid/liquid interfaces was the subject of much debate at the beginning of this century. There are in fact three different types of electrical potential difference which arise at the liquid/liquid interface[73] namely; diffusion potentials, adsorption potentials and distribution potentials.

3.1.1.1 Diffusion Potentials

The diffusion potential, also called the liquid junction potential, arises from a non equilibrium situation where electrolyte species present are not in thermodynamic equilibrium in adjoining phases[74]. Diffusion potentials may become relevant at reference electrode boundaries, but normally relative concentrations and transport numbers of electrolytes are arranged so that diffusion potentials either become negligibly small, or are constant during the lifetime of an experiment, and may thus be ignored.

3.1.1.2 Adsorption Potentials

Adsorption potentials are caused by selective ionic adsorption at the interface and hence only occur when there are surface active ionic species present.

3.1.1.3 Distribution Potentials

The distribution potential is due to an unequal distribution of electrolyte ions across the interface and its variation is that which we aim to measure, or control, at the ITIES. Karpfen and Randles[14] considered the thermodynamics of a salt MX dissolved in two contacting phases, α and β, (see (I) below) based on the equality of the electrochemical potentials of the ions in both phases and the electroneutrality condition for the bulk phases.

$$M^+ + X^- \text{ (solvated in } \alpha \text{ and totally dissociated)} \rightleftharpoons M^+ + X^- \text{ (solvated in } \beta \text{ and totally dissociated)} \qquad \text{(I)}$$

They tested their thermodynamic analysis by experiment and the results supported their equation (equation (1)) defining the potential difference, $\Delta_\alpha^\beta\phi_{mx}$ arising at the ITIES when a salt MX (M and X being univalent ions) is distributed between the water (α) and oil (β) phases.

$$\Delta_\alpha^\beta\phi_{mx} = \frac{RT}{2F}\ln\left[\frac{B_m\,\gamma_m^{\alpha\ sat}\,\gamma_x^{\beta\ sat}}{B_x\,\gamma_m^{\beta\ sat}\,\gamma_x^{\alpha\ sat}}\right] \qquad (1)$$

where $RT \ln B_m = \mu_m^{o,\,\alpha\ sat} - \mu_m^{o,\,\beta\ sat}$

and $RT \ln B_x = \mu_x^{o,\,\alpha\ sat} - \mu_x^{o,\,\beta\ sat}$

Superscripts refer to the standard state (o=infinite dilution, etc) and the water (αsat) or oil (βsat) phase respectively. Subscripts refer to the species concerned and γ to the activity coefficient. Note that αsat and βsat refer to water saturated with oil and oil saturated with water respectively.

As can be seen from equation (1) the distribution potential is independent of the electrolyte concentration (over the concentration range where the activity coefficients ratio is constant) and is controlled by the ionic distribution coefficients, B_m and B_x. It is distribution potentials which make up the potential differences normally observed at the ITIES.

3.1.2 Energies of Transfer and Partition

Considering the equilibrium **(I)** above the standard Gibbs energy of transfer for the salt MX from α to β, $\Delta G_{t,mx}$, is given by:

$$\Delta G_{t,mx}^{o,\alpha\rightarrow\beta} = \left[\mu_m^{o,\beta} + \mu_x^{o,\beta}\right] - \left[\mu_m^{o,\alpha} + \mu_x^{o,\alpha}\right] \qquad (2)$$

and corresponds to the difference in the energies of solvation of the salt MX between α and β which can be measured experimentally. Given that solvation results in complete dissociation of MX it can also be expressed as the sum of the standard Gibbs energies of transfer of the ions M^+ and X^-:

$$\Delta G_{t,mx}^{o,\alpha\rightarrow\beta} = \Delta G_{t,m}^{o,\alpha\rightarrow\beta} + \Delta G_{t,x}^{o,\alpha\rightarrow\beta} \qquad (3)$$

While the standard Gibbs energies of transfer for salts are thermodynamically measurable quantities a scale for the ionic standard Gibbs energies of transfer can only be established by using an extra-thermodynamic assumption. The most widely accepted assumption is the tetraphenylarsonium/tetraphenylborate ($TPAs^+/TBA^-$) assumption

which was proposed by Grunwald et al in 1960[75] and states that for any solvent:

$$\Delta G_{solvation,\ TPAs^+} = \Delta G_{solvation,\ TPB^-} = \frac{1}{2}\,\Delta G_{solvation,\ TPAs\ TPB} \qquad (4)$$

Thus the ΔG_t of any anion, A, or any cation, C, may be obtained from equations (5) and (6) respectively. Again complete dissociation on solvation is implied.

$$\Delta G^{o,\alpha\rightarrow\beta}_{t,A^-} = \Delta G^{o,\alpha\rightarrow\beta}_{t,TPAsA} - \Delta G^{o,\alpha\rightarrow\beta}_{t,TPAs^+} \qquad (5)$$

$$\Delta G^{o,\alpha\rightarrow\beta}_{t,C^+} = \Delta G^{o,\alpha\rightarrow\beta}_{t,TPB\,C} - \Delta G^{o,\alpha\rightarrow\beta}_{t,TPB^-} \qquad (6)$$

Another approach is to determine the potential of zero charge (pzc) for the system, e.g. by use of a streaming electrolyte electrode[76], and to take this point as corresponding to the absolute zero of the potential scale for the system.

The standard Gibbs energy of transfer of an ion is equivalent to the difference in the standard chemical potentials of the ion in the two pure phases α and β (equation (7)).

$$\Delta G^{o,\alpha\rightarrow\beta}_{t,i} = \left[\mu_i^{o,\beta} - \mu_i^{o,\alpha}\right] \qquad (7)$$

In contrast the Gibbs energy of partition, $\Delta G_{p,i}$, of the ion (related to the ionic partition coefficient, B_i, mentioned above) is given by the difference in the standard chemical potentials of the ion in the two *mutually saturated* phases α and β.

$$\Delta G^{o,\alpha\rightarrow\beta}_{p,i} = \left[\mu_i^{o,\beta\ sat} - \mu_i^{o,\alpha\ sat}\right] = -\ RT\ \ln\ B_i \qquad (8)$$

With solvents of low miscibility, e.g. water/nitrobenzene and water/1,2-dichloroethane, the ionic standard Gibbs energies of transfer and partition are nearly equal[73]. In this work the water/1,2-dichloroethane interface is used and hence the distinction between energies of partition and transfer is not made. While the solvents used are generally mutually saturated, the notation used hereafter refers to transfer, rather than partition, Gibbs energies (as is common in the literature).

3.1.3 Ideally Reversible and Ideally Polarised Electrodes

There are two main classes of ITIES: the "ideally polarisable" interface and the non polarisable or "ideally reversible" interface. The first occurs when the organic electrolyte is strongly hydrophobic and the aqueous electrolyte strongly hydrophilic (i.e. ΔG_t's are large and of the appropriate signs). This situation provides a "potential window" where the Galvani, or inner, potential difference between the two phases may be varied over a range of a few hundred millivolts without significant passage of current across the interface. A build up of charge in the form of electrolyte ions is thus created on either side of the interface to maintain the potential difference. Outside the potential window the potential difference is sufficiently extreme to induce electrolyte ions to cross the interface in quantity. The hydrophobic and hydrophilic salts used to produce this situation act as supporting electrolyte in a similar fashion to those used at the metal/electrolyte interface. Any charge transfer reaction to be studied must have a less extreme Gibbs energy of transfer than the supporting electrolytes in order for it to occur within the accessible potential window.

The non polarisable interface is one where the application of an external potential difference does not lead to charge accumulation at the interface, but to charge transfer. This situation arises when one or more ions present is able to cross the interface unhindered, i.e. if one or more ions present is readily soluble in both phases. The term "ideally reversible" means that an infinitesimal increase or decrease in potential from the equilibrium value will lead to charge transfer across the interface, thus depolarising it. Real interfaces only ever behave as ideally reversible or polarisable over a limited potential range.

3.1.4 Reference Electrodes

Reference electrodes consist of non polarisable interfaces (reversible to single ions) of defined and constant composition and therefore constant electrical potential. In liquid/liquid systems this is most frequently achieved using solid silver/silver halide (Ag/AgX) electrodes in aqueous halide salt solutions of specified concentration. The aqueous supporting electrolyte is often a chloride salt. The organic reference electrode commonly consists of a silver/silver chloride electrode in an aqueous solution of a chloride salt whose counter ion is the cation of the organic phase supporting electrolyte, thereby acting as a potential determining ion[77].

3.1.5 The Electrical Double Layer

The difference in ionic distribution coefficients which results in the formation of the distribution potential across the liquid/liquid interface results, by the same token, in the formation of an "electrical double layer". Put very simply the double layer is the form of the charge separation and distribution which occurs at the interface. It is this double layer which maintains the Galvani potential difference. The precise and detailed molecular scale structure of this double layer is the subject of a great deal of controversy. The model for the liquid/liquid interface has been developed from that used for the metal/electrolyte interface.

3.1.5.1 The Double Layer at the Metal/Electrolyte Interface

Charge separation at the metal/electrolyte interface was first considered by Helmholtz [78,79] who proposed that the excess charge resided at the surface of each phase in accordance with Gauss' law[74] which states that the excess charge of a conducting phase at equilibrium must reside at its surface. This model is the equivalent of a parallel plate capacitor and as such suggests that the interface should be of a constant capacitance. It is known by experiment that this is not the case. Gouy and Chapman [80-82] proposed independently that, while the charge on the metal is at the surface, the

counter charge in the solution is spread through a significant thickness of the solution called the diffuse layer. A statistical mechanical description of the excess charge carrier distribution through the diffuse layer was used. A further modification by Stern[83] introduced the concept of the distance of closest approach of charge carriers to the metal surface thereby making some allowance for the finite size of ions and ion solvation which was neglected by Gouy and Chapman. This Gouy Chapman Stern model has formed the basis for continued developments in double layer theory and studies at the electrified interface which now include such phenomena as inner layer compression, dielectric saturation, dipole-dipole interactions, non arbitrary dipole orientation and electron spillover from the metal electrode to the solution[84].

3.1.5.2 The Double Layer at the Liquid/Liquid Interface

Riesenfeld[13] first envisaged an electrical double layer at the ITIES in 1902, but the earliest quantitative treatment is attributed to Verwey and Niessen in 1939[16]. They proposed a model of the oil/water interface where there is a potential difference attributable to orientation of solvent dipoles where the two phases contact (the inner layer) and that the remainder of the interfacial potential difference is accounted for by a diffuse layer of excess ions in both the aqueous and organic phases analogous to the Gouy Chapman diffuse layer at the metal/electrolyte interface. Similar to Stern's modification Gavach et al proposed[85] an ion free inner layer of orientated solvent molecules defining planes of closest approach (outer Helmholtz planes) for both aqueous and organic sides of the interface. This model, termed the modified Verwey-Niessen model has been widely adopted by workers in the field[18,86]. The existence of an ion free inner layer is questioned however, especially by Girault and Schiffrin who propose that interfacial solvent mixing occurs[87]. Subsequently Samec et al, admitting a "non zero probability of finding ions in the inner-layer region" [47], have attempted to model ion penetration into the inner layer in analogy with the treatment of electron spillover at the metal/electrolyte

interface[88]. Exactly how this model should be interpreted physically if ions remain solvated, but solvents do not "mix", is unclear. Part of the difficulty in devising a satisfactory model for the liquid/liquid interface derives from the problems in interpreting experimental data in the same way as for the metal/electrolyte interface.

3.1.5.3 Thermodynamic Analysis

Application of the Gibbs adsorption isotherm to the mercury/electrolyte interface results in the electrocapillary equation which relates changes in surface tension to changes in interfacial electrical potential and the chemical potentials of components of the system. For example, the electrocapillary equation for mercury in contact with an aqueous solution of potassium chloride and a neutral species, X, is given by[74]:

$$-d\gamma = \sigma^m \, dE + \Gamma_{K^+(H_2O)} \, d\mu_{KCl} + \Gamma_{X\,(H_2O)} \, d\mu_X \qquad (9)$$

Where γ is surface tension, σ_m the excess charge density on the metallic side of the interface, E the potential of mercury with respect to the reference and Γ_{K^+} and Γ_X are the surface excesses of K^+ and X respectively relative to that of water.

The surface excess charge on the electrode is thus given by:

$$\sigma^m = -\left(\frac{\partial\gamma}{\partial E}\right)_{\mu_{KCl},\mu_X} \qquad (10)$$

and the differential capacitance of the interface, C_d, may be defined as:

$$Cd = \left(\frac{\partial\sigma^m}{\partial E}\right) \qquad (11)$$

Thus, in the absence of adsorption, the variation of surface tension with potential gives information on the surface excess charge and differential capacitance of the mercury/electrolyte interface, and vice versa.

The thermodynamic analysis for the ITIES is similar[60] but surface excess quantities are expressed relative to both solvents and incomplete dissociation of electrolytes and ion pair formation at the interface is considered. The resulting electrocapillary equation is:

$$-d\gamma = \left(\Gamma_{K^+}^{(o,w)} + \Gamma_{KA}^{(o,w)} + \Gamma_{KCl}^{(o,w)}\right)d\mu_{KCl} + \left(\Gamma_{A^-}^{(o,w)} + \Gamma_{KA}^{(o,w)} + \Gamma_{CA}^{(o,w)}\right)d\mu_{CA} + F\left[\left(\Gamma_{Cl^-}^{(o,w)} - \Gamma_{K^+}^{(o,w)}\right) + \left(\Gamma_{CCl}^{(o,w)} - \Gamma_{KA}^{(o,w)}\right)\right]dE_{+(-)} \quad (12)$$

$$\Gamma_X^{(o,w)} = \Gamma_X - n_X^{(w)}\frac{\Delta_w}{\Delta} - n_X^{(o)}\frac{\Delta_o}{\Delta} \quad (13)$$

where $\Delta = \begin{vmatrix} n_w^{(w)} & n_w^{(w)} \\ n_o^{(o)} & n_w^{(o)} \end{vmatrix}$, $\Delta_w = \begin{vmatrix} n_w^{(o)} & \Gamma_w \\ n_o^{(o)} & \Gamma_o \end{vmatrix}$ and $\Delta_o = \begin{vmatrix} n_o^{(w)} & \Gamma_o \\ n_w^{(w)} & \Gamma_w \end{vmatrix}$

In this case $(d\gamma/dE)$ is given by equation 14.

$$-\left(\frac{\partial\gamma}{\partial E}\right)_{\mu_{KCl},\mu_{CA}} = \left(\Gamma_{Cl^-}^{(o,w)} - \Gamma_{K^+}^{(o,w)}\right) + \left(\Gamma_{CCl}^{(o,w)} - \Gamma_{KA}^{(o,w)}\right) = Q \quad (14)$$

This is not simply a surface charge density as in equation (10) but represents the quantity of ions and ion pairs which must be brought to the interface to maintain a constant interfacial composition, constant chemical potentials of KCl and CA and constant E when the interfacial area is increased by unit amount[60]. Obviously in the case of ion pair formation the electrocapillary maximum is not necessarily the point of zero free charge. The point of zero free charge corresponds to the condition:

$$\Gamma_{Cl^-}^{(o,w)} = \Gamma_{K^+}^{(o,w)} \quad (15)$$

which may be experimentally determined using a streaming electrolyte electrode[76] when $\Gamma_{Cl} = \Gamma_{K^+} = 0$.

The differential interfacial capacitance, C_d, may be expressed as the sum of two components, one relating to the free surface charge, q, and the other to the ion pair contribution, q'.

$$Cd = \left(\frac{\partial Q}{\partial E}\right)_{\mu_{CA},\mu_{KCl}} = \left(\frac{\partial q}{\partial E}\right)_{\mu_{CA},\mu_{KCl}} + \left(\frac{\partial q'}{\partial E}\right)_{\mu_{CA},\mu_{KCl}} \qquad (16)$$

Double integration of differential capacitance data have been found to coincide well with electrocapillary curves[18,60] showing that the Gibbs adsorption equation and formalism is applicable.

While the precise structure of the double layer is not known it is generally agreed upon that the vast majority of the potential difference across the interface is dropped across the diffuse layers with only a small part being accounted for by any "inner layer" potential difference. The form of the potential profile across the interfacial region is of relevance to the interpretation of the variation in the electrochemical rate constant observed with applied potential[89].

3.2 INTERFACIAL CHARGE TRANSFER REACTIONS

All three reactions considered here: ion; assisted ion and electron transfer (see Introduction figure 2), are analogous to electron transfer at the metal/electrolyte interface in that: reactants are transported to an interface across which there is a potential gradient or electric field; charge is then transferred from one phase to the other and finally the products of the reaction move away from the interface. The thermodynamics, charge transfer kinetics and mass transport characteristics of each reaction must therefore be addressed in order to apply electrochemical methodology to them.

3.2.1 Thermodynamics (The Nernst Equation)

Consider the ubiquitous redox at a metal/electrolyte interface (II)

$$O^{z+} + ne^- \rightleftharpoons R^{(z-n)+} \qquad \text{(II)}$$

The equation which governs the relative concentrations of O and R at any given potential is the Nernst equation (equation (17)).

$$E = E^o + \frac{RT}{nF} \ln \frac{a_O}{a_R} \qquad (17)$$

where E is the electrode potential and E^o the standard electrode potential.

This equation is obtained quite simply from the necessary condition for equilibrium that the sum of the electrochemical potentials (μ) of the reactants must equal that of the products (equation(18)).

$$\tilde{\mu}_R = \tilde{\mu}_O + n\tilde{\mu}_e \qquad (18)$$

The electrochemical potential of a species i with charge z_i in phase α is defined as:

$$\tilde{\mu}_i^{\alpha} = \mu_i^{\alpha} + z_i F \phi^{\alpha} \qquad (19)$$

μ_i^{α} is the chemical potential of i in α, defined as:

$$\mu_i^{\alpha} = \left(\frac{\partial G}{\partial n_i}\right)_{T,P,n_j \neq i} \qquad (20)$$

and expressed in terms of the standard chemical potential, $\mu_i^{o,\alpha}$, as:

$$\mu_i^{\alpha} = \mu_i^{o,\alpha} + RT \ln a_i \qquad (21)$$

Substituting into equation (18) from (19) and (21) gives:

$$\mu_R^{o,s} + RT \ln a_R^s + (z - n)F\phi^s = \mu_o^{o,s} + RT \ln a_o^s + zF\phi^s + n\mu_e^{o,m} + nRT \ln a_e^m - nF\phi^m \qquad (22)$$

where superscripts s and m refer to the solution and metallic phases respectively.

Since the activity of electrons in a metal is unity this equation simplifies to:

$$nF(\phi^m - \phi^s) = \mu_o^{o,s} + \mu_e^{o,m} - \mu_R^{o,s} + RT \ln \frac{a_o^s}{a_R^s} \qquad (23)$$

By definition the molar Gibbs energy of the reaction ΔG_m^o is:

$$-\Delta G_m^o = \mu_o^{o,s} + \mu_e^{o,m} - \mu_R^{o,s} \qquad (24)$$

and

$$-\Delta G_m^o = -nFE_{abs}^o \qquad (25)$$

where E_{abs}^o is the standard redox potential on the absolute vacuum scale. Substitution of (24) and (25) into (23) finally gives the Nernst equation (17):

$$E = E^o + \frac{RT}{nF} \ln \frac{a_O}{a_R} \qquad (17)$$

The electrode potential E is the potential difference between the metal and solution phases:

$$E = \phi^m - \phi^s \qquad (26)$$

In practice electrode potentials can only be measured with respect to some reference system, this is conventionally the NHE and the standard electrode potential of any redox couple is that measured with respect to this system.

3.2.1.1 Ion Transfer

The general ion transfer reaction depicted in figure 2a is:

$$M^{z+}(\alpha) \rightleftharpoons M^{z+}(\beta) \qquad \text{(III)}$$

Equating the electrochemical potentials of the ions in each phase (equation(27))

$$\mu_m^{o,\alpha} + RT \ln a_m^{\alpha} + zF\phi^{\alpha} = \mu_m^{o,\beta} + RT \ln a_m^{\beta} + zF\phi^{\beta} \qquad (27)$$

leads to the Nernst equation for ion transfer:

$$\Delta_{\alpha}^{\beta}\phi = \Delta_{\alpha}^{\beta}\phi_m^{o} + \frac{RT}{zF} \ln \frac{a_m^{\alpha}}{a_m^{\beta}} \qquad (28)$$

where

$$\Delta_{\alpha}^{\beta}\phi = \phi^{\beta} - \phi^{\alpha} \qquad (29)$$

and

$$\Delta_{\alpha}^{\beta}\phi_m^{o} = \left(\mu_m^{o,\alpha} - \mu_m^{o,\beta}\right) / zF = -\Delta G_{t,m}^{o,\alpha\rightarrow\beta} / zF \qquad (30)$$

3.2.1.2 Assisted ion Transfer

The assisted ion transfer reaction depicted in figure 2b may be written:

$$M^{z+}(\alpha) + C(\beta) \rightleftharpoons CM^{z+}(\beta) \qquad \text{(IV)}$$

The equilibrium condition is expressed as:

$$\mu_m^{o,\alpha} + RT \ln a_m^{\alpha} + zF\phi^{\alpha} + RT \ln a_c^{\beta} = \mu_{cm}^{o,\beta} + RT \ln a_{cm}^{\beta} + zF\phi^{\beta} \quad (31)$$

$$\Rightarrow zF(\phi^{\beta} - \phi^{\alpha}) = \mu_m^{o,\alpha} + \mu_c^{o,\beta} - \mu_{cm}^{o,\beta} + RT \ln \frac{a_c^{\beta} a_m^{\alpha}}{a_{cm}^{\beta}} \quad (32)$$

$$\Rightarrow \Delta_{\alpha}^{\beta}\phi = \Delta_{\alpha}^{\beta}\phi_{react}^{o} + \frac{RT}{zF} \ln \frac{a_c^{\beta} a_m^{\alpha}}{a_{cm}^{\beta}} \quad (33)$$

$\Delta_{\alpha}^{\beta}\phi_{react}^{o}$ is $-\Delta G_{react}/zF$ and may also be expressed (equation(35)) in terms of the association constant, K_a, for reaction **(V)** below:

$$M^{z+}(\beta) + C(\beta) \rightleftharpoons CM^{z+}(\beta) \quad \textbf{(V)}$$

$$\mu_m^{o,\alpha} + \mu_c^{o,\beta} - \mu_{cm}^{o,\beta} = \mu_m^{o,\beta} + \mu_c^{o,\beta} - \mu_{cm}^{o,\beta} + \left(\mu_m^{o,\alpha} - \mu_m^{o,\beta}\right) \quad (34)$$

$$\Delta_{\alpha}^{\beta}\phi_{react}^{o} = -\frac{RT}{zF} \ln K_a + \Delta_{\alpha}^{\beta}\phi_m^{o} \quad (35)$$

Substitution of equation (35) into (33) gives:

$$\Delta_{\alpha}^{\beta}\phi = \Delta_{\alpha}^{\beta}\phi_m^{o} - \frac{RT}{zF} \ln K_a + \frac{RT}{zF} \ln \frac{a_c^{\beta} a_m^{\alpha}}{a_{cm}^{\beta}} \quad (36)$$

Under pseudo first order conditions when $a_{m,\alpha} >> a_{c,\beta}$ and $a_{m,\alpha} >> a_{cm,\beta}$ then $a_{m,\alpha}$ is effectively constant with potential and the effective Nernst equation for the reaction becomes:

$$\Delta_{\alpha}^{\beta}\phi = \Delta_{\alpha}^{\beta}\phi^{o}_{eff} + \frac{RT}{zF} \ln \frac{a_{c}^{\beta}}{a_{cm}^{\beta}} \qquad (37)$$

where $\Delta_{\alpha}^{\beta}\phi^{o}_{eff}$ is given by:

$$\Delta_{\alpha}^{\beta}\phi^{o}_{eff} = \Delta_{\alpha}^{\beta}\phi^{o}_{m} - \frac{RT}{zF} \ln K_a + \frac{RT}{zF} \ln a_{m}^{\alpha} \qquad (38)$$

The use of equations (34) and (35) asserts that the complexed ion product of reaction **(IV)** is identical to that of reaction **(V)**, ie that M^{z+} loses all of its solvation shell from solvent α upon transfer to the complexed species in β. This means that the thermodynamics of the direct interfacial complexation reaction **(IV)** is identical to that of the EC reaction given by combination of reactions **(III)** and **(V)** above. It is conceivable however, that some of solvent α is transported across the interface with M^{z+} in either, or both, of reactions **(III)** and **(IV)**. If reaction **(III)** involves complete desolvation and resolvation of M^{z+} then the assertion that the complexation reaction product involves no α solvent molecules can be tested by comparing the association constant, K_a, obtained experimentally from equation (36) and $\Delta_{\alpha}^{\beta}\phi^{o}_{m}$ with that obtained experimentally from studies in pure β. Unfortunately the determination of whether or not the simple ion transfer reaction **(III)** involves complete desolvation by use of ionic solvation energies involves the use of an extra-thermodynamic assumption and so is not entirely reliable. Hence such calculations cannot be used to unambiguously identify the product of the assisted ion transfer reaction.

3.2.1.3 Electron Transfer

The generalised electron transfer reaction between redox couples 1 and 2 across a liquid/liquid interface is written below **(VI)** and shown schematically in figure (2c).

$$O1_{\alpha} + R2_{\beta} \rightleftharpoons R1_{\alpha} + O2_{\beta} \qquad \textbf{(VI)}$$

Considering the case where the charges on O1 and R1 are p and q and those on O2 and R2 are x and y respectively. The number of electrons transfered is n, i.e.:

$$n = p - q = x - y \qquad \textbf{(39)}$$

Equating the electrochemical potentials of reactants and products in **(VI)** gives:

$$\mu_{O1}^{o,\alpha} + RT \ln a_{O1}^{\alpha} + pF\phi^{\alpha} + \mu_{R2}^{o,\beta} + RT \ln a_{R2}^{\beta} + yF\phi^{\beta} = \mu_{R1}^{o,\alpha} + RT \ln a_{R1}^{\alpha} + qF\phi^{\alpha} + \mu_{O2}^{o,\beta} + RT \ln a_{O2}^{\beta} + xF\phi^{\beta} \qquad \textbf{(40)}$$

This rearranges using equation (39) to a Nernst type equation for electron transfer:

$$\Delta_{\alpha}^{\beta}\phi = \Delta_{\alpha}^{\beta}\phi^{o} + \frac{RT}{nF} \ln \frac{a_{O1}^{\alpha} a_{R2}^{\beta}}{a_{R1}^{\alpha} a_{O2}^{\beta}} \qquad \textbf{(41)}$$

$\Delta_{\alpha}^{\beta}\phi^{o}$ is the standard Galvani potential of the electron transfer reaction[62,65] which is related to the standard molar Gibbs energy of reaction (VI), ΔG_{redox}^{o}, as shown in equation (42). It may be further related[65] to the standard potentials for the two redox couples in solvent α

and to the standard Gibbs energies of partition of R2 and O2 between solvents α and β equation (43).

$$\Delta_{\alpha}^{\beta}\phi^{o} = -\frac{\Delta G_{redox}^{o}}{nF} = \left(\left(\mu_{R2}^{o,\beta} - \mu_{O2}^{o,\beta}\right) - \left(\mu_{R1}^{o,\alpha} - \mu_{O1}^{o,\alpha}\right)\right) / nF \qquad (42)$$

$$-\frac{\Delta G_{redox}^{o}}{nF} = -E_{O2,R2}^{o,\alpha} + E_{O1,R1}^{o,\alpha} + \left(\Delta G_{t,R2}^{o,\alpha\rightarrow\beta} - \Delta G_{t,O2}^{o,\alpha\rightarrow\beta}\right) / nF \qquad (43)$$

The three Nernstian expressions above (equations (28), (37) and (41)) enable the Galvani, or inner, potential difference between the two phases, α and β, to be related to the ratio of activities of reactants and products in the three types of interfacial charge transfer considered.

3.2.2 Charge Transfer Kinetics

3.2.2.1 Ion Transfer

Consider the simple ion transfer reaction (III) as an elementary reaction.

$$M^{z+}(\alpha) \qquad <k_b k_f> \qquad M^{z+}(\beta) \qquad (III)$$

In this case the rates of forward, v_f, and back, v_b, reactions will be proportional to the interfacial concentrations of M, $C_m^{\sigma,\alpha}$ and $C_m^{\sigma,\beta}$ in phases α and β respectively, i.e.

$$v_f = k_f C_m^{\sigma,\alpha} \quad \text{and} \quad v_b = k_b C_m^{\sigma,\beta} \qquad (44)$$

where k_f and k_b are the forward and reverse rate constants.

Because electrochemical reactions take place at two dimensional interfaces the rate of reaction is measured by the flux of reactant or product across the reactive interface, ν_f and ν_b are therefore forward and reverse fluxes across the interface and the rate constants k_f and k_b have dimensions $l\ t^{-1}$. The net flux, or net rate, of charge transfer, ν_{net}, is the difference between the forward and reverse rates and is related to the net interfacial current density, i/A, by:

$$\nu_{net} = k_f C_m^{\sigma,\alpha} - k_b C_m^{\sigma,\beta} = \frac{i}{zFA} \qquad (45)$$

where i is the net interfacial current, A is the interfacial area and F the Faraday constant.

We consider the reaction kinetics using activated complex theory and suppose that in passing from phase α to phase β the ion crosses an energy barrier (see figure 10) whose height is the electrochemical Gibbs energy of activation for the reaction $\Delta G_f^{\neq}$. The activation barrier to the reverse reaction is denoted $\Delta G_b^{\neq}$. The electrochemical Gibbs energies of activation are formally separated into chemical and electrical components (equation (46))[74,89]. The chemical, or neutral, component, $\left(\Delta G^{\neq}\right)_n$, is assumed to be independent of potential and the electrical component, $\left(\Delta G^{\neq}\right)_e$ is assumed to be a fixed fraction of the electrical part of the electrochemical Gibbs energy of transfer for the reaction, $\left(\Delta G_{t,m}^{\alpha\rightarrow\beta}\right)_e$.

$$\Delta G_f^{\neq} = \left(\Delta G_f^{\neq}\right)_n + \left(\Delta G_f^{\neq}\right)_e \quad , \quad \Delta G_b^{\neq} = \left(\Delta G_b^{\neq}\right)_n + \left(\Delta G_b^{\neq}\right)_e \qquad (46)$$

$$\left(\Delta G_f^{\neq}\right)_e = \alpha \left(\Delta G_{t,m}^{\alpha\rightarrow\beta}\right)_e \qquad (47)$$

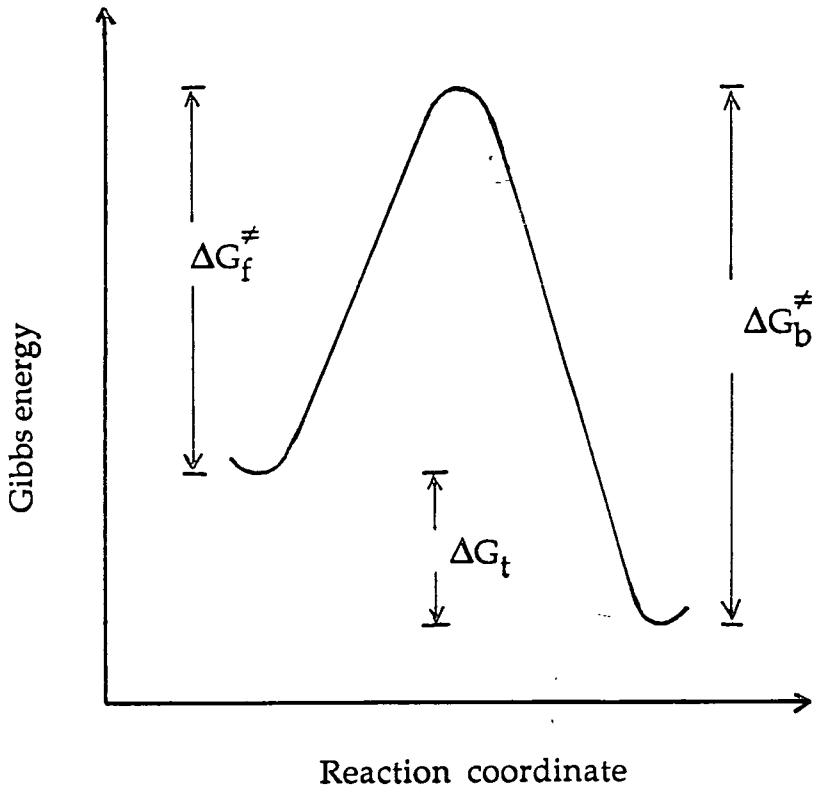

Fig. 10 Schematic diagram of energy barrier to charge transfer showing the Gibbs energies of activation for the forward and reverse reactions when ΔG_t is negative.

$$\left(\Delta G_b^{\neq}\right)_e = -(1-\alpha)\left(\Delta G_{t,m}^{\alpha\rightarrow\beta}\right)_e \qquad (48)$$

The electrical part of the Gibbs energy of transfer can be obtained from equation (49) assuming that $\left(\Delta G^{\neq}\right)_n$ is independent of the electrical potential as must be the case by definition.

$$\Delta G_{t,m}^{\alpha\rightarrow\beta} = \left(\mu_m^{\beta} + zF\phi^{\beta}\right) - \left(\mu_m^{\alpha} + zF\phi^{\alpha}\right) \qquad (49)$$

$$\left(\Delta G_{t,m}^{\alpha\rightarrow\beta}\right)_e = zF\left(\phi^{\beta} - \phi^{\alpha}\right) \qquad (50)$$

Supposing an Arrhenius like dependence of the rate constants on the activation energies:

$$k_f = Z_f \exp\left(\frac{-\left(\Delta G_f^{\neq}\right)_n}{RT}\right) \exp\left(\frac{-\alpha zF\left(\phi^{\beta} - \phi^{\alpha}\right)}{RT}\right) \qquad (51)$$

$$k_b = Z_b \exp\left(\frac{-\left(\Delta G_b^{\neq}\right)_n}{RT}\right) \exp\left(\frac{(1-\alpha)zF\left(\phi^{\beta} - \phi^{\alpha}\right)}{RT}\right) \qquad (52)$$

where Z_f and Z_b are similar to the pre-exponential or frequency factors of the Arrhenius equation. It should be noted[90] that Z_f and Z_b have the same dimensions as the rate constants, k_f and k_b, and hence are not equal to kT/h as sometimes erroneously stated[74,53,89,91]. Girault and Schiffrin[64] use the Eyring Transition State Theory of Diffusion to introduce a distance, d, into their pre-exponential factor, dkT/h, thus ensuring the correct dimensions. Equation (45) may now be rewritten using equations (47)-(52) to give:

$$\frac{i}{zFA} = Z_f \exp\left(\frac{-\left(\Delta G_f^{\neq}\right)_n}{RT}\right) \exp\left(\frac{-\alpha zF(\phi\beta - \phi\alpha)}{RT}\right) C_m^{\sigma,\alpha}$$

$$- Z_b \exp\left(\frac{-\left(\Delta G_b^{\neq}\right)_n}{RT}\right) \exp\left(\frac{(1-\alpha)zF(\phi\beta - \phi\alpha)}{RT}\right) C_m^{\sigma,\beta} \qquad (53)$$

The experimentally applied potential difference, E, between the phases α and β is related to $\phi^\beta - \phi^\alpha$ by a constant E_{ref}:

$$E = \phi^\beta - \phi^\alpha + E_{ref} \qquad (54)$$

$$\phi^\beta - \phi^\alpha = E - E_{ref}$$

Hence equation (53) may be rewritten to relate the measured current to the experimentally applied potential:

$$i = zFA\left[Z_f \exp\left(\frac{\left(\Delta G_f^{\neq}\right)_n}{RT}\right) \exp\left(\frac{\alpha zFE_{ref}}{RT}\right) \exp\left(\frac{-\alpha zFE}{RT}\right) C_m^{\sigma,\alpha} \right.$$

$$\left. - Z_b \exp\left(\frac{-\left(\Delta G_b^{\neq}\right)_n}{RT}\right) \exp\left(\frac{(\alpha-1)zFE_{ref}}{RT}\right) \exp\left(\frac{-\alpha zFE}{RT}\right) C_m^{\sigma,\beta} \right] \qquad (55)$$

By defining potential independent forward and reverse rate constants, k_f^o and k_b^o, as follows:

$$k_f^o = Z_f \exp\left(\frac{\alpha z F E_{ref}}{RT}\right) \exp\left(\frac{-\left(\Delta G_f^{\neq}\right)_n}{RT}\right) \quad (56)$$

$$k_b^o = Z_f \exp\left(\frac{(\alpha - 1) z F E_{ref}}{RT}\right) \exp\left(\frac{-\left(\Delta G_b^{\neq}\right)_n}{RT}\right) \quad (57)$$

The current potential characteristic (equation(55)) becomes:

$$i = zFA\left[k_f^o \exp\left(\frac{-\alpha z F E}{RT}\right) C_m^{\sigma,\alpha} - k_b^o \exp\left(\frac{(1-\alpha) z F E}{RT}\right) C_m^{\sigma,\beta}\right] \quad (58)$$

At the formal potential, $E^{o'}$ (which is equal to $\Delta_\alpha^\beta \phi^o + E_{ref}$), where $C_m^{\sigma,\alpha}=C_m^{\sigma,\beta}=C_m^{bulk}$ and no net current flows we can write from equation (58):

$$k_f^o \exp\left(\frac{-\alpha z F E^{o'}}{RT}\right) = k_b^o \exp\left(\frac{(1-\alpha) z F E^{o'}}{RT}\right) = k^o \quad (59)$$

where k^o is the standard rate constant for the reaction. At equilibrium the reactant and product electrochemical potentials are equal (i.e. $\Delta G_t=0$) hence the forward and reverse activation energies must be equal. For equilibrium at the formal potential the activation energy is denoted $\Delta \bar{G}^{o\neq}$ and k^o may be expressed as:

$$k^o = Z^o \exp\left(\frac{-\Delta \bar{G}^{o\neq}}{RT}\right) \quad (60)$$

Note that this means that $Z_f=Z_b=Z^o$.

Substitution of k^o into (58) gives the recognised form of the current-potential relationship:

$$i = zFAk^o\left[C_m^{\sigma,\alpha}\exp\left(\frac{-\alpha zF\left(E-E^{o'}\right)}{RT}\right)-C_m^{\sigma,\beta}\exp\left(\frac{(1-\alpha)zF\left(E-E^{o'}\right)}{RT}\right)\right] \qquad (61)$$

This equation describes the current which will be observed at any potential E when $E^{o'}$,k^o and the interfacial concentrations of M are known.

The most basic test for any kinetic theory is that in the limit of equilibrium it should agree with the thermodynamics. Taking equation (61) at equilibrium, i.e. at zero current, gives:

$$C_m^{\sigma,\alpha}\exp\left(\frac{-\alpha zF\left(E-E^{o'}\right)}{RT}\right)=C_m^{\sigma,\beta}\exp\left(\frac{(1-\alpha)zF\left(E-E^{o'}\right)}{RT}\right) \qquad (62)$$

$$\frac{C_m^{\sigma,\alpha}}{C_m^{\sigma,\beta}}=\frac{C_m^{b,\alpha}}{C_m^{b,\beta}}=\exp\left[\frac{(1-\alpha)zF\left(E-E^{o'}\right)}{RT}+\frac{\alpha zF\left(E-E^{o'}\right)}{RT}\right] \qquad (63)$$

$$\Rightarrow E-E^{o'}=\frac{RT}{zF}\ln\frac{C_m^{b,\alpha}}{C_m^{b,\beta}} \qquad (64)$$

This is indeed the equivalent of the Nernst equation (28).

3.2.2.2 Assisted ion transfer

In the case of assisted ion transfer (IV)

$$M^{z+}(\alpha) \quad + \quad C(\beta) \quad \langle k_b\, k_f\rangle \quad C\,M^{z+}(\beta) \qquad (IV)$$

the forward and reverse reaction rates are:

$$v_f = k_f C_m^{\sigma,\alpha} C_c^{\sigma,\beta} \qquad (65)$$

$$v_b = k_b C_{cm}^{\sigma,\beta} \qquad (66)$$

k_f in equation (65) is a second order rate constant and so experiments are usually conducted under pseudo first order conditions by using a very large concentration of $M^{z+}(\alpha)$ in relation to C (β) (or vice versa) hence the aqueous interfacial concentration of M^{z+} may be regarded as a constant and equal to the bulk concentration, C_m^{α}.

$$C_m^{\sigma,\alpha} = C_m^{\alpha} \qquad (67)$$

The derivation of the current potential characteristic then proceeds as for the ion transfer case. K_f and k_b are given by equations (51) and (52) above, but in this case Z_f is now a second order pre-exponential factor with dimensions $l^4 t^{-1} n^{-1}$.

The net current at any applied potential can be written similarly to equation (58) as:

$$i = zFA\left(k_f^o \exp\left(\frac{-\alpha zFE}{RT}\right) C_c^{\sigma,\beta} C_m^{\alpha} - k_b^o \exp\left(\frac{(1-\alpha)zFE}{RT}\right) C_{cm}^{\sigma,\beta} \right) \qquad (68)$$

where k_f^o and k_b^o are defined by equations (56) and (57) above.

Under equilibrium at the formal potential, $E^{o'}$, no net current flows and from the Nernst equation (33) for assisted ion transfer, $a_c^{\beta} a_m^{\alpha} = a_{cm}^{\beta}$

provided that all activity coefficients, γ, are unity. This means that:

$$\frac{C_m^{\alpha} C_c^{\beta}}{C^{\ominus}} = C_{cm}^{\beta} \qquad (69)$$

where $C^{\ominus}$ is the standard concentration term equal to one standard concentration unit. From equation (68) we can write, as with equation (59),

$$k_f^o \exp\left(\frac{-\alpha z F E^{o'}}{RT}\right) = k_b^o \exp\left(\frac{(1-\alpha) z F E^{o'}}{RT}\right) = k^o \qquad (70)$$

As previously the equilibrium condition means that the forward and reverse activation energies are equivalent and equal to $\Delta\bar{G}^{o\neq}$ at the formal potential, hence the pre-exponential factors Z_f and Z_b are again numerically equivalent and k^o can be expressed as in equation (60) above.

The generalised current potential characteristic for assisted ion transfer may therefore be written from equations (68) and (70)as:

$$i = zFAk^o \left[\frac{C_m^{\alpha} C_c^{\sigma,\beta}}{C^{\ominus}} \exp\left(\frac{-\alpha z F\left(E - E^{o'}\right)}{RT}\right) - C_{cm}^{\sigma,\beta} \exp\left(\frac{(1-\alpha) z F\left(E - E^{o'}\right)}{RT}\right) \right]$$

(71)

Note that $C_m^{\alpha}/C^{\ominus}$ is a constant.

At equilibrium, i.e. when the net interfacial current is zero, equation (71) collapses to the nernstian expression given in equation (33).

3.2.2.3 Electron Transfer

The forward and reverse rates, v_f and v_b, for the electron transfer reaction **(VI)** may be written:

$$v_f = k_f C_{01}^{\sigma,\alpha} C_{R2}^{\sigma,\beta} \qquad (72)$$

$$v_b = k_b C_{02}^{\sigma,\beta} C_{R1}^{\sigma,\alpha} \qquad (73)$$

The net rate of reaction expressed in terms of the net interfacial current, i, is:

$$i = nFA\left(k_f C_{01}^{\sigma,\alpha} C_{R2}^{\sigma,\beta} - k_b C_{02}^{\sigma,\beta} C_{R1}^{\sigma,\alpha}\right) \qquad (74)$$

where both k_f and k_b are second order rate constants which are commonly written in an Arrhenius form as for the ion transfer equations (51) and (52). For electron transfer both pre-exponential factors, Z_f and Z_b, are now second order.

The forward and reverse rate constants may again be expressed in terms of the standard rate constant at the formal potential, $E^{O'}$, where the net current is zero and $C_{01}^{\sigma,\alpha} C_{R2}^{\sigma,\beta} = C_{02}^{\sigma,\beta} C_{R1}^{\sigma,\alpha}$, thus the generalised current potential equation for electron transfer becomes:

$$i = nFAk^{o}\left[C_{01}^{\sigma,\alpha} C_{R2}^{\sigma,\beta} \exp\left(\frac{-\alpha nF\left(E-E^{o'}\right)}{RT}\right) - C_{02}^{\sigma,\beta} C_{R1}^{\sigma,\alpha} \exp\left(\frac{(1-\alpha)nF\left(E-E^{o'}\right)}{RT}\right)\right] \qquad (75)$$

The above kinetic treatment is a direct transposition of the Butler Volmer treatment of the metal/electrolyte redox to liquid/liquid charge transfer reactions.

Implicit in the above derivation was the assumption that the whole of the interfacial potential difference is dropped between the loci of product and reactant. This assumption is not crucial to the derivation and corrections for double layer effects are discussed elsewhere[74,89].

Two assumptions which are fundamental to the derivation are (i) that $\left(\Delta G_f^{\neq}\right)_n$ and $\left(\Delta G_b^{\neq}\right)_n$ are potential independent and (ii) that $\left(\Delta G_f^{\neq}\right)_e$ and $\left(\Delta G_b^{\neq}\right)_e$ are constant fractions of $\left(\Delta G_t\right)_e$. Assumption (i) will hold on condition that the actual location of the activated complex does not vary with potential. Assumption (ii) is integral to the treatment and its validity has been disputed by Van Rysselberghe[92].

Attempts have been made to formulate the charge transfer kinetics in other ways and each approach results in equations which are formally equivalent to those above. However differences do arise in the interpretation of the preexponential factor and of the transfer coefficient, α.

3.2.2.4 Pre-exponential Factors and Transfer Coefficients

In the present model, where use has been made of activated complex theory, the pre-exponential factor may be obtained by a thermodynamical formulation of the kinetics[93,94,95]. If we initially consider only the forward reaction and assume that the activated complex is in equilibrium with the reactants then the rate can be expressed as the concentration of the activated complex, $A^{\neq}$, times a frequency, ν:

$$\text{rate} = \nu \left[A^{\neq}\right] \qquad (76)$$

The normal rate equation for the forward reaction is written:

$$\text{rate} = k_f \text{ [reactants]} \qquad (77)$$

then the forward rate constant is given by:

$$k_f = \frac{\nu \left[A^{\neq}\right]}{\text{[reactants]}} = \nu K^{\neq} \qquad (78)$$

where $K^{\neq}$ is the equilibrium constant for the reaction of reactants to activated complex. The term ν is identified as the frequency of the very loose vibration in the activated complex which will lead to dissociation of the complex into products. As this vibration is loose its frequency is rather low and the vibrational partition function corresponding to it may be expressed as $kT/h\nu$. This partition function may be taken out of the equilibrium constant $K^{\neq}$ leaving a new function $K^{\neq}$ so that equation (78) may be rewritten:

$$k_f = \nu \frac{kT}{h\nu} K^{\neq} \qquad (79)$$

The unknown frequency ν then cancels out, however the thermodynamic function $K^{\neq}$ is left ill defined and although it is generally identified with $\exp(-\Delta G_f^{\neq}/RT)$ this identification cannot be rigourously justified[95]. The pre-exponential factor is effectively guessed as being of the order of kT/h.

As seen in equations (60), (70) and (75), under equilibrium conditions at the formal potential the forward and reverse pre-exponential factors are equivalent and indeed when this factor is identified with the vibrational frequency of the activated complex this is not surprising. However the difficulty with this formulation of the reverse rate of reaction is that the exponential expression for the ratio of concentration of activated complex to products necessitates that the product and activated complex are in thermal equilibrium. If this equilibrium condition applies simultaneously to both forward and reverse reactions then it might appear that the overall reaction must be at equilibrium and hence no net current would flow and no reaction rates would be measured. This difficulty is overcome by considering the activated complexes arising from the reactants and those arising from the products as distinguishable and in equilibrium with their respective precursors. To allow for the eventuality that not every vibration of an activated complex carries it through to product or reactant respectively a transmission coefficient, κ, may be introduced. At equilibrium this will be the same for the forward and reverse reaction, however away from equilibrium it may differ for the two cases and hence the pre-exponential factors are not necessarily equal or constant away from equilibrium.

A distance of some sort must now be introduced to give the correct dimensions for an electrochemical rate constant and this is generally taken to be the distance through which the ion, or electron must travel in crossing the interface. This may either be associated with the compact inner layer of Gavach et al[85] or, less obviously, with the mixed solvent layer of Girault and Schiffrin[87].

The problem of needing to introduce a distance into the pre-exponential factor in order to obtain the correct dimensions comes from the use of volume concentrations for the kinetic description of what is essentially an interfacial reaction. If the concentrations in the rate equations were expressed as surface concentrations the pre-exponential factor would have the normal dimensions of frequency in the unispecies case and an illspecified distance would not have to be included. The use of surface concentrations will be considered briefly in section **3.3.2.**

The charge transfer coefficient, α, may be taken as representing the proportion of the total applied potential difference which is effective at the activated state, i.e. if the potential at the locus of the activated state is ϕ^* then α is given by:

$$\alpha = \frac{\phi^* - \phi^\alpha}{\phi^\beta - \phi^\alpha} \qquad (80)$$

By analogy with equations (49) and (50) the electrical part of the Gibbs energy of activation is given by:

$$\left(\Delta G_f^{\neq}\right)_e = zF(\phi^* - \phi^\alpha) \qquad (81)$$

$$\left(\Delta G_b^{\neq}\right)_e = zF(\phi^* - \phi^\beta) \qquad (82)$$

Substitution of either equation (81) or (82) into equation (47) or (48) respectively results in equation (80) above. If the form of the potential profile across the interface is known accurately enough then α may be used to identify the location of the activated complex at the interface.

Melroy and Buck[91], when considering ion transfer, use what they term a "quasi-thermodynamic analysis of interfacial rate constants". This consists of an adaptation of the absolute rate theory approach to electrode kinetics presented by Parsons[96] and later Delahay[89] to the liquid/liquid interface. They use the standard result of $\kappa kT/h$ for the pre-exponential factor. The rate equations are initially formulated in terms of ion activities rather than concentrations and hence the expressions given for current density must be multiplied by a standard surface concentration term to give the correct dimensions. Melroy and Buck mention the possibility of using surface activities but conclude that for small currents and well stirred solutions it is satisfactory to use bulk values.

Samec[62] first formulated kinetic expressions for ion and electron transfer based on the quantum theory of charge transfer reactions in polar media. For the ion transfer case he expressed the pre-exponential factor as $B^* d$ where d is inprecisely defined as the linear dimension of the ion and B^* is described as involving the parameters of the quantum subsystem. In the case of electron transfer the bimolecular nature of the reaction requires the introduction of a further parameter, V_m, which is a small volume of molecular dimensions close to the phase boundary. In this treatment Samec refers to α as the formal charge transfer coefficient and it is said to have no physical significance however the true charge transfer coefficient, α_t, which is closely related to α, characterises the change in activation

energy of the classical subsystem with change in ΔJ^* (the difference in the ground state energies of the initial and final states of the whole system). ΔJ^* is then equated to the difference in the electrochemical free energies of the system at the planes of closest approach and the treatment becomes effectively equivalent to that used here.

More recently Gurevich and Kharkats, Samec and others[97,48,63] have suggested a stochastic method for the treatment of ion transfer. Stochastic theories are essentially more refined collision theories, hence the pre-exponential factor is a function of the collision frequency $(kT/2\pi m)^{1/2}$, the frequency of ion vibration at the potential energy maximum and a friction coefficient estimated at kT/D^W. The pre-exponential factors thus calculated[48] were noted to be significantly smaller (10-5 times) than those calculated from transition type methods. Reference is again made to a true charge transfer coefficient, α_t, which is found to be approximately equal to the ratio $(x^* - x_2^W)d^{-1}$ where x^* is the ion coordinate at the potential energy maximum, x_2^W is the position of the aqueous outer Helmholtz plane and d is the total distance between the two outer Helmholtz planes.

3.3 MASS TRANSPORT

3.3.1 Background

Three modes of mass transfer occur in electrolyte solutions: convection, migration and diffusion. Convection may occur both naturally, due to thermal fluctuations causing density gradients in solution, and through forcing, such as stirring of the electrolyte solution and rotation of electrodes. Here we consider situations in which only natural convection

occurs. For environments controlled at a uniform temperature such as those encountered experimentally it is quite satisfactory to neglect natural convective mass transport as it generally occurs only in the bulk of the solution and does not effect the area close the electrode or interface which we are concerned with.

If there is a gradient of electrochemical potential of a species in a solution, a flux of that species will occur in order to alleviate the gradient. The flux is proportional to the gradient causing it. A gradient in electrochemical potential may arise due to an electric field, leading to a migration flux, or due to a concentration, or activity, gradient, leading to a diffusional flux. At any time the total current density, i, passing in the bulk of the solution is made up of diffusion, i_d, and migration, i_m, contributions from all species, j, present. i.e.:

$$i = \sum_j i_{d,j} + i_{m,j} \qquad (83)$$

The relative contributions of diffusion and migration to the flux of a species, and of the flux of a particular species to the total flux differ at different locations in the solution. In the bulk of the solution distant from the interface concentration gradients are generally small and the vast proportion of the current is due to migration to which all charged species will contribute. This means that if an excess of supporting electrolyte is added (i.e. a high concentration of non electroactive ions) then the migration component of the current is essentially carried entirely by non electroactive species[74]. Conversely, near to and across the interface itself the electroactive species carries most of the current. Hence it is frequently sufficient to disregard migration and consider only the diffusional mass transport near the interface. This greatly simplifies the mathematical

analysis. A supporting electrolyte concentration ten times that of the electroactive species is usually sufficient for this purpose.

3.3.2 Diffusion

Fick's laws describe the flux, J, of a substance, M, and its concentration as functions of time, t, and position, x. The flux of M is the number of moles of M passing a given location x per unit time, per unit area. Fick's first law states that the flux of M in the x direction is proportional to the concentration gradient in that direction, $\frac{\partial C_m(x,t)}{\partial x}$:

$$-J_m(x,t) = D_m \frac{\partial C_m(x,t)}{\partial x} \qquad (84)$$

This equation may be derived from a microscopic model[74] where the location x is considered which has N_m (x) molecules of M to its left and N_m (x+Δx) molecules to its right at time t. During the time increment Δt the molecules move by a random walk process so that half of each set of molecules move Δx to the right and half move Δx to the left. Thus the net flux through an area A at x is the difference in the number of molecules moving from left to right ($N_m(x)/2$) and those moving from right to left ($N_m(x+\Delta x)/2$), i.e.:

$$J_m(x,t) = \frac{1}{A}\left[\frac{N_m(x)}{2} - \frac{N_m(x+\Delta x)}{2}\right] \Big/ \Delta t \qquad (85)$$

Multiplying through by $\Delta x^2/\Delta x^2$ and substituting the concentration, C_m, for $N_m/A\Delta x$ gives:

$$-J_m(x,t) = \frac{\Delta x^2}{2\Delta t} \frac{C_m(x+\Delta x) - C_m(x)}{\Delta x} \qquad (86)$$

By equating $\Delta x^2/2\Delta t$ with the diffusion coefficient, D_m, and allowing Δx and Δt to tend to zero, gives Fick's first law as expressed in equation (84). Δx may be considered as the mean free path of the molecule , λ, and $\Delta x/\Delta t$ as the mean speed, $\bar{c}$. Taking into account the probability that one molecule may collide with another before passing through the area, A, as not all molecules will be travelling normal to the area[94], equation (86) needs to be multiplied by a factor of 2/3 and hence the diffusion coefficient is given by:

$$D_m = \frac{1}{3}\lambda \bar{c} \qquad (87)$$

Fick's second law is derived from the first law. The change in concentration with time at a point x is given by the difference in the fluxes into and out of an element of width dx:

$$\frac{\partial C_m(x,t)}{\partial t} = \frac{J_m(x,t) - J_m(x + dx,t)}{dx} \qquad (88)$$

The flux at x + dx is given by:

$$J_m(x + \Delta x,t) = J_m(x,t) + \frac{\partial J_m(x,t)}{\partial x} dx \qquad (89)$$

The partial derivative of J with x is obtained from Fick's first law and is:

$$-\frac{\partial J_m(x,t)}{\partial x} = \frac{\partial}{\partial x}\left(D_m \frac{\partial C_m(x,t)}{\partial x}\right) \qquad (90)$$

Substituting equations (89) and (90) into (88) and assuming that D_m is independent of x gives Fick's second law:

$$\frac{\partial C_m(x,t)}{\partial t} = D_m \frac{\partial^2 C_m(x,t)}{\partial x^2} \qquad (91)$$

Equation (91) applies specifically to a linear geometry, the general formulation for any geometry is:

$$\frac{\partial C_m}{\partial t} = D_m \nabla^2 C_m \qquad (92)$$

where ∇^2 is the Laplacian operator. This second order differential may be solved for different experimental circumstances, given appropriate boundary conditions, to give concentration profiles through the solution close to the interface. Similarly Fick's first law may be solved and the flux at the electrode surface equated to the current density (cf equation (45)).

During an electrochemical experiment both Fick's laws and the charge transfer kinetics equations must be obeyed at all times, however which of these processes will be rate limiting depends on the individual reaction and the prevailing experimental conditions. The solution of the diffusion equations and the conditions under which reactions are diffusion controlled or controlled by the electrode kinetics is discussed in the Methodology chapter. Here the idea that the electrode processes are better to be considered using surface concentrations is developed briefly by recasting Fick's laws in these terms.

Equation (84) may be written in terms of the surface concentration, Γ, and a speed, v, as follows:

$$-J_m(x,t) = -v_m \frac{\partial \Gamma_m(x,t)}{\partial x} \qquad (93)$$

where v has dimensions of $l\ t^{-1}$ and is dx/dt, or the mean speed, $\bar{c}$. The derivation of the rate of change of Γ with time leads to the expression:

$$\frac{\partial \Gamma_m(x,t)}{\partial t} = v \frac{\partial^2 \Gamma_m(x,t)}{\partial x^2} dx \qquad (94)$$

if

$$D_m = v\, dx \qquad (95)$$

then Fick's second law becomes:

$$\frac{\partial \Gamma_m(x,t)}{\partial t} = D_m \frac{\partial^2 \Gamma_m}{\partial x^2} \qquad (96)$$

The relation between surface concentration is derived from the geometry of the cube:

$$\Gamma_m = \left[\frac{C_m^2}{N}\right]^{1/3} \qquad (97)$$

Where N is Avogadro's number. Differentiation of (97) with respect to x leads to:

$$\frac{\partial \Gamma_m}{\partial x} = \frac{2}{3} \left[N C_m\right]^{-1/3} \frac{\partial C_m}{\partial x} \qquad (98)$$

combining this expression with equations (84) and (93) above gives an expression for v in terms of D_m:

$$v_m = \frac{3}{2} \left[C_m N\right]^{1/3} \qquad (99)$$

Hence the value of dx in equation (95) is given by:

$$dx = \frac{2}{3} \left[C_m N\right]^{-1/3} \qquad (100)$$

METHODOLOGY

4.1 BACKGROUND

All the classical methodology developed for the study of the metal/electrolyte interface may be used at the ITIES. The many techniques devised are variations on the same basic theme of measuring the current response of a system to an electrical potential perturbation, or vice versa. The differences between methods derive from: (i) differences in the frequency and waveform of the electrical stimulus applied; (ii) differences in mass transport arising from different cell designs and mechanically agitated solutions and (iii) differences in the mathematical manipulation of the experimental data.

The wide variety of techniques developed has arisen from the variety of requirements of the experimenter. Some techniques are particularly suited to quantitative analytical work and others are useful in more fundamental investigations into electrochemical processes.

In every study of charge transfer reactions at the electrified interface there are two major practical problems to be overcome :

1) Compensation or correction for the electrical potential required to drive the current through the resistance of the electrolytes and electrodes, rather than that required to drive the reaction.

2) The separation of effects arising from the charge and discharge of the electrical double layer from those due to the charge transfer under investigation.

As the charging of the electrical double layer is a rather fast process versus charge transfer, the latter problem may be solved by using a relatively long experimental time scale although for very fast charge transfer reactions this difference in time scale may not be adequate. The former problem of resistance is tackled by the use of reference electrodes, as mentioned in chapter 2, and by the use of concentrated supporting electrolyte. The low dielectric constant of organic solvents does however limit the solubility of

electrolytes substantially and furthermore supporting electrolytes may not necessarily be inert, for example Samec et al.[35] found that Cs^+ transfer is assisted by TPB^-.

The primary technique used in the present work was cyclic voltammetry which is discussed in detail below for the electron transfer case, a less general treatment of which has been produced previously[98]. Some of the other procedures which have been used at the ITIES are also outlined briefly for comparison.

4.2 CYCLIC VOLTAMMETRY

During cyclic voltammetry a system is initially held at an electrical potential, ϕ_i or E_i, this potential is then varied linearly with time at a rate ν until a potential ϕ_λ or $E\lambda$ is reached. The direction of the potential scan is then reversed and the potential returned to ϕ_i or E_i, normally at the same rate, ν. At a large planar interface (i.e. >100 μm diameter) diffusion is essentially linear and the mass transport equations to be solved are Fick's laws for the linear case as given in equations (84) and (91) above.

4.2.1 Ion Transfer

The process of ion transfer at the ITIES (III) is formally identical to the electron transfer at the metal/electrolyte interface (II) and hence the theory derived for cyclic voltammetry at the metal/electrolyte interface may be used without modification.

The solution of the diffusion equations for cyclic voltammetry under reversible conditions was first considered by Randles[99] and Ševčik[100]. Reversible conditions means a charge transfer that is rapid enough for the concentrations of species O and R (or $M^z{}_\alpha$ and $M^z{}_\beta$) at the interface to adjust immediately to the ratio dictated by the Nernst equation. Nicholson and Shain[101] later considered the quasi-reversible case (reaction rate controlled by the charge transfer kinetics) together with the reversible and other cases and the results of their analysis are used in the discussion

of the results for ion transfer at a large interface. It need only be noted here that the boundary conditions used in the solution of the diffusion equations require that the initial concentration of M^z in the β phase is zero and that the volume of the cell versus the interfacial area is sufficiently large that constant bulk concentrations are maintained distant from the interface (in the case of M^z in the β phase this is zero).

4.2.2 Assisted ion Transfer

Homolka et al[40] have presented the theory for single scan cyclic voltammetry of assisted ion transfer under reversible conditions. They considered only the case where the bulk concentration of the metal cation in the aqueous phase is much greater than that of the ligand in the organic phase and therefore assumed that the reaction is controlled only by the diffusion of the ligand. Their results showed that the potential separation of the forward and reverse current peaks, ΔE_p, was dependent on the stoichiometry of the reaction. The 1:1, metal to ligand, stoichiometry gave the classical, Nicholson and Shain, 59/z mV separation, where z is the charge number of the transferring ion. When 2 or 3 ligands complexed with each ion the peak separations were 87/z mV and 112/z mV respectively. For the 1:1 complex the midpeak potential was independent of concentration, however for the 1:2 and 1:3 complexes the midpeak potentials varied linearly with the logarithm of the ligand concentration.

Given a 1:1 complexation reaction under reversible conditions the voltammetric behaviour is therefore expected to be the classical behaviour as with the simple ion transfer. This prediction could easily have been foreseen as the assumption that the diffusion of the more highly concentrated metal cation may be neglected makes the assisted ion transfer reaction **(IV)** formally equivalent to the ion transfer and redox reactions, **(III)** and **(II)**.

The detailed theory for the kinetic case has not been considered in the literature and the present procedure is to assume the validity of ignoring the diffusion of either the metal or ligand, whichever is in vast excess, and to make the kinetic analysis as for a simple ion transfer or redox reaction[41]. The results from the electron transfer diffusion problem given

below suggest that a concentration ratio of >50 will ensure pseudo first order conditions.

4.2.3 Electron Transfer

Electron transfer at the ITIES is a second order reaction involving the encounter of a redox species from each phase and therefore the diffusion of the redox couples in both phases must be considered.

4.2.3.1 The Reversible Case

The solution of the diffusion equations under reversible conditions taking into account the diffusion of all species in reaction **(VI)** was considered in the course of the present work (also Appendix) by extending the approach of Nicholson and Shain as follows.

Fick's second law for all species gives equations (101) - (104):

$$\frac{\partial C^{\alpha}_{O1}(x,t)}{\partial t} = D^{\alpha}_{O1} \frac{\partial^2 C^{\alpha}_{O1}(x,t)}{\partial x^2} \qquad \textbf{(101)}$$

$$\frac{\partial C^{\alpha}_{R1}(x,t)}{\partial t} = D^{\alpha}_{R1} \frac{\partial^2 C^{\alpha}_{R1}(x,t)}{\partial x^2} \qquad \textbf{(102)}$$

$$\frac{\partial C^{\beta}_{O2}(x,t)}{\partial t} = D^{\beta}_{O2} \frac{\partial^2 C^{\beta}_{O2}(x,t)}{\partial x^2} \qquad \textbf{(103)}$$

$$\frac{\partial C^{\beta}_{R2}(x,t)}{\partial t} = D^{\beta}_{R2} \frac{\partial^2 C^{\beta}_{R2}(x,t)}{\partial x^2} \qquad (104)$$

The initial and semi-infinite boundary conditions which apply are:

$$C^{\alpha}_{O1}(x,0) = C^{b,\alpha}_{O1} \quad , \quad C^{\alpha}_{R1}(x,0) = C^{b,\alpha}_{R1} \qquad (105)$$

$$C^{\beta}_{O2}(x,0) = C^{b,\beta}_{O2} \quad , \quad C^{\beta}_{R2}(x,0) = C^{b,\beta}_{R2} \qquad (106)$$

$$\lim_{x\to\infty} C^{\alpha}_{O1}(x,t) = C^{b,\alpha}_{O1} \quad , \quad \lim_{x\to\infty} C^{\alpha}_{R1}(x,t) = C^{b,\alpha}_{R1} \qquad (107)$$

$$\lim_{x\to\infty} C^{\beta}_{O2}(x,t) = C^{b,\beta}_{O2} \quad , \quad \lim_{x\to\infty} C^{\beta}_{R2}(x,t) = C^{b,\beta}_{R2} \qquad (108)$$

Application of the Laplace transform to equations (101) - (104) and insertion of the boundary conditions yields expressions for the Laplace transforms of the concentrations of each species, i, in the form:

$$\bar{C}_i(x,s) = \frac{C^{b}_{i}}{s} + A_i(s) \exp\left[-x\sqrt{\frac{s}{D_i}}\right] \qquad (109)$$

Fick's first law gives the flux of each species at the interface in terms of the concentration gradients and given that the fluxes of oxidised and reduced species must balance, equation(110), they may be used as boundary conditions to determine the constants $A_i(s)$. Equation (109) may thus be solved to give the concentration of each species at the interface (x=0) as a function of time (Equations 111-114).

$$\bar{i}(s) = nFAD_{O1}^{\alpha}\left[\frac{\partial \bar{C}_{O1}^{\alpha}}{\partial x}\right]_{x=0} = -nFAD_{R1}^{\alpha}\left[\frac{\partial \bar{C}_{R1}^{\alpha}}{\partial x}\right]_{x=0}$$

$$= nFAD_{R2}^{\beta}\left[\frac{\partial \bar{C}_{R2}^{\beta}}{\partial x}\right]_{x=0} = -nFAD_{O2}^{\beta}\left[\frac{\partial \bar{C}_{O2}^{\beta}}{\partial x}\right]_{x=0} \quad (110)$$

$$C_{O1}^{\alpha}(0,t) = C_{O1}^{b,\alpha} - \frac{I(t)}{\sqrt{D_{O1}^{\alpha}}} \quad (111)$$

$$C_{R1}^{\alpha}(0,t) = C_{R1}^{b,\alpha} + \frac{I(t)}{\sqrt{D_{R1}^{\alpha}}} \quad (112)$$

$$C_{O2}^{\beta}(0,t) = C_{O2}^{b,\beta} + \frac{I(t)}{\sqrt{D_{O2}^{\beta}}} \quad (113)$$

$$C_{R2}^{\beta}(0,t) = C_{R2}^{b,\beta} - \frac{I(t)}{\sqrt{D_{R2}^{\beta}}} \quad (114)$$

Where I(t) is the convoluted current defined as:

$$I(t) = \frac{1}{\sqrt{\pi}} \int_0^t \frac{f(\tau)}{\sqrt{t-\tau}}\, d\tau \quad (115)$$

$$f(\tau) = \frac{i(\tau)}{nFA} \quad (116)$$

The further condition that the Nernst equation is obeyed at the interface at all potentials is utilised to obtain an expression for the convoluted current in terms of the potential, the concentrations and the diffusion coefficients of all species. By defining the following parameters:

$$\theta = \exp\left[\frac{nF}{RT}\left(\Delta_{\alpha}^{\beta}\phi_i - \Delta_{\alpha}^{\beta}\phi^{o'}\right)\right] \qquad (117)$$

$$\sigma = \frac{nFv}{RT} \qquad (118)$$

$$S(t) = \begin{cases} \exp(-\sigma t) & \text{for } t < \lambda \\ \exp(\sigma t - 2\sigma\lambda) & \text{for } t \geq \lambda \end{cases} \qquad (119)$$

the Nernst equation (41) may be rewritten in the form of equation (120)

$$\theta S(t) = \frac{C_{O1}^{\alpha} C_{R2}^{\beta}}{C_{R1}^{\alpha} C_{O2}^{\beta}} \qquad (120)$$

where the concentrations are at x=0 and all activity coefficients are assumed to be unity.

Substitution of equations (111) - (114) into equation (120) gives the quadratic equation (121) for the convoluted current.

$$AI(t)^2 + BI(t) + C = 0 \qquad (121)$$

The constants A, B and C are defined as:

$$A = \frac{\theta S(t)}{\sqrt{D_R^{\alpha} D_O^{\beta}}} - \frac{1}{\sqrt{D_O^{\alpha} D_R^{\beta}}} \qquad (122)$$

$$B = \theta S(t)\left[\frac{C_R^{b,\alpha}}{\sqrt{D_O^{\beta}}} + \frac{C_O^{b,\beta}}{\sqrt{D_R^{\alpha}}}\right] + \frac{C_O^{b,\alpha}}{\sqrt{D_R^{\beta}}} + \frac{C_R^{b,\beta}}{\sqrt{D_O^{\alpha}}} \qquad (123)$$

$$C = C_R^{b,\alpha} C_O^{b,\beta} \theta S(t) - C_O^{b,\alpha} C_R^{b,\beta} \qquad (124)$$

Obviously equation (121) has two roots, one of which is the convoluted current. The choice between the two roots stems from the fact that the convoluted current is a continuous function of time and therefore the correct solution reads:

$$I(t) = \frac{-B + \sqrt{B^2 - 4AC}}{2A} \qquad (125)$$

The continuity of I(t) is ensured at A=0 by taking I(t) equal to $-C/B$

In order to integrate equation (121) in the general case the following dimensionless constants for the bulk concentrations and diffusion coefficients are introduced:

$$\alpha = \frac{C_O^{b,\alpha}}{C^{\alpha}} \qquad (126)$$

where C^{α} is the total concentration of redox couple 1 in phase α, given by:

$$C^{\alpha} = C_O^{b,\alpha} + C_R^{b,\alpha} \qquad (127)$$

and

$$\beta = \frac{C_O^{b,\beta}}{\kappa C^{\alpha}} \tag{128}$$

where κ represents the ratio of the total concentrations of the redox couples 1 and 2:

$$\kappa = \frac{C_O^{b,\beta} + C_R^{b,\beta}}{C^{\alpha}} = \frac{C^{\beta}}{C^{\alpha}} \tag{129}$$

$$\xi^{\alpha} = \sqrt{\frac{D_O^{\alpha}}{D_R^{\alpha}}} \tag{130}$$

$$\xi^{\beta} = \sqrt{\frac{D_O^{\beta}}{D_R^{\beta}}} \tag{131}$$

and finally

$$\zeta = \sqrt{\frac{D_O^{\alpha}}{D_O^{\beta}}} \tag{132}$$

These dimensionless coefficients are substituted into equations (122)-(124) to give the convoluted current equation (121) in terms of dimensionless parameters, the convoluted current is then seen to be proportional to $C^{\alpha}\sqrt{D_{O1}^{\alpha}}$.

Equation (121) may then be integrated using Nicholson and Shain's[101] numerical method based on the integration by parts of equation (115). This integration by parts produces a dimensionless current parameter, $\chi(\sigma t)$, which is related to the current by:

$$i(t) = nFA\sqrt{\pi D_O^{\alpha}\sigma}\ C^{\alpha}\chi(\sigma t) \qquad (133)$$

This equation shows that the normal dependence of the current on the square root of sweep rate is still applicable.

The values of $\chi(\sigma t)$ have been calculated as a function of the parameters α, β and κ. The results of the integration are given in tables 1 and 2 which give the values of the forward dimensionless peak current, $\chi(\sigma t)_{f,p}$, the peak potentials and the midpeak potential for a range of κ values. For simplicity all the results presented assume the equality of the diffusion coefficients of all species.

Table 1 refers to case 1 with zero initial concentration of products (i.e. the situation normally assumed in classical cyclic voltammetry), so that α=1 and β=0. In this case κ is equivalent to the ratio of concentrations of the reactants: $C_{O1}^{b,\alpha}/C_{R2}^{b,\beta}$, and equation (133) now reads

$$i(t) = nFA\sqrt{\pi D_O^{\alpha}\sigma}\ C_O^{b,\alpha}\chi(\sigma t) \qquad (134)$$

For case 1 and when the concentration of reactants in phases α and β is equal (i.e. κ=1), it is seen that the midpeak potential, $E_{1/2} = \Delta_{\alpha}^{\beta}\phi_{1/2} - \Delta_{\alpha}^{\beta}\phi^{o'}$,

Table 1

κ	$E_{p,f}$/mV	$E_{p,b}$/mV	ΔE_p/mV	$E_{1/2}$/mV	$\chi(\sigma t)_{f,p}$	$\chi(\sigma t)_{f,p}/\kappa$
0.01	88.3	172.4	84.1	130.4	0.00217	0.217
0.05	46.0	131.5	85.5	88.8	0.0108	0.216
0.1	27.2	113.8	86.6	70.5	0.0215	0.215
0.5	–26.5	71.7	98.2	22.6	0.103	0.206
1.0	–57.0	58.8	115.8	0.9	0.178	0.178
2.0	–27.0	72.2	99.2	22.6	0.206	
10.0	26.5	114.3	87.8	70.4	0.215	
20.0	45.7	132.3	86.6	89.0	0.216	
100.0	87.9	173.7	85.5	130.8	0.217	

Dimensionless current function $\chi(\sigma t)$ and other cyclic voltammogram characteristics for Case 1 ($\alpha = 1$, $\beta = 0$). $E = \Delta_\alpha^\beta\phi - \Delta_\alpha^\beta\phi^{o\prime}$, scanning from E = +500 mV to –500 mV, step increment 0.3 mV.

Table 2

κ	$E_{p,f}$/mV	$E_{p,b}$/mV	ΔE_p/mV	$E_{1/2}$/mV	$\chi(\sigma t)_{f,p}$	$\chi(\sigma t)_{f,p}/\kappa$
0.01	–29.5	29.0	58.5	–0.3	0.00251	0.251
0.05	–33.4	28.3	61.7	–2.6	0.0123	0.246
0.1	–37.8	27.5	65.3	–5.2	0.0241	0.241
0.5	–70.1	27.5	97.6	–21.3	0.0955	0.191
1.0	–41.3	42.1	83.4	0.4	0.111	0.111
2.0	–15.9	59.3	75.2	21.7	0.115	
10.0	30.1	101.0	70.9	65.6	0.118	
20.0	48.6	119.7	71.1	84.2	0.118	
100.0	90.4	161.6	71.2	126.0	0.118	

Dimensionless current function $\chi(\sigma t)$ and other cyclic voltammogram characteristics for Case 2 ($\alpha = 0.5$, $\beta = 0$). $E = \Delta_\alpha^\beta\phi - \Delta_\alpha^\beta\phi^{o\prime}$, scanning from E = +500 mV to –500 mV, step increment 0.3 mV.

is equal to the formal potential and that the peak separation, ΔE_p, is 116 mV. This case is equivalent to the classical reversible redox case, but with n = 1/2. Because the concentration profiles of the reactants in adjacent phases are symmetrical, as are those of the products, the concentration ratio in the Nernst equation (41) may in fact be written as $(C^{\alpha}_{O1}/C^{\alpha}_{R1})^2$.

The dependence of the current on the square root of sweep rate is illustrated in figure 11.

When the concentration of the reduced species in phase β exceeds that of the oxidised species in phase α (i.e. κ>1), the midpeak potential shifts towards values as high as 131 mV positive of the formal potential. At the same time the peak separation decreases and the peak dimensionless current approaches a limiting value of 0.217. This variation of $\chi(\sigma t)$ with κ is illustrated in figure 12.

When, by contrast, the concentration of the oxidised species in phase α exceeds that of the reduced species in phase β (i.e. κ<1), the dimensionless current $\chi(\sigma t)$ is governed by the lower concentration, $C^{b,\beta}_{R2}$. As would obviously be expected, the normalised current $\chi(\sigma t)/\kappa$ behaves as for the situation with κ>1 described above.

Table 2 shows the results for case 2 where the α phase contains an equimolar concentration of electron donor and acceptor, i.e. α=0.5. As in table 1, β=0 and κ takes a range of values. It is seen in table 2 that when the equimolar redox in phase α is in large excess relative to the reduced species in phase β (κ<<1) the system is controlled only by the diffusion of the latter reactant. Thus the behaviour approaches that of a simple reversible system, i.e. ΔE_p = 59 mV, $E_{1/2}$=0 and $\chi(\sigma t)/\kappa$=0.251. Under these conditions phase α is equivalent to a metallic phase, able to donate or accept electrons on demand. As κ is increased the peak separation augments, passing through a maximum value around κ=0.5. The position

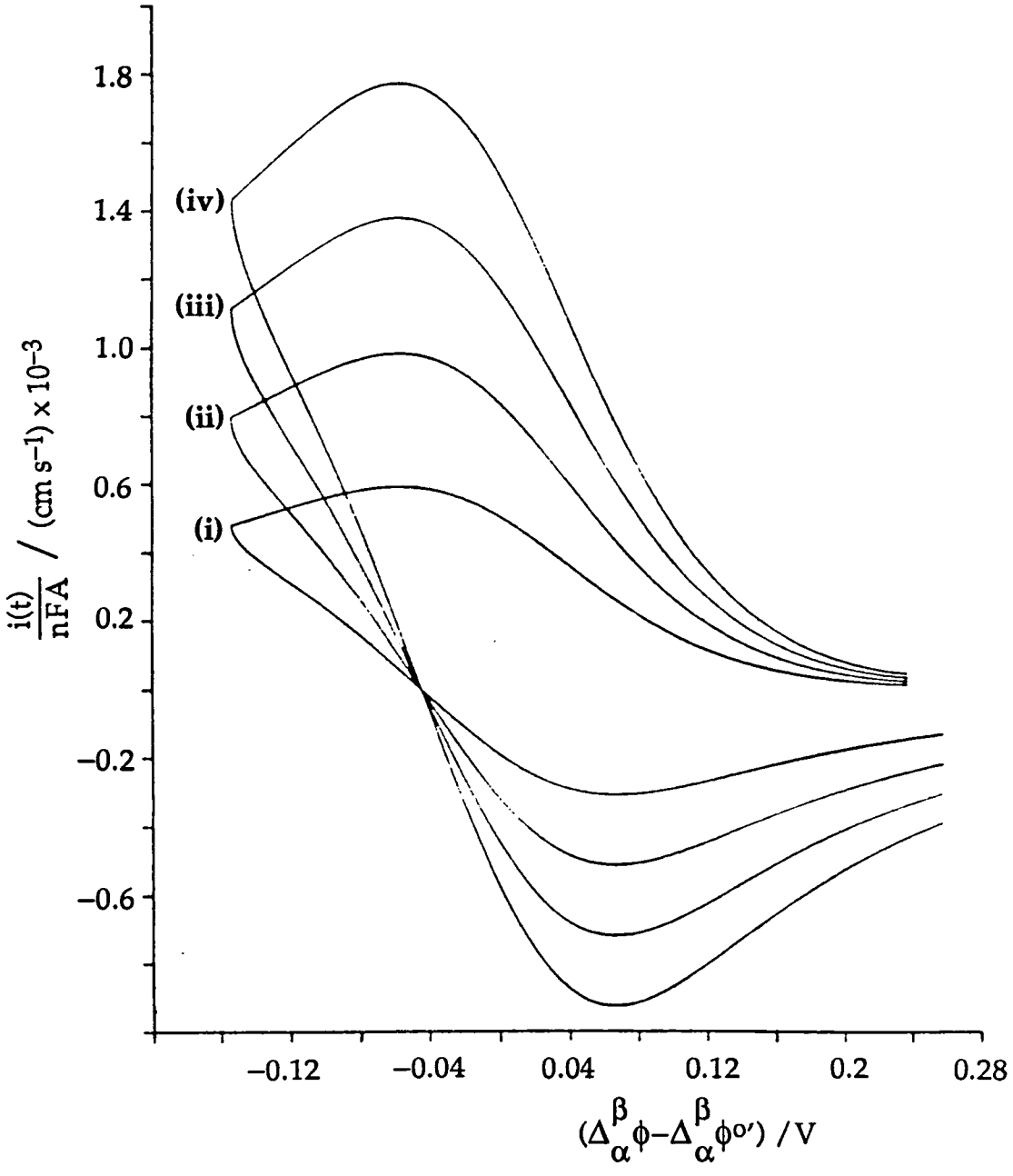

Fig. 11 Cyclic voltammograms for $\alpha = 1$, $\beta = 0$ and $\kappa = 1$ at various sweep rates: (i) 9, (ii) 25, (iii) 49, and (iv) 81 mV s^{-1}.

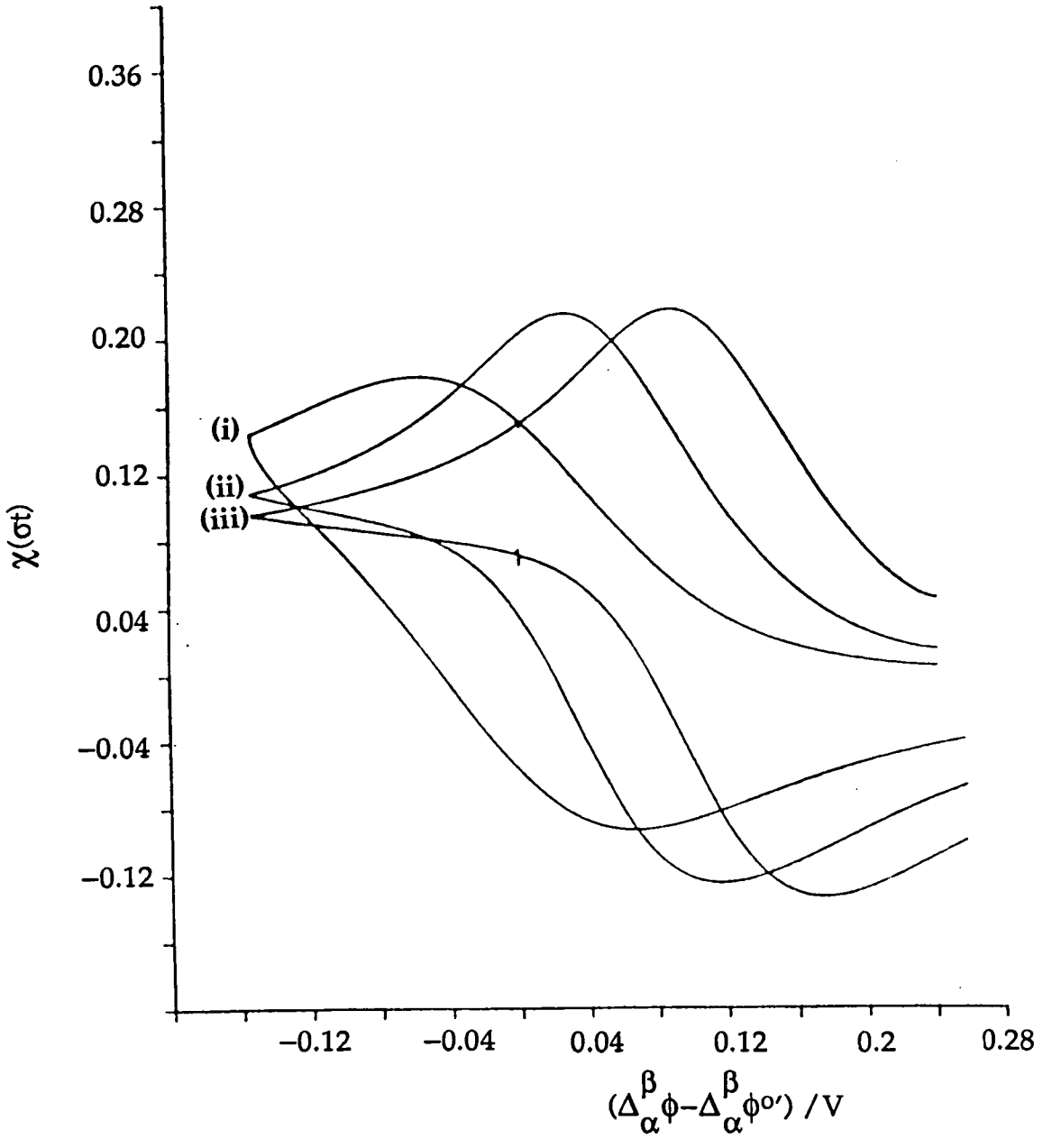

Fig. 12 Cyclic voltammograms for $\alpha = 1$, $\beta = 0$, with various κ values: (i) 1, (ii) 10, (iii) 100.

of the midpeak potential first of all shifts negative with respect to the formal potential and then moves positive versus the formal potential for values of $\kappa>1$. At $\kappa=1$ the formal and midpeak potentials are coincident, but the peak separation is 83 mV. Figure 13 displays cyclic voltammograms of the normalised current, $\chi(\sigma t)/\kappa$, for case 2 with various values of κ.

The results of the integration described above show that pseudo first order conditions leading to the classical criteria for a reversible single electron transfer (ΔE_p=59mV and $E_{1/2}=E^{O'}$) only apply when both oxidised and reduced forms of the excess redox species are present in excess. The necessary concentration ratio of species in β to species in α for first order conditions to prevail was found to be <0.05 with equal concentrations of oxidised and reduced forms in the α phase. With less extreme concentration ratios the peak separation, ΔE_p, increased and the midpeak potential, $E_{1/2}$, was displaced significantly from $E^{O'}$ and hence such deviations from more normal reversible behaviour should not necessarily be interpreted as control by charge transfer kinetics. When only one form of the redox species is present in excess a direct transposition of the classical voltammetry technique cannot be used, either to measure the formal potential, or to extract kinetic information.

4.2.3.2 Ferrocene Oxidation at the Water/Nitrobenzene Interface

The electrochemical oxidation of ferrocene in nitrobenzene by hexacyanoferrateIII in water has been reported by Samec et al[55]. Table 3 compares the results obtained in their study, at a sweep rate of 5 mV s^{-1}, with results obtained from the numerical analysis described under the same experimental conditions at 25 °C. The variations in the potential peak separation, ΔE_p, and the position of the half wave potential, $\Delta E_{1/2}$, agree reasonably well between the numerically calculated and experimentally determined results. The most significant disagreement occurs in the first and last rows in the table where the experimental shifts in $E_{1/2}$ are 0 and 2 mV respectively compared with calculated shifts of 12 and 24 mV. For these two experimental cases the peak currents observed

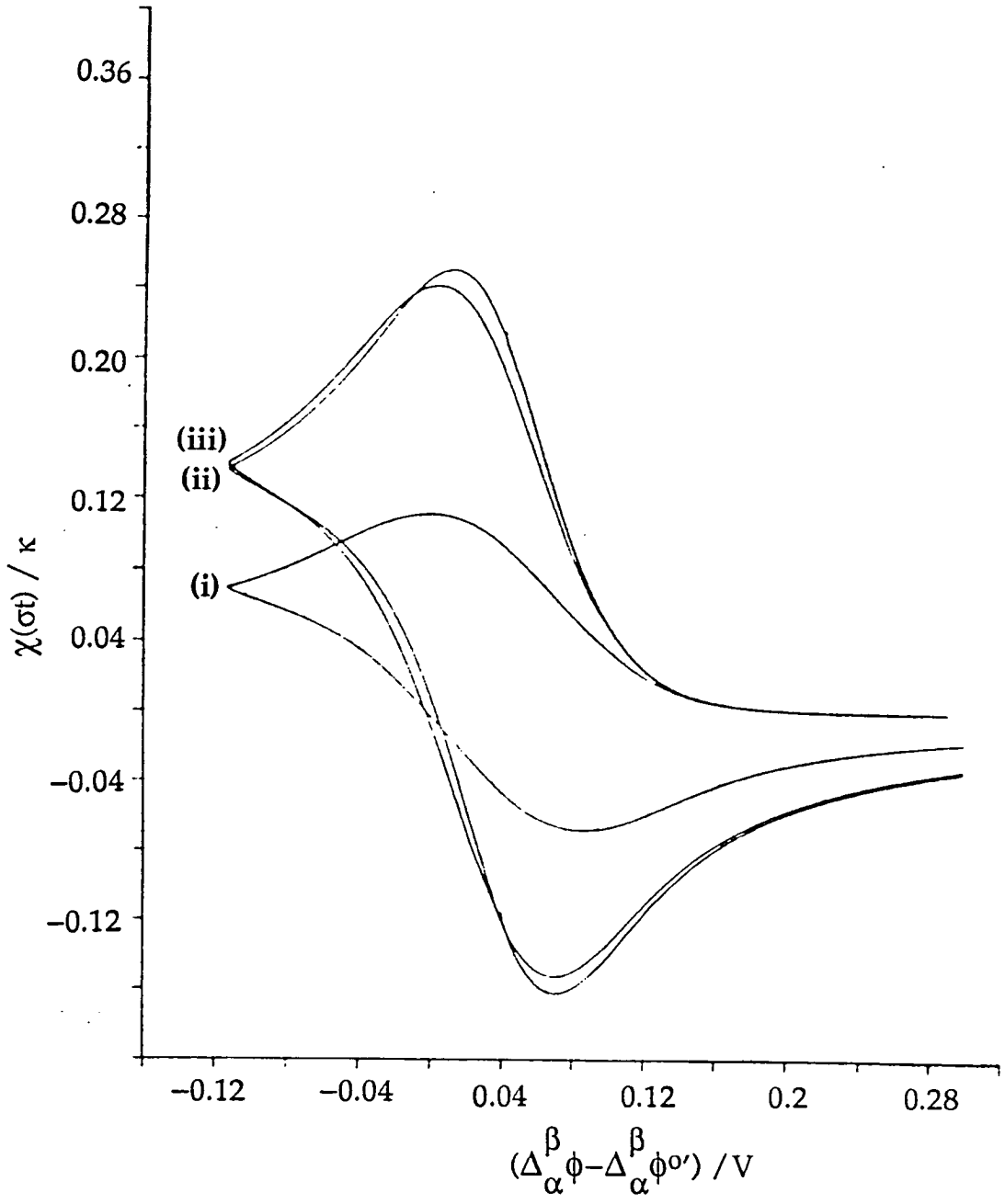

Fig. 13 Cyclic voltammograms, normalised dimensionless current for $\alpha = 0.5$, $\beta = 0$, with various κ values: (i)1, (ii) 10, (iii) 100.

Table 3

α	κ	ΔE_p/mV		$E_{1/2}$/mV		$\Delta E_{1/2}$/mV		$\chi(\sigma t)_{fp}$
		calc	exp	calc	exp	calc	exp	
0.909	9.09	87	85	75	–318			0.200
0.909	18.18	86	85	87	–318	12	0	0.200
0.909	45.45	85	85	111	–298	24	20	0.201
0.909	90.90	85	80	128	–285	17	13	0.201
0.909	181.18	84	85	145	–263	17	22	0.201
0.833	83.33	82	90	126	–288			0.187
0.909	45.45	85	85	111	–298	15	10	0.201
0.952	23.81	85	85	94	–315	17	17	0.208
0.980	9.80	87	90	70	–319	24	2	0.212

Comparison of calculated cyclic voltammogram characteristics (calc) for electron transfer with experimental values (exp) obtained by Samec et al[55]

were not proportional to the square root of potential sweep rate, whereas in every other case there was a direct proportionality of the peak current height to the square root of sweep rate. This direct proportionality indicates that the reactions were reversible and hence the reversible numerical analysis applies. The discrepancies which occur when the proportionality of current to square root of sweep rate is lost can be attributed to kinetic effects arising. The fitting of this experimental data to the numerical solution of the electron transfer diffusion problem confirms that electron transfer was indeed the process observed by Samec et al and explains the origin of the concentration dependence of the half wave potential they observed.

4.2.3.3 The Quasireversible Case

The above treatment may be extended to the kinetic case by using the current potential characteristic described in equation (75) as a condition in place of the Nernst equation which no longer applies. Dimensionless parameters θ, σ and S(t) are defined as in equations (117)-(119) and the kinetic expression for the current (equation (75)) may then be expressed in the form:

$$i(t) = nFAk^{o}(\theta S(t))^{-\alpha}\left[C_{O}^{\alpha}C_{R}^{\beta} - \theta S(t)C_{R}^{\alpha}C_{O}^{\beta}\right] \qquad (135)$$

Substitution of the mass transport equations (111)-(114) then gives a quadratic expression for the convoluted current, equation (136), similar to that obtained before.

$$AI(t)^2 + BI(t) + C^1 = 0 \qquad (136)$$

Where A and B are defined as in equations (122) and (123) above and C^1 is defined as:

$$C^1 = C_R^{b,\alpha} C_O^{b,\beta} \theta S(t) - C_O^{b,\alpha} C_R^{b,\beta} + \frac{i}{nFAk^o(\theta S(t))^{-\alpha}} \qquad (137)$$

Equation (136) has two roots, the correct one being given by the equivalent of equation (125) above:

$$I(t) = \frac{-B + \sqrt{B^2 - 4AC^1}}{2A} \qquad (138)$$

As $k^o \rightarrow \infty$ it can be seen that $C^1 \rightarrow C$ and equation (138) collapses to equation (125) for the reversible case above.

The integration of equation (138) is then performed in a similar manner to that of equation (125) and has been done by Stewart[102]. Due to the extra kinetic term in C^1 a dimensionless kinetic parameter, Ψ, is defined by:

$$\Psi = \frac{k^o C^\alpha}{\sqrt{\pi \sigma D_O^\alpha}} \qquad (139)$$

This is similar to the dimensionless kinetic parameter defined for a simple redox, however a concentration term C^α must be included in this case as the rate constant is second order rather than the first order rate constant of a simple redox. The concentration C^α appears elsewhere in the integration in the term κ (equation (129)) and so variation of the concentration of the redox couple in the α phase does not have the same effect as variation in the rate constant as might appear to be the case from equation (139).

While the analysis of the kinetic case is not yet complete some preliminary results have been obtained for the case, similar to case 1 above, where only one form of each redox couple is present in either

phase, and some initial conclusions may be made. Under reversible conditions decreasing C^{α} (where C^{α} is the lower of the two redox couple concentrations, i.e. $\kappa>>1$) leads to a variation in $E_{1/2}$ because κ varies with C^{α}, but it does not change the peak separation ΔE_p. Under quasireversible conditions variation in C^{α} changes both the $E_{1/2}$ and the ΔE_p. It does not appear that changing C^{α} alone, or any other reactant concentration, can change the reaction from reversible through quasireversible to irreversible as has been suggested by Samec[62].

4.3 CHRONOPOTENTIOMETRY

As its name suggests this technique is concerned with measuring the electrical potential of a system as a function of time. In contrast to cyclic voltammetry the current is the controlled, or independent, variable and the potential is the dependent variable to be measured. Normally a constant current step is applied to the system and the potential is recorded until it reaches some preset value. Charge is transfered by the electroactive species at the rate dictated by the current until the concentration drops to levels where the rate of reactant arrival at the interface is insufficient to maintain the applied current. The potential then changes very rapidly to more extreme values where other species become electroactive and are able to contribute to the current. The time at which this rapid potential change occurs is called the transition time, τ. The shape of the E.t wave recorded is governed by the reversibility, or charge transfer kinetics, of the reaction.

One of the advantages of chronopotentiometry is that relatively simple instrumentation can be used without the need for feedback control circuitry. A high voltage source with a large resistance and a voltage follower provide the minimum requirements. The constant current conditions used mean that the potential drop due to solution resistance is constant and its approximate value may be easily identified and corrected for. The major disadvantage of the method is that because the rate of change of potential with time, $d\phi/dt$, is changing throughout the experiment so is the charging current. This means that while the total

current passing is held constant, the proportion of that current due to the charge transfer reaction of interest (faradaic current), as opposed to double layer charging, varies during the experiment and this can be very difficult to correct for adequately.

Samec and Mareček[44] have used this technique for the study of tetrabutyl, tetrapropyl and tetraethylammonium ion transfers across the water/nitrobenzene interface. They used an iterative technique to correct for iR drop but made no correction for double layer charging. Rate constants in the range 0.1 to 4.1 $x10^{-2}$ cm s^{-1} were calculated with charge transfer coefficients ranging from 0.4 to 0.6.

4.4 AC VOLTAMMETRY AND IMPEDANCE

AC voltammetry has been used at the metal/electrolyte interface for many years, much of the early work being done by Smith[103]. At the ITIES Solomon, Alemu and Hundhammer[45,104] employed this method to obtain thermodynamic data for some ion transfer reactions and Osakai, Kakutani and Senda[46] have used phase sensitive ac voltammetry to measure kinetic parameters. Kinetic measurements have also been made by Wandlowski et al[47,48] with impedance methods. There is no essential difference between impedance measurements and ac voltammetry, however impedance tends to refer to the case where impedances are measured directly through sophisticated instrumentation whereas ac voltammetry refers to the case where impedances are calculated from current values measured through slightly less sophisticated phase sensitive detection.

The ac method for obtaining kinetic parameters is inherently different from other methods such as potential sweep and current steps which involve large perturbations of a system driving it far from equilibrium and then observing the transient response. In the ac case a small magnitude, ΔE, alternating potential is superimposed on a potential ramp which is slow with respect to the ac frequency so that the mean interfacial concentrations of reactants on the ac time scale are those given by the Nernst equation for the dc potential. The low amplitude of the applied ac potential ($\Delta E \leq 10/n$ mV) ensures that the system is always close to

equilibrium. The ac response is usually recorded at the applied frequency as a function of the dc potential.

In the simplest experiment to obtain thermodynamic data the resultant current amplitude alone may be recorded. For a reversible reaction the observed current peak occurs at the half wave potential, $E_{1/2}$ and has a width at half height of 90/n mV independent of frequency, ω. The amplitude of the peak current is proportional to ΔE and $\omega^{1/2}$ and forward and reverse peaks are superimposed, as found by Solomon Alemu and Hundhammer[104].

To gain kinetic information it is necessary to use phase sensitive detection by which the complex impedance of the system may be determined. Correction for solution resistance and double layer capacitance is crucial in this technique as the relatively high operating frequency means that the charging current is significant in relation to the faradaic current. Feedback iR compensation cannot be used satisfactorily as it introduces noise into the system. The solution resistance and double layer capacitance contributions to the impedance therefore have to be subtracted, either algebraically or graphically, from the total complex impedance. This is often achieved by measuring the cell response in the absence of electroactive species.

While ac techniques demand relatively expensive equipment they have resulted in the fastest rate constants for ion transfer so far reported with a value as high as 13.6 $x10^{-2}$ cm s^{-1} for tetrapropyl and tetramethyl ammonium[48].

4.5 CHRONOCOULOMETRY

Shao and Girault have recently used chronocoulometry to gain kinetic information on charge transfer at the ITIES[105]. The technique consists of integrating the current response of the system to an applied potential step and plotting the charge passed, Q(t), versus the square root of time, $t^{1/2}$. As the time increases Q(t) becomes linearly dependent on $t^{1/2}$ and the reaction is diffusion controlled, however extrapolation to the intercept on the time axis allows the forward rate constant to be determined by using also the

slope of the Q(t) vs $t^{1/2}$ plot. By stepping up to different potentials in different experiments the variation of k_f with potential may be determined without any a priori assumptions on the relationship. Thus while a large amount of data and data manipulation is required to produce a full set of results these results are obtained without the usual assumption of an Arrhenius dependence of the rate constants on potential.

It is essential to this method that solution resistance is correctly compensated. In the above cited work the ohmic resistance was reckoned to be fully corrected for by feedback iR compensation. This was verified by a 59/n mV peak separation in cyclic voltammetry experiments and through direct measurement of the iR drop using a current step. Correction for double layer charging involves measurement of the capacitance in a separate experiment, e.g. by current step without electroactive species. In the error from double layer charging was assumed to be negligible. Formal rate constants in the range 3 to 0.6 $x10^{-2}$ cm s^{-1} were determined for the transfer of the acetylcholine cation from water-sucrose mixtures to 1,2-dichloroethane.

4.6 MICROELECTRODE TECHNIQUES

4.6.1 Background

Electrodes with dimensions on the micrometre scale have been investigated intensively since the end of the 1970's. Such small electrodes offer advantages over more conventional electrodes, when operated on the time scale of seconds, as the dimensions of the electrode are then smaller than the diffusion distance for species in the solution. The main positive attributes of microelectrodes are sited as follows[106]:

(i) The high rates of steady state diffusion obtained allow relatively fast charge transfer reactions to be studied without recourse to transient techniques on a short time scale.

(ii) The low currents produced lead to negligible iR drop and hence accurate measurements may be made in highly resistive media.

(iii) Charging currents are reduced and so the ratio of charging to faradaic current is enhanced.

The electrochemical use of microelectrodes has been constrained up until recently to metallic (often platinum) and carbon based solid electrodes. Such microelectrodes have been used successfully to determine kinetic parameters by both steady state and fast sweep cyclic voltammetry methods. Andrieux and Saveant[107] determined a standard rate constant of 3.3 ± 0.2 cm s^{-1} for the reduction of anthracene in DMF using sweep rates of up to 2 x10^5 V s^{-1} and a 5 μm diameter gold disc electrode. At such high sweep rates involved corrections for resistive losses and charging currents had to be made, however the result obtained was consistent with that of 5 ± 3 cm s^{-1} reported from impedance measurements[108]. Oldham, Bond and others[109] presented a method for determining the standard rate constant for charge transfer under steady state conditions from the shift in half wave potential with electrode radius, although the condition that the reaction be very nearly reversible so that the exponential dependence on $E^{O'} - E_{1/2}$ can be linearised does restrict its applicability. More recently Oldham, Bond and Zoski have provided analytical or semianalytical solutions for reversible, irreversible and quasireversible kinetic control under steady state conditions[71].

4.6.2 The Micro-ITIES

Although patch clamp pipettes are used in electrophysiology to measure trans membrane potentials and other characteristics of living cell tissue, it was not until 1986 that Girault and Taylor[52] initiated the use of microelectrodes in liquid/liquid electrochemistry by supporting an interface at the tip of a patch clamp pipette of internal radius 25 μm. These authors used cyclic voltammetry to demonstrate the transfer of tetraethylammonium across the water/1,2-dichloroethane interface. During the course of the present work further supports for micro-ITIES have been developed which display different diffusion characteristics, namely microholes and microhole arrays. These diffusion geometries are described below and illustrated in figure 14.

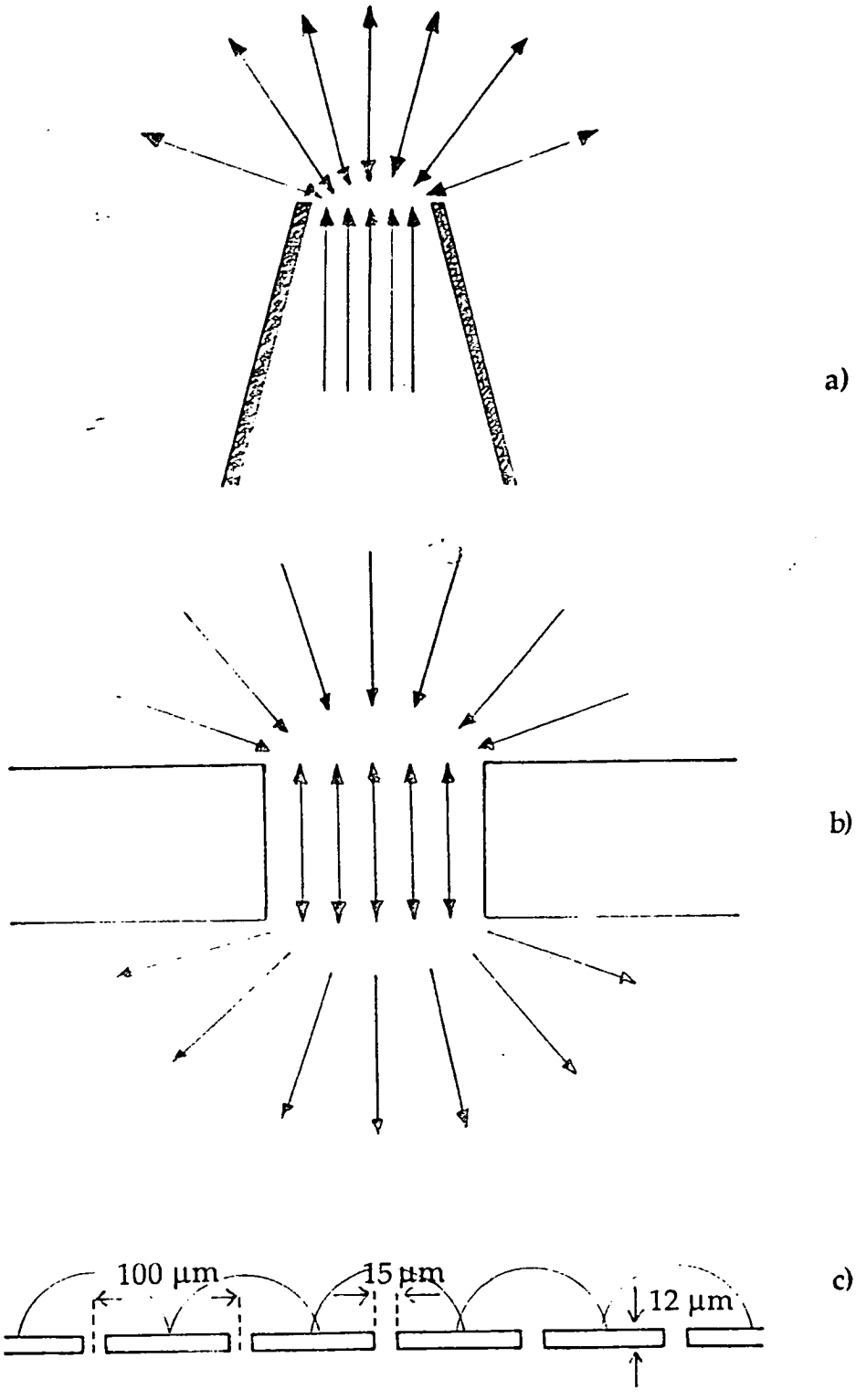

Fig. 14 Sections through; a) a micropipette, b) a single microhole, and c) part of a microhole array, showing diffusion flux lines and, for the microhole array, showing diffusion fields and where they might interfere if the holes were too closely spaced.

4.6.2.1 Diffusion at a Micropipette

The diffusion regime at a micro-ITIES supported at the tip of a micropipette is unique in its asymmetry. Diffusion of species from outside the pipette, to and from the interface, has a significant radial contribution and is largely cylindrical in nature, whereas that of species inside the pipette is constrained to be linear (fig 14a). An accurate treatment of the diffusion extant is rather complex and is being considered elsewhere[72]. Qualitatively, for cyclic voltammetry, the asymmetric diffusion regime leads to a sweep rate dependent current peak for species crossing out of the pipette and a steady state, sweep rate independent, current wave for species crossing into the pipette. This can prove a useful diagnostic criterion in determining whether species are diffusing from inside or outside the pipette and hence what reaction is being observed and which species are responsible for limiting the accessible potential window[110].

For accurate quantitative procedures it is necessary to simplify the diffusion problem by transforming it into a symmetrical system dependent only on diffusion external to the pipette. This cannot be achieved for a simple ion transfer reaction, but for both assisted ion transfer and electron transfer the concentration of the reactant species inside the pipette may be used in a vast excess such that the reaction rate is dependent solely on the diffusion of the species outside. The microinterface is assumed to be flat and in a plane perpendicular to the axis of the pipette at its tip. The mathematics of the diffusion is thus similar to that at a microdisc electrode.

4.6.2.2 Diffusion at a Microhole

For the case of an interface supported at a microhole of 5-50 μm diameter in a 12 μm thick membrane the geometry is symmetrical (fig 14b) and if the thickness of the membrane is ignored the diffusion may be treated, to a first approximation, as that at a microdisc electrode in an infinite insulating plane. Where the diffusion layer thickness is significantly larger than the membrane thickness this approximation seems reasonable. A rough measure of diffusion layer thickness may be obtained from the

root mean square displacement, $\bar{\Delta}$, at time t given by the random walk treatment as:

$$\bar{\Delta} = \sqrt{2Dt} \qquad (140)$$

For a diffusion coefficient of 5×10^{-5} cm^2 s^{-1} a diffusion layer thickness of 12 μm is built up in 0.15 s. This indicates that at low sweep rates the microdisc approximation is adequate.

4.6.2.3 Diffusion at Microhole Arrays

The diffusion to an array of microholes can be treated merely as the sum of that to all the individual microholes in the array so long as the holes are sufficiently distant from one another for their diffusion fields not to interact (fig 14c). Given that the diffusion field of a microelectrode extends for about 6 radii from the electrode centre, an array with N holes centred 12 radii apart should give a response equivalent to the sum of N isolated holes of the same size. Analysis of microhole array results therefore proceeds as for the case of a single microhole.

4.6.3 Steady State Diffusion at a Microdisc

Fick's second law for diffusion at a microdisc (also applicable to species external to a micropipette and all species at a microhole or microhole array, as described above) contains both linear and cylindrical parts. It is expressed in terms of the distance from the centre of the interface and in the plane of the interface, r, and the distance from the interface and perpendicular to the plane of the interface, z, as follows:

$$\frac{\partial C}{\partial t}(r,z,t) = D\left(\frac{\partial^2 C}{\partial r^2}(r,z,t) + \frac{1}{r}\frac{\partial C}{\partial r}(r,z,t) + \frac{\partial^2 C}{\partial z^2}(r,z,t)\right) \qquad (141)$$

The time dependence of the current at a microdisc is rather complex, however the system rapidly reaches a steady state in which case $\partial C/\partial t = 0$. It is from this point that Bond, Oldham and Zoski[71] develop a

semianalytical solution to the diffusion problem. These authors re-express equation (141) in terms of a bivariate dimensionless current function, G(r,z), which is then replaced by the integrated product of two bivariate functions, R(x,r) and Z(x,z), thus allowing the separation of variables r and z. The mathematical treatment then becomes rather complex and results in a number of candidate weighting functions which are applicable to different experimental circumstances. These weighting functions generate infinite sets of simultaneous equations requiring numerical methods for their solution. A more naive approach to the solution of the steady state problem is adopted here (also Appendix) which applies a Nernst diffusion layer approximation.

The current passed at an electrode is proportional to the concentration gradient of the electroactive species at the interface:

$$\frac{i}{zFA} = D\left(\frac{\partial C}{\partial z}(r,0,t)\right) \qquad (142)$$

where A is the area of the interface.

The concentration gradient at the interface, $\partial C(r,0,t)/\partial z$, is approximated in a linear fashion by introducing a distance, δ, which is the thickness of a hypothetical Nernst diffusion layer as illustrated in figure 15, thus:

$$\frac{\partial C}{\partial z}(r,0,t) = \frac{C^b - C^\sigma(r,t)}{\delta} = \frac{i}{zFAD} \qquad (143)$$

It is assumed that under steady state conditions δ is constant through the experiment. The magnitude of δ may be obtained from the diffusion limited, or plateau, current, i_d, observed at a microdisc at extreme polarisation when the surface concentration of the electroactive species, $C^\sigma(r,t)$, is zero. This is given by:

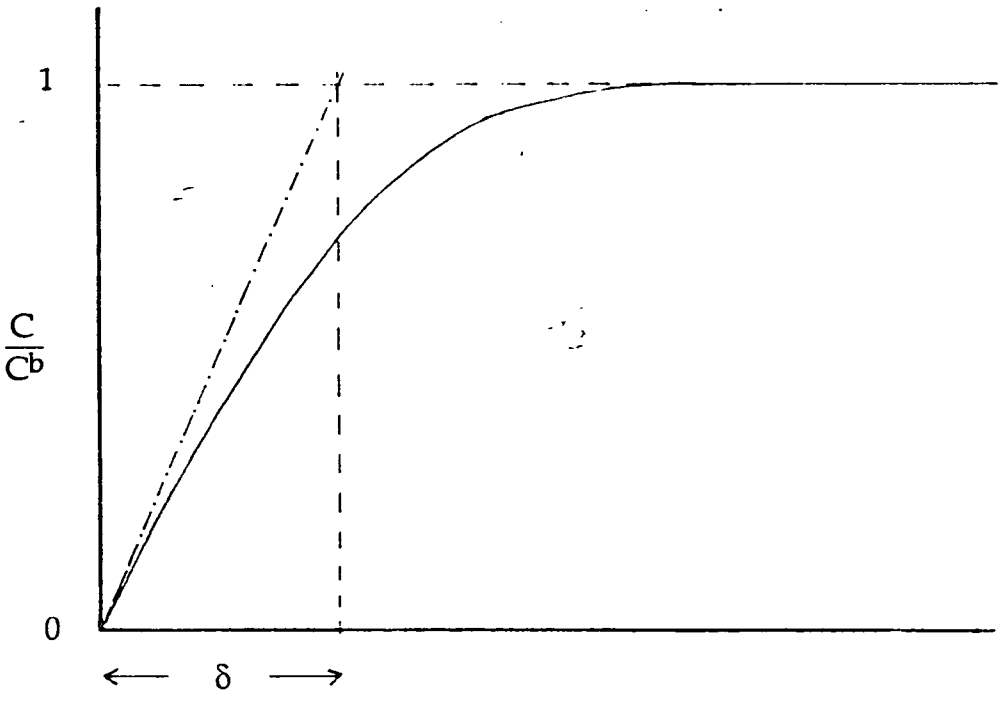

Fig. 15 Concentration of the electroactive species out from the electrode surface. The Nernst diffusion layer thickness is denoted δ. The dashed line (—·—·—·—·—) extrapolates the concentration gradient at the electrode surface (x=0).

$$i_d = 4\,z\,F\,D\,r_o\,C^b \qquad (144)$$

where r_o is the radius of the disc, or interface. Combination of equations (142), (143) and (144) gives the value of δ at a microdisc as:

$$\delta = \frac{\pi}{4}\,r_o \qquad (145)$$

4.6.3.1 Voltammetry in the Reversible Case

Consider the simple ion transfer reaction (III). Under reversible conditions the Nernstian equation (28) applies and assuming unit activity coefficients the concentration ratio of reactant to product at the interface may be written:

$$\frac{C_m^{\sigma,\alpha}}{C_m^{\sigma,\beta}} = \exp\left[\frac{zF}{RT}\left(\Delta_\alpha^\beta\phi - \Delta_\alpha^\beta\phi^{o'}\right)\right] \qquad (146)$$

The surface concentration of either reactant or product species may be expressed in terms of the current and the bulk concentration by use of equations (143) and (145) giving:

$$C_m^{\sigma,\alpha} = C_m^{b,\alpha} - \frac{i}{4\,z\,F\,D^\alpha\,r_o} \qquad (147)$$

$$C_m^{\sigma,\beta} = \frac{i}{4\,z\,F\,D^\beta\,r_o} - C_m^{b,\beta} \qquad (148)$$

Given that the bulk concentration in phase β is zero and that the bulk concentration in phase α is given by equation (144), equation (147) may be written as:

$$C_m^{\sigma,\alpha} = \frac{i_d - i}{4\,z\,F\,D^{\alpha}\,r_o} \qquad (149)$$

and the Nernst equation (146) may be expressed in terms of the current at any potential as:

$$\frac{i_d - i}{i} = \frac{D^{\alpha}}{D^{\beta}} \exp\left[\frac{zF}{RT}\left(\Delta_{\alpha}^{\beta}\phi - \Delta_{\alpha}^{\beta}\phi^{o'}\right)\right] \qquad (150)$$

This is the equation of a typical reversible polarographic or voltammetric wave[74] except that the half wave potential is dependent on $\frac{D^{\alpha}}{D^{\beta}}$ rather than $\left(\frac{D^{\alpha}}{D^{\beta}}\right)^{1/2}$ and is identical to the expression obtained by Bond, Oldham and Zoski[71].

4.6.3.2 The Quasireversible Case

In the quasireversible case the rate expression for the current may be given in terms of the forward and reverse potential dependent rate constants and the surface concentrations in each phase as follows:

$$i = zFA\left(k_f C_m^{\sigma,\alpha} - k_b C_m^{\sigma,\beta}\right) \qquad (151)$$

The forward and reverse rate constants are related by:

$$k_b = k_f \exp\left[\frac{zF}{RT}\left(\Delta_\alpha^\beta\phi - \Delta_\alpha^\beta\phi^{o'}\right)\right] \quad (152)$$

Hence equation (151) may be recast in terms of the diffusion limited current, the forward rate constant and the electrical potential by substitution from equations (148), (149) and (152) to give:

$$i = zFAC_m^{b,\alpha}k_f\left[\left(1-\frac{i}{i_d}\right) - \xi\frac{i}{i_d}\exp\left(\frac{zF}{RT}\left(\Delta_\alpha^\beta\phi - \Delta_\alpha^\beta\phi^{o'}\right)\right)\right] \quad (153)$$

where ξ is the ratio (D^α/D^β). The potential dependent forward rate constant is thereby given by:

$$k_f = \frac{i}{zFAC_m^{b,\alpha}}\left[\left(1-\frac{i}{i_d}\right) - \xi\frac{i}{i_d}\exp\left(\frac{zF}{RT}\left(\Delta_\alpha^\beta\phi - \Delta_\alpha^\beta\phi^{o'}\right)\right)\right]^{-1} \quad (154)$$

Equivalent results are obtained for the assisted ion transfer (IV) and electron transfer (VI) cases under pseudo first order conditions:

$$k_f = \frac{i}{zFAC_c^{b,\beta}}\left[C_m^{b,\alpha}\left(1-\frac{i}{i_d}\right) - \xi\frac{i}{i_d}C^{\ominus}\exp\left(\frac{zF}{RT}\left(\Delta_\alpha^\beta\phi - \Delta_\alpha^\beta\phi^{o'}\right)\right)\right]^{-1} \quad (155)$$

$$k_f = \frac{i}{zFAC_{O2}^{b,\beta}C^\alpha}\left[\left(1-\frac{i}{i_d}\right) - \xi\frac{i}{i_d}\exp\left(\frac{zF}{RT}\left(\Delta_\alpha^\beta\phi - \Delta_\alpha^\beta\phi^{o'}\right)\right)\right]^{-1} \quad (156)$$

Note that equation (156) assumes $C_{R2}^{b,\beta}=0$.

Under irreversible conditions the reverse transfer reaction rate becomes negligible and equation (153) reduces to:

$$i = zFA\,C_m^{b,\alpha}\,k_f\left(1-\frac{i}{i_d}\right) \qquad (157)$$

The semi-empirical solution to the quasi-reversible steady state problem expressed in equation 153 above was tested for accuracy by application to the numerical simulations of Heinze[70] and Taylor[111] and the semi-analytical solution of Bond, Oldham and Zoski[71] (using the empirical formula subsequently published by Oldham and Zoski[112]). Taylor's numerical simulation agrees very closely with the solution of Bond, Oldham and Zoski[71,112] and hence the two are quoted as the same below. The test was conducted by taking current and potential data points from the results of Heinze and Taylor and inserting them into equation (154) to determine the potential dependent rate constant. The charge transfer coefficient was then determined from the gradient of a plot of lnk(E) versus potential. The results of this comparison are summarised in tables 4 and 5. It can be seen from these tables that the naive semi-empirical solution to the diffusion problem is largely satisfactory in providing a straightforward analysis of steady state waves. The large error in the rate constant of 0.1 cm s^{-1} in table 4 derives from the fact that, using an electrode radius of 5 μm, diffusion is no longer sufficiently fast relative to charge transfer kinetics (i.e. the reaction approaches reversible) and there is mixed diffusion and kinetic control. A smaller electrode would need to be used to make an accurate determination of such a rate constant by this analysis.

The Nernst diffusion layer approximation can similarly be used to derive kinetic expressions for any polarographic or other steady state wave as well as for the microelectrode case considered here. The advantage of the method over that of Oldham, Zoski, Bond and Sweigart[109] is that it does not have to be used under "near reversible" conditions and that it does not require a range of experiments using electrodes of different radii. Further it gives the potential dependent rate constant and so allows the

Table 4

Simulation Conditions			Analysis Results	
ψ	σ	disc radius/m	α	$k^o/10^{-4}$cm s^{-1}
1.0	5.0	3.54×10^{-4}	0.36	1.08
0.1	5.0	3.54×10^{-5}	0.35	1.19
1.0	8.0	2.216×10^{-4}	0.41	0.88
0.1	8.0	2.216×10^{-5}	0.42	1.15

Comparison with Heinze's simulation, ψ and σ are defined as follows: $\psi = k^o/[D\pi\nu F/(RT)]^{1/2}$, $\sigma = [D/(n\nu Fr^2/RT)]^{1/2}$. Other simulation conditions were: $D = 1 \times 10^{-5}$ cm^2 s^{-1}, $k^o = 1 \times 10^{-4}$ cm s^{-1}, $\alpha = 0.5$

Table 5

Simulation Conditions		Analysis Results	
k^o/cm s^{-1}	α	k^o/cm s^{-1}	α
0.1	0.5	0.35	
0.01	0.5	0.010	0.49
0.001	0.5	0.00088	0.52
0.0001	0.5	0.000070	0.53
0.00001	0.5	0.0000075	0.51
0.0001	0.3	0.00011	0.29
0.0001	0.8	0.00011	0.77

Comparison with Taylor's simulation and Bond, Oldham and Zoski's solution, simulation conditions: $D = 1 \times 10^{-5}$, disc radius = 5×10^{-6} m.

determination of the charge transfer coefficient, α, rather than just k^o as is the case for Oldham's treatment. The naive treatment does not however provide a simulation and it does not give any information on the variation in current density across the disc interface, or on the real concentration profiles in the solution. The current density at a microdisc is in fact known to be quite heterogeneous, with the greatest fluxes occuring at the edges of the disc. This factor is taken into account in Bond Oldham and Zoski's semi-analytical treatment[71], as is mixed diffusion and kinetic control, although their simulation does not provide an analysis for experimental results other than the restricted one already mentioned[109]. More recently Oldham, Myland, Zoski and Bond have produced kinetic indicator diagrams[113] for the determination of k^o and α by steady state cyclic voltammetry at microdisc electrodes. They suggest the use of a number of electrodes of different radii to confirm the result. Zoski, Bond, Allinson and Oldham have also considered the problem of how long an electrode takes to reach steady state[114] and have developed a method of convolutive forecasting[115] for producing a steady state voltammogram from one with significant linear diffusion.

4.6.4 Effects of iR and Capacitance

Although one of the most frequently sited advantages of microelectrodes is their freedom from the distorting effects of iR drop, the effects of solution and electrode resistance cannot necessarily be ignored. It should be noted that at sweep rates and microelectrode radii where steady state conditions are obtained the current is proportional to electrode radius rather than area and the ohmic solution resistance to the reciprocal radius, hence the product iR is independent of electrode radius and cannot be reduced by a further decrease in electrode dimensions[117]. Oldham[118] has pointed out that close to the microelectrode the term "ohmic" is inappropriate as Ohm's law is far from being obeyed, the resistance of the solution being heavily dependent on the current passed. His calculations show that under steady state conditions with a simple one electron reversible reaction (ignoring any electrode resistance) concentrations of supporting electrolyte greater than or equal to the electroactive species behave as "excess supporting electrolyte". However it should be noted

that at lower concentrations of electrolyte when iR effects were observed the influence on steady state cyclic voltammograms was qualitatively the same as charge transfer kinetics.

For measurements of reaction kinetics using solid microelectrodes (10 μm diameter range) in dimethylformamide electrolyte at very high sweep rates (10 - 1000 kV s^{-1}) when linear diffusion is dominant Andrieux, Saveant and others[107] found it necessary to introduce comprehensive correction for the ohmic drop taking into account the mutual dependence of the faradaic and double layer charging currents. They determined the solution resistance between reference and working electrodes in their experiments to be 55 kΩ. At sweep rates of up to 20 kV s-1 using electrodes of under 14 μm diameter in acetonitrile with supporting electrolyte Howell and Wightman[116] concluded that cyclic voltammograms were obtained with minimal distortion from iR drop and double layer capacitance.

The above experimental findings give confidence that at solid microelectrodes under steady state conditions the effects of iR will be negligible. Unfortunately there is a significant difference at the micro-ITIES. When the ITIES is supported at the tip of a micropipette the resistance of the column of aqueous electrolyte in the tip of the pipette is even more significant than that of the organic solution outside the pipette. In analogy to the solid microelectrode this is similar to having a highly resistive electrode. For this reason the aqueous supporting electrolyte is generally used in very high concentration, and the narrow shank before the pipette tip made as short as possible. At the microhole the thickness of the constriction around the interface is fixed at 12 μm due to the thickness of the supporting membrane. Reference electrodes should be placed as close to this as possible.

With reference to Oldham's calculations[118] it has been noted that uncompensated resistance will appear to the experimenter in the same form as charge transfer kinetics, as indeed it does at large electrodes with linear diffusion. To ensure reliable results the resistance of systems should therefore be measured, or the absence of resistive effects confirmed by the use of a known reversible reaction. An alternative method of confirming that reaction kinetics rather than solution resistance is

responsible for deviations from reversible behaviour is to increase the concentration of electroactive species, and thus increase the faradaic current passed. Distortions due to iR will increase proportionately, whereas the shape of the wave dictated by reaction kinetics, notably the position of the half wave potential, will be unaltered. In the case of charged electroactive species it can be argued that changing their concentration may change the resistance of the electrolytes significantly, however in the case of assisted ion transfer this should not be the true, and such a check could prove very effective.

ION TRANSFER

5.1 RESULTS

The first results for ion transfer at a microhole supported liquid/liquid interface were achieved using the tetraethylammonium cation (TEA^+) and a single, isolated, microhole of 20 μm diameter. Figure 16 shows the cyclic voltammetric wave obtained for TEA^+ crossing from the DCE phase to the water phase of CELL1 over a range of sweep rates. Figure 17 shows the result of a similar experiment performed when no hole was present in the membrane in order to test for pin holes, leakages and capacative currents.

Ag/AgCl	10mM NaCl 1mM NaTPB water	1mM CVTPB 150μM TEATPB DCE	10mM LiCl	AgCl/Ag

CELL1

Further studies used the acetylcholine cation as the electroactive species because the crystal violet based supporting electrolyte, necessary for the study of the TEA^+ transfer, was awkward to use. The acetylcholine cation crosses conveniently near the middle of the tetrabutylammonium-tetrakis(4-chlorophenyl)borate potential window. All experiments were conducted at room temperature, $20 \pm 2\ ^{o}C$.

Cyclic voltammograms recorded when no hole was present in the cell membrane, using the electrochemical CELL2, are given in figure 18. Figure 18a shows voltammograms recorded immediately after the cell was filled, whereas those in figure 18b were taken approximately half an hour later. The variation in current with sweep rate in figure 18a is directly proportional to sweep rate and may therefore be attributed to charging current. The capacitance of the hole free membrane was thus calculated to be $1.78 \pm 0.05 \times 10^{-10}$ F. Figure 18 also shows a variation in the slope of the current with potential which increases substantially with the length of time the cell is filled. This indicates that the membrane is conducting to a certain extent and that its conductivity increases with time. The resistance of the membrane was measured from figure18b and found to be $8.1 \pm 0.1 \times$

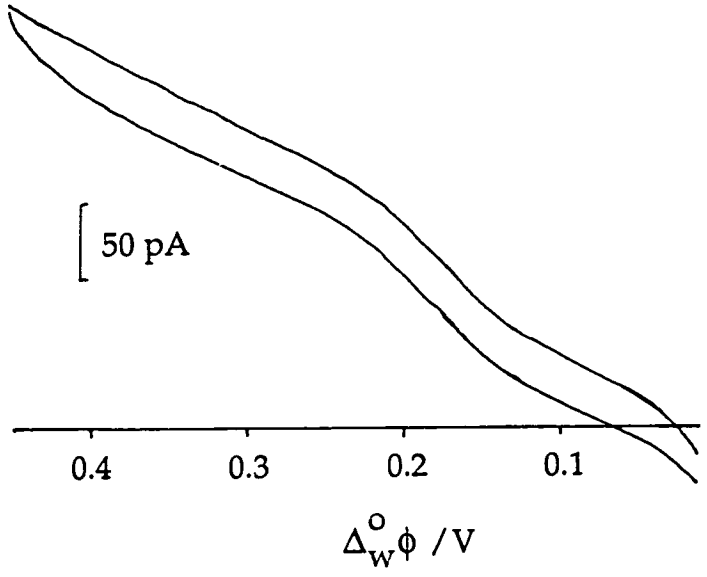

Fig. 16 Cyclic voltammogram for the transfer of TEA^+ from DCE to water at a 20 μm diameter hole and at 10 mV s^{-1}.

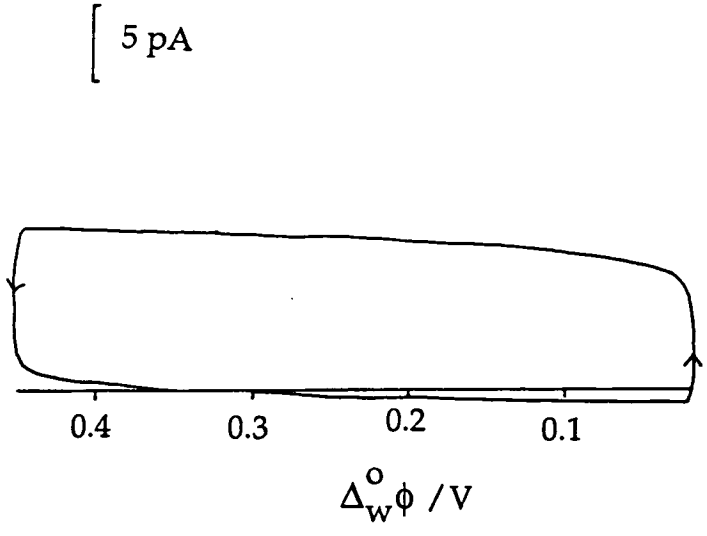

Fig. 17 Cyclic voltammogram with electroactive species present, but no hole in the membrane, at 100 mV s^{-1}.

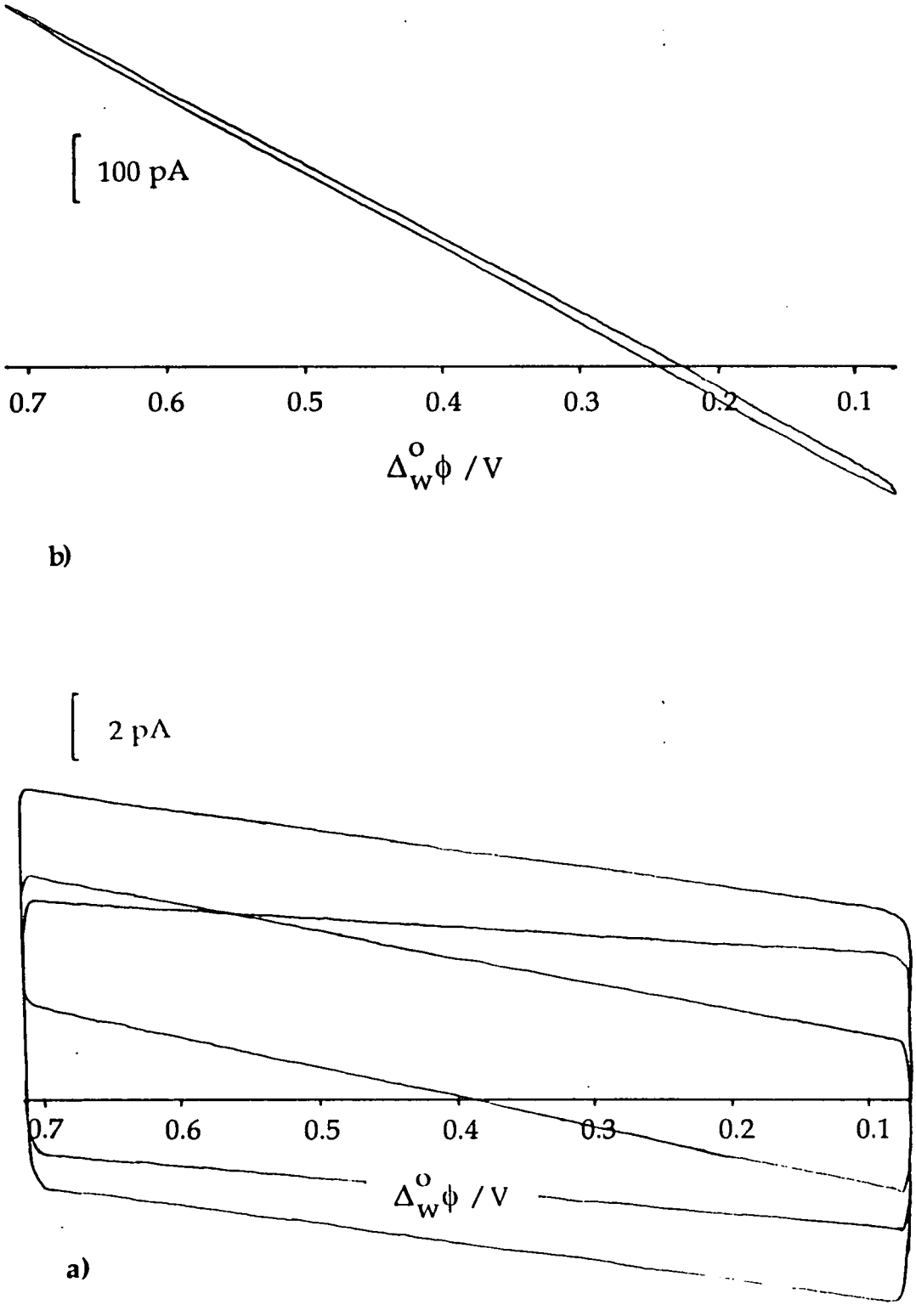

Fig. 18 Cyclic voltammograms from membrane without hole; a) immediately after filling cell at sweep rates of: 1) 200 mV s^{-1}, 2) 300 mV s^{-1}, and b) approximately 30 minutes later at 200 mV s^{-1}.

$10^8\ \Omega$. The initial resistance of the membrane, measured from the 200 mV s^{-1} scan in Figure 18a, was $3.2 \pm 0.2 \times 10^{11}\ \Omega$.

Ag/AgCl	10mM LiCl X mM AChCl water	10mM TBATPBCl DCE	10mM TBACl	AgCl/Ag

CELL2

The current potential characteristic for the base electrolyte (i.e. CELL2 with X=0) at an interface supported at a 20 μm diameter hole is displayed in figure 19 from which it can be seen that the accessible potential window extends for approximately 600 mV and has a good horizontal baseline indicating little leakage current. The current potential characteristic for the acetylcholine cation crossing the same interface at various sweep rates is shown in figure 20. It can be seen that the current wave is steady state, i.e. sweep rate independent, at low sweep rates. At higher sweep rates some peaking in the current wave becomes apparent. The diffusion coefficient for the acetylcholine cation in water was calculated from the diffusion limited current of 4.65×10^{-9} A to be 6.1×10^{-6} cm^2 s^{-1}. This compares with a value of 5.2×10^{-6} cm^2 s^{-1} obtained from cyclic voltammetry at a large interface. Similar steady state waves were obtained from CELL2 at holes of 50 μm, 10μm and 5 μm diameter and are shown in figure 21. Figure 21 also shows the sweep rate dependence of the current at the 5 μm diameter hole which continues to be steady state up to 400 mV s^{-1}. The variation in current with sweep rate at a 50 μm diameter hole is illustated in figure 22a. This shows a peaked response developing on both forward and reverse sweeps as the sweep rate is increased. Figure 22b illustrates the current-potential response at a 20 μm diameter hole with a sweep rate of 500mV s^{-1}. Here the peaked current response is no longer obviously symmetrical, but is much more pronounced on the forward than on the reverse sweep.

According to equation (144) the diffusion limited current at a microdisc is directly proportional to the disc radius and the concentration of electroactive species. A plot of the diffusion limited current (normalised to concentration) against microhole radius is given in figure 23. The results show a lack of quantitative reproducability between experiments. The dashed line in the figure corresponds to the theoretical response

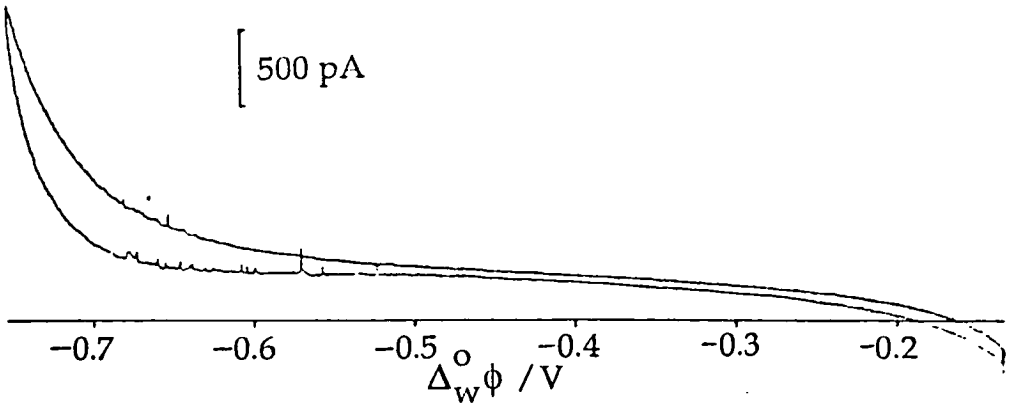

Fig. 19 Cyclic voltammogram of background electrolyte at 10 mV s^{-1} at a 20 μm diameter hole.

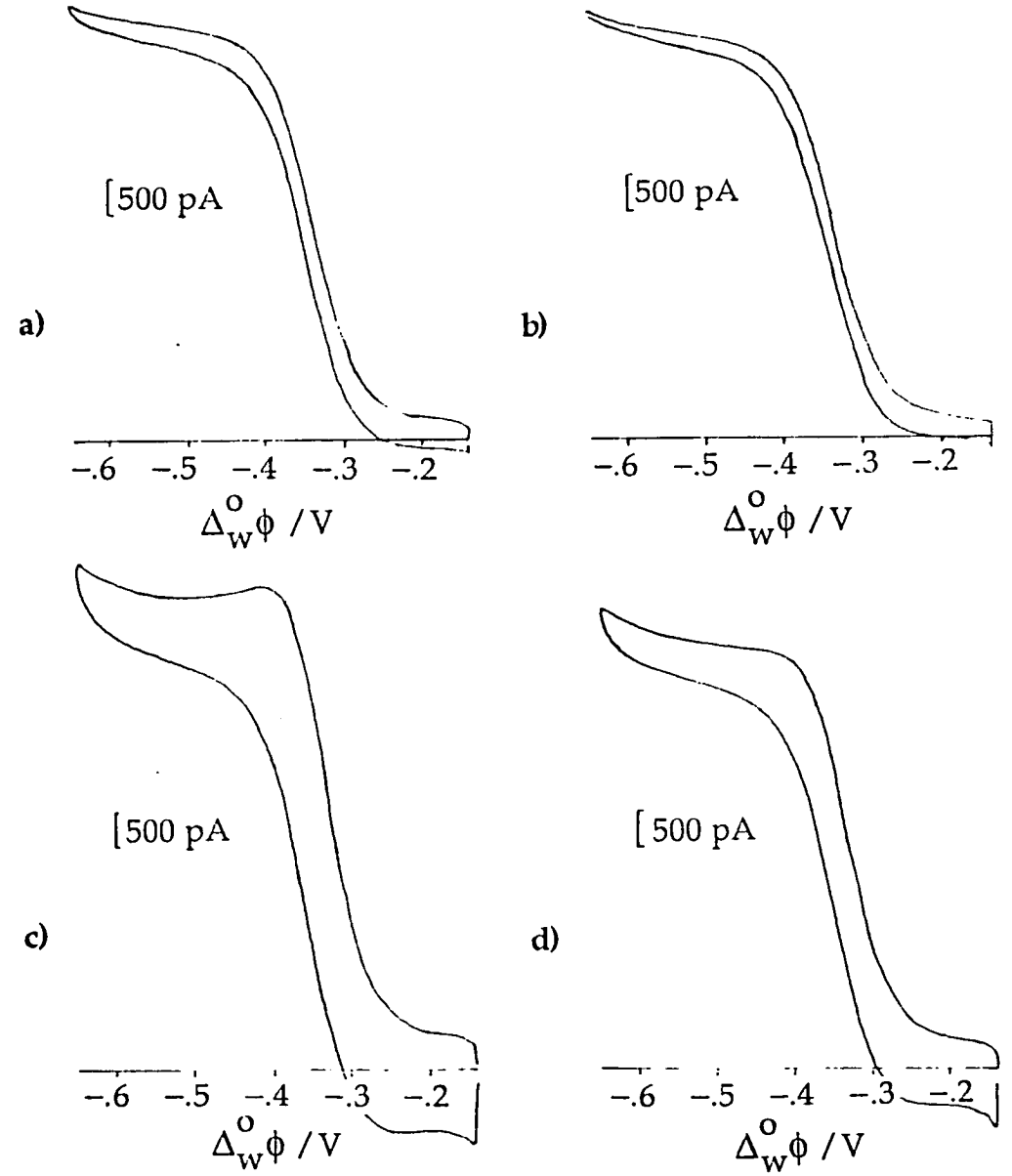

Fig. 20 Sweep rate dependence of acetylcholine cation transfer at a 20 μm diameter hole, a) 20 mV s^{-1}, b) 10 mV s^{-1},.c)200 mV s^{-1}, and d) 100 mV s^{-1}.

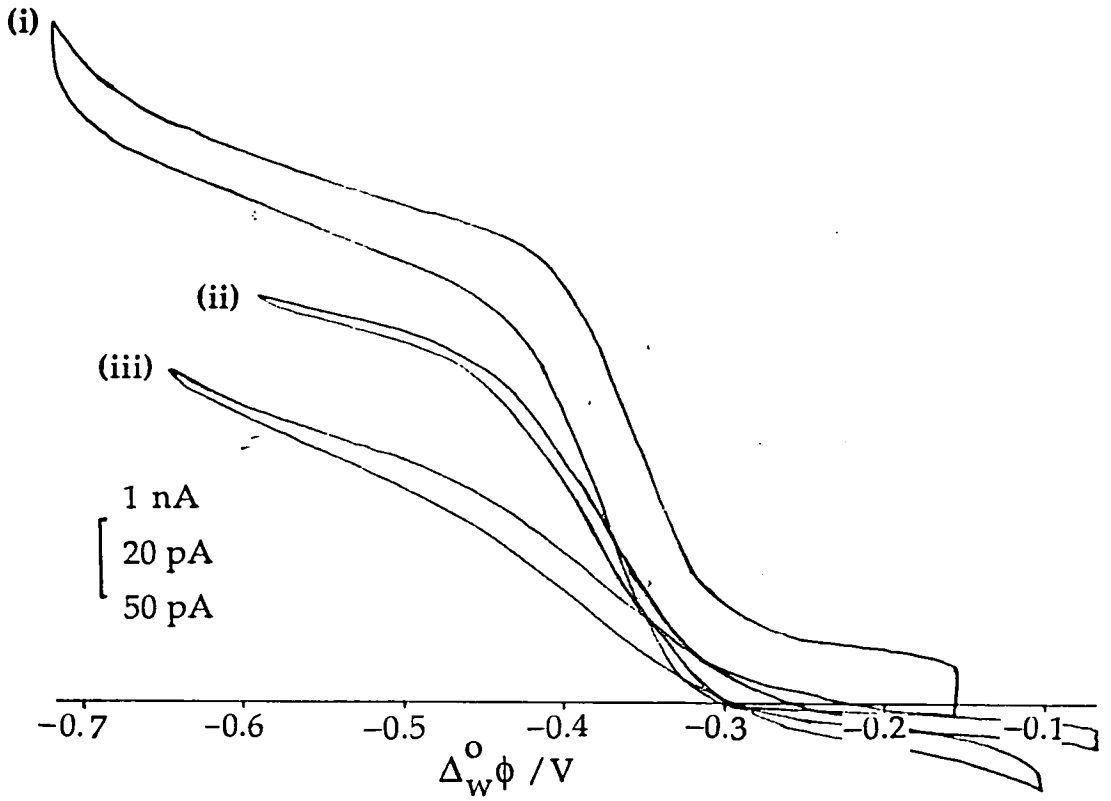

Fig. 21a Cyclic voltammograms from CELL2 at single holes, (i) 50 μm, ν =20 mV s^{-1}, X=2, (ii) 10μm, ν =10 mV s^{-1}, X=0.2, (iii) 5μm, ν =50 mV s^{-1}, X=0.2

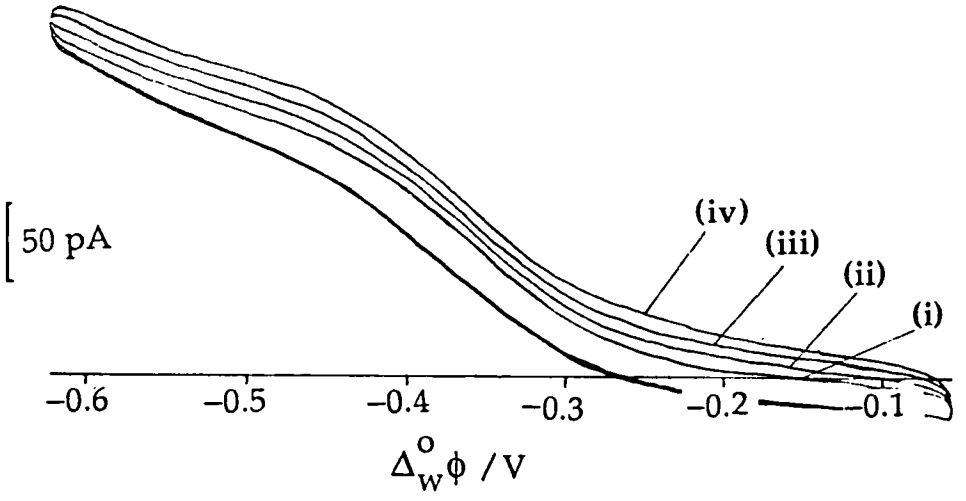

Fig. 21b Cyclic voltammograms from CELL2, X=0.2, at varying forward sweep rates: (i) 100 mV s^{-1}, (ii) 200 mV s^{-1}, (iii) 300 mV s^{-1}, and (iv) 400 mV s^{-1}, and at a constant reverse sweep rate of 50 mV s^{-1}.

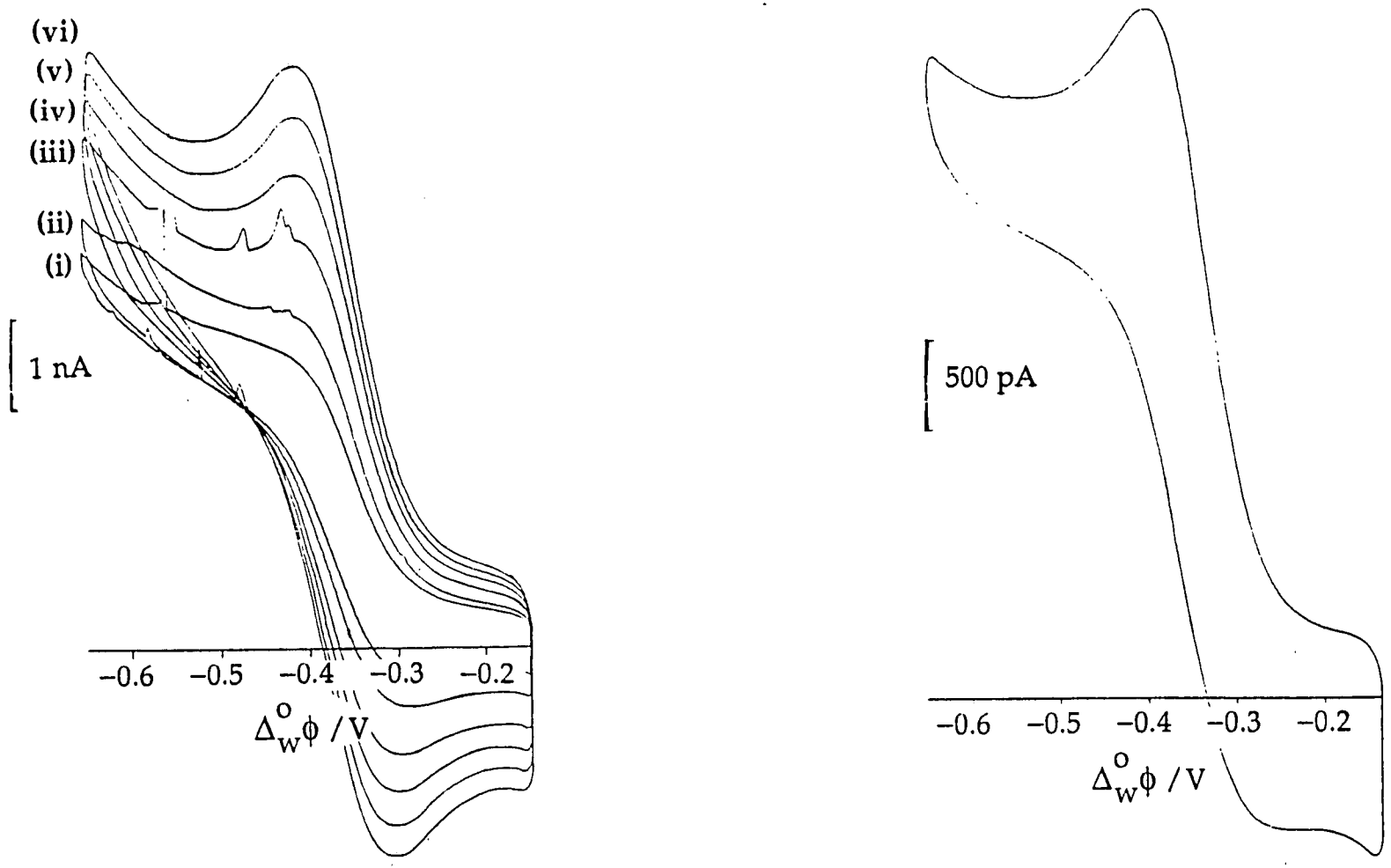

Fig. 22 a) Cyclic voltammograms of ACh^+ crossing at a 50 μm diameter hole at various sweep rates: (i) 50, (ii) 100, (iii) 200, (iv) 300, (v) 400 and (vi) 500 mV s^{-1}. b) Cyclic voltammograms of ACh^+ crossing at a 20 μm diameter hole showing asymmetry at high sweep rate - 500 mV s^{-1}.

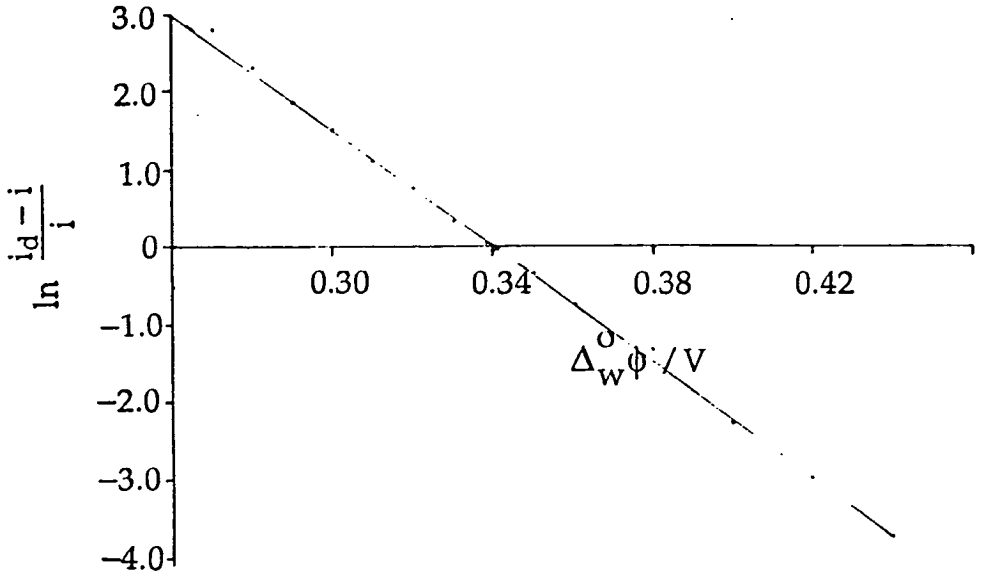

Fig. 24. Semi-logarithmic plot of $\ln((i_d-i)/i)$ v $\Delta\phi$ for the current response at a 20 μm diameter hole.

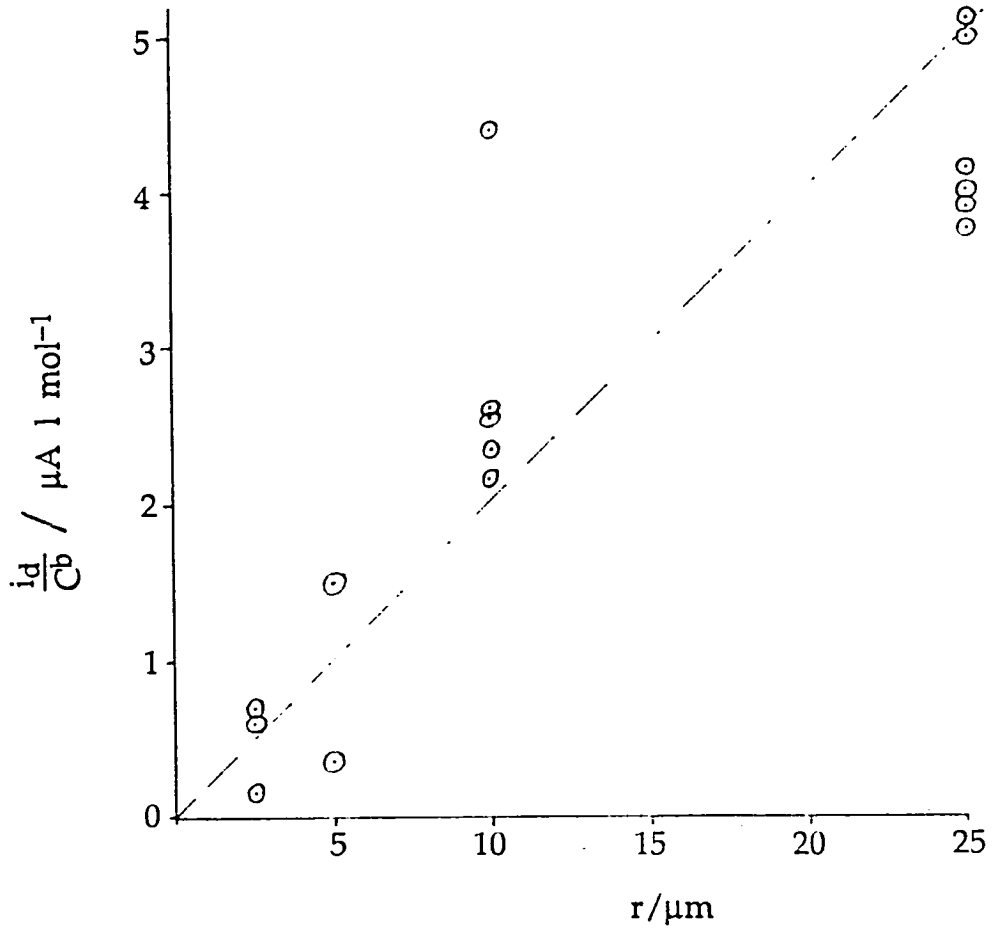

Fig. 23 Plot of diffusion limited current, normalised with concentration, against microhole radius. The dashed line represents the theoretical response using $i_d = 4nFDCr$

expected for diffusion of a species with diffusion coefficient 5.2×10^{-6} cm^2 s^{-1} to microdiscs of the same radii. A plot of ln $(i_d-i)/i$ versus potential for a typical single hole (20 μm) steady state wave is shown in figure 24 and gives a straight line of gradient 37.6 ± 2 V^{-1}. The gradients of such plots for the 50 μm, 10 μm and 5μm holes were 40.5 ± 1 V^{-1}, 35.6 ± 2 V^{-1} and 24.5 ± 2 V^{-1} respectively. The slopes for the 50 μm and 20 μm holes thus agree with the Nernst slope of F/RT for a reversible, single charge, transfer, that for the 5 μm hole is considerably less than this.

The array of microholes, 15 μm in diameter and centred 100 μm apart, again gives a steady state response and figure 25 shows the current potential characteristics thus obtained at various sweep rates from CELL3. This figure demonstrates that apart from an increase in charging current, which is proportional to sweep rate, the current is independent of potential sweep rate up to values of 400 mV s^{-1}. Figure 26 shows the current response of CELL2 at an array when only a two, as opposed to four, electrode system is used. It can be seen that while there remains a steady state, the cyclic voltammograms are severely distored by the associated ohmic resistance of the two electrode experiment. An analysis of $\ln(i_d-i)/i$ versus potential for the microhole array experiment with four electrodes gives a straight line of slope 26 ± 2 V^{-1}, which is well below the expected Nernst slope of 39 V^{-1}. This indicates that even with four electrodes there is a problem of iR losses.

Ag/AgCl	10mM LiCl 0.2 mMAChCl water	1mM TBATPBCl DCE	1mM TBACl	AgCl/Ag

CELL3

A cyclic voltammogram for the acetylcholine cation transfer at the more conventional large scale ITIES is given in figure 27 for comparison. This shows the typical linear diffusion response of a reversible system with forward and reverse current peaks 60 mV apart and height of peak current proportional to the square root of sweep rate.

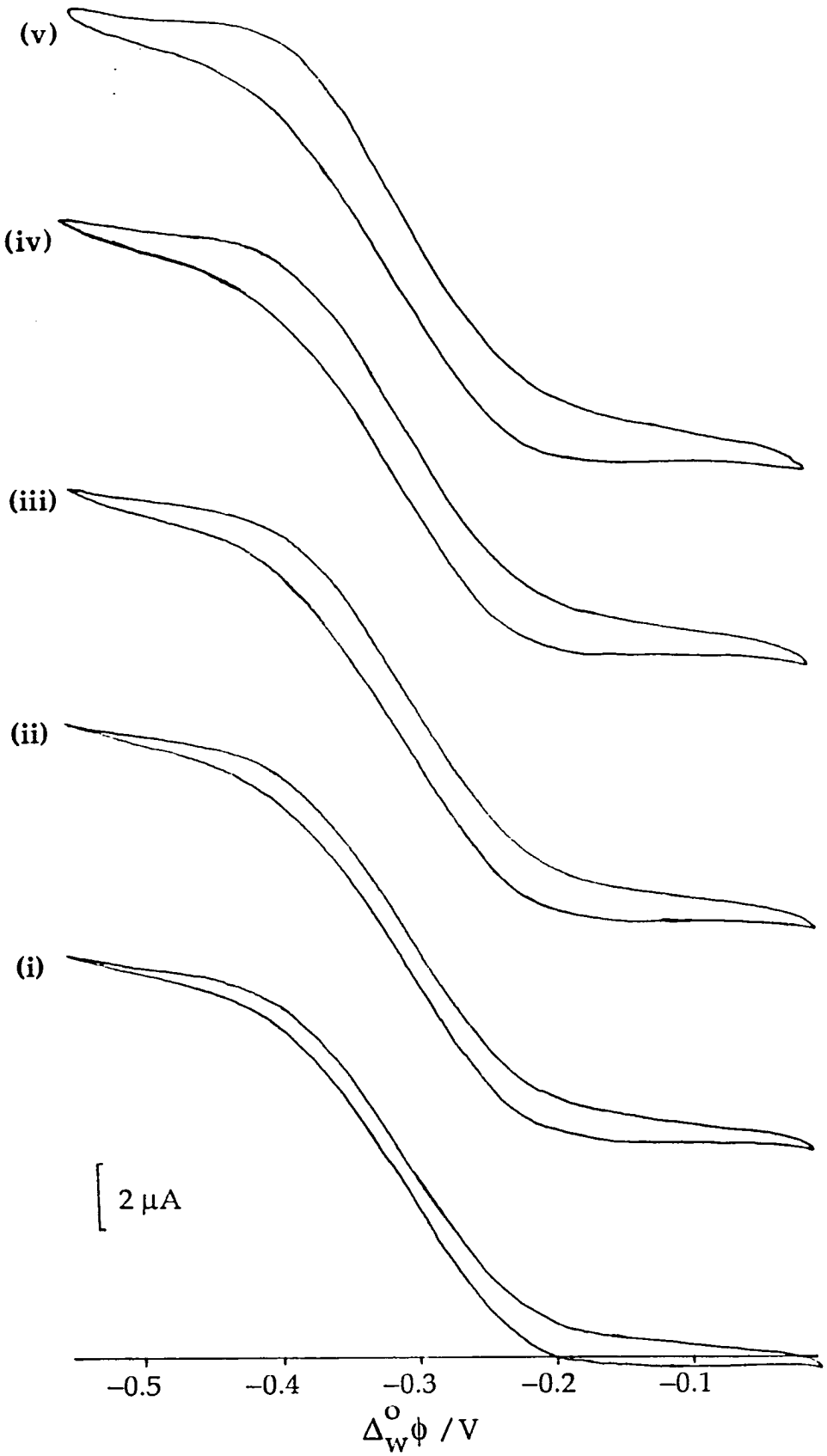

Fig. 25 Cyclic voltammograms from CELL3 at a microhole array using four electrodes and at varying sweep rates; (i) 50 mV s^{-1}, (ii) 100 mV s^{-1}, (iii) 200 mV s^{-1}, (iv) 300 mV s^{-1}, and (v) 400 mV s^{-1}.

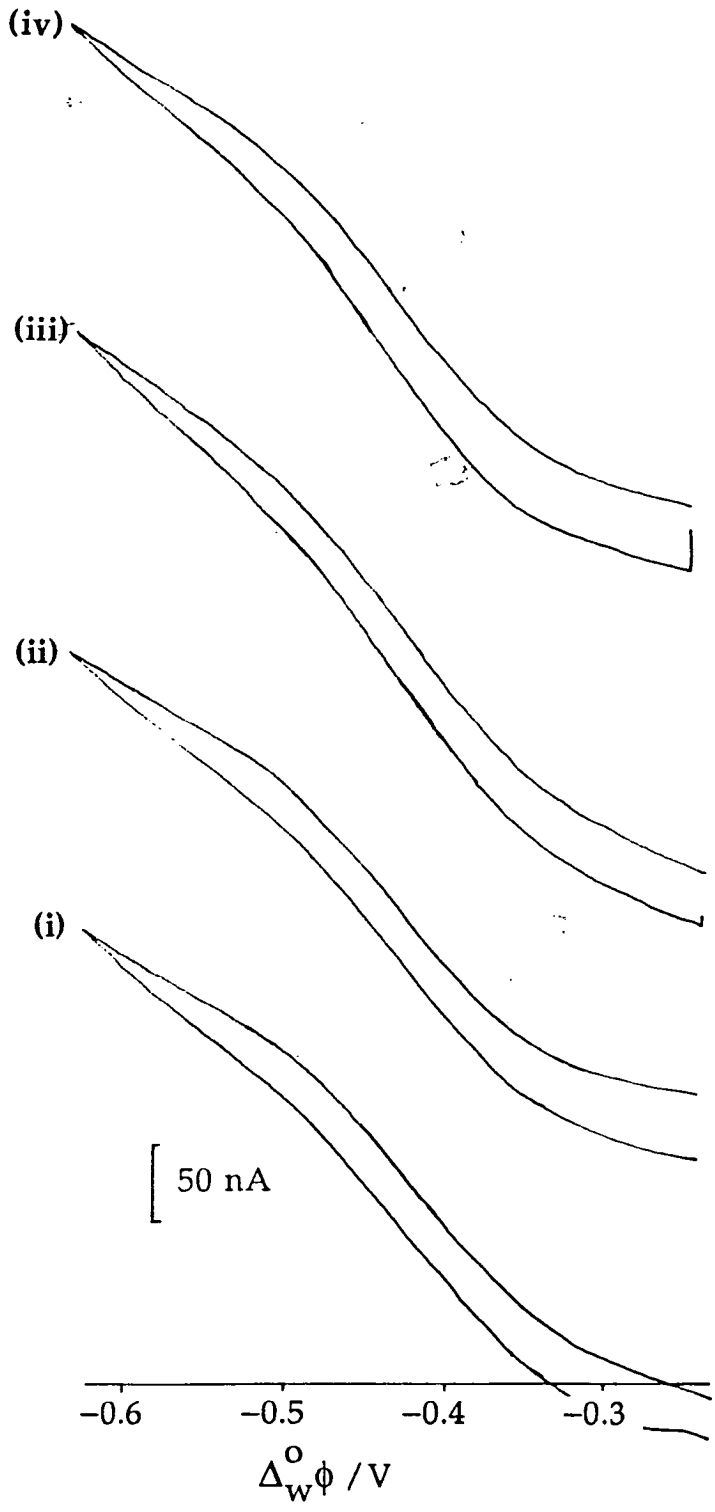

Fig. 26 Cyclic voltammograms from CELL2 (X=1) at a microhole array using two electrodes and at varying sweep rates; (i) 10 mV s^{-1}, (ii) 40 mV s^{-1}, (iii) 100 mV s^{-1}, (iv) 200 mV s^{-1}.

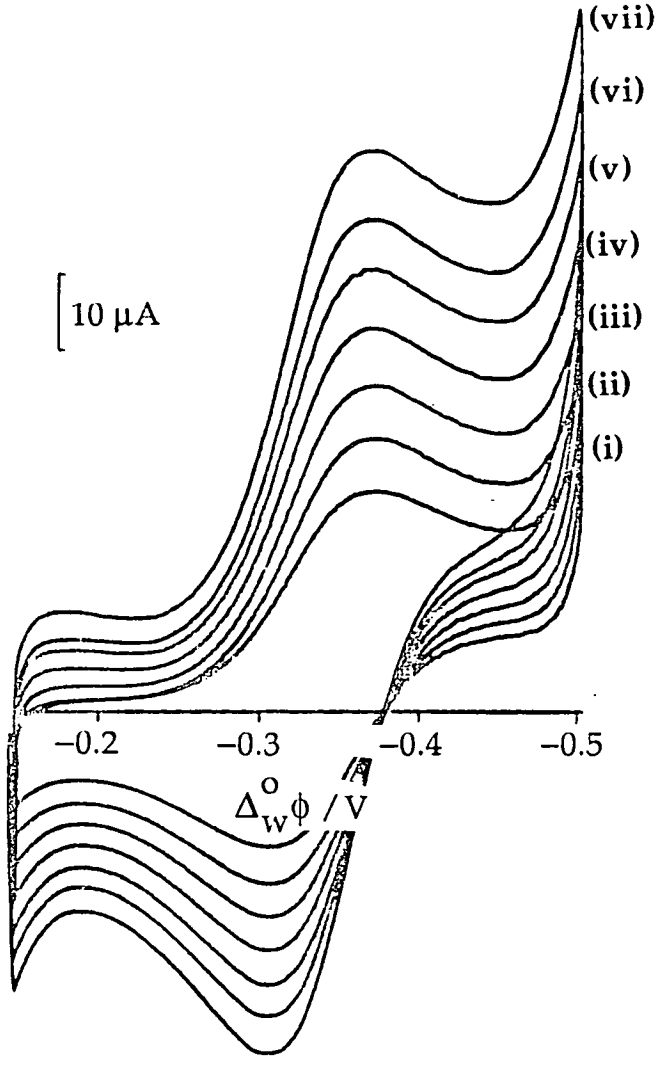

Fig. 27 Cyclic voltammetry of ACh^{+} crossing a large (12 mm diameter) water/DCE interface at various sweep rates: (i) 16, (ii) 25, (iii) 36, (iv) 49, (v) 64, (vi) 81 and (vii) 100 mV s^{-1}. Courtesy of Y. Shao.

5.2 DISCUSSION

5.2.1 Properties of the Membrane

It can be seen from figures 17 and 18 that the 12 μm thick membrane used to separate the two liquid phases is both pin hole free and highly resistive. This is a basic requirement for the cell to be able to operate properly, that is to provide a small and controlled area of contact between two otherwise isolated phases. The capacitance of the membrane itself is low enough to avoid problems with charging current obscuring faradaic currents and the capacitance of the micro-liquid/liquid interface is in fact more significant.

The observation that the resistance of the membrane decreases with time means that the composition of the membrane is not constant during an experiment. It is thought that the decrease in membrane resistance which is seen in figure 18 is caused by the adsorption of electrolyte solution into the membrane. This adsorption may also lead to some change in the size of the microholes, although no progressive changes in faradaic currents passed were noted during experiments to provide any evidence of significant hole distortion.

5.2.2 Properties of the Current Wave

5.2.2.1 The Shape of the Wave

The current waves observed at all the single holes clearly show steady state behaviour at low sweep rates which is typical of a large radial contribution to diffusion. At higher sweep rates radial contributions become less dominant at the larger interfaces and linear diffusion effects become apparent. For the 50μm diameter hole current peaks appear on forward and reverse scans at sweep rates as low as 50 mV s^{-1}. In contrast the 5 μm diameter hole voltammogram does not show any current peaking, even up to sweep rates of 400 mV s^{-1}. This means that despite the fact that through the thickness of the membrane the diffusion is constrained to a linear geometry (figure 28), the membrane is still thin enough for diffusion inside the membrane not to be limiting.

5.2.2.2 The Magnitude of the Wave

The quantitative response of the microholes is not as satisfactory as their qualitative response. Figure 23 shows that results are not reproducible, and that the limiting currents observed are not usually those expected

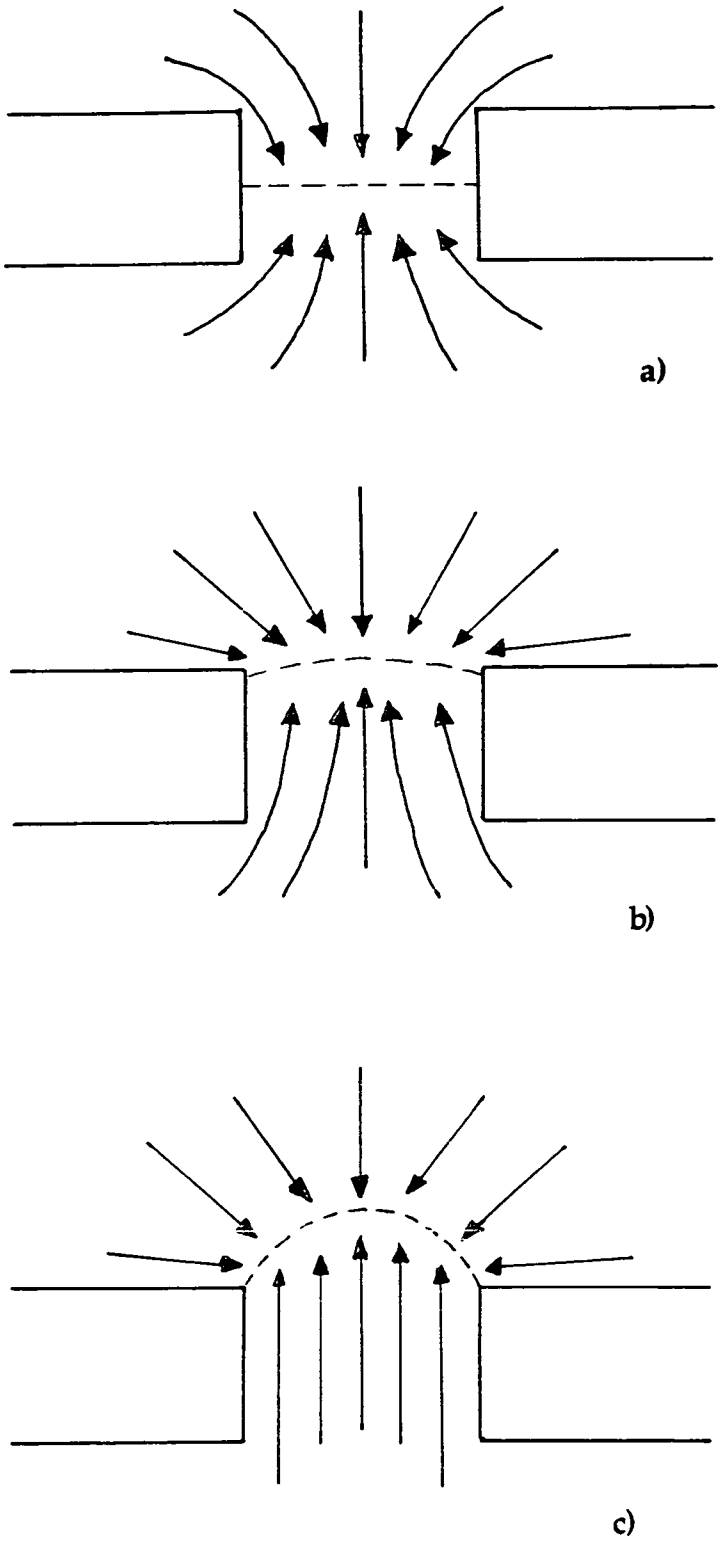

Fig. 28 Possible positions of the liquid/liquid interface at a microhole and lines of flux to the interface. a) symmetric, b) asymmetric, and c) asymmetric and highly curved.

from microdisc interfaces of the same radii as the microholes used. This irreproducibility is thought to derive from the variation in position and shape of the microinterfaces in different experiments. These differences will lead to altered diffusion characteristics and to a variety of interface sizes occuring at the same membrane hole. Membranes were inspected under the microscope after washing and drying between experiments and no obvious mechanical change in the membranes or holes was evident.
It was observed that in many experiments the onset of current peaking, indicating linear diffusion, was asymmetric as shown in figure 22b. This asymmetric behaviour is probably due to the interface being sited asymmetrically in the microhole. Indeed there are a whole range of positions which the interface may adopt from being flat and central in the membrane to a hemispherical or more extremely curved interface at either the aqueous or organic side of the membrane, as illustrated in figure 28. The asymmetric development of current peaking occured on both forward and reverse scans in different experiments and hence there did not appear to be a preferential siting of the interface on either the hydrophobic or the hydrophilic side of the membrane. It is likely that when the onset of current peaking is observed at the same sweep rate on forward and reverse scans the interface is in the centre of the membrane, although some asymmetry may be obscured by the potential window.

Attempts were made to alter the position of the interface by means of pressure control both by variation of electrolyte levels in the cell, and by sealing the aqueous compartment and varying its internal pressure with a syringe. Neither of these approaches altered the asymmetry or symmetry of onset of current peaking in experiments. This obstinate behaviour indicates that there must be some very strong interactions between the electrolyte solutions and the inside of the membrane which are not easily altered. The consequent lack of control over the position and size of the microinterface limits the quantitative usefulness of this technique at present.

The quantitative difference between the experimental results and those predicted from the theory for microdiscs is not significant in comparison with the lack of consistency between experiments. As the diffusion situation is rather different from a microdisc, even for the symmetrically

placed interface (in fact it is equivalent to a recessed disc), it would be surprising if the microhole results agreed precisely with those for a microdisc. Although it will be necessary to make a full mathematical simulation of the experiment for comparison before precise and reliable quantitative data can be obtained, if the results at a "symmetrical" interface proved consistent then an approximate formula for the limiting current could be used satisfactorily in place of that for the microdisc.

5.2.3 Kinetic Observations

The gradients of plots of $\ln(i_d-i)/i$ against potential gave the Nernst slope, showing reversible behaviour, for holes of 50 μm and 20 μm diameter. The decrease in gradient observed at holes of 10 μm and 5 μm diameter may be attributed in part to uncertainties from the sloping current baseline and the rather indistinct 5 μm hole wave, however the deviation from Nernstian behaviour is so significant for the 5 μm hole that there must either be a contribution from reaction kinetics, or solution resistance. Given that the voltammograms at 50 μm and 20 μm holes are undistorted by iR drop it is unlikely that the 5 μm hole voltammogram will be greatly distorted by iR drop. Unfortunately the wave cannot at present be analysed for kinetic data due to the uncertainty in the interface profile in the hole and therefore in the interfacial area.

5.2.4 Capacitance and Hysteresis

Although there is a small amount of capacitive current observed at the microholes which leads to a hysteresis which increases with sweep rate as seen in figures 20, 21b and 22a, there is also a residual hysteresis effect which is not proportional to sweep rate. It appears from figure 19 that this effect arises from background current due to supporting electrolyte and trace impurities.

5.2.5 Microhole Arrays

Qualitatively and quantitatively the microhole array results are similar to those obtained from the single microholes. It is clear from the steady state waves observed, that the holes are sufficiently separated to behave as isolated interfaces. It is hoped that the use of arrays of large numbers of holes may average out effects caused by the position of membranes in holes and therefore make results much more reproducible, but there has

not yet been time to test this hypothesis. Despite the use of four electrodes the plot of $\ln(i_d-i)/i$ does indicate significant distortion by iR drop due to the large currents being passed and these results would probably be improved by the use of feedback iR compensation.

ASSISTED ION TRANSFER

6.1 RESULTS

The transfers of the alkali metal cations, Li^+, Na^+, K^+, Rb^+ and Cs^+, with the complexing crown ether dibenzo-18-crown-6 (DB18C6) were studied, as well as the transfer of Li^+ with benzo-15-crown-5 (B15C5) as a complexing agent. All experiments were conducted using cells similar to CELL4 with reactant concentrations varying as specifiedin the text. MCl represents the alkali metal chloride and crown represents a crown ether.

Ag/AgCl	0.1M MCl	XmM Crown 10mMTBATPBCl DCE	10mM TBACl 45mM $MgCl_2$	AgCl/Ag

CELL4

6.1.1 The Large ITIES

Slow cyclic voltammetry experiments at a large interface (0.196 cm^2, fig 9) were conducted for all the above reactions under pseudo first order conditions, i.e. with the alkali metal ion concentration in vast excess in comparison with that of the crown ether. These experiments with the lithium, sodium and potassium cations gave cyclic voltammograms with a 60 mV peak separation and a peak current proportional to the square root of sweep rate. Figures 29 and 30 show the cyclic voltammetry of Li^+/B15C5 and Na^+/DB18C6 as typical examples of this behaviour. The diffusion coefficients of the two crown ethers in dichloroethane were determined from these sweep rate dependencies and were found to be 7.3×10^{-6} and 6.3×10^{-6} $cm^2\ s^{-1}$ for B15C5 and DB18C6 respectively.

The DB18C6 assisted transfer of rubidium ion showed similar large scale cyclic voltammetry (figure 31) with peak separations of 60 mV and proportionality of peak current to square root of sweep rate. The magnitude

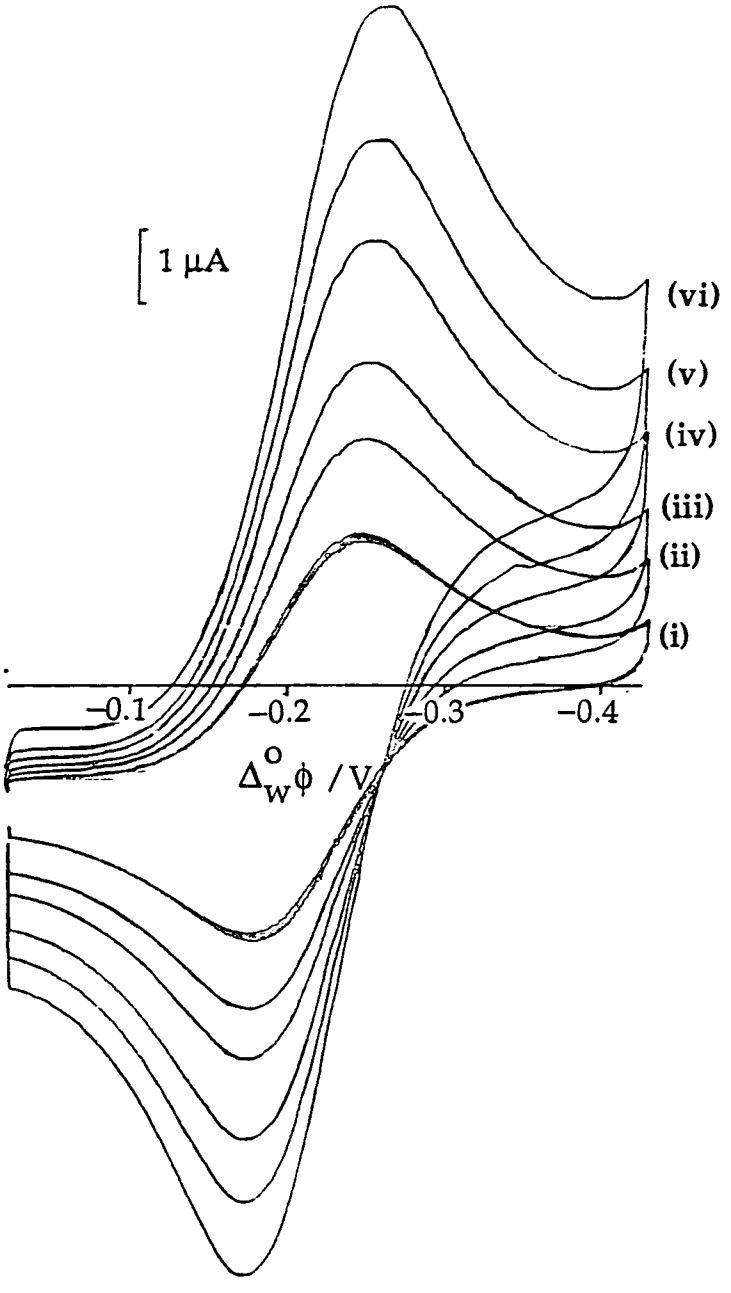

Fig. 29 Cyclic voltammograms of Li^+ crossing assisted by B15C5, concentration X (CELL4) = 0.2, sweep rates were: (i) 10, (ii) 20, (iii) 30, (iv) 50, (v) 70, and (vi) 100 mV s^{-1}.

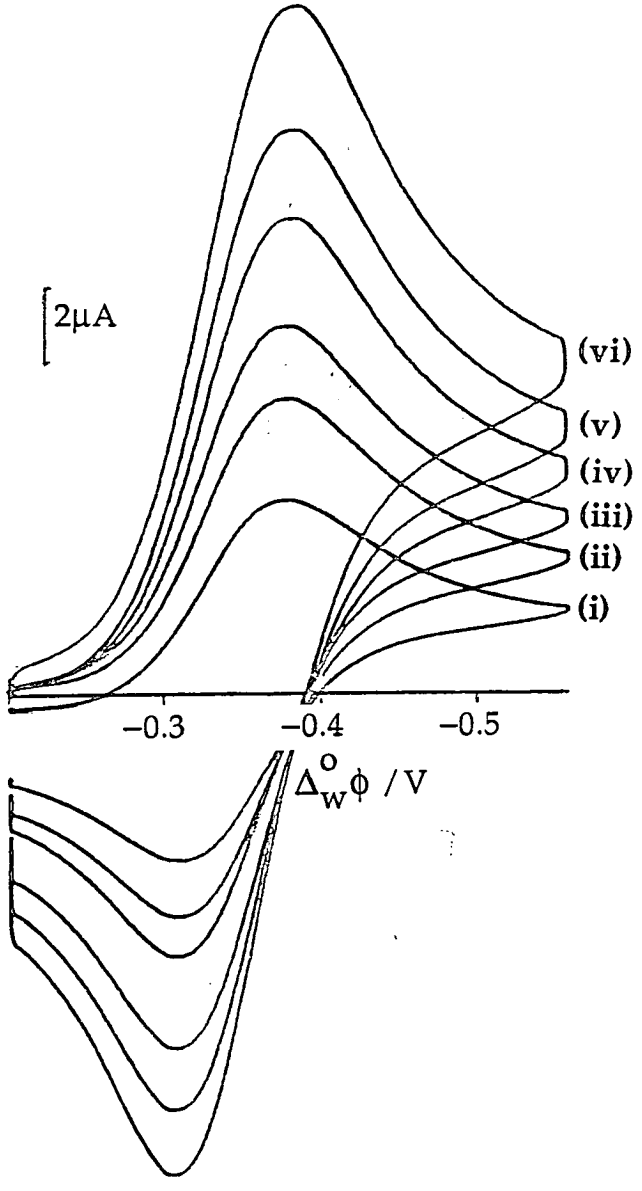

Fig. 30 Cyclic voltammograms of Na^+ crossing assisted by DB18C6, concentration X (CELL4) = 0.2, sweep rates were: (i) 10, (ii) 20, (iii) 30, (iv) 50, (v) 70, and (vi) 100 mV s^{-1}.

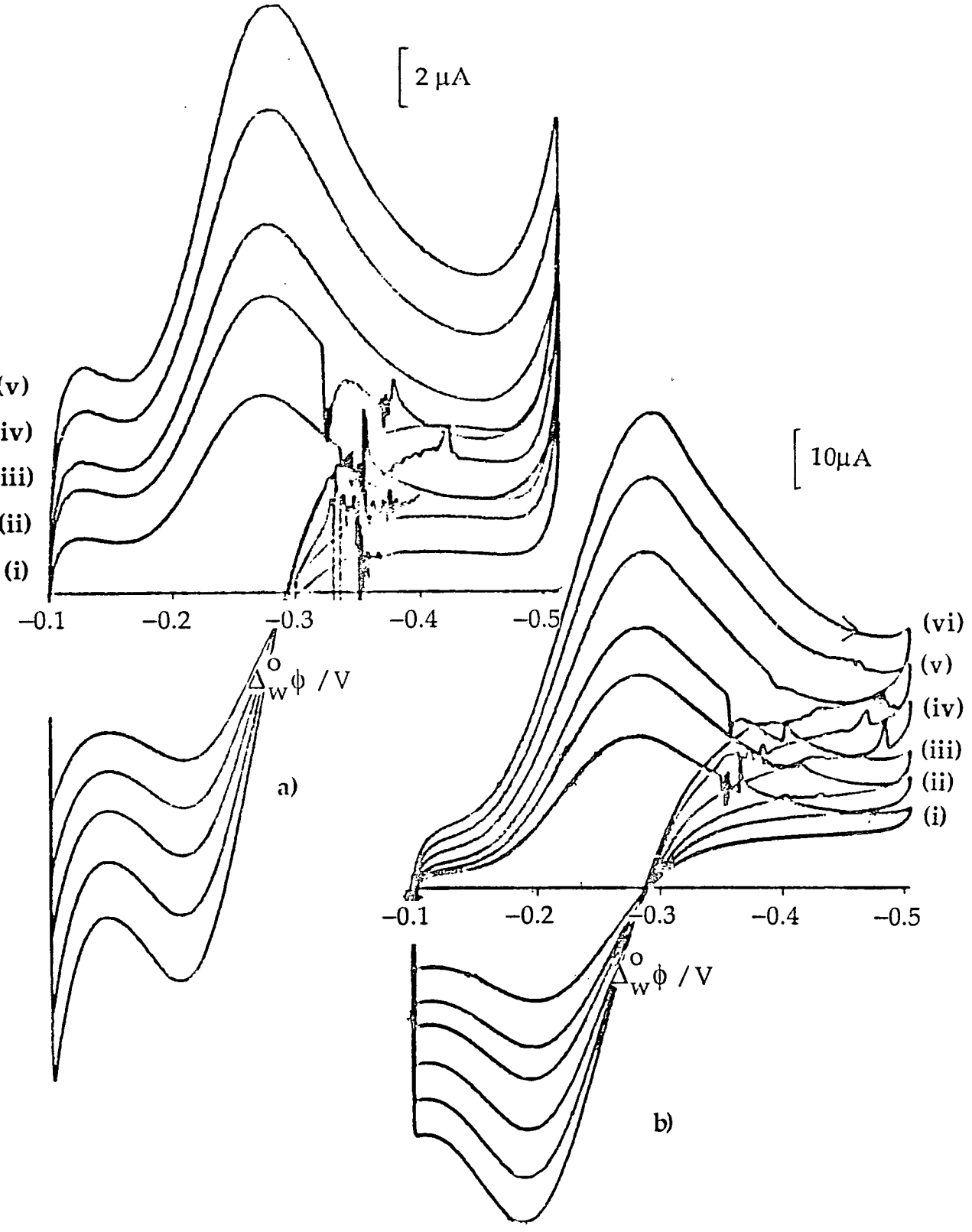

Fig. 31 Cyclic voltammograms of Rb^+ crossing assisted by DB18C6 (CELL4). a) X = 0.4, b) X = 1.6. Sweep rates were: (i) 10, (ii) 20, (iii) 30, (iv) 50, (v) 75, and (vi) 100 mV s^{-1}.

of the peak current was however, a little lower than that expected for the concentration of crown ether used.

The large interface cyclic voltammograms for the DB18C6 assisted transfer of the caesium cation were recorded at various concentrations of crown ether as shown in figure 32 (p. 120 & 121). The voltammograms consisted of broad forward and reverse current peaks which increased in separation with increasing concentration. With 1.6mM DB18C6 the voltammogram appeared as two closely spaced and unresolved current peaks. The forward and reverse peak separations varied from 150 mV at higher concentrations to 60 mV at lower concentrations. The peak current was always proportional to the square root of sweep rate, but current densities were significantly lower than those expected on the basis of a 1:1 stoichiometry. The values of the peak separations, ΔE_p, the mid peak potentials, E_{mid}, and the apparent diffusion coefficients of DB18C6 (calculated from the sweep rate dependence assuming a 1:1 stoichiometry) are given in table 6 (p. 122) for different concentrations of crown ether and CsCl. An experiment was also conducted outwith pseudo first order conditions. Figure 33 (p. 123) shows cyclic voltammograms obtained from a 0.5mM CsCl solution in water, in contact with a 0.2mM DB18C6 solution in dichloroethane. The voltammograms show two current peaks on the forward sweep, the first corresponds to the assisted ion transfer reaction and the second to the non assisted ion transfer reaction of caesium. An association constant of $10^{6.86}$ dm^3 mol^{-1} for the complexation reaction was estimated from the difference in the mid peak potentials of the assisted and non assisted reactions using equation (38).

6.1.2 The Micro-ITIES

Cyclic voltammograms were also recorded for each system at a micro-ITIES supported at the tip of a micropipette. These experiments were all conducted under pseudo first order conditions with the aqueous phase situated inside the pipette. Typical cyclic voltamograms for these systems are given in figures 34-39 (p. 124-129) together with the plot for each current wave of $\ln((i_d - i)^n/i)$ versus potential, where i_d is the diffusion limited plateau current, i the instantaneous current at the given potential and n the stoichiometric coefficient for the crown ether. These figures display the sigmoidal shaped current waves expected from electrodes with dominant radial diffusion.

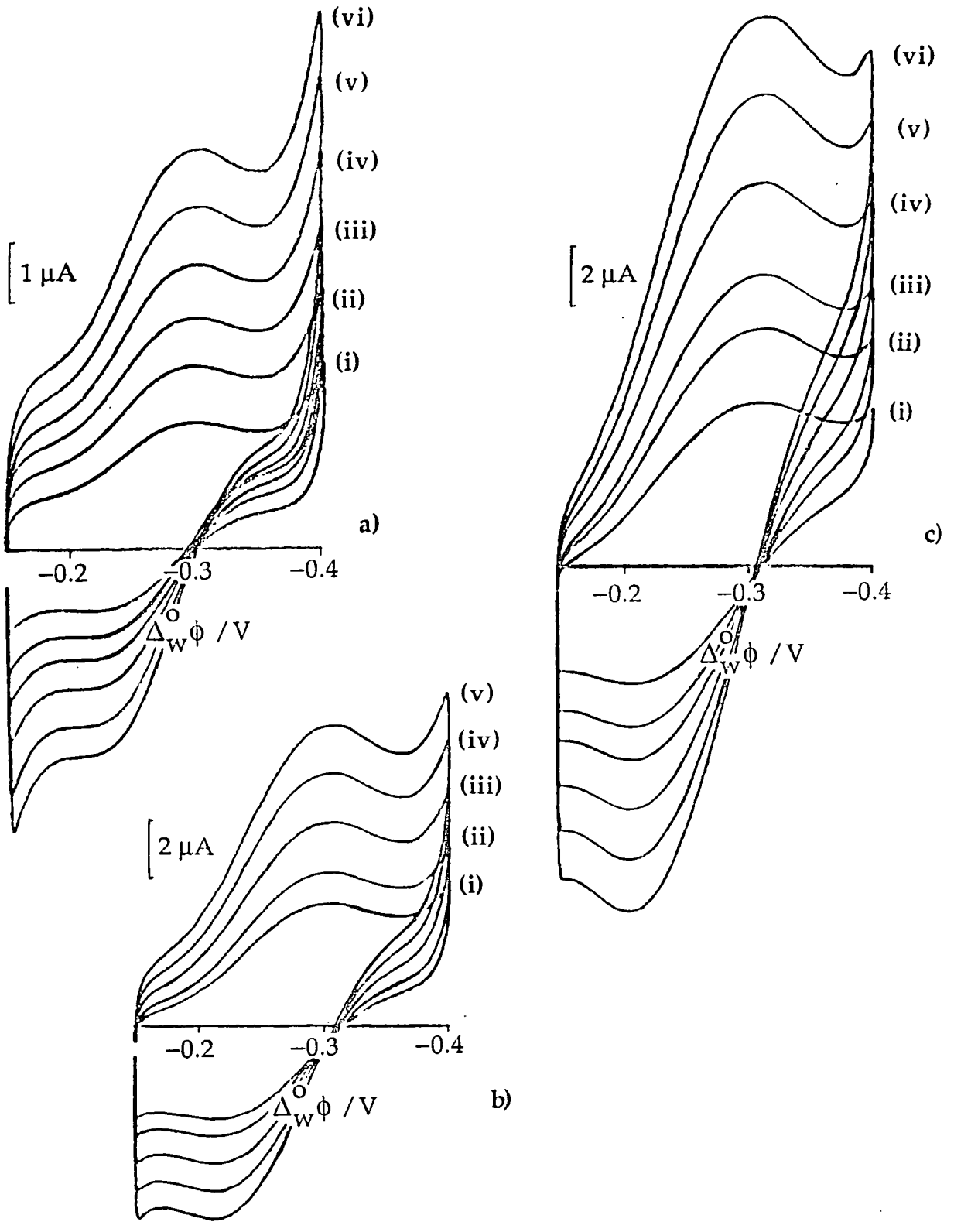

Fig. 32 Cyclic voltammograms of Cs^+ crossing assisted by DB18C6 at various concentrations: a) X = 0.1, b) X = 0.2, c) X = 0.4, d) X = 1.6, see next page, sweep rates were : (i) 10, (ii) 20, (iii) 30, (iv) 50, (v) 75, and (vi) 100 mV s^{-1}.

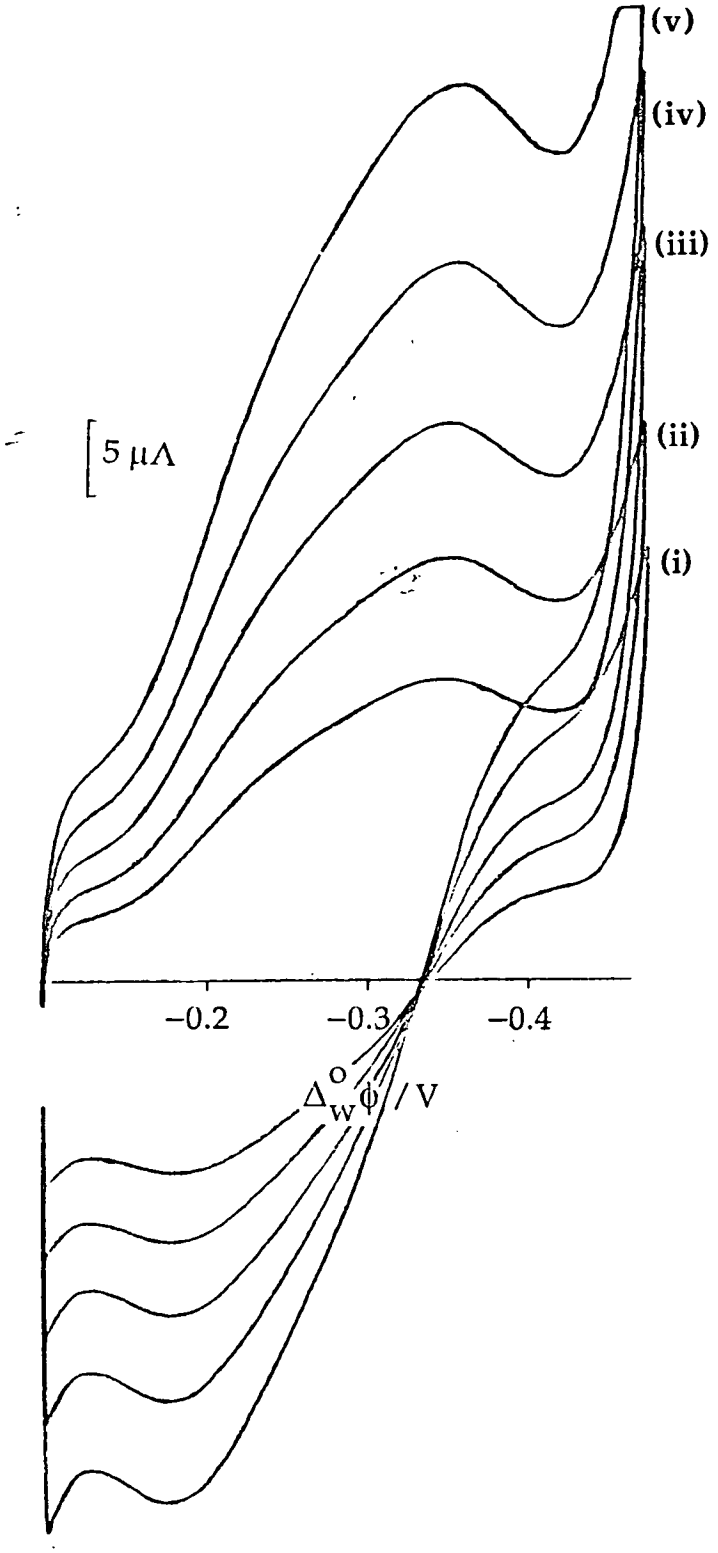

Fig. 32 **d)** As legend for fig. 32 on previous page.

Table 6

$[Cs^+]$ / mol l^{-1}	[crown]/ mol l^{-1}	$[Cs^+]$ / [crown]	ΔE_p/ m V	E_{mid}/ m V	D_{app}*/ $cm^2\ s^{-1}$	$(D_{real}/D_{app})^{1/2}$	T/°C
0.1	1.6×10^{-3}	62	150	−255	3.39	1.31	17
0.1	4×10^{-4}	250	100	−256	4.16	1.23	20
0.1	2×10^{-4}	500	75	−260	3.88	1.27	20
0.1	1×10^{-4}	1000	60	−253	3.55	1.33	20
5×10^{-4}	7×10^{-4}	0.7	135	−385	–	–	10
5×10^{-4}	2×10^{-4}	2.5	61	−381	4.6	1.07	10
			58	−584	–	–	

*D_{app} is D calculated assuming a 1:1 complexation

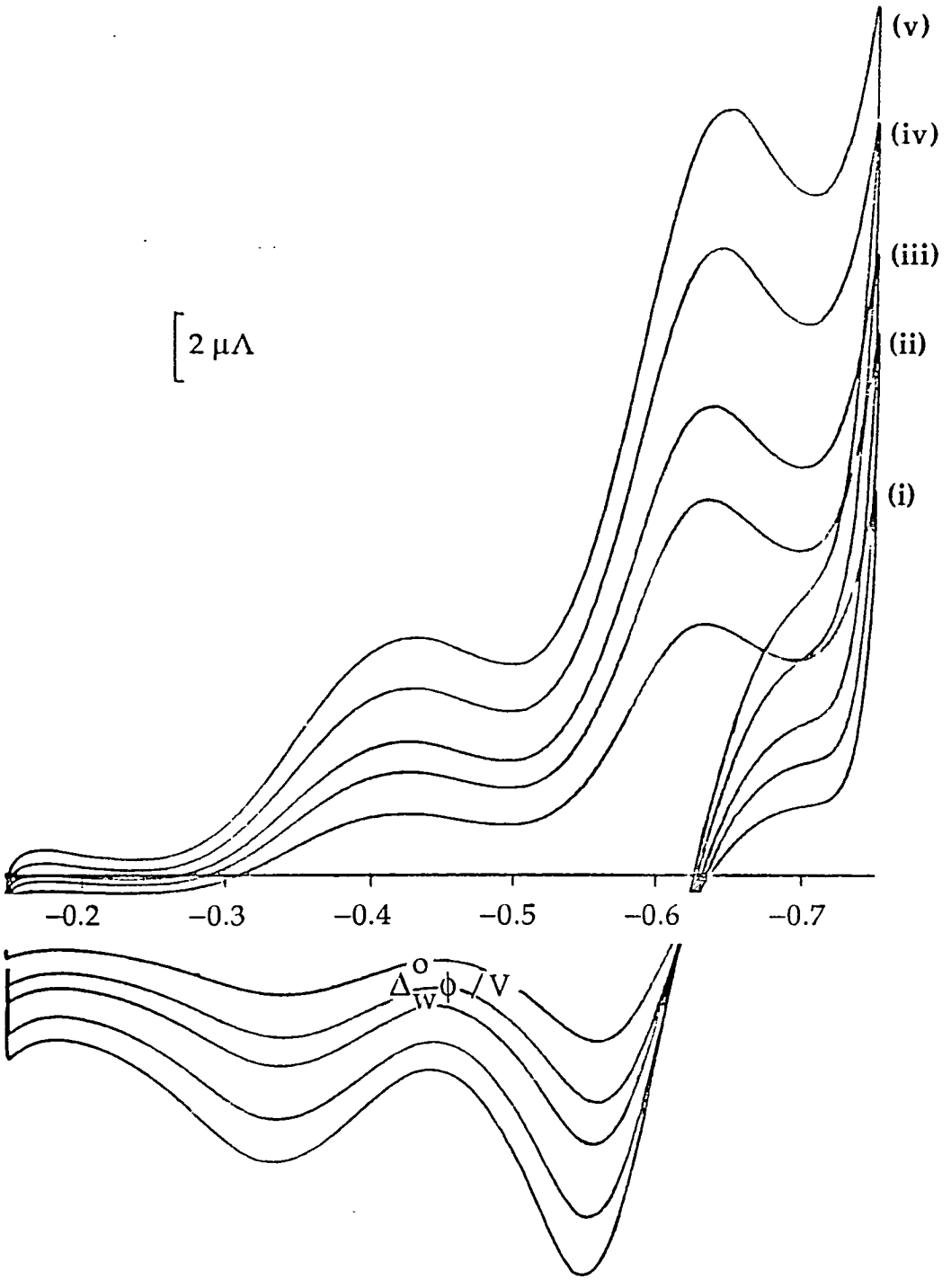

Fig. 33 Cyclic voltammograms of Cs^+ crossing assisted by DB18C6. CsCl concentration = 0.5 mM, DB18C6 concentration = 0.2 mM. Sweep rates: (i) 10, (ii) 20, (iii) 30, (iv) 50, and (v) 75 mV s^{-1}.

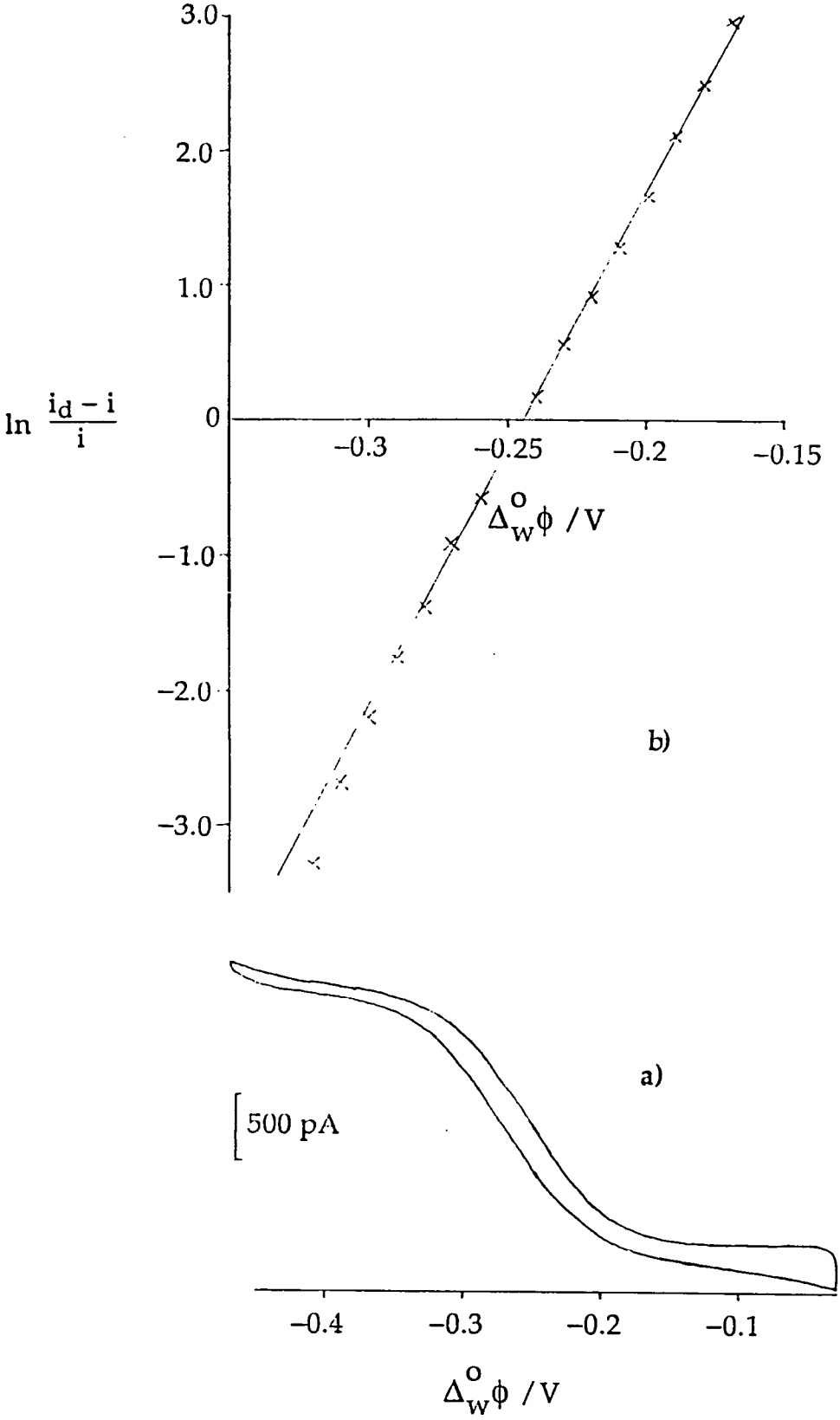

Fig. 34 a) Cyclic voltammogram of Li^+ crossing assisted by B15C5 (CELL4) X = 0.2, at a 10 µm diameter pipette and a sweep rate of 10 mV s^{-1}.

b) Semi-logarithmic plot from current wave.

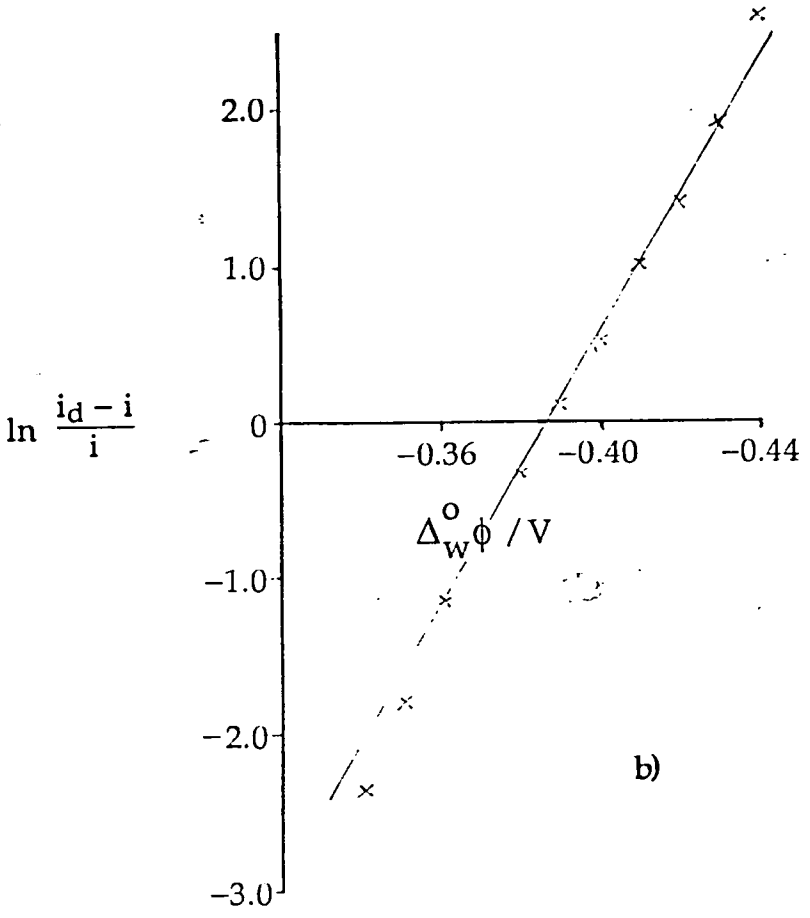

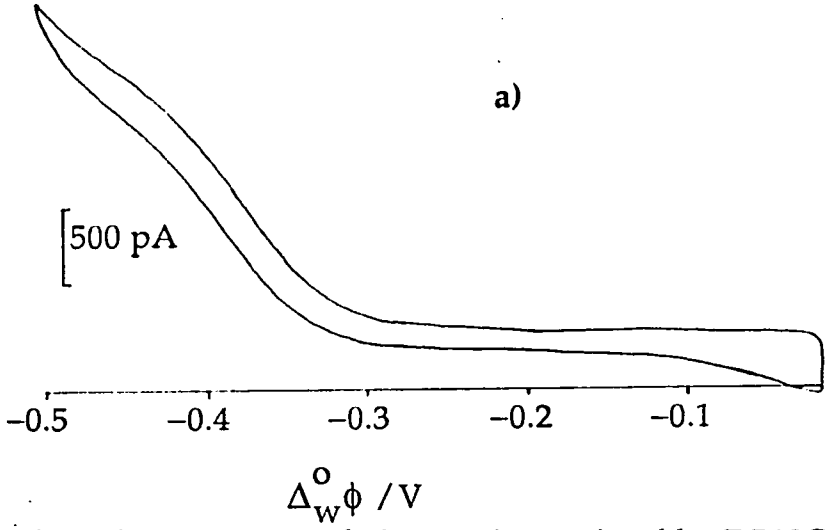

Fig. 35 a) Cyclic voltammogram of Li^+ crossing assisted by DB18C6 (CELL4) X = 0.2, at a 10 μm diameter pipette and a sweep rate of 10 mV s^{-1}.

b) Semi-logarithmic plot from current wave.

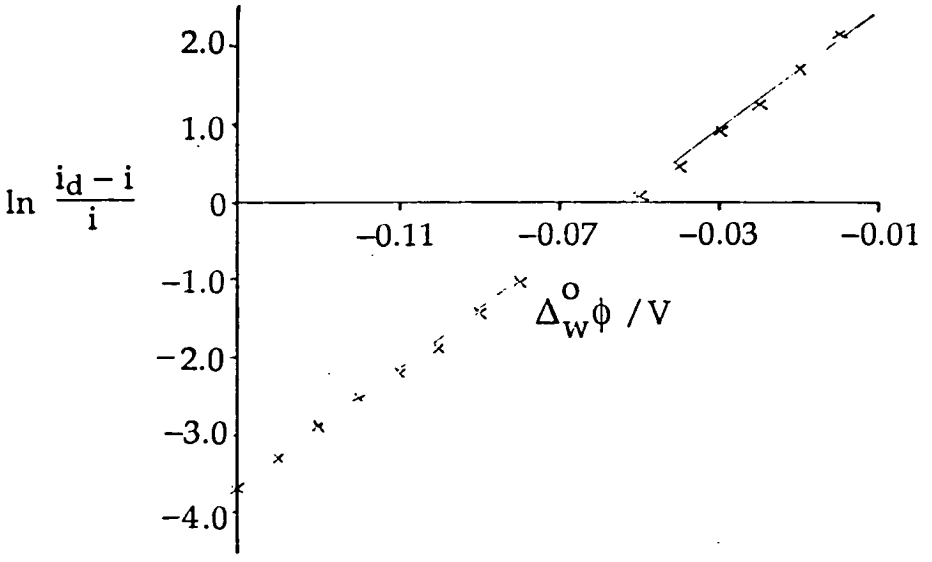

b) Semi-logarithmic plot from current wave.

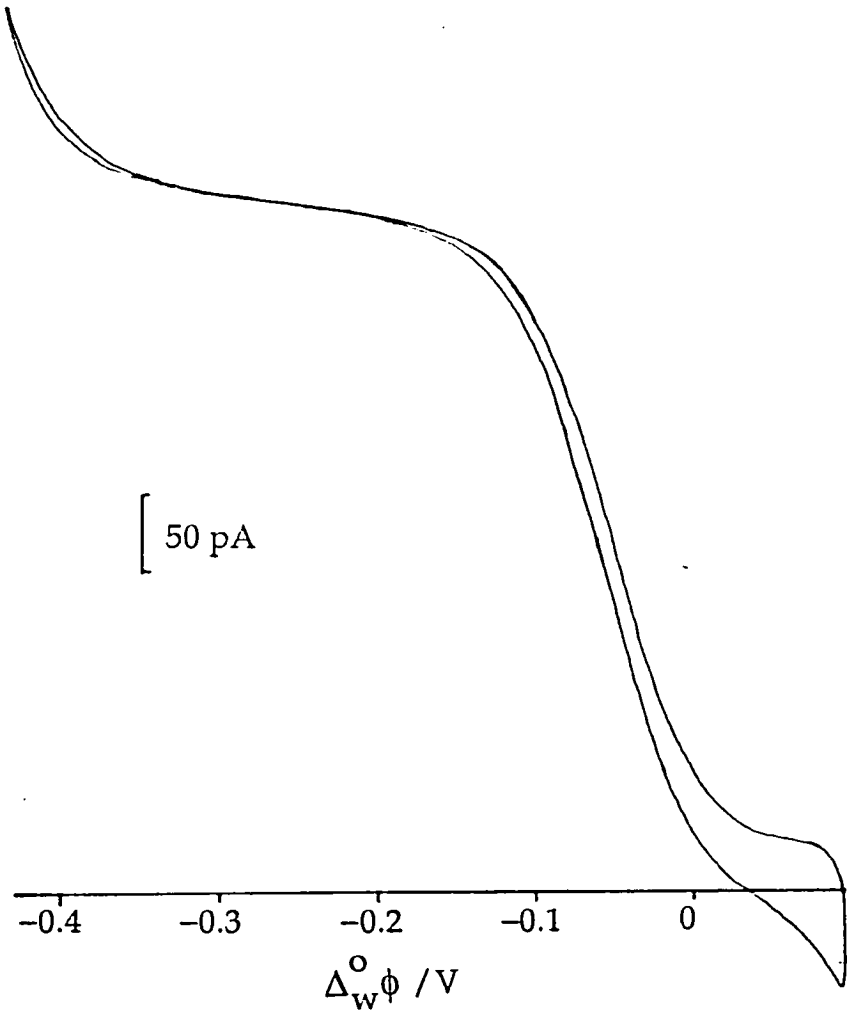

Fig. 36 a) Cyclic voltammogram of K^+ crossing assisted by DB18C6 (CELL4) X = 0.2, at a 4.5 μm diameter pipette and a sweep rate of 100 mV s^{-1}.

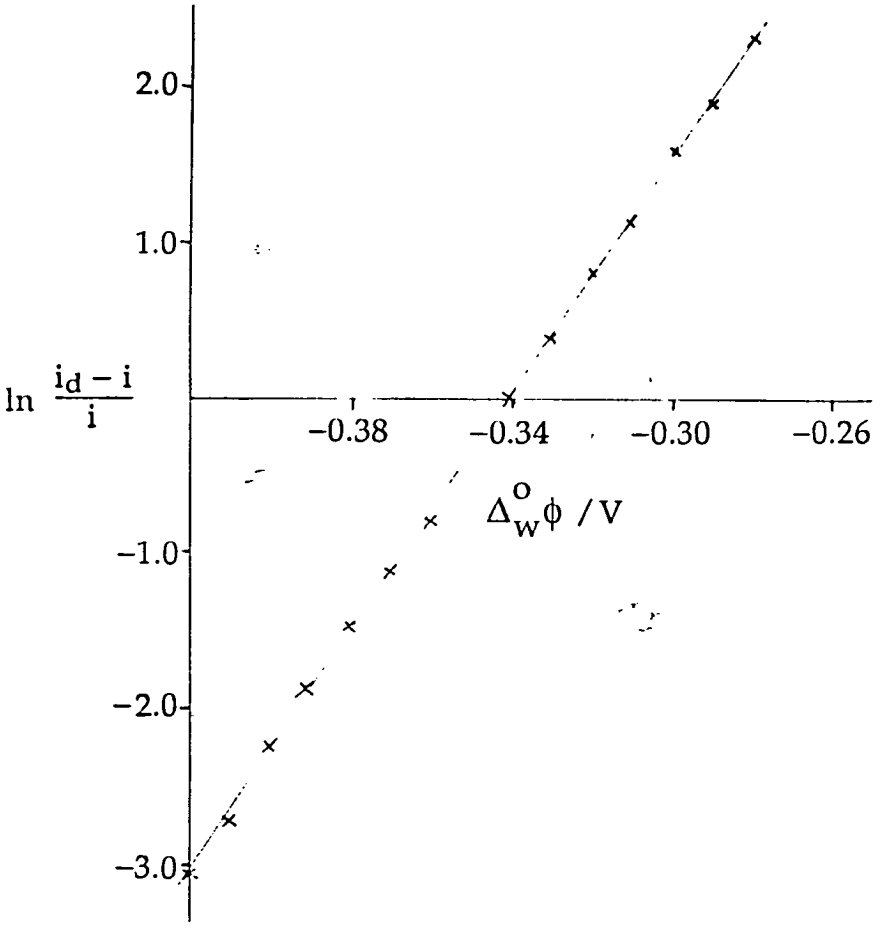

b) Semi-logarithmic plot from current wave.

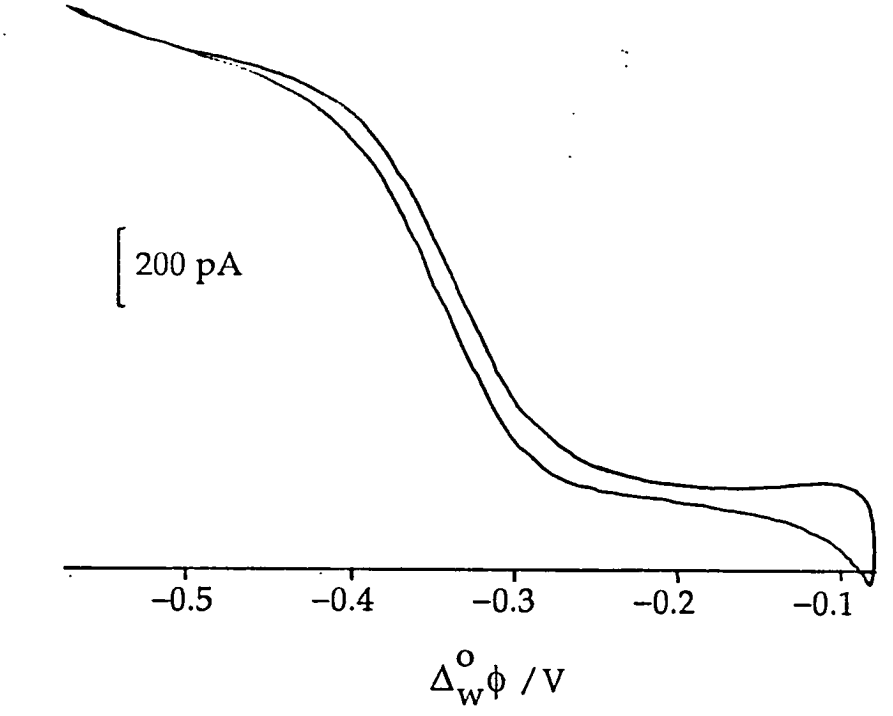

Fig. 37 a) Cyclic voltammogram of Na^+ crossing assisted by DB18C6 (CELL4) X = 0.2, at a 9.7 μm diameter pipette and a sweep rate of 100 mV s^{-1}.

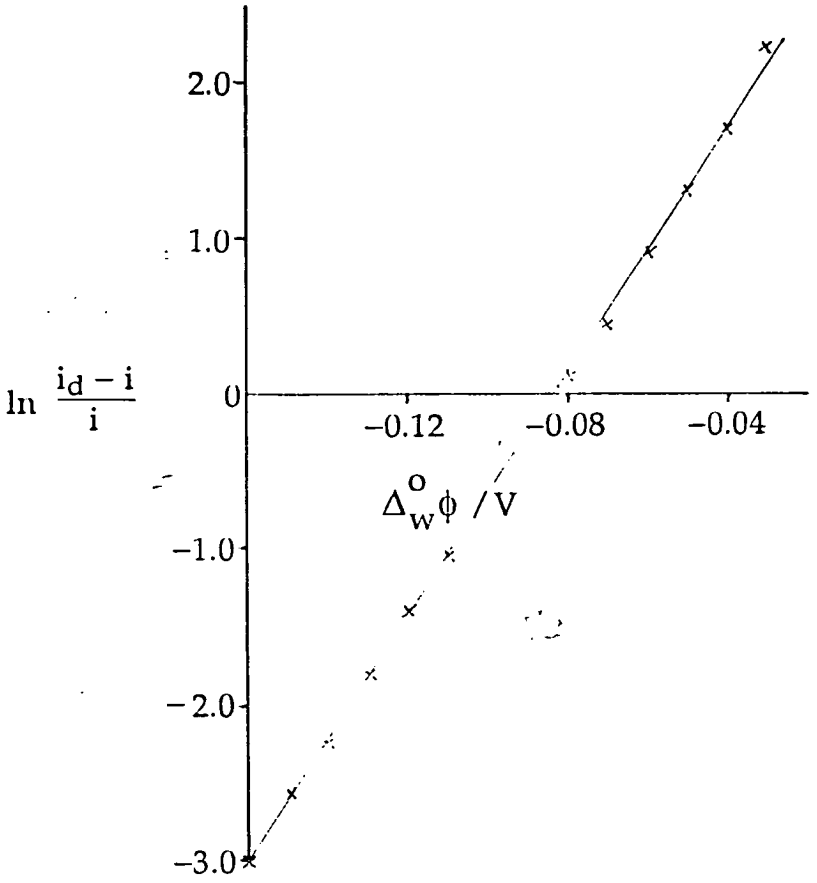

b) Semi-logarithmic plot from current wave.

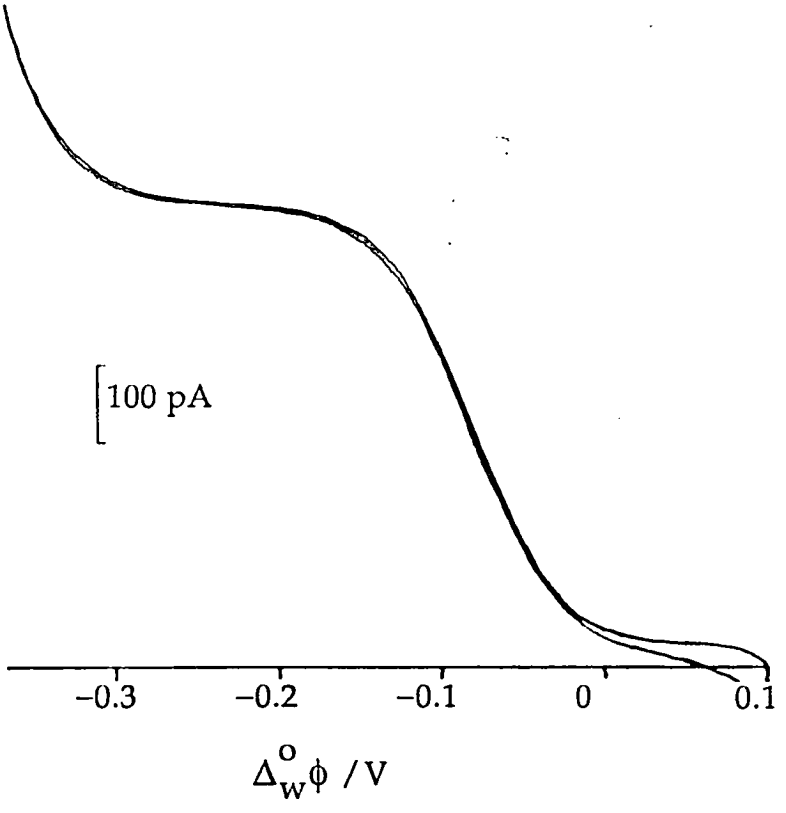

Fig. 38 a) Cyclic voltammogram of Rb^+ crossing assisted by DB18C6 (CELL4) X = 0.2, at a 6 μm diameter pipette and a sweep rate of 10 mV s^{-1}.

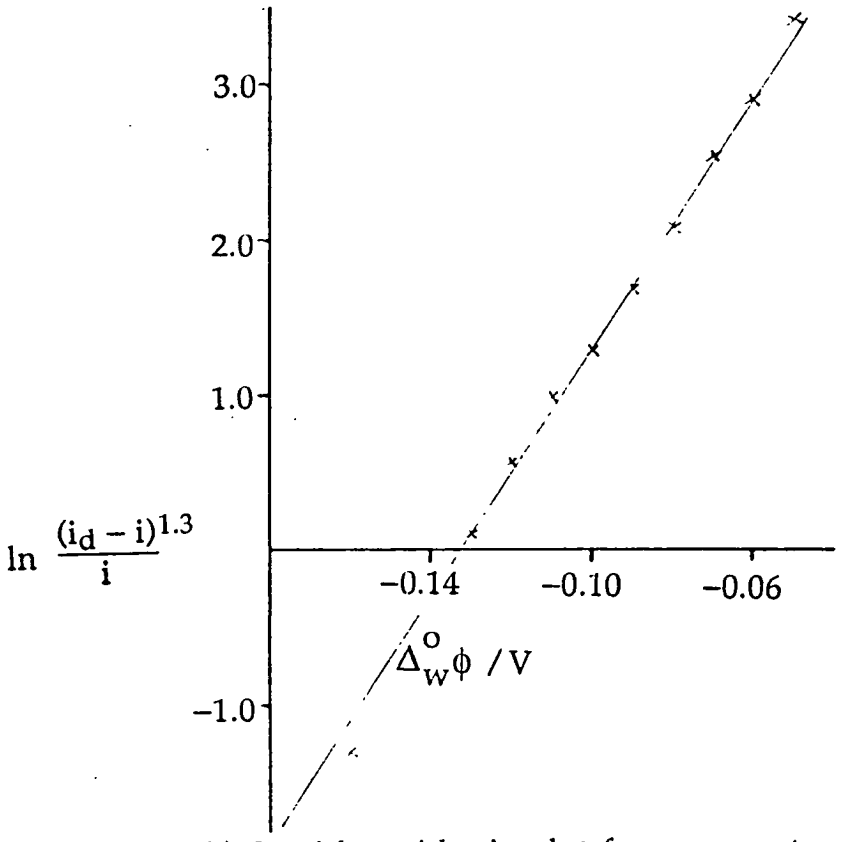

b) Semi-logarithmic plot from current wave.

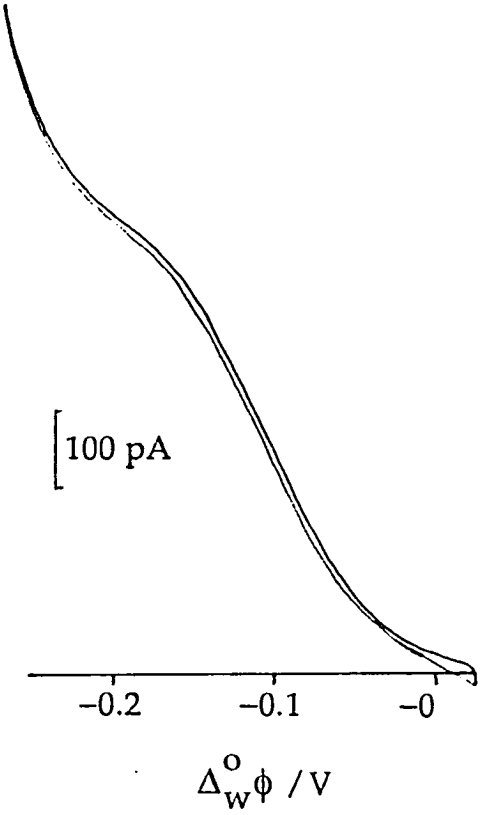

Fig. 39 a) Cyclic voltammogram of Cs^+ crossing assisted by DB18C6 (CELL4) X = 0.2, at a 20 μm diameter pipette and a sweep rate of 10 mV s^{-1}.

The gradients of the plots of $\ln((i_d - i)^n/i)$ are given in table 7 together with the Tomeš criteria, $E_{1/4} - E_{3/4}$.

Although the height of the current plateau is independent of the sweep rate in the range 20 – 200 mV s^{-1}, showing that the wave is "steady state", the magnitude of the plateau current was not directly proportional to the pipette radius as would be expected for a microdisc or a microhemisphere electrode. There was no reproducible proportionality between the plateau current and the micropipette radius, but the currents observed were consistently higher than those that would be predicted from either a disc or a hemisphere of the same radius. Table 7 shows the plateau currents divided by crown ether concentration obtained from different pipette radii together with the expected current from a hemispherical electrode of the same radius and the effective interface radius if a hemispherical electrode is assumed.

Under the pseudo first order conditions employed, and using TBATPBCl as the organic phase supporting electrolyte, the oil negative end of the potential window is formed in every case by the non assisted alkali metal ion transfer reaction. Using the value of the association constant determined above for the assisted caesium ion transfer reaction it was thus possible to estimate the association constant for each of the other reactions from the potential difference between the half wave potential and the end of the potential window. This method assumes that the half wave potential is coincident with the effective formal potential for the assisted ion transfer, i.e. that the ratio of complexed and non complexed crown diffusion coefficients is equal to one and that the wave is electrochemically reversible (see below). Determining the position of the foot of the current wave forming the end of the potential window can only be regarded as a rather approximate procedure and, together with the above assumption, this results in rather large error bound estimates for the values of K_1 given. It would have been preferable to undertake a determination from a voltammogram such as that for caesium in figure 33, however it is only in the case of caesium that a sufficiently inert aqueous supporting electrolyte is available to allow the non assisted ion transfer to be observed. The association constants thus determined are listed in table 8 together with values published by other investigators[43].

Table 7

Reaction	[crown]/ mM	grdt $\ln(i_d-i)^n/i$ /V^{-1}	$E_{3/4}-E_{1/4}$ /mV	pipette radius/ μm	effective pipette radius/μm	i_d/[crown]/ mA l mol^{-1}	$i_{d,\,expected}$/ [crown]/ mA l mol^{-1}
Li/B15C5	0.2	38.8	57.5	5.0	20	9.05	22.1
Li/DB18C6	0.2	43.0	50.0	5.0	19	7.25	19.1
Na/DB18C6	0.2	35.8	57.5	2.7	4.6	1.75	10.3
K/DB18C6	0.2	38.6	57.5	2.3	5.0	1.90	8.78
Rb/DB18C6	0.2	38.9	56.0	3.0	9.9	2.65	8.00
Cs/DB18C6	0.2	33.5	57.5	10.0	9.6	2.15	22.4

Using B15C5 diffusion coefficient of 7.3 $x10^{-6}$ cm^2 s^{-1}
Using DB18C6 diffusion coefficient of 6.3 $x10^{-6}$ cm^2 s^{-1} for Li, K and Na, 4.4 $x10^{-6}$ cm^2 s^{-1} for Rb and 3.7 $x10^{-6}$ cm^2 s^{-1} for Cs.

Table 8

Reaction	$Log_{10} K_1$ +/− 0.3 DCE	$Log_{10} K_1$ DCE*	$Log_{10} K_1$ nitrobenzene*
Li/B15C5	8.42	–	–
Li/DB18C6	6.86	11.3	4.8
Na/DB18C6	10.4	11.2	7.3
K/DB18C6	10.4	9.9	7.2
Rb/DDB18C6	8.87	8.3	5.2
Cs/DB18C6	6.86	–	–

From Samec' and Papoff's data, ref 43

6.2 DISCUSSION

6.2.1 Reaction Stoichiometry

In order to interpret the experimental results it is first of all necessary to determine the reaction stoichiometries involved as these effect both the peak height and the peak separation of cyclic voltammograms. Reaction stoichiometries have been determined for various crystalline complexes of polyethers and alkali metal salts as reported by Pedersen[1,119]. In the crystalline case the stoichiometries were observed to be dependent on the diameter of the alkali metal cation relative to the diameter of the oxygen ringed hole in the crown ether compound, see figure 40. Ions smaller than the crown hole gave 1:1 stoichiometries whereas larger ions required two crown ethers to form a complex. In the case of DB18C6, sodium and potassium salts gave a 1:1 stoichiometry, rubidium both 1:1 and 1:2 (ion:crown) stoichiometries and caesium 1:2 and 2:3 stoichiometries. The only lithium salt reported was that of a 14-crown-4 complex which gave 1:1 stoichiometry. As the lithium cation is smaller than both the 15-crown-5 and 18-crown-6 "holes" it is reasonable to predict a 1:1 complexation stoichiometry.

In the present situation, where complexes are being formed in an interfacial process with a limiting concentration of crown ether, it is reasonable to expect that 1:1 complexation reactions will dominate, even where a different stoichiometry is thermodynamically favoured[41], due to restrictions imposed by limiting transport of the complexing crown to the interface. If the complexation reaction actually occurs "at the interface" the two dimensional nature of the interface may impose steric and kinetic constraints on a 1:2 or 2:3 complexation reaction. In other words there is a possibility of formation of a kinetic product over a thermodynamic product. How this phenomenon might be manifested experimentally is unclear.

The large scale cyclic voltammetry of the Li^+, Na^+ and K^+ assisted reactions herein observed (figures 29 and 30) give a 60mV peak current separation independent of potential sweep rate. This indicates a reversible 1:1 stoichiometry which is in agreement with the crystalline salt stoichiometries mentioned above. The Na^+ and K^+ assisted transfer reactions have also been reported by other workers as reversible and of 1:1 stoichiometry at the large interface[120,2,38]. The diffusion coefficients, at 20 ^oC, for DB18C6 in

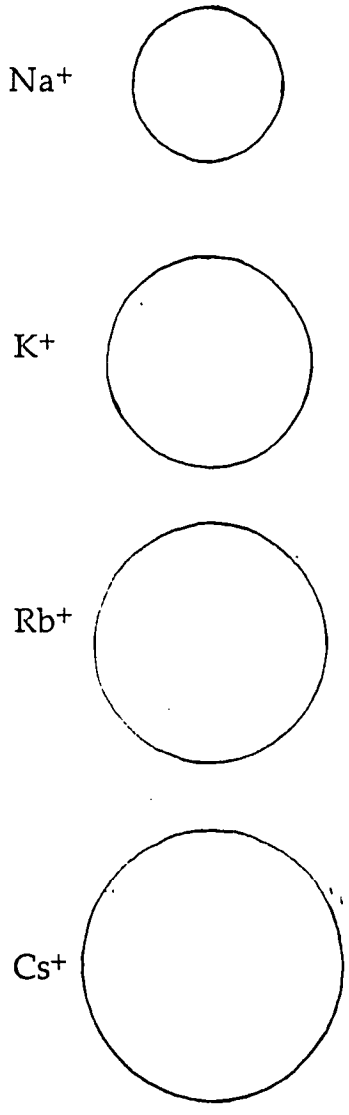

dibenzo-18-crown-6, cavity diameter 0.4 nm

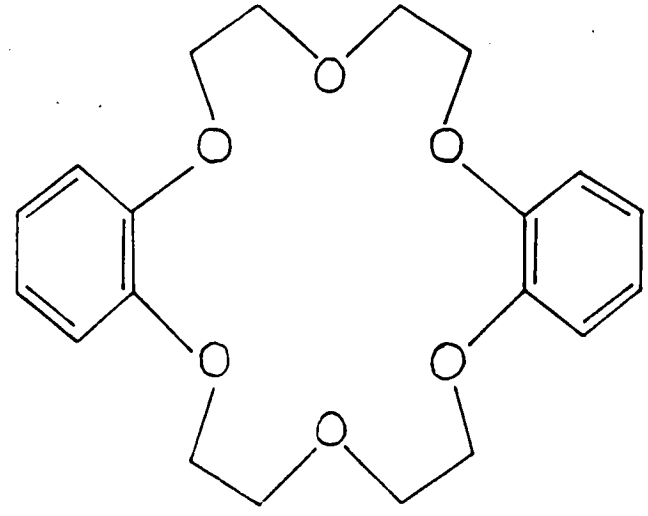

Fig. 40 Comparison of DB18C6 cavity with alkali metal ion diameters

dichloroethane of $6.3 \pm 0.3 \times 10^{-6}$ $cm^2 s^{-1}$, quoted above, is a little larger than that of 5.9×10^{-6} $cm^2 s^{-1}$ reported by Freiser et al[120]. A literature value for B15C5 in dichloroethane is not available for comparison.

The large ITIES cyclic voltammetry of the assisted caesium transfer reaction showed a marked variation with crown ether concentration, as described in the results section above. To summarise; the peak current separation is independent of sweep rate but appears to increase with increasing crown ether concentration (fig 32 and table 6) until, at a concentration of 1.6 mM DB18C6, the current signal begins to look like two distinct, but unresolved, current peaks. The midpoint potential of the peak(s) is constant over the concentration range investigated, within the limits of experimental error. The peak currents were directly proportional to the square root of potential sweep rate, but the diffusion coefficients calculated from this dependence (assuming a 1:1 stoichiometry) ranged from 3.4×10^{-6} $cm^2 s^{-1}$ to 4.6×10^{-6} $cm^2 s^{-1}$, and are significantly smaller than the 6.3×10^{-6} $cm^2 s^{-1}$ determined above. The ratio of the square roots of the actual and expected diffusion coefficients is about 0.75. This means that the concentration of crown ether at the interface is resulting in the transfer of only 75% of the charge that would be expected given a 1:1 reaction. A 1:2 stoichiometry reaction is expected to result in approximately 50% of charge transfer versus the 1:1 reaction. These results indicate that there are in fact two interfacial complexation reactions occuring. One involves the formation of a 1:1 complex and the other the formation of a 1:2 complex (ion:crown). At lower crown ether concentrations the two reactions appear to take place at the same potential giving only one current wave , but an increase in crown ether concentration causes the 1:2 complexation to occur at a less negative potential than the 1:1 complexation.

This conclusion is confirmed by Kakiuchi's recent theoretical analysis of the current potential curves for facilitated ion transfer across the liquid/liquid interface[121]. Kakiuchi considers the case where two complex species may be formed, having ion:ligand ratios 1:1 and 1:2, and calculates the cyclic voltammograms for the reversible pseudo first order case over a range of association constants and ligand concentrations. Kakiuchi and Senda's results show that two peaks will occur, the separation of which is dependent on the ratio of the dimensionless association constants, b_2/b_1, which is equal to $K_2C_1^b$, where K_2 is the association constant for the complexation of the second

ligand and C_l^b is the bulk concentration of the ligand in the oil phase. A reduction in C_l^b is shown to lead to a merging of the two waves while the mid point potential is unaltered, as is observed experimentally here. According to Kakiuchi the mid point potential of the merged waves and the two separate waves corresponds to the mid point potential for the isolated 1:1 complexation reaction. This means that the difference between this potential and the mid peak potential for the non assisted transfer reaction may reasonably be used to calculate the association constant for the 1:1 complexation reaction, K_1.

Figure 33, which is obtained with only 0.5mM CsCl and 0.2mM DB18C6, shows two distinct and well separated waves. The first wave corresponds to the assisted transfer reaction (both 1:1 and 1:2 stoichiometries) and the second, at the more negative oil versus water potential, corresponds to the non assisted transfer reaction. The mid point potential of the assisted transfer wave is shifted negative by approximately 130 mV relative to that obtained under pseudo first order conditions due to the decrease in the concentration of the Cs^+ ion by a factor of 200. The association constant of $10^{6.86}$ calculated in the results section from this voltammogram may, according to the results of Kakiuchi, be deduced to be that for the 1:1 complexation reaction.

Under pseudo first order conditions a further increase in the crown ether concentration over the maximum of 1.6 mM used here may allow complete resolution of the 1:1 and 1:2 complexation waves and hence a calculation of K_2, but there was not time to fully investigate this aspect of the reaction. Performance of the experiment with an excess of crown ether would also be interesting, but is difficult to achieve due to the low solubility of the crown ether and the likelihood of competing transfer reactions from the aqueous supporting electrolyte .

The large scale rubidium cyclic voltammetry results gave a sweep rate independent peak separation of 60 mV with 0.4 mM DB18C6, typical of a reversible 1:1 complexation reaction. The peak currents observed are however somewhat smaller than would be expected for this case. The diffusion coefficient for DB18C6, calculated on the basis of 1:1 complexation, was 4.43×10^{-6} , 5.62×10^{-6} and 5.90×10^{-6} $cm^2 s^{-1}$ for 0.4 mM, 0.8 mM and 1.6 mM concentrations of crown ether respectively. Experimental error is estimated at $\pm 0.3 \times 10^{-6}$ $cm^2 s^{-1}$. These low diffusion coefficients indicate

that some 1:2 complexation may be occuring. The cyclic voltammograms in figure 31 do not show the distortion evident in the caesium assisted transfer voltammograms under similar concentration conditions and it is difficult to draw a firm conclusion as to the stoichiometry of the reaction, except that any 1:2 complexation occuring is less thermodynamically favoured over the 1:1 complex than in the case for the caesium complexation reaction.

6.2.2 The Micro-ITIES

6.2.2.1 The Shape of the Wave

The micropipette results displayed in figures 34 - 39 are characteristic in shape of those obtained from redox reactions at solid microelectrodes. The existence of a plateau current independent of sweep rate, rather than a sweep rate dependent peaked current, shows that radial rather than linear diffusion is controlling, and that the micropipettes are being operated in "steady state" mode. This symmetrical wave is different from the shape exhibited by non assisted ion transfer at a micropipette which consists of a plateau current when the ion is transfering from outside to inside the pipette and a peak current when the ion is transfering from inside the pipette to outside[52,122]. In the present case of assisted ion transfer conducted under pseudo first order conditions (with the species inside the pipette in vast excess to that outside) the current is limited on both forward and reverse sweeps by the low concentration species which, being very hydrophobic in both the complexed and free form, always remains in the organic phase outside the pipette, and hence always diffuses in a radial fashion for both forward and reverse reactions.

6.2.2.2 Thermodynamic Observations

It is useful to note that the oil negative end of the potential window is formed by the non-assisted, alkali metal cation, transfer from water to dichloroethane. This may be deduced from the fact that there is no current peak at the end of the potential window on the return sweep, and hence the returning ion transfer must be occuring by radial diffusion and hence by diffusion of a species from the outside of the pipette[110]. This knowledge enabled the

calculation of the association constants, K_1, as described in section 6.1.2 above and displayed in table 8. Table 8 also gives K_1 values in dichloroethane and nitrobenzene as determined by Samec and Papoff in a recent publication[43]. The present results show a trend in stability constants, and hence selectivity, similar to that observed by Samec and Papoff with nitrobenzene, but they are significantly different from those reported by the same authors for dichloroethane. According to the results herein reported the selectivity sequence of DB18C6 in dichloroethane is $Na^+ \approx K^+ > Rb^+ > Li^+ \approx Cs^+$, whereas Samec and Papoff report; $Li^+ \approx Na^+ > K^+ > R^+ > Cs^+$. Knowing that the oil negative end of the potential window in the micro-ITIES experiments is caused by the non assisted alkali metal ion transfer means that a simple comparison of the positions of the assisted ion transfer waves in the windows in figures 34-39 confirms the order of stability constants reported here and the results reported by Samec for dichloroethane must therefore be in error. It should be noted that the magnitudes of the association constants for K^+ and Rb^+ in dichloroethane given by Samec, and those determined here, probably agree within experimental error (Samec does not give error bound estimates). It is likely that the disagreement in the Na^+ and Li^+ values observed arises from errors in the formal potentials, $E^{o'}$, for the non assisted transfers of these ions from water to dichloroethane. These were determined by Samec and Papoff "by extrapolation" [43]. These extrapolated values of formal potential were then used to calculate the association constants in disagreement with those determined here and are most likely incorrect. Using the more reliable association constants determined here it would be possible to back calculate the formal potentials of Na^+ and Li^+.

As noted by Samec and Papoff [43], the association constants in dichloroethane are about 10^3 times larger than those in nitrobenzene and their conclusion that this difference is largely due to the lower donating ability of dichloroethane and hence the lower stability of the uncomplexed cations in the dichloroethane versus the nitrobenzene phase seems reasonable. Further conclusions about the cation solvation becoming dominant over crown ether cavity size effects, and hence changing the selectivity sequence of DB18C6 for the different cations in different solvents, are no longer substantiated by a change in the selectivity order from nitrobenzene to dichloroethane. There are however changes in potassium ion selectivity over sodium when comparing methanol, 1,2-propylene carbonate and water with acetonitrile, nitrobenzene and dichloroethane[43]. In the former solvents DB18C6

preferentially complexes K^+ over Na^+, whereas in the latter solvents there is slight selectivity for Na^+ over K^+, or equal selectivity. This evidence indicates that while crown cavity size effects are significant they are not entirely dominant in determining selectivity in some solvents.

6.2.2.3 The Magnitude of the Wave

The observation (table 7) that the diffusion limited currents are generally significantly higher than expected from a flat or hemispherical interface of the same radius as the pipette tip means that the interfaces formed have a geometry giving a significantly greater surface area than a hemisphere. This could be caused by the formation of a pendant drop or by the aqueous phase wetting the outer surface of the pipette to a certain extent. The plateau currents were not reproducible for a given pipette radius, hence implying that the interface was not of a reproducible geometry.

The unreproducible nature of the plateau current observed here differs from that observed for the non assisted transfer of the acetylcholine cation at a micropipette[122]. With an assisted ion transfer the plateau current is proportional to the pipette radius and approximately half way in magnitude between that expected from hemispheres and discs of the same radius. The difference in the present experiments probably stems from the surface active nature of the crown ethers which reduce the interfacial tension leading to wetting of the glass at the pipette tip and the formation of pendant drops.

In order for micropipettes to prove quantitatively useful beyond the measurement of half wave potentials it is necessary either to provide a reproducible interface, or to be able to measure the interfacial geometry for each experiment. It appears that the use of surface active substances disrupts the reproducibility of the interface. Control of the hydrostatic pressure in the pipette should enable control of the geometry of the interface. In work with patch clamp pipettes on cell membranes the pressure inside micropipettes is controlled by various syringe systems. A similar system was used to try and control the position of a liquid/liquid interface at the tip of a micropipette at Edinburgh, but attempts conducted so far have not proved successful[123] and further work is required. In situ microscopic observation of the pipette tip has also been undertaken. Throughout the above experiments the tips of the

pipettes were monitored using the zoom microscope and video camera previously described, however it was not possible to identify and precisely locate the interface due to optical distortions. It may be possible to partially remedy the poor optical properties of the system by the use of a flat optical glass cell, rather than the "U" tube presently employed, and this modification is currently being implemented. Optical magnification is not however likely to be sufficient to make accurate measurements of interfacial geometry on such small systems and a combination of interfacial control and optical observation is likely to be necessary to produce good quantitative results.

6.2.2.4 Kinetic Observations

As discussed above the lack of knowledge of the interfacial geometry means that it is not possible to use the kinetic analysis proposed in the Methodology as neither the effective interfacial area, nor the Nernst diffusion layer thickness is known. The gradients of $\ln((i_d - i)^n/i)$ versus potential plots and the Tomeš criteria ($E_{1/4} - E_{3/4}$) given in table 7 do however indicate that all the reactions observed were electrochemically reversible under the conditions used. The reversible slope of the logarithmic plot at 17 °C for a single charge transfer is 40 V^{-1}. The Tomeš criterion for reversibility given a 1:1 stoichiometry is 55 mV at 17 °C. The results in table 7 agree with these reversible values to within experimental error. The estimated experimental error arises from inaccuracy in the determination of the limiting current. There may also be small effects from solution resistance, unfortunately the lack of reproducibility in the position, shape and size of the interface precluded the investigation of resistive effects by changing crown ether concentration as suggested in the Methodology chapter.

The fact that all the reactions behaved reversibly with the radii of pipettes used means that at least a lower bound for the rate constants can be estimated. According to Oldham et al[113] the fastest reaction that a 2.5 μm radius electrode will render usefully, i.e. measurably, quasireversible has a rate constant of 10^{-3} m s^{-1} assuming a diffusion coefficient of 1×10^{-9} m^2 s^{-1}. A 25 μm radius electrode will measure rate constants up to 10^{-4} m s^{-1}, or 10^{-2} cm s^{-1}. Thus a conservative estimate would give all the complexation reactions a minimum first order rate constant of 10^{-2} cm s^{-1}, equivalent to a second order rate constant at 0.1M of 10^{-1} cm s^{-1} M^{-1}.

The observed reversibility of the reactions also means that the half wave potentials can be used as formal potentials in the calculation of association constants above, although there remains the assumption that the ratio of crown and complexed crown diffusion coefficients is unity.

ELECTRON TRANSFER

7.1 RESULTS

Two electron transfer systems were studied experimentally at the water/1,2-dichloroethane interface. The aqueous redox couple in both cases was the hexacyanoferrate II/III (FeII/FeIII) couple. The organic redox couples investigated were: ferrocene/ferrocinium (FeC/FeC^+) and di-n-butyl ferrocene/di-n-butyl ferrocinium (DBFeC/$DBFeC^+$). The electrochemistry of the organic redox species was studied both at the Pt/DCE interface and at the water/DCE interface.

7.1.1 Oxidation on Platinum

A solid Pt microdisc electrode was used for the oxidation of the two organic species in DCE. The resultant voltammograms for FeC and DBFeC both gave linear semi-logarithmic plots with a slope $\approx 39\ V^{-1}$, as shown in figures 41 and 42. The potential scale in figure 41 is that for a 1mM TBACl/AgCl/Ag reference electrode with 1mM TBATPB supporting electrolyte to enable comparison with CELL6 in the ITIES case below. The cell used for figure 42 was as follows:

$$\text{Pt} \;\Big|\; \begin{matrix}\text{10mM TBATPBCl} \\ \text{2 mMDBFeC} \\ \text{DCE}\end{matrix} \;\Big|\; \text{10mM TBACl} \;\Big|\; \text{AgCl/Ag}$$

CELL5

i.e. as for CELL6 in the equivalent ITIES experiment below, less the aqueous phase. The half wave potentials of the two reactions versus the specified reference electrodes were -450 ± 5mV and -412 ± 5mV for FeC and DBFeC respectively. The difference in the half wave potentials of the two oxidations relative to each other was determined from figure 43 to be 150 ± 5 mV. Diffusion coefficients for FeC and DBFeC in DCE were calculated from the diffusion limited currents observed using equation (144) and found to be 8×10^{-6} $cm^2\ s^{-1}$ and 7×10^{-6} $cm^2\ s^{-1}$ respectively. The radius of the Pt microdisc was taken to be 12.5 μm as it was constructed from 25μm diameter platinum wire (see experimental). The FeC diffusion coefficient of 8×10^{-6} $cm^2\ s^{-1}$ in DCE was consistent with that determined by Samec and others[55] for FeC in nitrobenzene given the

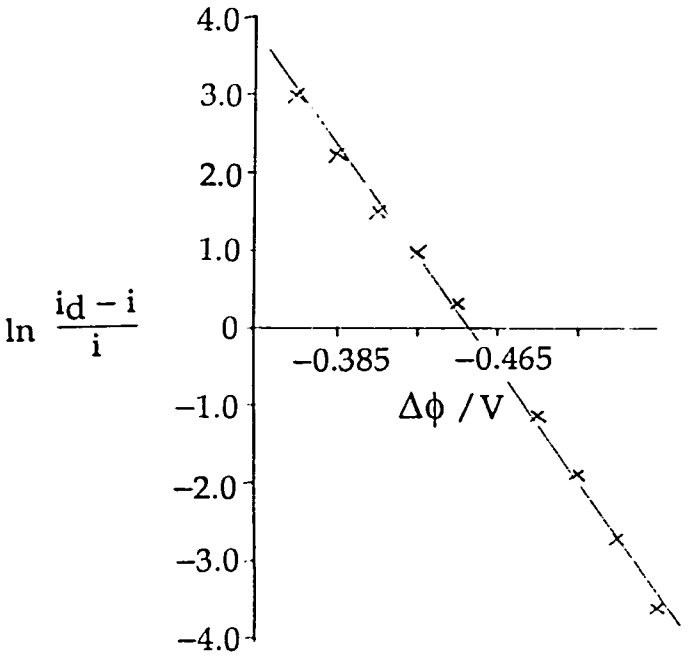

b) Semi-logarithmic plot from current wave.

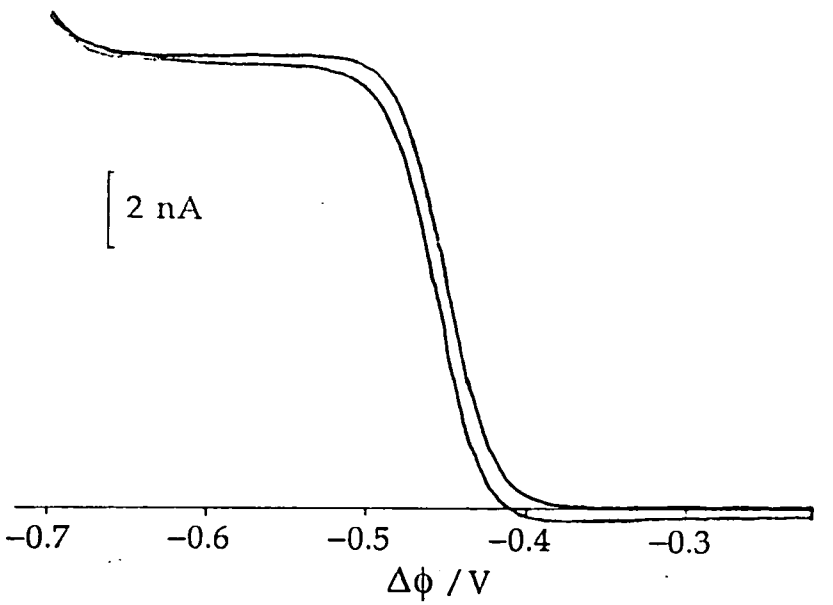

Fig. 41 a) Cyclic voltammogram for the oxidation of FeC at a 25 μm microdisc.

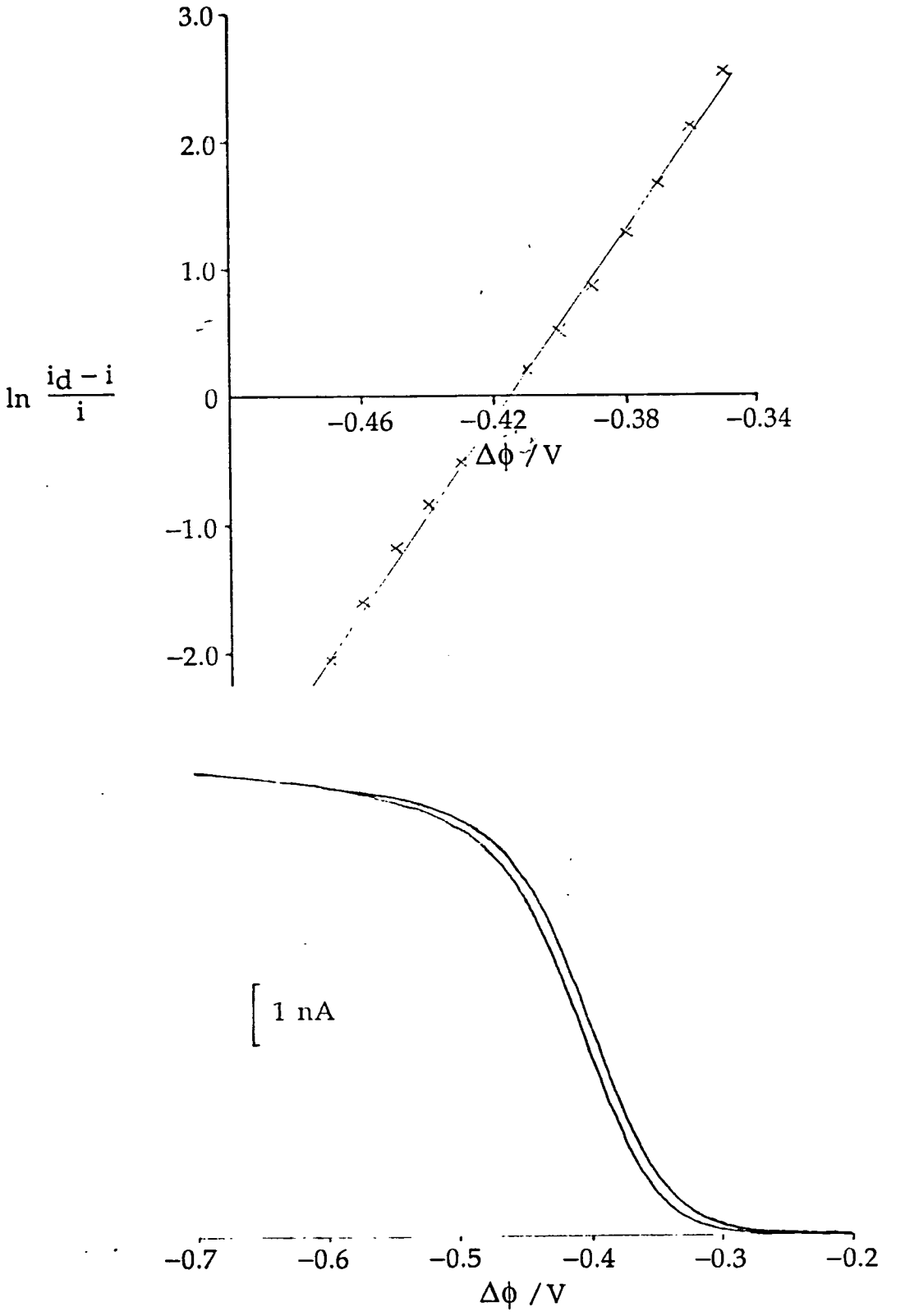

Fig. 42 a) Cyclic voltammogram for the oxidation of DBFeC at a 25 μm microdisc.
b) Semi-logarithmic plot from current wave.

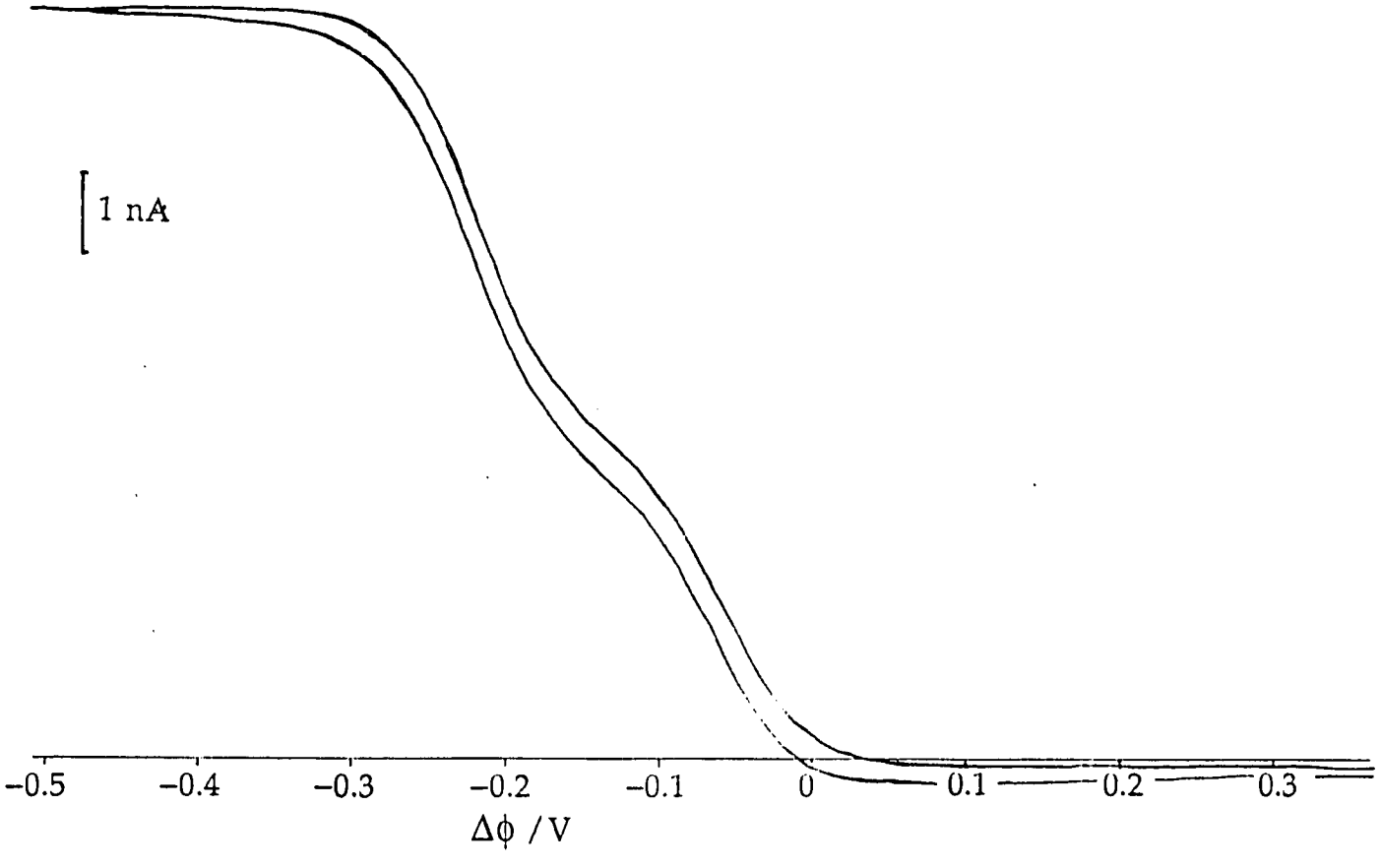

Fig. 43 Cyclic voltammogram showing the oxidation of FeC and DBFeC on a 25 μm diameter platinum microdisc at 10 mV s^{-1}.

proportionality of diffusion coefficient to solvent viscocity, thus confirming the validity of the microdisc radius.

7.1.2 Ion Transfer at the ITIES

Both FeC^+ and $DBFeC^+$ have been electrogenerated in situ at an ITIES and their transfer from DCE to water observed by A. Brown using a five electrode system[124]. The results for the construction of figure 44 were generously provided by A. Brown. Figure 44 shows the transfers of FeC^+ and $DBFeC^+$ from DCE to water. The separations of forward and reverse peaks for both transfer reactions were ≈ 60 mV, consistent with a reversible reaction. The FeC^+ transfer gave a peak current proportional to the square root of sweep rate. The $DBFeC^+$ transfer was too close to the end of the potential window for a reliable dependence on the square root of sweep rate to be made. The half wave potentials of the reactions were –340 mV and –115 mV for FeC^+ and $DBFeC^+$ respectively. The separation of the half wave potentials was thus 225 mV, $DBFeC^+$ being more hydrophobic than FeC^+. Using the tetramethylammonium cation (TMA^+) as an internal reference (and with the use of the half wave potential for the transfer of TMA^+ against the reference system in CELL6 provided by Y. Shao[29]) the half wave potentials of these ion transfer reactions could be related to the reference electrodes used in CELLs 6 and 7. The half wave potential for FeC^+ ion transfer with respect to CELL6 was determined to be –290 mV oil v water, at that for $DBFeC^+$ transfer with respect to CELL7 was –5 mV oil v water.

7.1.3 Oxidation at the ITIES

7.1.3.1 Ferrocene

Ag/AgCl	0.05MFeIII 0.01MFeII 0.1M KCl		xmM FeC 1mMTBATPB DCE		1mM TBACl	AgCl/Ag

CELL6

Figure 45 shows a cyclic voltammogram obtained from CELL6 with 1mM ferrocene at a sweep rate of 50 mV s^{-1}. This cyclic voltammogram is identical to that obtained from supporting electrolyte alone. Figure 46 was again obtained from CELL6, but in this case a quantity of ferrocene was added to the organic phase *in situ* and so that its concentration was very

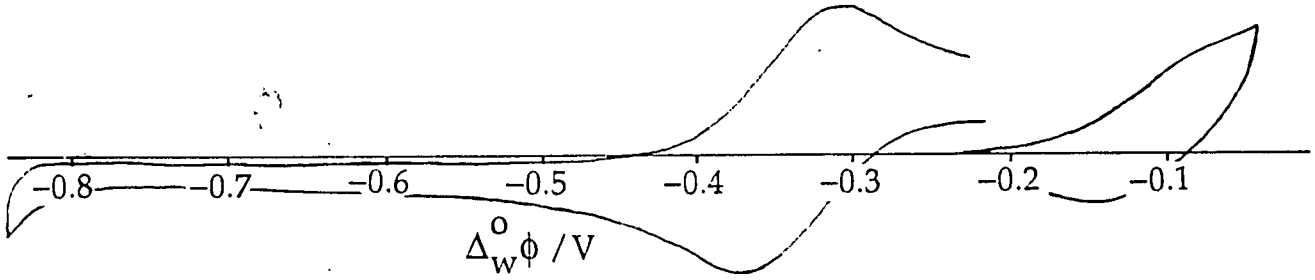

Fig. 44 Cyclic voltammograms showing ion transfer of FeC^+ and $DBFeC^+$ from DCE to water, sweep rate 50 mV s^{-1}, courtesy of A. Brown.

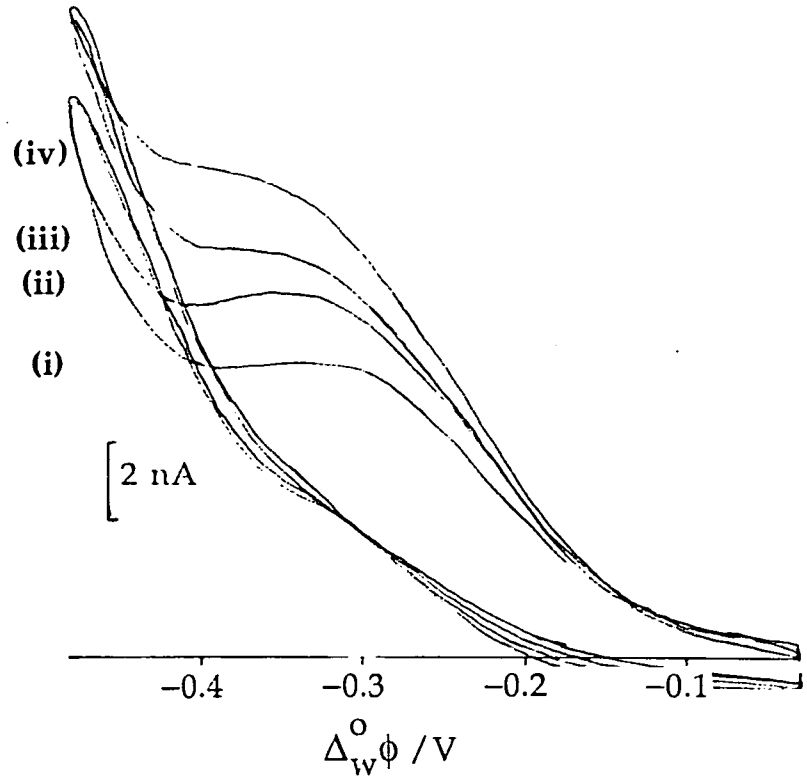

Fig. 46 Cyclic voltammograms from CELL6 with excess FeC at a 17 μm diameter pipette and various sweep rates: (i) 30, (ii) 50, (iii) 70 and (iv) 100 mV s^{-1}.

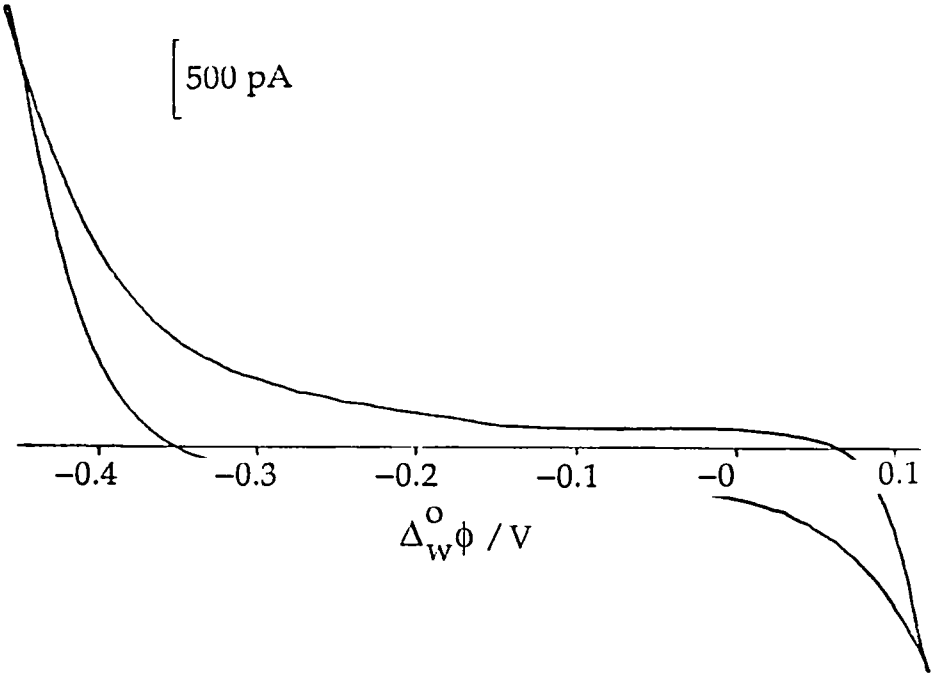

Fig. 45 Cyclic voltammogram from CELL6 (x=1) at a 34 μm diameter pipette and 50 mV s^{-1}.

high. The aqueous solution in the pipette tip was observed to turn a blue green colour after the addition of the excess ferrocene. The resultant current potential characteristic of figure 46 is asymmetric with a peaked current proportional to the square root of sweep rate on the forward sweep, but no current peak on the return sweep. This is typical of an ion transfer reaction and cannot be attributed to electron transfer at the ITIES which must give a symmetric response at a pipette tip. The half wave potential for this ion transfer is approximately –240 mV oil v water.

7.1.3.2 Di-n-butylferrocene

Pt	100mMFeIII 100mMFeII 1.5M Li_2SO_4	ymMDBFeC 10mMTBATPBCl DCE	10mM TBACl	AgCl/Ag

CELL7

The oxidation of DBFeC at the ITIES was studied using CELL7.

7.1.3.2.1 The Large ITIES

The cyclic voltammetric response of the system at a large ITIES is shown in figure 47 where it is seen that the peak current is proportional to the square root of sweep rate and of appropriate sign for the interfacial oxidation of DBFeC. The peak separation, ΔE_p, is 65 mV. Assuming a reversible single charge transfer involving DBFeC as the diffusion limiting electroactive species a diffusion coefficient of 4.2×10^{-6} cm^2 s^{-1} for DBFeC in DCE may be calculated. The half wave potential is –420 mV, oil v water.

7.1.3.2.2 The Micro-ITIES

Figure 48 is the cyclic voltammogram at 20 mV s^{-1} of the background electrolytes only in a 13 μm diameter pipette (i.e. for CELL7, y=0). Figure 49 shows cyclic voltammograms at various sweep rates in the presence of 2 mM DBFeC. The shape of the wave is clearly sweep rate dependent and the wave is not simply steady state. The direction of the current corresponds to a transfer of negative charge from oil to water or of positive charge from water to oil.

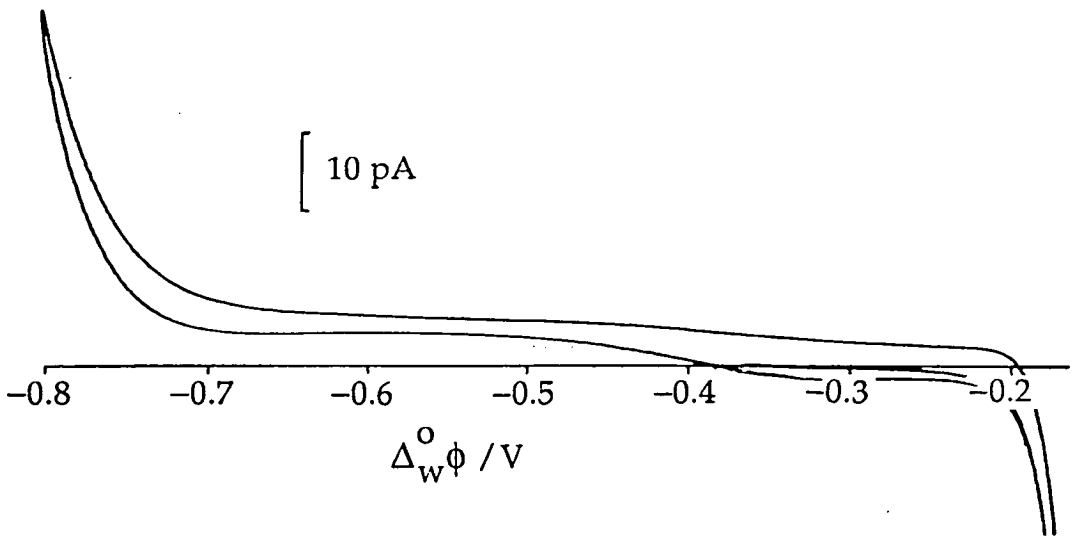

Fig. 48 Cyclic voltammogram of background electrolyte, CELL7 (y=0), at a 13 μm diameter micropipette and a sweep rate of 20 mV s^{-1}.

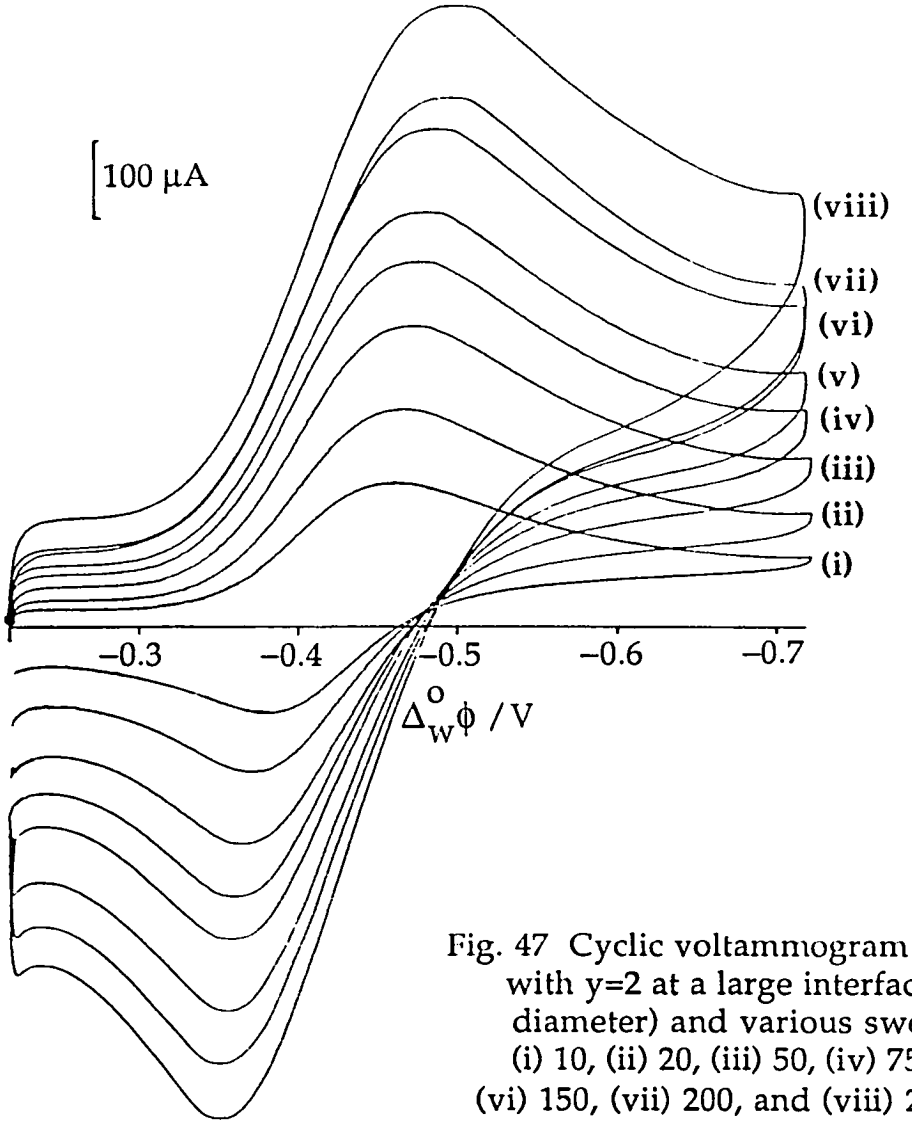

Fig. 47 Cyclic voltammogram from CELL7 with y=2 at a large interface (12 mm diameter) and various sweep rates: (i) 10, (ii) 20, (iii) 50, (iv) 75, (v) 100, (vi) 150, (vii) 200, and (viii) 250 mV s^{-1}.

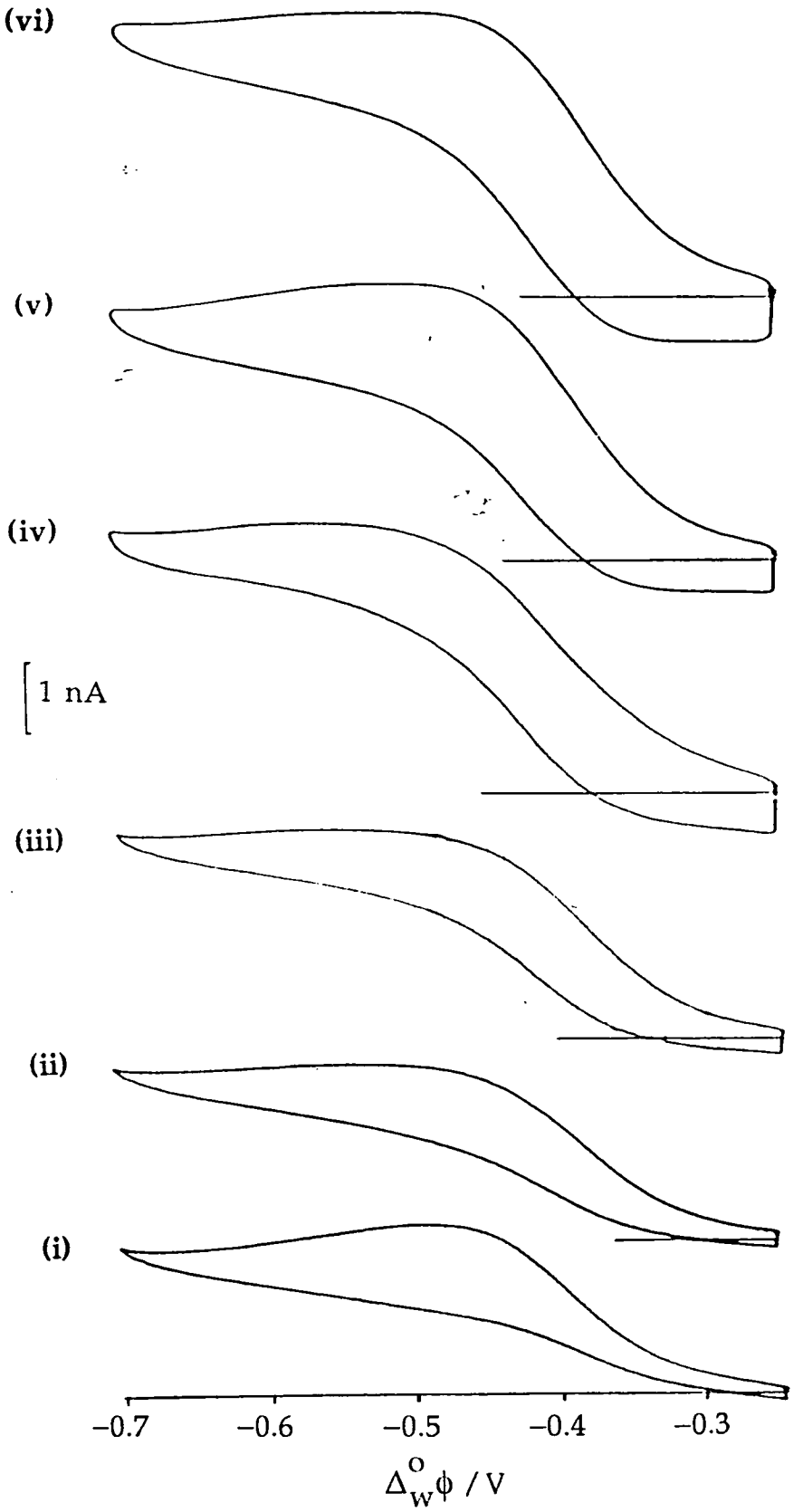

Fig. 49 Cyclic voltammogram from CELL7 (y=2), at a 13 μm diameter micropipette and various sweep rates: (i) 20, (ii) 50, (iii) 100, (iv) 200, (v) 300, and (vi) 500 mV s^{-1}.

7.2 DISCUSSION

7.2.1 Oxidation on Platinum

The oxidation of both FeC and DBFeC on a platinum microdisc gave semi-logarithmic plots with reversible gradients thus indicating a rapid and chemically reversible charge transfer. The half wave potential of DBFeC was 150 mV less positive than that of FeC showing that the dibutyl derivative is significantly easier to oxidise. This was expected to be the case due to the electron donating effect of the two butyl groups into the aromatic rings which stabilise the positive central iron in DBFeC to a greater extent than the unsubstituted rings in the FeC.

The formal potentials of the reactions on Pt may be related to those at the ITIES. Comparison of CELLs 5 and 7 above show that thermodynamically the only difference between the solid electrode and ITIES oxidations is that an extra layer of conducting material is introduced between the organic phase and the Pt electrode. The conducting material in this instance is a redox couple in aqueous solution in large excess to the organic redox species and hence a ready electron conductor. There is thus no net effect on the overall cell potential as the metal/aqueous and the aqueous/organic potential differences are summed and the aqueous potential is cancelled.

The above thermodynamic argument means that the formal oxidation potential observed at the platinum electrode should be identical to that at the ITIES. In order to relate the formal potential to the half wave potential which is measured experimentally the diffusional characteristics of the system must be addressed. The diffusional characteristics of the electron transfer cyclic voltammetry experiment at the ITIES were considered in the Methodology chapter for the case of a reversible reaction. The results given therein showed that the half wave potential was only coincident with the formal potential (oxidised and reduced species diffusion coefficients being assumed equal) in the case where:

a) Redox couple 1 was one hundred times more concentrated than the redox couple 2 in the other phase.

b) Only one oxidation form of redox couple 2 was present initially.

and

c) Where the oxidised and reduced forms of redox couple 1 were present in equal concentration.

It is only under these conditions that the half wave potentials of the oxidation at the ITIES and on Pt may be expected to be coincident. Where a different ratio of redox species is present the half wave potential observed in the ITIES experiment will be offset from that determined on Pt by the same amount as the offset from the formal potential at the ITIES calculated in chapter 4. For the experiment on Pt alone the formal and half wave potentials are coincident when both forms of the redox species have the same diffusion coefficient[101]. The half wave potential of DBFeC in CELL7 is therefore expected to occur at −412 mV for an equimolar mixture of FeII/FeIII. The potential of the Ag/AgCl reference system used in CELL6 was measured with respect to Pt in FeIII/FeII and the potential difference determined to be −160 ± 10 mV. The expected interfacial oxidation potential of FeC in CELL6 was thus calculated from the half wave potential on Pt to be −380 ± 12 mV.

7.2.2 Oxidation at the ITIES

7.2.2.1 Ferrocene

As described above there was no distinguishable oxidation wave for ferrocene at the ITIES when the concentration of FeC in CELL6 was 1mM. There was no difference between the voltammogram with supporting electrolyte alone and that with the electroactive species present. When a large excess of FeC was added to the oil phase an asymmetric wave typical of ion transfer[122,52] was observed as illustrated in figure 46. It is believed that this wave corresponds to the transfer of FeC^+ from water to oil on the forward potential sweep, where the oil phase is made more negative, and that transfer of FeC^+ from oil to water occurs on the reverse sweep. FeC^+ is known to be blue in colour and the fact that the aqueous phase turns blue green at the tip of the pipette in the presence of excess FeC is consistent with the presence of FeC^+ in the aqueous phase. The following mechanism is postulated:

Step 1 The FeC partitions between the oil and water phases.

$$FeC_{(DCE)} \rightleftharpoons FeC_{(aq)}$$

Step 2 The aqueous FeC is readily oxidised by the FeIII present.

$$FeC_{(aq)} + Fe(CN)^{3-}_{6\,(aq)} \rightleftharpoons FeC^{+}_{(aq)} + Fe(CN)^{4-}_{6\,(aq)}$$

Although the partition of FeC to water from DCE is only slight, the oxidation of $FeC_{(aq)}$ to $FeC^{+}_{(aq)}$ displaces equilibrium in step 1 and thus drives the FeC partition so that more of the neutral FeC transfers to the aqueous phase to be oxidised. These processes occur without application of an external electric field. The formal potential of FeC in water has not been determined, however it is known that ferric iron readily oxidised FeC (and DBFeC) in 1:1 propylalcohol:water mixtures[125].

During cyclic voltammetry the oil phase is made sufficiently negative relative to the aqueous phase to cause the $FeC^{+}_{(aq)}$ which has built up in the pipette tip as a result of the reaction in step 2 to cross out of the pipette into the oil phase. Inside the pipette the diffusion is constrained to be linear and hence a current peak proportional to the square root of sweep rate is generated. On the return sweep the $FeC^{+}_{(DCE)}$ ion is able to diffuse radially to the interface at the pipette tip and hence there is no current peak[122,52]. Since the equilibrium constant for the partition of FeC is rather low, it is only when a high concentration of FeC is present in the DCE that sufficient will partition at a great enough rate for the $FeC^{+}(aq)$ concentration to build up to detectable levels. The idea that the redox reaction takes place in the aqueous phase without the application of any electrical potential difference is supported by the observation that when an aqueous solution of FeII/FeIII was shaken together with a solution of FeC in DCE the aqueous phase turned from yellow to a green blue colour after two to five minutes.

The half wave potential for FeC^{+} transfer was predicted above (section 7.1.2) to occur at a potential of –290 mV in CELL6. The ion transfer wave observed during the attempted oxidation of FeC in CELL6 occurs at approximately –240 mV. Although there is a difference of 50 mV in these two potentials this can be explained by the instability of the aqueous reference system used in CELL6. The Ag/AgCl reference electrode was

rather unsatisfactory when in contact with a significant concentration of the FeII/FeIII redox couple and therefore was replaced by a Pt electrode for the experiments with DBFeC. Discrepancies of up to 100 mV could occur between half wave potentials when experiments were repeated. The formal potential of FeIII/FeII is approximately 500 mV more positive than that of Ag^+/Ag and therefore the composition of the AgCl/Ag reference system was expected to remain constant when in contact with FeIII/FeII as the solid AgCl would form a passive layer on the Ag electrode, however this was not the case in practice. The FeC experiments were not repeated using a Pt reference electrode as the interfacial electron transfer which it was sought to investigate was not observable with FeC.

It is not clear why the oxidation of FeC was not observed at the ITIES. The expected half wave potential for the oxidation in CELL6 was calculated above to be -380 ± 12mV, this is close to the oil negative end of the potential window, however it would still be expected to be distinguishable from the end of the potential window. It may be that the reaction is slow at the ITIES and hence the half wave potential is displaced in the oil negative direction.

7.2.2.2 Di-n-butylferrocene

Experiments with DBFeC were conducted using a Pt reference electrode which afforded proper stability and reproducible results. The aqueous phase was rendered virtually saturated in Li_2SO_4 in order to help prevent the oxidation product $DBFeC^+$ transferring to the aqueous phase. The ion transfer data provided later by A Brown showed that this precaution was unnecessary, the $DBFeC^+$ prefering to remain in the DCE phase at the oxidation potential. The experimental results at the ITIES indicate that the interfacial electron transfer from $DBFeC_{(DCE)}$ to $FeIII_{(aq)}$ does occur, but that the reaction is not a simple, uncomplicated, reversible charge transfer.

7.2.2.2.1 The Large ITIES

Cyclic voltammetry at the large ITIES results in a current peak on both forward and reverse sweeps which is proportional to the square root of sweep rate (figure 47) and of appropriate sign for the interfacial oxidation/reduction of DBFeC. The current peak separation of 65 mV is close to the 59 mV expected from a reversible reaction and the half wave

potential occurs at −420 mV, just 8 mV away from that expected from the oxidation on Pt, and acceptable within experimental error. This evidence could indicate a reversible electron transfer except that the DBFeC diffusion coefficient in DCE (calculated from the sweep rate dependence of the forward current peak) is only $4.2 \pm 0.5 \times 10^{-6}$ cm^2 s^{-1} in comparison with $7.0 \pm 0.5 \times 10^{-6}$ cm^2 s^{-1} obtained from the Pt micro electrode oxidation. The current densities at the ITIES are therefore much lower than expected.

7.2.2.2.2 The Micro-ITIES

Cyclic voltammetry at the micro-ITIES shows that there is not merely a reduction in current density, but the shape of the wave indicates that more than one interfacial reaction is occuring. The wave is not sweep rate independent, but increases in intensity with increasing sweep rate. At low sweep rates (eg 20 mV s^{-1}) the wave is quite asymmetric with a definite maximum in the forward current. At intermediate sweep rates (100 mV s^{-1} and 200 mV s^{-1}) the wave appears to be more plateau like on the forward sweep and the wave height increases with sweep rate. The wave becomes more symmetric with a large amount of hysterisis. At higher sweep rates the asymmetry becomes more obvious again with a current maximum beginning to show about 50 mV negative of the first one as indicated by the arrow in figure 49. The hysterisis between the forward and reverse waves is greater at higher sweep rates. The sweep rate dependence and peak of the current wave at the micro interface shows that there is a significant contribution from linear diffusion over radial diffusion.

It is difficult to calculate any diffusion coefficient from the micro-ITIES results as there does not appear to be a steady state diffusion limited current. The "plateau" current observed at the end of the 50 mV s^{-1} wave gives a diffusion coefficient of 3.6×10^{-6} cm^2 s^{-1} based on the assumption that it is a diffusion limited current according to equation (144) which, although not a reliable figure, does support the observation from the large interface that the current densities at the ITIES are anomalously low.

As the wave at the micro ITIES is not steady state a half wave potential cannot be measured, however the wave does occur in approximately the expected region for the oxidation of DBFeC.

7.2.2.2.3 Reaction Mechanism

It is difficult to envisage what can be occuring to reduce current densities at the ITIES in comparison to those at a solid Pt surface. As the concentration of $FeIII_{(aq)}$ is 100 times that of $DBFeC_{(DCE)}$ it is extremely unlikely that the FeIII could be quenched sufficiently, due to some unknown bulk aqueous process, to inhibit DBFeC oxidation. There does not appear to be any following reaction of the oxidation product $DBFeC^+$ which might consume starting material for the reaction as the reaction is apparently reversible with the reverse current peaks in figure 47 equally as intense as the forward current peaks. Lower current densities are unlikely to result from reductions in DBFeC concentrations due to any bulk homogeneous reaction as the bulk DCE phase is the same as that used at the solid Pt electrode and an interfacial reaction must therefore be considered.

Ion pairing of supporting electrolytes or film deposition at the interface might reduce the effective electrode area and hence current density. The concentration of K^+ in the aqueous phase is very high as it is the counter ion for the FeIII/FeII mixture and this may result in association with the TPBCl in the DCE phase although no precipitation was actually observed at the interface. Geblewicz and Schiffrin[56,57], using a very similar combination of supporting electrolyte and electroactive species in the aqueous phase, found diffusion coefficients of the lutetium biphthalocyanine at the solid Pt micro electrode and the large ITIES to be in close agreement, as were those obtained in similar experiments on tin diphthalocyanine. A blocking of the reactive interface due to supporting electrolyte interactions is not therefore supported.

An alternative explanation is that there is adsorption of the oxidation product, $DBFeC^+$, at the interface where there is a high concentration of anions on the aqueous side such as the oxidising species itself, its reduced counterpart and sulphate ions. There are three possibilities after DBFeC is oxidised to $DBFeC^+$ at the interface:

1. The $DBFeC^+$ may diffuse away from the interface resulting in a net charge transfer.

2. The $DBFeC^+$ may adsorb at the interface in association with an aqueous anion resulting in no net charge transfer and possibly reducing the active interfacial area.

3. The $DBFeC^+$ may adsorb without association resulting in an overall charge transfer with a different free energy from process 1 and possibly reducing the active interfacial area.

Adsorption of the product of an electro oxidation results in a prepeak or prewave before the main oxidation wave[94]. At a large interface the intensity of the prepeak is proportional to ν and symmetric, occuring at the same potential on forward and reverse sweeps, whereas the non adsorbed redox current is proportional to $\nu^{1/2}$ and forward and reverse peaks are separated. Redox reactions complicated by adsorption have not been considered at micro interfaces in the literature, however it is reasonable to deduce that a prewave will also occur for an adsorbed product at a microinterface as the interfacial thermodynamics are not affected by the diffusional properties of the system. Such a peak is also expected to be proportional to ν at the microinterface as this sweep rate proportionality arises from the fact that there is no diffusion required (or possible) of the adsorbed species to and from the interface.

The strange shape of the wave observed at the micro-ITIES may therefore arise from a combination of waves resulting from reactions 1, 2 and 3 above. The plateau current density is depressed by reactions 2 and 3 above. Reaction 3 would result in a sweep rate dependent peak and hysterisis due to a negative peak on the reverse sweep. A sweep rate dependence will also arise in reaction 1 at higher scan rates as linear diffusion increases in importance relative to radial diffusion and hence the shape of the wave may be expected to change somewhat with scan rate as is observed.

Although no obvious prepeak occurs at the large ITIES, differences in current density may effect the relative dominance of reactions 1, 2 and 3, so that at the large ITIES reactions 1 and 2 are predominant giving a fairly

undistorted reversible wave of reduced intensity. Comparison of the expected plateau current density at a micropipette of 7 μm radius with the expected peak current density at a large ITIES at sweep rates of 10 to 100 mV s^{-1} shows that the fluxes at the microinterface are between 17 times and 4 times greater than those at the large ITIES for a diffusion coefficient of 7×10^{-6} cm^2 s^{-1}.

7.2.3 Other Electron Transfers at the ITIES

Kihara et al[27] have published data on a number of different electron transfer reactions at the water/nitrobenzene interface using current scan polarography at the ascending water electrode. Most of the redox couples they studied gave reversible waves at the ITIES which were attributed to electron transfer. These included FeIII/FeII, or hydroquinone, and 7,7,8,8-tetracyano-quinodimethane, FeIII/FeII, or Ce_4^+, and FeC. It is unlikely that the waves they have observed were due to ion transfer of a product formed from a homogeneous redox following partition (as suggested for the FeC in DCE experiment above) as the ascending water electrode they used gives little opportunity for the build up of such a product to detectable levels. They found that the presence of both aqueous and organic redox species was necessary to give interfacial charge transfer and it seems reasonable to conclude that interfacial electron transfer does indeed occur under their conditions.

Under pseudo first order conditions the limiting currents recorded by Kihara et al[27] were dependent on the dilute reactant, however the results were not quantified to give diffusion coefficients of electroactive species, hence current densities could not be compared with those expected. The results confirmed that the half wave potentials for redox reactions at the ITIES depend on the relative concentrations of the reactants. The reactions which they investigated did not show any of the more complex behaviour described in the present work. It may be that complications would become apparent if the consistency of diffusion coefficients was checked or if a microinterface were used.

Geblewicz and Schiffrin[56] have published work on electron transfer at the water/DCE interface using an FeIII/FeII – lutetium diphthalocyanine ($Lu(PC)_2$) system. As mentioned above the current densities they observed

were consistent with the diffusion coefficients measured from oxidation on Pt. These workers measured a rate constant for electron transfer of 0.9 x 10^{-3} cm s^{-1} from the shift in peak separation with sweep rate at the large ITIES. This rate constant may however be an artefact caused by uncompensated solution resistance. The authors state that currents measured were of less than 1 μA:

"and therefore the results are free from uncompensated resistance errors."

however this assertion is not necessarily true. Interestingly the ratio of the aqueous FeIII/FeII is 10:1, rather than the 1:1 required for "classical" linear diffusion behaviour and thus the reversible peak separation is calculated from numerical analysis to be about 80 mV. This is indeed the peak separation shown in figure 3 of Geblewicz and Schiffrin's paper[56] and may have misled the authors into believing that they were observing some kinetic control, when in fact the reaction behaviour was reversible.

Although it has not proved possible in the present study to measure the kinetics of an electron transfer at the ITIES, the micropipette has proved useful in distinguishing between ion transfer and electron transfer. The asymmetric diffusion regime at a micropipette is diagnostic in this respect under pseudo first order conditions. It also appears that complicating processes such as adsorption may be more obvious at microinterfaces as the normal reversible process should be sweep rate independent, hence any sweep rate dependence at the microinterface is also diagnostic of complications. A significant problem with microinterfaces is that current densities vary greatly across the interface diameter[71]. This variation in current density, which may affect the reaction occuring, is not within the experimenters control. Average current densities may be controlled through concentration and electrode radius, but uniformity across the electrode diameter cannot be achieved.

CONCLUSION

8.1 KINETIC METHODOLOGY

The approximate analytical solution for the current potential characteristic at the microdisc interface presented in chapter 4 is show to agree satisfactorily with the semi-analytical solutions of Zoski, Oldham and Bond[71] and the numerical solution of Heinze[70]. This analytical solution is applicable under steady state conditions only and is based on the Nernst diffusion layer approximation. The Nernst diffusion layer approximation may be applied in a similar way to any steady state situation in which the relation of the diffusion limited current to the electrode area is known.

The analytical solution may be used to determine the forward potential dependent rate constant and the charge transfer coefficient, α, from any quasireversible, steady state, current potential wave obtained at a microdisc of known radius if the formal potential for the reaction is also known. It was not possible to determine kinetic parameters in this manner for the reactions studied herein as the steady state waves recorded were reversible, not quasireversible, under the reaction conditions employed.

8.2 MICROINTERFACE SUPPORTS

It has been shown that a micro-liquid/liquid interface may be supported at a microhole in a thin polyester membrane. For the first time this provides the opportunity to make a micro-liquid/liquid interface with a symmetrical diffusion geometry, i.e. with the plane of the interface as a mirror plane. The interface geometry and diffusion regime at the microhole is the same as that at a recessed microdisc. This symmetric design may potentially allow the extension of methodology developed for solid microelectrodes to the liquid/liquid interface. At present it has enabled steady state reversible current waves to be obtained from an ion transfer reaction at the ITIES by cyclic voltammetry. A regular array of microholes has also successfully supported an array of microinterfaces

generating a steady state current wave for ion transfer with plateau currents of the order of 10 μA.

There are some problems with control of the position of the interface which result in a certain irreproducibility and this problem will have to be solved before such membrane supports can be used quantitatively.

8.3 ASSISTED ION TRANSFER

Values for the association constants, K_1, of the alkali metal ions; lithium, sodium, potassium, rubidium and caesium, with dibenzo-18-crown-6 and lithium with benzo-15-crown-5, in 1,2-dichloroethane were determined to be $10^{6.86}$, $10^{10.4}$, $10^{10.4}$, $10^{8.87}$, $10^{6.86}$ and $10^{8.42}$ respectively. Steady state, reversible waves were produced by all these association reactions at the water/dichloroethane interface supported at the tips of micropipettes between 5 and 20 μm in diameter and all the reactions were thus concluded to have pseudo first order rate constants in excess of 10^{-2} cm s^{-1}.

The usefulness of the micropipette support was limited by the fact that the position of the interface at the pipette tip, and hence the size of the interface, could not be well controlled.

The interfacial association of caesium with dibenzo-18-crown-6 was concluded to involve the formation of both the 1:1 and 1:2, ion:crown, complexes. The cyclic voltammetry of this reaction at the large interface displayed characteristics similar to those calculated by Kakiuchi and Senda[121] to arise under such circumstances.

8.4 ELECTRON TRANSFER AT THE ITIES

$$O1_{\alpha} + R2_{\beta} \rightleftharpoons R1_{\alpha} + O2_{\beta} \qquad \text{(VI)}$$

The solution of the diffusion mass transport equations for electron transfer at the ITIES (VI) allows the specification of experimental conditions under which the interfacial charge transfer may be regarded as truly pseudo first order and where the cyclic voltammetry of the reversible

reaction will give the classical reversibility criteria, i.e. ΔE_p = 59 mV and $E^{o'} = E_{1/2}$, when all diffusion coefficients are equivalent.

These initial conditions are:

(i) $C_{O1} = C_{R1}$

(ii) $C_{O1} + C_{R1} \geq 100\, C_{O2}$

(iii) Initially $C_{R2} = 0$

Values of ΔE_p and $E_{1/2}$ are also given for different ratios of reactants under reversible conditions. These agreed with those measured by Samec[55] for electron transfer between ferrocene in nitrobenzene and hexacyanoferrate III in water and confirm that an interfacial electron transfer is indeed occuring.

Results at the water/1,2-dichloroethane interface show that it is likely that ferrocene partitions into the aqueous phase and undergoes a homogeneous oxidation reaction with the hexacyanoferrate III ions present producing ferrocinium which is then seen to transfer back to the organic phase under the influence of an applied potential. The interfacial oxidation is thought to occur beyond the end of the potential window.

Di-n-butylferrocene oxidation is observed at the water/1,2-dichloroethane interface, but appears to be complicated by other interfacial reactions which are thought to involve the interfacial adsorption of the oxidation product di-n-butlylferrocinium at the interface.

8.5 FUTURE USE OF THE MICRO-ITIES

The work presented here has shown that the micro-ITIES supported at the tip of a micropipette can prove a useful diagnostic tool in identifying the electroactive species, e.g. in distinguishing between ion and electron

transfer and determining which ions form the end of the potential window.

One of the main aims of the present work, however, was to use the micro-ITIES in determination of kinetic parameters and this aim has not been fulfilled. The barrier to the kinetic application of the micro-ITIES is the difficulty in controlling the precise location of the interface at the microsupport and this problem needs to be addressed further.

Control of the interface at the micropipette should be fairly tractable through the use of techniques already applied to "patch clamp" work. It is expected that micropipettes might form a useful route to kinetic measurement of assisted ion transfer and electron transfer reactions in the future. The control of the interface at the microhole support is more difficult as while in principle it can be controlled by pressure this has not been achieved in practice. Another drawback is the minimum dimension of the interface which cannot be reduced below 12 μm diameter at present due to the thickness of the supporting membrane. Thinner supporting membranes can be manufactured, but these are likely to become mechanically fragile and difficult to handle, hence partially negating one advantage of microelectrodes, the simplified apparatus. Another possible approach is to use an aqueous gel electrolyte which may provide a means of more firmly defining the interface.

The prospect of extending microelectrode techniques to the liquid/liquid interface is very attractive, but the fluid nature of the interface itself makes the achievement of this goal elusive.

REFERENCES

1 C.J. Pedersen, Angew. Chem. Int. Ed. Engl. 27 (1988) 1021

2 E. Makrlík, L.Q. Hung and A. Hofmanová, Electrochim. Acta. 28 (1983) 847

3 J. Koryta, J. Electroanal. Chem. 213 (1986) 323

4 J. Koryta, J. Electroanal. Chem. 229 (1987) 265

5 C. Gavach and P. Seta, Anal. Chim. Acta. 50 (1970) 407

6 C. Gavach and C. Bertrand, Anal. Chim. Acta. 55 (1971) 385

7 J. Koryta, Ion-Selective Electrode Rev. 5 (1983) 131

8 H. Ti Tien Bilayer Lipid Membranes (BLM), Theory and Practice, Marcel Dekker, New York, 1974

9 M. Cremer, Z. Biologie 47 (1906) 562

10 J. Koryta, Electrochim. Acta. 24 (1979) 293

11 J. Koryta et al., Bioelectrochem. and Bioenergetics 7 (1980) 61

12 W. Nernst and E.H. Riesenfield, Ann. Phys. 8 (1902) 600

13 E.H. Riesenfield, Ann. Phys. 8 (1902) 616

14 F.M. Karpfen and J.E.B. Randles, Trans. Farad. Soc. 49 (1953) 823

15 J.T. Davies, Proc. Third Int. Cong. Surf. Activity, Cologne, 2 (1960) 254 (Review)

16 E.J.W. Verwey and K.F. Niessen, Philos. Mag. 28 (1939) 435

17 Z. Samec, V. Mareček and D. Homolka, Farad. Disc. Chem. Soc. 77 (1984) 197

18 M. Senda, T. Kakiuchi, T. Osakai and T. Kakutani, in The Interface, Structure and Electrochemical Processes at the Boundary Between Two Immiscible Liquids. ed. V.E. Kazarinov, Springer-Verlag Berlin, Heidelberg 1987

19 Z. Samec, V. Mareček, K. Holub, S. Racinsky and P. Hajkova, J. Electroanal. Chem. 225 (1987) 65

20 J. Guastalla, J. Chim. Phys. 53 (1956) 470

21 C. Gavach, T. Mlodnicka and J. Guastalla, Compt. Rend. C266 (1968) 1196

22 J. Guastalla, Nature 227 (1970) 485

23 C. Gavach and F. Henry, Compt. Rend. C274 (1972) 1545

24 C. Gavach, J. Chim. Phys. 70 (1973) 1478

25 J. Koryta, P. Vanýsek and M. Brezina, J. Electroanal. Chem. 75 (1977) 211

26 C. Gavach and F. Henry, J. Electroanal. Chem. 54 (1974) 361

27 S. Kihara, M. Suzuki, K. Maeda, K. Ogura, M. Matoui and Z. Yoshida, J. Electroanal. Chem. 247 (1989) 107

28 K. Maeda, S. Kihara, M. Suzuki and M. Matsui, J. Electroanal. Chem. in press (1991) accepted Sept 1990

29 Y.Shao, personal communication

30 Z. Samec, V. Mareček, J. Koryta and M.W. Khalil, J. Electroanal. Chem. 83 (1977) 393

31 Z. Samec, V. Mareček and J. Weber, J. Electroanal. Chem. 100 (1979) 841

32 Z. Samec, J. Electroanal. Chem. 111 (1980) 211

33 J.C. Imbeaux and J.M. Saveant, J. Electroanal. Chem. 44 (1973) 169

34 R.S. Nicholson, Anal. Chem. 37 (1965) 1351

35 Z. Samec, V. Mareček, J. Weber and D. Homolka, J. Electroanal. Chem. 126 (1981) 105

36 D. Homolka and V. Mareček, J. Electroanal. Chem. 112 (1980) 91

37 D. Homolka, V. Mareček, Z. Samec, O. Ryba and J. Petranck, J. Electroanal. Chem. 125 (1981) 243

38 A. Hofmanová, L.Q. Hung and W. Khalil, J. Electroanal. Chem. 135 (1982) 257

39 P. Vaný́sek, W. Ruth and J. Koryta, J. Electroanal. Chem. 148 (1983) 117

40 D. Homolka, K. Holub and V. Mareček, J. Electroanal. Chem. 138 (1982) 29

41 Z. Samec, D. Homolka and V. Mareček, J. Electroanal. Chem. 135 (1982) 265

42 Z. Samec, V. Mareček and D. Homolka, J. Electroanal. Chem. 158 (1983) 25

43 Z. Samec and P. Papoff, Anal. Chem. 62 (1990) 1010

44 Z. Samec and V. Mareček, J. Electroanal. Chem. 200 (1986) 17

45 B. Hundhammer, T. Solomon and H. Alemu, J. Electroanal. Chem. 149 (1983) 179

46 T. Osakai, T. Kakutani and M. Senda, Bull. Chem. Soc. Jpn., 57 (1984) 370

47 T. Wandlowski, V. Mareček and Z. Samec, J. Electroanal. Chem. 242 (1988) 291

48 T. Wandlowski, V. Mareček, K. Holub and Z. Samec, J. Phys. Chem. 93 (1989) 8204

49 Z. Koczorowski and G. Geblewicz, J. Electroanal. Chem. 108 (1980) 117

50 Z. Koczorowski and G. Geblewicz, J. Electroanal. Chem. 139 (1982) 177

51 Z. Koczorowski and G. Geblewicz, J. Electroanal. Chem. 152 (1983) 55

52 G. Taylor and H.H. Girault, J. Electroanal. Chem. 208 (1986) 179

53 V.J. Cunnane, D.J. Schiffrin, M. Fleischman, G. Geblewicz and D. Williams, J. Electroanal. Chem. 243 (1988) 455

54 Z. Samec, V. Mareček and J. Weber, J. Electroanal. Chem. 96 (1977) 245

55 Z. Samec, V. Mareček and J. Weber, J. Electroanal. Chem. 103 (1979) 11

56 G. Geblewicz and D.J. Schiffrin J. Electroanal. Chem. 244 (1988) 27

57 V.J. Cunnane, D.J. Schiffrin, C. Beltram, G. Geblewicz and T. Solomon, J. Electroanal. Chem. 247 (1988) 203

58 L.Q. Hung, J. Electroanal. Chem. 115 (1980) 159

59 L.Q. Hung, J. Electroanal. Chem. 149 (1983) 1

60 H.H. Girault and D.J. Schiffrin, J. Electroanal. Chem. 170 (1984) 127

61 T. Kakiuchi and M. Senda, Bull. Chem. Soc. Jpn. 56 (1983) 2912

62 Z. Samec, J. Electroanal. Chem. 99 (1979) 197

63 Z. Samec, Y.I. Kharkats and Y.Y. Gurevich, J. Electroanal. Chem. 204 (1986) 257

64 H.H. Girault and D.J. Schiffrin, J. Electroanal. Chem. 195 (1985) 213

65 H.H. Girault and D.J. Schiffrin, J. Electroanal. Chem. 244 (1988) 15

66 Z. Samec, J. Electroanal. Chem. 103 (1979) 1

67 E. Makrlík, Electrochim. Acta. 29 (1984) 11

68 R.A. Marcus J. Phys. Chem. 94 (1990) 1050

69 R.A. Marcus J. Phys. Chem. 94 (1990) 4152

70 J. Heinze and M. Storzbach, Ber. Buns. Phys. Chem. 90 (1986) 1043

71 A.M. Bond, K.B. Oldham and C.G. Zoski, J. Electroanal. Chem. 245 (1988) 71

72 G. Taylor, PhD Thesis, Edinburgh University, 1991

73 H.H. Girault and D.J. Schiffrin in Electroanalytical Chem. Vol15 ed. A.J. Bard, Marcel Dekker inc. NY 1989

74 A.J. Bard and R.L. Faulkner, Electrochemical Methods, Fundementals and Applications, John Wiley & Sons, New York 1980

75 E. Grunwald, G. Baughman and G. Kohnstan, J. Amer. Chem. Soc. 82 (1960) 5801

76 H.H. Girault and D.J. Schiffrin, J. Electroanal. Chem. 161 (1984) 415

77 Z. Koczorowski, "Galvani and Volta Potentials" in The Interface, Structure and Electrochemical Processes at the Boundary Between Two Immiscible Liquids. ed. V.E. Kazarinov, Springer-Verlag berlin, Heidelberg 1987

78 H.L.F. von Helmholtz, Ann. Phys. 89 (1853) 211

79 H.L.F. von Helmholtz, Ann. Phys. 7 (1879) 337

80 G. Gouy, J. Phys. Radium 9 (1910) 457

81 G. Gouy, Compt. Rend. 149 (1910) 654

82 D.L. Chapman, Phil. Mag. 25 (1913) 475

83 O. Stern, Z. Electrochem. 30 (1924) 508

84 J.R. MacDonald, Proc. R.A. Welch Found. XXX Adv. in Electrochem. (1986) 7

85 C. Gavach, P. Seta and B. d'Epenoux, J. Electroanal. Chem. 83 (1977) 225

86 Z. Samec, Chem. Rev. 88 (1988) 617

87 H.H. Girault and D.J. Schiffrin, J. Electroanal. Chem. 150 (1983) 29

88 Z. Samec, V. Mareček and D. Homolka, J. Electroanal. Chem. 187 (1985) 31

89 P. Delahay, "Double Layer and Electrode Kinetics" Wiley-Interscience, 1965, p155 et seq

90 W.J. Albery, "Electrode Kinetics" Clarendon Press, Oxford, 1975

91 O.R. Melroy and R.P. Buck, J. Electroanal. Chem. 136 (1982) 19

92 P. van Rysselberghe, Electrochim. Acta. 8 (1963) 583

93 K.J. Laidler, "Chemical Kinetics" McGraw-Hill, New York, 2nd ed. 1950

94 P.W. Atkins, "Physical Chemistry" O.U.P. 2nd ed. 1982, p978 et seq.

95 F. Wilkinson, "Chemical Kinetics and Reaction Mechanisms" Van Nostrand Reinhold, England, 1980

96 R. Parsons, Trans. Farad. Soc. 47 (1951) 1332

97 Y.Y. Gurevich and Y.I. Kharkats, J. Electroanal. Chem. 200 (1986) 3

98 M. Eddowes, personal communication

99 J.E.B. Randles, Trans. Farad. Soc. 44 (1948) 327

100 A. Sevčik, Coll. Czech. Chem. Comm. 13 (1948) 349

101 R.S. Nicholson and I. Shain, Anal. Chem. 36 (1964) 706

102 A.A. Stewart, PhD thesis, Edinburgh University, 1990

103 D.E. Smith, Electroanal. Chem. 1 (1966) 1-155 (review)

104 T. Solomon, H. Alemu and B. Hundhammer, J. Electroanal. Chem. 169 (1984) 303

105 Y. Shao and H.H. Girault, J. Electroanal. Chem. 282 (1990) 59

106 M.I. Montenegro, Port. Electrochim Acta., 3 (1985) 165

107 C.P. Andrieux, D. Garreau, P. Hapiot, J. Pinson and J.M. Saveant, J. Electroanal. Chem. 243 (1988) 321

108 H. Hojima and A.J. Bard, J. Amer. Chem. Soc. 95 (1975) 6317

109 K.B. Oldham, C.G. Zoski, A.M. Bard and D.A. Sweigart, J. Electroanal. Chem. 248 (1988)467

110 C.M. Pereira, A.A. Stewart and H.H. Girault, J. Electroanal. Chem. to be published

111 G. Taylor, H.H. Girault and J. McAleer, , J. Electroanal. Chem. 293 (1990) 19

112 K.B. Oldham and C.G. Zoski, J. Electroanal. Chem. 256 (1988) 11

113 K.B. Oldham, J.C. Myland, C.G. Zoski and A.M. Bard, J. Electroanal. Chem. 270 (1989) 79

114 C.G. Zoski, A.M. Bond, E.T. Allinson and K.B. Oldham, Anal. Chem. 62 (1990) 37

115 C.G. Zoski, A.M. Bond, C.L. Colyer, J.C. Myland and K.B. Oldham, J. Electroanal. Chem. 263 (1989) 1

116 J.O. Howell and R.M. Wightman, Anal. Chem. 56 (1984) 524

117 R.M. Wightman and D.O. Wipf in Electroanalytical Chem. Vol 15 ed. A.J. Bard, Marcel Dekker inc. NY 1989

118 K.B. Oldham, J. Electroanal. Chem. 250 (1988) 1

119 C.J. Pedersen and H.K. Frensdorff, Angew. Chem. Int. Ed. 11 (1972) 16

120 L. Sinru, Z. Zaofan and H. Freiser, J. Electroanal. Chem. 210(1986) 137

121 T. Kakiuchi and M. Senda J. Electroanal. Chem. in press

122 A.A. Stewart, G. Taylor, H.H. Girault and J. McAleer, , J. Electroanal. Chem. 296 (1990) 491

123 G. Taylor, personal communication

124 A. Brown PhD Thesis, Edinburgh University 1991

125 J.R. Pladziewicz and J.H. Espenson, J. Amer. Chem. Soc. 95:1 (1973) 56

APPENDIX

published papers

J. Chem. Soc., Faraday Trans. 1, 1989, 85(4), 843–853

Determination of the Kinetics of Facilitated Ion Transfer Reactions across the Micro Interface between Two Immiscible Electrolyte Solutions

Jane A. Campbell, Alan A. Stewart and Hubert H. Girault*

Department of Chemistry, University of Edinburgh, West Mains Road, Edinburgh EH9 3JJ, Scotland

The transfer of K^+ from water to dichloroethane assisted by dibenzo-18-crown-6 has been studied at a liquid–liquid interface supported at the tip of a micropipette. The apparent electrochemical rate constant and apparent charge-transfer coefficient have been determined by analysis of the quasi-reversible steady-state wave observed. A kinetic model is proposed and the true electrochemical rate constant for the complexation reaction is thereby calculated.

Since the first investigation of the kinetics of ion transfer across the interface between two immiscible electrolyte solutions (ITIES) by Gavach *et al.*,[1] who studied the transfer of tetra-alkylammonium ions from water to nitrobenzene by chronopotentiometry, much work has been dedicated to this topic. The main conclusion of the results hitherto obtained[2–7] for simple ion transfer and facilitated ion transfer[8] is that these reactions are fast and therefore difficult to measure.

The standard electrochemical methodology for studying quasireversible charge transfer circumvents mass-transport limitations either by rapid variation of the electrode potential (*e.g.* Chronoamperometry, a.c. polarography, a.c. impedance and fast-sweep voltammetry) or by enhancing the rate of arrival of the reactants (e.g. rotating-disc, wall-jet and microelectrodes). To date the published investigations of the kinetics of ion transfer have relied only on the first category of techniques, and the purpose of the present paper is to show that, in the case of facilitated ion transfer, data can also be obtained by enhancing the diffusion using a microITIES.

The main problem with electrochemical measurements at liquid–liquid interfaces resides in the low polarity of the organic phase. The consequently large *iR* drop is usually either compensated by positive feedback or decreased by the use of concentrated supporting electrolyte. The effect of analogue compensation is to introduce, by definition, a large amount of noise, which limits the accuracy of current acquisition and hence makes techniques such as cyclic voltammetry non-ideal. Furthermore, in this particular case, 100% analogue compensation is never achieved, and the residual *iR* drop also contributes to the peak shift observed. Alternatively, the use of a concentrated supporting electrolyte in the organic phase causes significant ion-pairing effects between the transferring ion and the supporting electrolyte counter-ion. Such interactions complicate the determination of the data sought, and investigations in dilute media are to be preferred.

The difficulties just described render most of the techniques used so far inherently inaccurate, as reviewed recently by Samec.[9] According to this author the most reliable method is a.c. impedance, *i.e.* measurement of the charge-transfer resistance. However, as shown in ref. (9), full semi-circles are difficult to obtain, and the accuracy of the measurement is heavily dependent on the reliability of the curve-fitting algorithm employed.

More generally, all transient techniques require relatively sophisticated instrumentation, including a potentiostat with a fast rise time and high-speed transient recording equipment. However, the accuracy of these techniques at liquid–liquid interfaces is intrinsically limited at short times by the low impedance of the double layer, in parallel with the faradaic processes.

An entirely different experimental approach to the study of ion-transfer reaction kinetics is to increase the rate of mass transport of the reactants to the interface. Taylor and Girault[10] showed that micro-liquid–liquid interfaces supported at the tip of the micro-pipette can be used to provide a spherical diffusion pattern similar to that observed at solid microelectrodes.[11] This enhanced mass transport produces a steady-state current when the transferring species enters the pipette, whereas classical linear diffusion behaviour is observed when the ion exits from the pipette. Consequently a theory similar to that employed at solid-state microelectrodes may be applied in the special case of facilitated ion transfer, where both the rate of arrival of the reactants and the rate of departure of the products is enhanced. This can be achieved experimentally by, for example, using an excess of the concentration of the ion to be transferred inside the pipette together with a low concentration of the ionophore outside the pipette.

Theory

When the concentration of the transferring ion in the aqueous phase is in excess relative to the ionophore in the organic phase, the observed current for facilitated ion transfer is equal to the rate of departure of the complexed ion. In the case of spherical diffusion this reads as

$$i = \frac{z_i FAD_C}{r}(C_C^b - C_C^\sigma) = \frac{z_i FAD_{CI}}{r}(C_{CI}^\sigma - C_{CI}^b) \tag{1}$$

where the subscripts C and CI refer to the ionophore and complexed ion, respectively, the superscripts b and σ refer to bulk and surface concentrations and where F is the Faraday constant, D the diffusion coefficient, A the area of the microITIES and r the radius of the tip of the pipette. The observed limiting current for the case where the initial concentration of the complexed ion is zero in the organic phase is given by

$$i_d = \frac{z_i FAD_C}{r} C_C^b = \frac{z_i FAD_{CI}}{r} C_{CI}^\sigma. \tag{2}$$

Also, the kinetic expression for the current is

$$i = z_i FA(\vec{k}_{app} C_C^\sigma - \overleftarrow{k}_{app} C_{CI}^\sigma) \tag{3}$$

where $\vec{k}_{app}$ and $\overleftarrow{k}_{app}$ are the apparent forward and reverse electrochemical rate constants.

By substituting eqn (1) and (2) into eqn (3) we have

$$i = z_i FAC_C^b[\vec{k}_{app}(1 - i/i_d) - \overleftarrow{k}_{app}\xi i/i_d] \tag{4}$$

where ξ is the ratio D_C/D_{CI}.

Note that the concentration of the ion, C_i, does not appear in eqn (3). This is because in the present case the ionic concentration in the pipette is taken to be orders of magnitude greater than that of the ionophore. The complexation reaction

$$C^{org} + I^{water} \rightarrow CI^{org}$$

can be compared to a reduction reaction at an electrode, and is therefore pseudo-first-order.

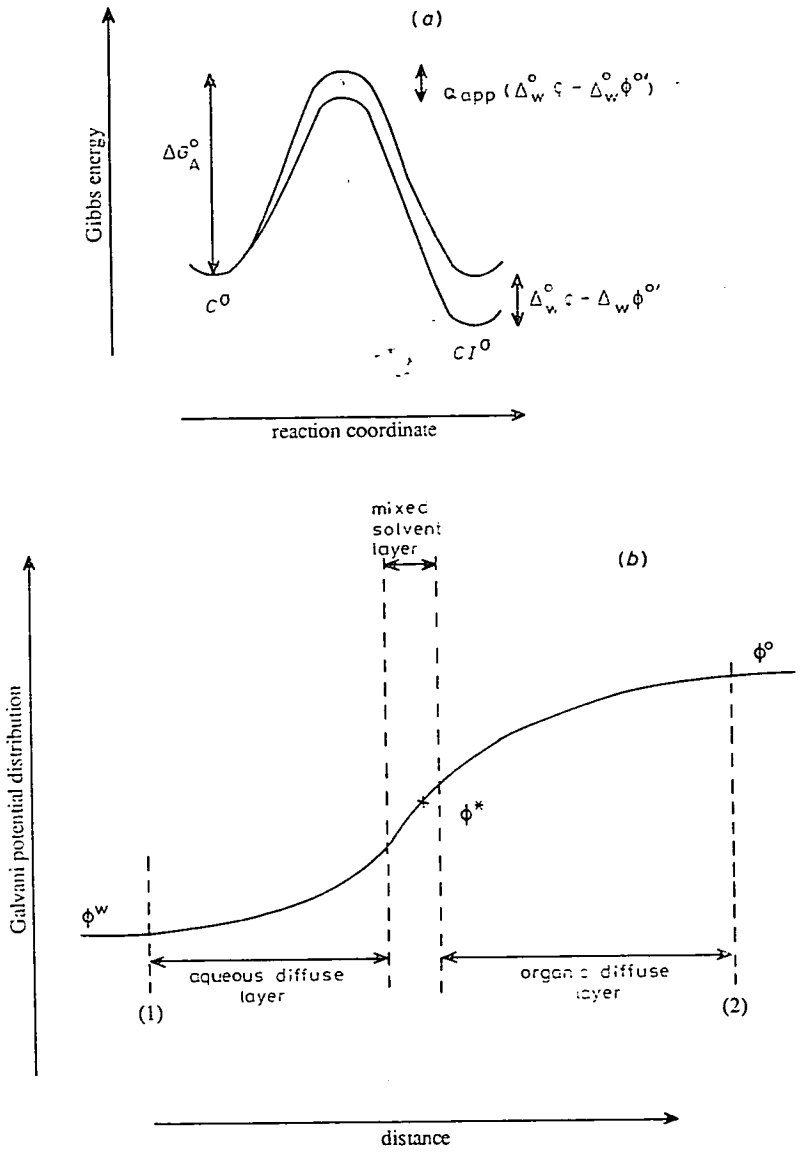

Fig. 1. (*a*) Simple representation of potential energy of Gibbs-energy changes during an ion-ionophore reaction at an ITIES. (*b*) Schematic Galvani potential distribution across an ITIES.

The potential dependence of electrochemical rate constants for charge-transfer reactions across a liquid–liquid interface has been the cause of many discussions.[12] However, the present situation is distinct from a classical non-assisted ion transfer in that the reaction coordinate does not correspond to the position of the ion with respect to the plane of the interface. As shown in fig. 1, the reaction can be modelled according to the transition-state theory. However, the initial and final positions (1) and (2) in fig. 1 correspond to positions just outside the back-to-back double layer, and consequently the rate constants $\bar{k}_{app}$ and $\bar{k}_{app}$ correspond to a global transfer and not to the elementary complexation-reaction step occurring somewhere in the mixed-solvent layer between positions (1) and (2).

In the apparent standard case where the activation energy barrier is symmetrical and the concentration of the ionophore is equal to that of the complexed ion (*i.e.* at the boundary of the space-charge region assumed to be thin compared to the diffusion layer), the equilibrium is described by the equality

$$\vec{k}_{app} C_C^c = \overleftarrow{k}_{app} C_{CI}^c. \tag{5}$$

Hence the apparent standard rate constant k_{app}° can be classically defined as

$$k_{app}^\circ = \vec{k}_{app} = \overleftarrow{k}_{app} = Z \exp(-\Delta G_A^\circ / RT). \tag{6}$$

In the apparent standard case the Galvani potential difference between the two phases is defined as the formal potential $\Delta_w^o \Phi^{o\prime}$. The formal potential for facilitated ion transfer is related to the standard potential for ion transfer of the species i, $\Delta\Phi_i^\circ$ ($= -\Delta G_{t,i}^\circ / z_i F$, where $\Delta G_{t,i}^\circ$ is the Gibbs energy of transfer) by

$$\Delta_w^o \Phi^{o\prime} = \Delta_w^o \Phi_i^\circ - \frac{RT}{z_i F} \ln K_c + \frac{RT}{z_i F} \ln \frac{\gamma_C}{\gamma_{CI}} \tag{7}$$

where K_c is the complexation constant in the organic phase and γ is the activity coefficient.

When the potential is varied from the formal potential, *e.g.* by making the oil phase more negative *vs.* water, the Gibbs energy of the uncharged ionophore remains unchanged and that of the complexed ion is lowered by an amount $z_i F(\Delta_w^o \Phi - \Delta_w^o \Phi^{o\prime})$. The activation energy barrier for the ion transfer to the oil phase, ΔG_A, is itself lowered by a fraction of this Gibbs-energy difference:

$$\Delta \vec{G}_A = \Delta G_A^c - \alpha_{app} z_i F(\Delta_w^o \Phi - \Delta_w^o \Phi^{o\prime}) \tag{8}$$

whereas the activation energy barrier for the reverse process, $\Delta \overleftarrow{G}_A$, is increased according to

$$\Delta \overleftarrow{G}_A = \Delta G_A^\circ + (1 - \alpha_{app}) z_i F(\Delta_w^o \Phi - \Delta_w^o \Phi^{o\prime}). \tag{9}$$

From eqn (8) and (9) it can be shown that the reverse rate constant is related to the forward rate constant by

$$\overleftarrow{k}_{app} = \vec{k}_{app} \exp\left(\frac{z_i F}{RT}(\Delta_w^o \Phi - \Delta_w^o \Phi^{o\prime})\right). \tag{10}$$

Consequently eqn (4) can be more generally expressed as

$$i = z_i F A C_C^b \vec{k}_{app} \left[\left(1 - \frac{i}{i_d}\right) - \xi \frac{i}{i_d} \exp\left(\frac{z_i F}{RT}(\Delta_w^o \Phi - \Delta_w^o \Phi^{o\prime})\right)\right] \tag{11}$$

from which the potential dependent rate constant for the assisted-transfer reaction can be obtained. In the case of an irreversible facilitated ion-transfer reaction, the reverse transfer can be neglected and consequently eqn (11) reduces to

$$i = z_i F A C_C^b \vec{k}_{app} \left(1 - \frac{i}{i_d}\right). \tag{12}$$

Experimental

The micropipettes were made from Kwik-Fil capillaries (1.5 mm o.d., 0.86 mm i.d., Clark Electromedical) pulled with a vertical pipette puller (Kopf 102, U.S.A.). The puller was adjusted to provide pipettes with a short shank and a fine tip, which were then polished on an optically flat glass of a pipette beveller (K. T. Brown, BV-10, U.S.A.).

During polishing the resistance of the pipette was constantly monitored, as it decreases until a flat polish is obtained. Following this procedure, pipettes with circular sections can be made with external radii comprised between 5 and 50 μm. Outside these limits, polishing becomes extremely difficult.

Tetrabutylammonium tetraphenylborate (TBATPB) was prepared by mixing equimolar aqueous solutions of TBABr (Fluka) and NaTPB (Aldrich), the precipitate being dried and recrystallized from acetone. Dibenzo-18-crown-6 was used as supplied (Aldrich). The solvents consisted of doubly deionized water and AnalaR grade 1,2-dichloroethane. The voltage ramp was produced by a PPRI waveform generator (Hitek) and the current was measured by a home-made battery-powered current follower based on a high-input impedance FET operational amplifier (Burr Brown OAP 104).

The electrochemical cell simply consisted of a glass U-tube in which the micropipette was immersed [see ref. (10) for further details]. The separation distance between the tip of pipette and the reference interface was within a 1 mm. During the experiment the tip of the pipette was monitored with a zoom microscope (Olympus, SZH, maximum magnification 384 ×) together with a colour video attachment (Sony, CCD camera, DXC–102). This constant observation was necessary to ensure that the interface remained located at the tip of the pipette.

Results

The potential window containing the K^+ ion transfer facilitated by DB18C6 across a water–1,2-dichloroethane interface supported at the tip of a micropipette is shown in fig. 2. The corresponding electrochemical cell is

$$\mathrm{Ag}\left|\mathrm{AgCl}\right|\begin{matrix}10^{-1}\ \mathrm{mol\ dm^{-3}}\ \mathrm{MgSO_4}\\ 10^{-2}\ \mathrm{mol\ dm^{-3}}\quad \mathrm{KCl}\end{matrix}\Big\|\Big\|\begin{matrix}10^{-3}\ \mathrm{mol\ dm^{-3}}\ \mathrm{TBATPB}\\ 10^{-4}\ \mathrm{mol\ dm^{-3}}\ \mathrm{DB18C6}\end{matrix}\Big|10^{-3}\ \mathrm{mol\ dm^{-3}}\ \mathrm{TBACl}\left|\mathrm{AgCl}\right|\mathrm{Ag}. \quad \text{(I)}$$

Steady-state properties are observed for K^+ transferring out of and into the pipette. This behaviour is due to spherical-diffusion mass transport for the foward and return charge transfers and contrasts with typical behaviour observed[12] for non-assisted ion transfer across micro-ITIES (*i.e.* peak-shape voltammogram for transfer out, steady-state wave voltammogram for transfer into the pipette). Steady-state voltammograms for this transfer have been analysed using the theory described above, and fig. 3 shows the result obtained when $\ln \vec{k}_{app}$ is plotted *vs.* the applied potential difference $\Delta_w^o\Phi - \Delta_w^o\Phi^{o\prime}$. The linear relationship observed indicates that the ion transfer is quasi-reversible, with a standard rate constant, k°_{app}, equal to *ca.* 2.0×10^{-3} cm s^{-1}, assuming that $\xi = 1$. The potential-difference scales given in all the figures are real Galvani potential differences calculated after measurement of the potential of zero charge (taken to be equal to the zero Galvani potential difference). The potential of zero charge (p.z.c.) for the following cell

$$\mathrm{Ag}\left|\mathrm{AgCl}\right|\begin{matrix}10^{-1}\ \mathrm{mol\ dm^{-3}}\ \mathrm{MgSO_4}\\ 10^{-2}\ \mathrm{mol\ dm^{-3}}\quad \mathrm{KCl}\end{matrix}\Big\|\Big|10^{-3}\ \mathrm{mol\ dm^{-3}}\ \mathrm{TBATPB}\Big|10^{-3}\ \mathrm{mol\ dm^{-3}}\ \mathrm{TBACl}\left|\mathrm{AgCl}\right|\mathrm{Ag} \quad \text{(II)}$$

was measured at room temperature by the streaming method as described in ref. (16). The value measured herewith was -136 mV.

The accuracy of the value of k°_{app} measured depends chiefly on the exact determination of the formal potential. This difficulty is inherent to this type of study, and there are

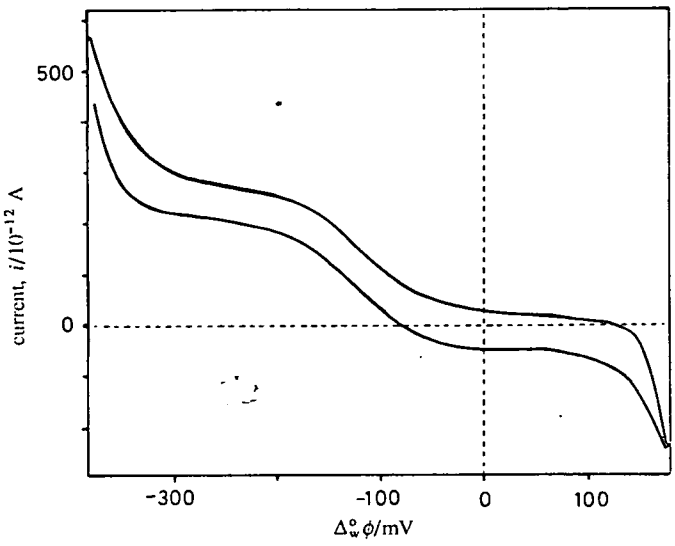

Fig. 2. Cyclic voltammogram for DB18C6-facilitated K^+ transfer at a micro ITIES for cell I. Scan rate 0.05 V s^{-1}.

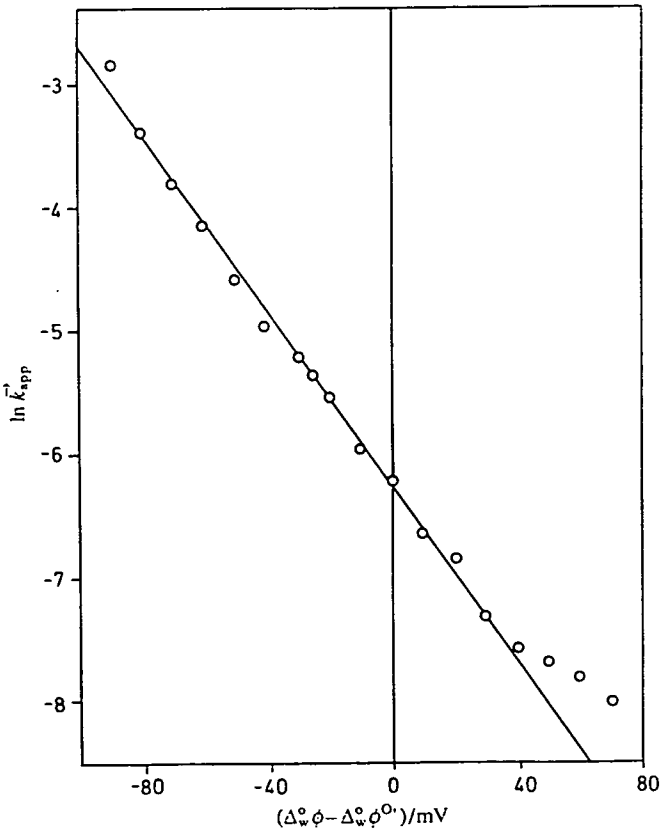

Fig. 3. Plot of $\ln \vec{k}_{app}$ *vs.* $\Delta_w^o \Phi - \Delta_w^o \Phi^{o'}$.

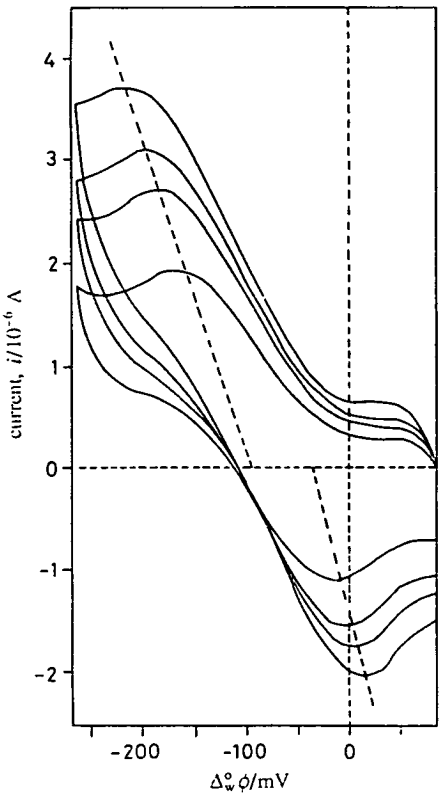

Fig. 4. Cyclic voltammogram for cell (I) at large planar liquid–liquid interface used to evaluate the formal potential. Scan rates: 0.025, 0.049, 0.064 and 0.1 V s^{-1}.

Table 1. Values of k°_{app} and α_{app} obtained for a range of formal potentials

$\Delta^{o}_{w}\Phi^{o\prime}$/V	k°_{app}/cm s^{-1}	α_{app}
−0.050	9.92×10^{-4}	0.92
−0.055	1.15×10^{-3}	0.92
−0.060	1.52×10^{-3}	0.91
−0.065[a]	1.96×10^{-3}[a]	0.91[a]
−0.070	2.46×10^{-3}	0.90
−0.075	3.08×10^{-3}	0.89
−0.0080	4.46×10^{-3}	0.87

[a] Values for the formal Galvani potential obtained by the mid-peak potential method.

basically two ways to evaluate the formal potential. On the one hand, we could relate the potential scale to a real Galvani potential-difference scale using, for example, the TPATPB assumption[14] or by measuring the potential of zero charge[13] and then evaluating the formal potential from the standard potential and the dissociation constant according to eqn (7). In this approach the activity coefficients of the ionophore and complexed ion in the organic phase are required, and their approximation can lead to large inaccuracies. On the other hand, we can take the empirical approach based on

the measurement of the mid-peak potential of cyclic-voltammetry experiments at a large planar liquid–liquid interface extrapolated to zero sweep rate. The result of this approach is shown in fig. 4. The value thus obtained using cell (I) is −201 mV (oil with respect to water) and compares with a value of apparent half-wave potential equal to −236 mV (oil with respect to water) measured from a plot of ln $[(i_d - i)/i]$ *vs.* potential difference. The formal Galvani potential difference, when related to the absolute Galvani potential scale established by the p.z.c. measurement, is −65 mV (oil with respect to water). The importance of the determination of an accurate value of the formal potential is highlighted in table 1, where values of k°_{app} are calculated from eqn (11) for a range of different formal potentials.

Discussion

Before discussing the present results it may be worth explaining why the theory outlined here is not applicable to non-assisted ion-transfer reactions. In this case the Nernst diffusion layer thickness is not fixed inside the pipette, where linear diffusion takes place. Consequently eqn (1) no longer holds and the kinetic analysis fails.

The results presented show that steady-state measurements are a powerful and straightforward route to kinetic information, especially for the determination of the apparent charge-transfer coefficient and the apparent standard rate constant. This, however, is not very informative about the process itself, as the real goal is the obtention of kinetic parameters for the rate-limiting step occurring somewhere in the mixed solvent layer separating the two diffuse layers. As recently shown[15] for the case of simple ion transfer, the desired kinetic parameters can be obtained from the apparent measured values. A similar analysis is used here for the case of facilitated ion-transfer reactions.

Let us consider that the complexation reaction occurs somewhere in the mixed solvent layer where $\vec{k}_t$ and $\overleftarrow{k}_t$ are the rate constants for the local reaction. Assuming again that the complexation reaction is pseudo-first-order (*i.e.* an excess of transferring ion) the real standard case for this local reaction is defined by

$$C^*_C = C^*_{Cl} \tag{13}$$

where the superscript * refers to the local concentration at the plane of the reaction. These concentrations are related to the surface concentrations just outside the diffuse layer by

$$C^*_C = C^{\sigma}_C \tag{14}$$

and

$$C^*_{Cl} = C^{\sigma}_{Cl} \exp\left(\frac{-z_i F}{RT}(\Phi^* - \Phi^{o})\right) \tag{15}$$

where Φ^* is the Galvani potential at the local plane where the complexation reaction occurs and Φ^{o} is the Galvani potential in the bulk of the organic phase. Substituting eqn. (14) and (15) into (13) gives

$$\frac{C^{\sigma}_C}{C^{\sigma}_{Cl}} = \exp\left(\frac{z_i F}{RT}(\Delta^{o}_{w}\Phi - \Delta^{*}_{w}\Phi^{o})\right) \tag{16}$$

where $\Delta^{*}_{w}\Phi$ is the Galvani potential difference between the water phase and the reaction plane. If we neglect mass transport and assume that the surface concentrations just outside the diffuse layer obey the Nernst equation, in this case

$$\Delta^{o}_{w}\Phi = \Delta^{o}_{w}\Phi^{o\prime} + \frac{RT}{z_i F}\ln\frac{C^{\sigma}_C}{C^{\sigma}_{Cl}} \tag{17}$$

it can be deduced that

$$\Delta^{*}_{w}\Phi^{c} = \Delta^{o}_{w}\Phi^{c} . \tag{18}$$

Note that in the real standard case the potential drop in the aqueous phase, $\Delta_w^* \Phi^\circ$, is equal to the formal potential, *i.e.* the total Galvani potential difference for the apparent standard case when $C_C^\alpha = C_{CI}^\alpha$. At this point it is possible to define the real standard rate constant, k_t°, as

$$k_t^\circ = \vec{k}_t = \overleftarrow{k}_t \tag{19}$$

and to express the true rate constant, k_t, as

$$\vec{k}_t = k_t^\circ \exp\left(\frac{-\alpha z_i F}{RT}(\Delta_w^* \Phi - \Delta_w^* \Phi^\circ)\right) \tag{20}$$

and similarly

$$\overleftarrow{k}_t = k_t^\circ \exp\left((1-\alpha)\frac{z_i F}{RT}(\Delta_w^* \Phi - \Delta_w^* \Phi^\circ)\right) \tag{21}$$

where α is the classical charge-transfer coefficient defined for the local reaction. Because in the present case the reaction is pseudo-first-order, the local charge-transfer coefficient α is shifted to unity as the potential at which the activated state occurs coincides with the reaction plane defined above as Φ^*. Eqn (20) and (21) thus reduce to

$$\vec{k}_t = k_t^\circ \exp\left(\frac{-z_i F}{RT}(\Delta_w^* \Phi - \Delta_w^* \Phi^\circ)\right) \tag{22}$$

and

$$\overleftarrow{k}_t = k_t^\circ. \tag{23}$$

These two equations can now be used to express the apparent rate constants $\vec{k}_{app}$ and $\overleftarrow{k}_{app}$ by combining eqn (14) and (15) with eqn. (22) and (23), respectively:

$$\vec{k}_{app} = k_t^\circ \exp\left(\frac{-z_i F}{RT}(\Delta_w^* \Phi - \Delta_w^* \Phi^\circ)\right) \tag{24}$$

$$\overleftarrow{k}_{app} = k_t^\circ \exp\left(\frac{-z_i F}{RT}(\Delta_o^* \Phi)\right). \tag{25}$$

We can now identify the apparent charge-transfer coefficient, α_{app}, introduced earlier in eqn (8) and (9) with

$$\alpha_{app} = \frac{\Phi^* - \Phi^w}{\Phi^o - \Phi^w}. \tag{26}$$

Using eqn (18), eqn (24) and (25) can be rewritten as

$$\vec{k}_{app} = k_t^\circ \exp\left(\frac{-z_i F}{RT}(\alpha_{app} \Delta_w^\circ \Phi - \Delta_w^\circ \Phi^{o\prime})\right) \tag{27}$$

$$\overleftarrow{k}_{app} = k_t^\circ \exp\left(\frac{(1-\alpha_{app}) z_i F}{RT}(\Delta_w^\circ \Phi)\right). \tag{28}$$

As in ref. (12), we see that the apparent charge-transfer coefficient refers to the total Galvani potential difference between the two phases and not to the local interfacial potential drop. It represents the ratio of the potential drop between the locus of the activated state and the bulk aqueous phase to the total Galvani potential difference. By definition α_{app} is dependent on the applied potential difference and will be a function of the concentrations of the supporting electrolytes.

The measured rate constant k_{app}° is defined for the equality

$$C_C^\alpha = C_{CI}^\alpha \tag{29}$$

and is obtained when $\Delta\Phi = \Delta\Phi^{o'}$: it reads

$$k^{o}_{app} = k^{c}_{t} \exp\left((1-\alpha_{app})\frac{F\Delta^{o}_{w}\Phi^{o'}}{RT}\right). \tag{30}$$

The apparent charge-transfer coefficient derived from fig. 3 by employing the following equation:

$$\alpha_{app} = -\frac{RT}{z_i F}\left[\frac{\delta \ln \vec{k}}{\delta \Delta^{o}_{w}\Phi}\right]_{\Delta^{o}_{w}\Phi = \Delta^{o}_{w}\Phi^{o'}} \tag{31}$$

was found to be 0.9.

The true standard rate constant k^{o}_{t} can therefore be calculated directly from eqn (30) using the value of the apparent standard rate constant computed from eqn (11) and inserting the corresponding value of α_{app} and the formal potential obtained by the graphical method described above. This calculation leads to a true standard rate constant of 2.5×10^{-3} cm s^{-1}. Another way to evaluate k^{o}_{t} is by use of eqn (27) at the p.z.c. for which the Galvani potential difference $\Delta^{o}_{w}\Phi$ is defined to be zero. This second approach can only be used when the formal Galvani potential difference is small enough to provide accurate values of k_{app} at the p.z.c.

The analysis of the values obtained for these interfacial complexation reactions in comparison with the corresponding bulk reactions is beyond the scope of the present paper and will be discussed in a future publication on the mechanism of ion-ionophore reactions in heterogeneous media.

To test the applicability of eqn (26) it is interesting to compare the apparent charge-transfer coefficient value thereby defined with the ratio $\Delta^{w}_{\sigma}\Phi/\Delta^{w}_{0}\Phi$, where $\Delta^{w}_{\sigma}\Phi$ is the potential drop in the aqueous diffuse layer, which can be calculated for example using the Gouy–Chapman theory. Indeed for the 1:1 organic electrolytes used in the present experiment the Gouy charge is given by

$$q^{o} = -\varepsilon^{o}\left[\frac{d\Phi}{dx}\right]_{x=0} = -(8RTC^{o}\varepsilon^{o})^{\frac{1}{2}}\sinh\left(\frac{F}{2RT}\Delta^{\sigma}_{o}\Phi\right) \tag{32}$$

whereas the aqueous charge for the 2:2 aqueous electrolyte is given by

$$q^{w} = +\varepsilon^{w}\left[\frac{d\Phi}{dx}\right]_{x=0} = (4RTC^{w}\varepsilon^{w})^{\frac{1}{2}}\sinh\left[\frac{F}{RT}\Delta^{\sigma}_{w}\Phi\right]. \tag{33}$$

The electroneutrality of the interface allows us to calculate the potential drop in the aqueous diffuse layer, $\Delta^{w}_{\sigma}\Phi$. When the Galvani potential drop is equal to the formal potential (*i.e.* -0.065 V) $\Delta^{w}_{\sigma}\Phi$ was found to be equal to 2.2 mV. This leads to an apparent charge-transfer coefficient of 0.97. Given the inadequacy of the Gouy–Chapman theory in application to 2:2 electrolytes and also that $MgSO_4$ is significantly ion-paired at such a high concentration in water, this calculated value of α_{app} compares relatively well with the measured value of 0.9 and justifies *a posteriori* the definition of α_{app} given by eqn (26).

Conclusion

The present work shows for the first time that the measurement of steady-state current occurring during assisted ion transfer across a micro-liquid–liquid interface supported at the tip of a micropipette allows direct access to the apparent kinetic parameters of these processes. Furthermore, the accompanying kinetic theory proposed enables the calculaton of the true kinetic parameters corresponding to the local interfacial complexation reaction, and this without referring to any *a priori* model of the interface.

We acknowledge the S.E.R.C. for supporting this work and for providing an Information Technology studentship to J.A.C. and a CASE award studentship in collaboration with Genetics International (U.K.) to A.A.S. The support of the Nuffield Foundation is also gratefully acknowledged.

References

1 C. Gavach, B. d'Epenoux and F. Henry, *J. Electroanal. Chem.*, 1975, **64**, 107.
2 T. Osakai, T. Kakutani and M. Senda, *Bull. Chem. Soc. Jpn.* 1984, **57**, 370.
3 B. d'Epenoux, P. Seta, G. Amblard and C. Gavach, *J. Electroanal. Chem.*, 1979, **99**, 77.
4 Z. Samec, V. Marecek, J. Weber and D. Homolka, *J. Electroanal. Chem.*, 1981, **126**, 105.
5 Z. Samec, V. Marecek and J. Weber, *J. Electroanal. Chem.*, 1979, **100**, 841.
6 T. Osakai, T. Kakutani and M. Senda, *Bull. Chem. Soc. Jpn.* 1985, **58**, 2626.
7 Z. Samec and V. Marecek, *J. Electroanal. Chem.*, 1986, **200**, 17.
8 T. Kakutani, Y. Nishiwaki, T. Osakai and M. Senda, *Bull. Chem. Soc. Jpn*, 1986, **59**, 781.
9 T. Wandlowski, V. Marecek and Z. Samec, *J. Electroanal. Chem.*, 1988, **242**, 291.
10 G. Taylor and H. H. Girault, *J. Electroanal. Chem.*, 1986, **208**, 179.
11 M. I. Montenegro, *Port. Electrochim. Acta*, 1985, **3**, 165.
12 H. H. Girault and D. J. Schiffrin, *J. Electroanal. Chem.*, 1985, **195**, 213.
13 H. H. Girault and D. J. Schiffrin, *Electrochim. Acta*, 1986, **31**, 1341.
14 H. H. Girault and D. J. Schiffrin, *Electroanal. Chem.*, 1988, **15**, 1.
15 H. H. Girault, *J. Electroanal. Chem.*, in press.
16 H. H. Girault and D. J. Schiffrin, *J. Electroanal. Chem.*, 1984, **161**, 415.

Paper 8/01473F; *Received* 15*th April*, 1988

J. Electroanal. Chem., 266 (1989) 465–469
Elsevier Sequoia S.A., Lausanne – Printed in The Netherlands

Preliminary note

Steady state current for ion transfer reactions at a micro liquid/liquid interface

J.A. Campbell and H.H. Girault

Department of Chemistry, University of Edinburgh, West Mains Road, Edinburgh EH9 3JJ, Scotland (Great Britain)

(Received 22 May 1989)

INTRODUCTION

The advantages of microelectrodes in electrochemistry, both for the study of fast charge transfer reactions, and for investigations in resistive media have been widely reported [1].

Charge transfer reactions across the Interface between Two Immiscible Electrolyte Solutions (ITIES) which include ion transfer, assisted ion transfer and electron transfer reactions are generally fast ($10^{-3} < k^\circ < 10^{-1}$ cm s^{-1}) and the measurement of reliable kinetic data for these processes is largely hampered by the high resistivity of the organic phase. For this reason, the use of micro ITIES offers advantages in circumventing most of the difficulties generally encountered with larger interfaces where planar diffusion mass transport dominates.

The first method proposed to obtain a micro ITIES was to support the interface at the tip of a micropipette similar to those used in electrophysiology for intracellular measurements. In this case, however, it was shown that an asymmetric diffusion field prevailed, comprising a linear component inside the pipette and a radial component outside [2]. This first approach permitted the study of charge transfer with solvents of low permittivity such as 1,2-dichloroethane but kinetic studies had to rely on a model derived from the computer simulation of this asymmetric mass transport regime [3]. The only kinetic studies at micropipettes which could be analysed following the methodology generally used at solid microelectrodes were pseudo-first order bimolecular reactions where the concentration of the reactant inside the pipette was in excess compared to that of the reactant outside. With this approach the mass transport was controlled by the radial diffusion of the reactants and products outside the pipette. In this way it was possible to study ion/ionophore interfacial complexation reactions [4] such as

$$M^+(aq) + C(org) \rightleftharpoons CM^+(org)$$

0022-0728/89/$03.50

and interfacial electron transfer reactions [5] of the type

$O_1(aq) + R_2(org) \rightleftharpoons R_1(aq) + O_2(org)$

in cells where the aqueous phase was located inside the pipette.

The micropipette approach generates steady state currents and is thus potentially very useful for analytical applications especially for the in vivo amperometric determination of ionic species but because of the large resistance of the electrolyte in the micropipette tip ($R > 10^4$ Ω) this technique does not permit the use of very fast sweep cyclic voltammetry.

The purpose of the present note is to show that micro ITIES can be formed in a microhole in a treated thin polymer film. Both the hole drilling and the polymer film treatment are relatively new processes based on laser technology. This new approach to micro ITIES fabrication allows the establishment of a diffusion field with radial contributions on both sides of the interface thereby enabling all the methodology developed for microdisc electrodes to be transposed for use with micro ITIES.

EXPERIMENTAL

The cell consisted of a 20 μm diameter hole formed in a 12 μm thick polyester film (Melynex.ICI) using a laser micro-machining technique developed by Exitech Ltd (Oxford, U.K.) in which bursts of UV laser photons are directed onto the surface using image projection techniques to define a pattern. The resolution provided by this technique is well below 1 μm and the microholes obtained are circular and very well defined. Because the process is based on UV irradiation by excimer lasers, the drilling occurs by laser photo ablative decomposition of the polymer and thermal effects such as melting, flowing and debris formation are eliminated.

Previous attempts to use microholes, in membranes such as nucleopore, for the support of micro ITIES have hitherto proved useless due to the hydrophilic, or hydrophobic, nature of the membranes which leads to the creep of one or the other solvent through the holes thereby wetting the whole surface of the membrane. This difficulty is herewith overcome by "hydrophilising" one side of the normally hydrophobic polyester film using a laser process especially developed by Exitech Ltd. The success of this treatment was verified by comparing the wetting properties of water and 1,2-dichloroethane on the treated and untreated film.

The film was mounted on the end of a glass tube (2 mm i.d., 6 mm o.d.) and the cell used in a conventional two electrode mode (Fig. 1). As a model system, the transfer of the acetylcholine cation (ACh) across the water/1,2-dichloroethane (DCE) interface was studied using Cell (I):

Ag	AgCl	10 m*M* LiCl 2 m*M* AChCl water	10 m*M* TBATPBCl DCE	10 m*M* TBACl water	AgCl	Ag

(I)

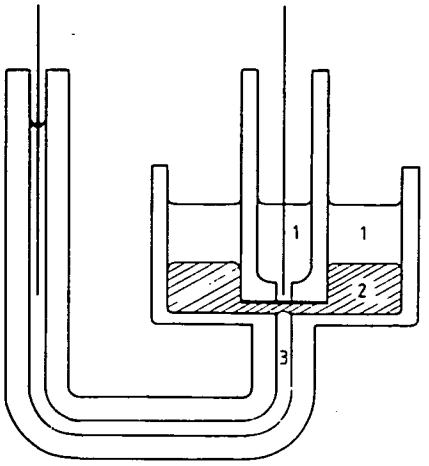

Fig. 1. Cell for ITIES at a microhole in a thin polymer film. (1) Aqueous electrolyte 10 m*M* LiCl + 2 m*M* AChCl. (2) Organic electrolyte 10 m*M* TBATPBCl. (3) Organic reference electrolyte 10 m*M* TBACl. The reference/counter electrodes are Ag/AgCl.

A voltage ramp was applied at the organic reference electrode using a PPR1 waveform generator (Hitek, U.K.) and the current through the aqueous reference electrode measured with a current follower based on a high-input impedance FET operational amplifier (Burr Brown OAP 104). Experiments were conducted at room temperature, i.e. 22 °C ± ~ 1 °C.

RESULTS AND DISCUSSION

Figure 2 shows the cyclic voltammograms obtained from Cell (I). The potential window is limited at the negative end by Li^- crossing from water to dichloroethane and at the positive end by TBA^+ crossing from dichloroethane to water.

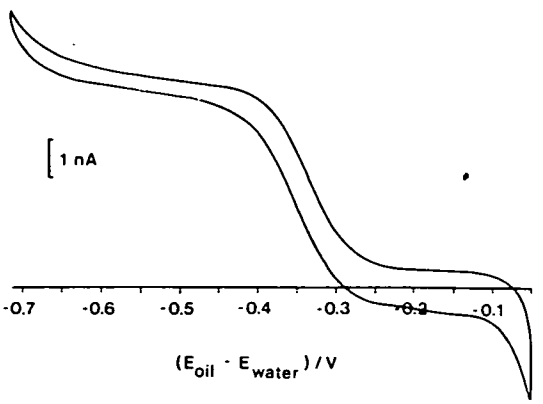

Fig. 2. Cyclic voltammogram for the transfer of ACh^- from water to 1.2-dichloroethane at 50 mV s^{-1}.

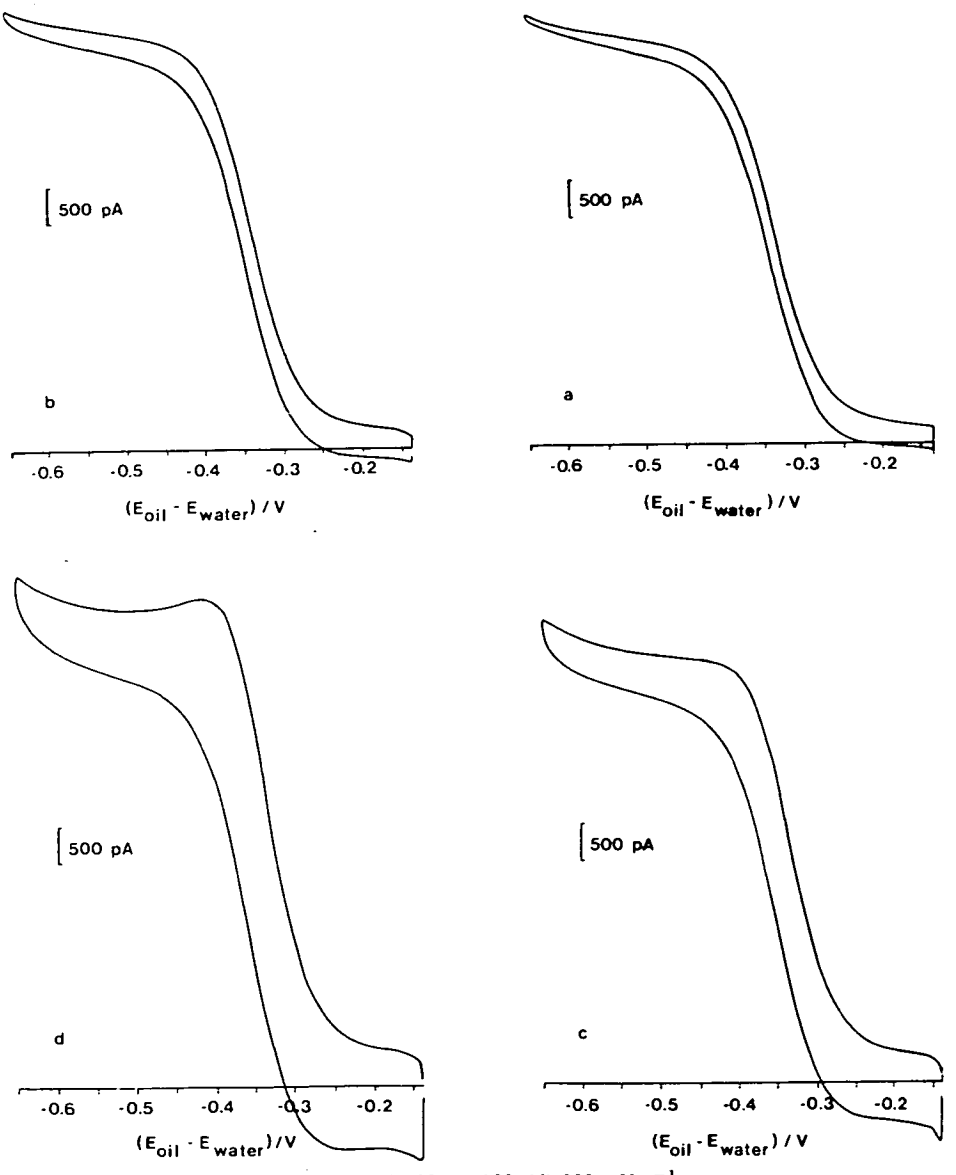

Fig. 3. Sweep rate dependence. (a) 10, (b) 20. (c) 100. (d) 200 mV s^{-1}.

Figure 3 shows that at sweep rates of 10 and 20 mV s^{-1} steady state waves are observed with a limiting current of 4.65×10^{-9} A. Using the equation for the diffusion limited current, i_d, at a microdisc:

$$i_d = 4FDcr$$

where F is the Faraday constant, D and c are the diffusion coefficient and bulk

concentration respectively of the ion transferred and r the radius of the electrode. we obtain a value of 6.06×10^{-6} cm^2 s^{-1} for the diffusion coefficient of the acetylcholine cation in water. This compares with a value of 5.2×10^{-6} cm^2 s^{-1} obtained from cyclic voltammetry at a large interface at 20 °C.

At scan rates of 100 and 200 mV s^{-1} the current begins to peak as linear diffusion becomes more significant. The peaking with increasing sweep rate appears to be slightly more pronounced when scanning negatively, with respect to the aqueous phase, than positively. This may be due to the interface being disposed asymmetrically in the microhole or an artefact arising from the masking of the peak by the end of the potential window.

Ideal microdisc behaviour requires a small film thickness to hole radius ratio and the present approach will be limited by the availability of pinhole free super thin films. This inherent limitation is currently under investigation. A further very interesting aspect of the laser technology involved in this work is the possibility of fabricating well defined microhole arrays.

The results reported herein illustrate that micro ITIES can be fabricated in such a way that the methodology developed for microdisc electrodes can be extended to the study of charge transfer across liquid/liquid interfaces.

ACKNOWLEDGEMENTS

The authors wish to thank Dr. J. McAleer and Medisense U.K. for financial support and Exitech for stimulating discussions regarding the laser technology. One of us (J.A.C.) received an Information Technology postgraduate studentship from SERC.

REFERENCES

1 R.M. Wightman and D.O. Wipf in A.J. Bard (Ed.). Electroanalytical Chemistry. Vol. 15. Marcel Dekker. New York. 1989. p. 267.
2 G. Taylor and H.H. Girault. J. Electroanal. Chem.. 208 (1986) 179.
3 G. Taylor. J. McAleer and H.H. Girault. in preparation.
4 J.A. Campbell. A.A. Stewart and H.H. Girault. J. Chem. Soc.. Faraday Trans. 1. 85 (1989) 843.
5 J.A. Campbell and H.H. Girault. in preparation.

Cyclic Voltammetry for Electron Transfer Reactions at Liquid/Liquid Interfaces

A. A. Stewart, J. A. Campbell, H. H. Girault*)

Department of Chemistry, University of Edinburgh, West Mains Road, Edinburgh, EH9 3JJ, Scotland

M. Edddowes

Thorn EMI Central Lab., Dawley Road, Hayes, England

Voltammetry / Electrochemistry / Electron Transfer / Immiscible Electrolytes

y for cyclic voltammetry at liquid/liquid interfaces for electron transfer is proposed, and the numerical solution of the resulting equation is evaluated. This theory has been used to show how the cyclic voltammograms, for electron transfer at ITIES, vary ifferent ratios of reactants and products, in both phases, are used, and how these voltammograms differ from classical cyclic voltammograms.

Introduction

nterface between two immiscible electrolyte solutions has proven to be a suitable interface at which to eterogeneous electron transfer, the general scheme ch is outlined in Fig. 1.

the early work of Samec et al. [1] at the water/ nzene interface, different pairs of redox couples have vestigated [2–4]. The study of these systems has stricted mainly to pseudo first order reactions with ctant in excess. In this way the situation was thought milar to the metal.electrolyte interface, as the diffu- the dilute reactant would be the limiting process, ng a reversible reaction.

n the concentration of the reactants in the two ad- phases are of similar magnitude, diffusion of both ts to the interface should be taken into account. The e of this communication is to show that the combined diffusion of the reactants produces cyclic voltammograms which do not follow the classical behaviour as derived by Nicholson and Shain [5].

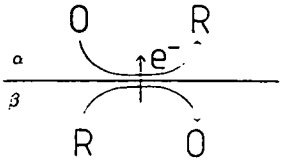

Fig. 1
Reaction scheme for electron transfer, across an ITIES, between redox couples in phases α and β

Theory

If we assume that the diffusion of the reactants and products for the process illustrated in Fig. 1 is linear, the concentration of any of the four species is given by

hom correspondence should be addressed.

nsenges. Phys. Chem. *94*, 83–87 (1990) –
0005–9021/90/0101–0083 $ 02.50/0

$$\frac{c_i^*}{s} + A_i(s)\exp\left[-x\sqrt{\frac{s}{D_i}}\right] \tag{1}$$

epresents the bulk concentration of species i, $\bar{c}_i$ e transform of the concentration with respect to e diffusion coefficient and x the absolute value of e from the interface. The constants $A_i(s)$ have to ned from the boundary conditions which in the se are given by the mass balance at the interface:

$$\begin{aligned} {}^{\alpha}D_O^{\alpha}\left[\frac{\partial\bar{c}\bar{c}_O^{\alpha}}{\partial x}\right]_{x=0} &= -nFAD_R^{\alpha}\left[\frac{\partial\bar{c}\bar{c}_R^{\alpha}}{\partial x}\right]_{x=0} \\ {}^{\beta}D_R^{\alpha}\left[\frac{\partial\bar{c}\bar{c}_R^{\beta}}{\partial x}\right]_{x=0} &= -nFAD_O^{\beta}\left[\frac{\partial\bar{c}\bar{c}_R^{\beta}}{\partial x}\right]_{x=0} \end{aligned} \tag{2}$$

s the Laplace transform of the current. The super- d β refer to the phases, and the subscripts O and the oxidised and the reduced species respectively. bining Eqs. (1) and (2), the interfacial concentra- four species can be written as:

$$c_O^{\alpha *} - \frac{I(t)}{\sqrt{D_O^{\alpha}}} \tag{3}$$

$$c_R^{\alpha *} + \frac{I(t)}{\sqrt{D_R^{\alpha}}} \tag{4}$$

$$c_O^{\beta *} + \frac{I(t)}{\sqrt{D_O^{\beta}}} \tag{5}$$

$$c_O^{\beta *} - \frac{I(t)}{\sqrt{D_R^{\beta}}} \tag{6}$$

is the convoluted current [5] defined as

$$\bar{\tau} \int_0^t \frac{f(\tau)}{\sqrt{t-\tau}}\,d\tau \tag{7}$$

$$\frac{\tau)}{A}. \tag{8}$$

a totally reversible system, the concentrations of species at the interface are related via the Nernst

$$\Delta_{\alpha}^{\beta}\phi^{0'} + \frac{RT}{nF}\ln\frac{c_O^{\alpha}\,c_R^{\beta}}{c_R^{\alpha}\,c_O^{\beta}} \tag{9}$$

the number of electrons exchanged at the interface

$$z_R^{\alpha} = z_O^{\beta} - z_R^{\beta}. \tag{10}$$

$\Delta_{\alpha}^{\beta}\phi$ is the Galvani potential difference $\phi^{\beta} - \phi^{\alpha}$ $^{0'}$ is the formal potential (see Ref. [6] for details).

By defining the following parameters

$$\theta = \exp\left[\frac{nF}{RT}(\Delta_{\alpha}^{\beta}\phi_i - \Delta_{\alpha}^{\beta}\phi^{0'})\right] \tag{11}$$

$$\sigma = \frac{nFv}{RT} \tag{12}$$

$$S(t) = \begin{cases} \exp(-\sigma t) & \text{for } t < \lambda \\ \exp(\sigma t - 2\sigma\lambda) & \text{for } t \geq \lambda \end{cases} \tag{13}$$

with $\Delta_{\alpha}^{\beta}\phi_i$ the starting potential, v the sweep rate, and λ the time at which the scan is reversed, it is possible to express the Nernst Eq. (5) as

$$\theta S(t) = \frac{c_O^{\alpha}\,c_R^{\beta}}{c_R^{\alpha}\,c_O^{\beta}}. \tag{14}$$

By substituting Eqs. (3)–(6) into Eq. (14), we obtain the following quadratic expression for the convoluted current

$$AI(t)^2 + BI(t) + C = 0 \tag{15}$$

with the constants A, B, and C defined as

$$A = \frac{\theta S(t)}{\sqrt{D_R^{\alpha}\,D_O^{\beta}}} - \frac{1}{\sqrt{D_O^{\alpha}\,D_R^{\beta}}} \tag{16}$$

$$B = \theta S(t)\left[\frac{c_R^{\alpha *}}{\sqrt{D_O^{\beta}}} + \frac{c_O^{\beta *}}{\sqrt{D_R^{\beta}}}\right] + \frac{c_O^{\alpha *}}{\sqrt{D_R^{\beta}}} + \frac{c_R^{\beta *}}{\sqrt{D_O^{\alpha}}} \tag{17}$$

$$C = c_R^{\alpha *}\,c_O^{\beta *}\theta S(t) - c_O^{\alpha *}\,c_R^{\beta *}. \tag{18}$$

Obviously Eq. (15) has two roots, one which is the convoluted current. The choice between the two roots stems from the condition that the convoluted current is a continuous function of time and therefore the correct solution reads

$$I(t) = \frac{-B + \sqrt{B^2 - 4AC}}{2A}. \tag{19}$$

The continuity of $I(t)$ is verified for $A = 0$ by taking $I(t)$ equal to $-C/B$.

In order to integrate Eq. (19) in the general case the following dimensionless coefficients are introduced

$$\alpha = \frac{c_O^{\alpha *}}{c^{\alpha}} \tag{20}$$

with c_{α} the total concentration of the redox couple in α given by

$$c^{\alpha} = c_O^{\alpha *} + c_R^{\alpha *} \tag{21}$$

and

$$\beta = \frac{c_O^{\beta *}}{\kappa c^{\alpha}} \tag{22}$$

κ represents the ratio of the total concentrations of ox couples

$$\frac{c_O^{\alpha *} + c_R^{\beta *}}{c^{\alpha}} = \frac{c^{\beta}}{c^{\alpha}} . \tag{23}$$

fusion coefficients of the reactions and products can expressed by a set of dimensionless parameters

$$\sqrt{\frac{D_O^{\alpha}}{D_R^{\alpha}}} \tag{24}$$

$$\sqrt{\frac{D_O^{\beta}}{D_R^{\beta}}} \tag{25}$$

ally

$$\sqrt{\frac{D_O^{\alpha}}{D_O^{\beta}}} . \tag{26}$$

dimensionless coefficients can be substituted into Eqs. 18) and it can be shown that the convoluted current portional to $\sqrt{c^{\alpha} D_O^{\alpha}}$.

integration of Eq. (19) can be carried out by following ssical Nicholson and Shain [5] numerical method on the integration by parts of Eq. (7). This integration (19) leads to a dimensionless current parameter $\chi(\sigma t)$ is related to the current by

$$nFA\sqrt{\pi D_O^{\alpha} \sigma}\, c^{\alpha} \chi(\sigma t) . \tag{27}$$

be seen from Eq. (27) that the normal sweep rate dence is still applicable in the present situation.

Computation

program for the calculation of the dimensionless cur- (σt) was written in FORTRAN77 on the University nburgh main frame computer (EMAS) and the results lotted using the graphics facilities of Edinburgh Uni- Computing Services. All calculations were carried double precision to enhance accuracy of the results. umerical integration of Eq. (19) was carried out with ensionless time step value of 0.01 as proposed by Ni- n and Shain [5].

opy of the programme is available by request on elec- mail.

Results and Discussion

values of the dimensionless current $\chi(\sigma t)$ have been ated as a function of the parameters α, β, and κ. All sults presented herewith assume the equality of the on coefficient of the reactants and products i.e.

$$\alpha = \zeta^{\beta} = 1 . \tag{28}$$

1: $\alpha = 1$, $\beta = 0$

Case 1 represents the simple reaction condition with a zero initial concentration of the products (i.e. the situation normally assumed in classical cyclic voltammetry).

In this case the coefficient κ represents the ratio of concentrations of the reactants $c_O^{\alpha *}/c_R^{\beta *}$. Eq. (27) then reads

$$i = nFA\sqrt{\pi D_O^{\alpha} \sigma}\, c_O^{\alpha *} \chi(\sigma t) \tag{29}$$

and shows that the peak current is proportional to the square root of the sweep rate with a slope value of $nFA \cdot \sqrt{\pi D_O^{\alpha} \frac{nF}{RT}}\, \chi_p(\sigma t)$, where $\chi_p(\sigma t)$ is the dimensionless peak current, given in Table 1 for different values of κ.

Table 1
Dimensionless current function $\chi(\sigma t)$ and other cyclic voltammogram characteristics for Case 1 ($\alpha = 1$, $\beta = 0$). $E = \Delta_{\alpha}^{\beta}\phi - \Delta_{\alpha}^{\beta}\phi^{0'}$, scanning from $E = +500$ mV to -500 mV, step increment 0.5 mV

κ	$E_{p,f}$/mV	$E_{p,b}$ mV	ΔE_p/mV	$E_{1/2}$/mV	$\chi(\sigma t)_{f,p}$	$\chi(\sigma t)_{f,p}\cdot\kappa$
0.01	88.3	172.4	84.1	130.4	0.00217	0.217
0.05	46.0	131.5	85.5	88.8	0.0108	0.216
0.1	27.2	113.8	86.6	70.5	0.0215	0.215
0.5	−26.5	71.7	98.2	22.6	0.103	0.206
1.0	−57.0	58.8	115.8	0.9	0.178	0.178
2.0	−27.0	72.2	99.2	22.6	0.206	
10.0	26.5	114.3	87.8	70.4	0.215	
20.0	45.7	132.3	86.6	89.0	0.216	
100.0	87.9	173.7	85.8	130.8	0.217	

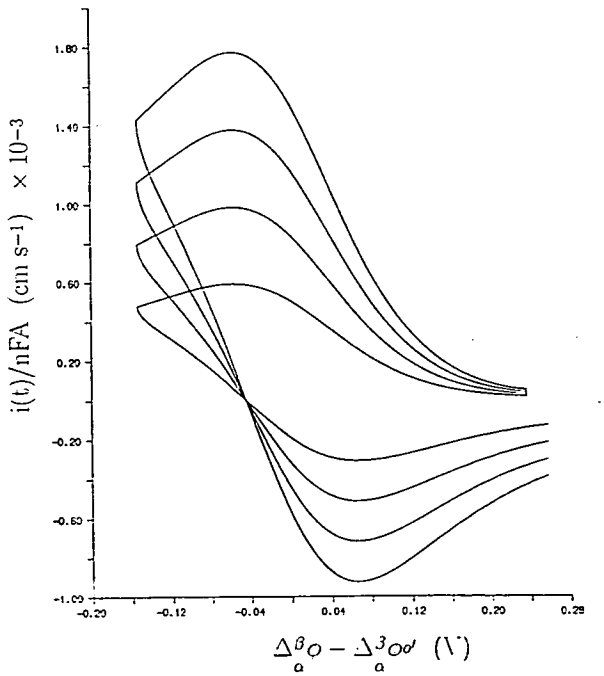

Fig. 2
Cyclic voltammograms (i nFA vs. $\Delta_{\alpha}^{\beta}\phi - \Delta_{\alpha}^{\beta}\phi^{0'}$) showing sweep rate dependence for $\alpha = 1$, $\beta = 0$, and $\kappa = 1$. Scan rates 0.009, 0.025, 0.049, 0.081 V s^{-1}

When the concentration of the reactants is equal (i.e. $\kappa = 1$) it can be seen from Table 1 that the midpeak potential $E_{1/2} = \Delta_{\alpha}^{\beta}\phi^{1/2} - \Delta_{\alpha}^{\beta}\phi^{0'}$ is equal to the formal potential and

eparation ΔE_p is equal to 123 mV. This case is valent to a classical cyclic voltammogram with 1/2 as the concentration profiles of the reactants ent phases are symmetrical. This symmetry also ie products and consequently the concentration . (9) reads $(c_O^{\alpha}/c_O^{\beta})^2$. The sweep rate dependence, in Fig. 2, follows Eq. (29) and can be used to her the diffusion coefficient D_O^{α} or the bulk con- of the oxidised species in the phase α.

e concentration of the reduced species in the eeds that of the oxidised species in the phase α he midpeak potential shifts towards positive val- as 131 mV when κ is equal to 100. On the other peak separation decreases and the peak current a limiting value of 0.217. This behaviour is il- Fig. 3.

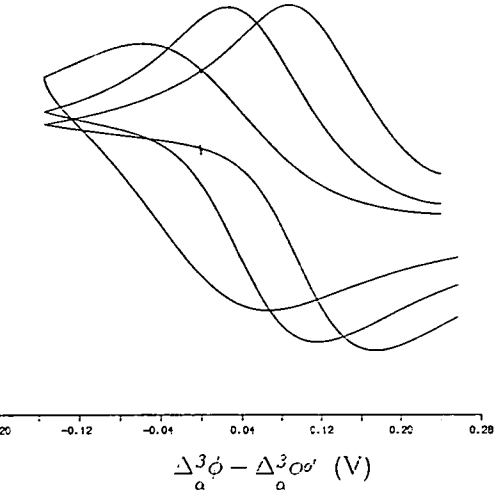

Fig. 3
mmograms of $\chi(\sigma t)$, dimensionless current, vs. $\Delta^{\beta}_{\alpha}\phi$ – = 1, β = 0, with varying κ. (a) κ = 1, (b) κ = 10, (c) κ = 100

ely, when the concentration of the oxidised spe- phase α exceeds that of the reduced species in the e. $\kappa < 1$), the dimensionless current $\chi(\sigma t)$ is gov- he concentration $c_R^{\beta *}$. The normalised current wever shows a similar behaviour to that described shift of midpeak potential to positive values, de- ie peak separation and same limiting value of the l plateau current.

sent numerical analysis shows that even in the udo first order reactions (i.e. κ very large of very system is not controlled only by the diffusion of it of low concentration and therefore that a direct on of the classical cyclic voltammetry technique used, either to measure the formal potential or kinetic information from the sweep rate depend- peak separation.

Case 2: $\alpha = 0.5$, $\beta = 0$

An interesting situation for the study of electron transfer reactions at ITIES is the case where one phase contains an equimolar concentration of electron donor and acceptor, i.e. $\alpha = 0.5$.

Table 2
Dimensionless current function $\chi(\sigma t)$ and other cyclic voltammogram characteristics for Case 2 ($\alpha = 0.5$, $\beta = 0$). $E = \Delta^{\alpha}_{\alpha}O - \Delta^{\beta}_{\alpha}\phi^{0'}$, scanning from E = +500 mV to −500 mV, step increment 0.3 mV

κ	$E_{p,f}$/mV	$E_{p,b}$ mV	ΔE_p mV	$E_{1/2}$ mV	$\chi(\sigma t)_{f,p}$	$\chi(\sigma t)_{f,p}/\kappa$
0.01	−29.5	29.0	58.5	−0.3	0.00251	0.251
0.05	−33.4	28.3	61.7	−2.6	0.0123	0.246
0.1	−37.8	27.5	65.3	−5.2	0.0241	0.241
0.5	−70.1	27.5	97.6	−21.3	0.0955	0.191
1.0	−41.3	42.1	83.4	0.4	0.111	0.111
2.0	−15.9	59.3	75.2	21.7	0.115	
10.0	30.1	101.0	70.9	65.6	0.118	
20.0	48.6	119.7	71.1	84.2	0.118	
100.0	90.4	161.6	71.2	126.0	0.118	

*) To whom correspondance should be addressed.

It can be seen from Table 2 that when this equimolar mixture is in large excess compared with that of the concentration of the reduced species in phase β then the system is controlled only by the diffusion of the later reactant. Hence the behaviour approaches that of a standard reversible system [5]. (ΔE_p = 60 mV, $E^{1/2}$ = 0, and $\chi(\sigma t)/\kappa$ = 0.251). In this case, therefore, the phase α is equivalent to a metallic phase, able to donate and accept electrons on demand. When the value of κ is increased the peak separation augments to a maximum value of 85 mV at κ = 1 and the midpeak potential shifts positively for large values of κ.

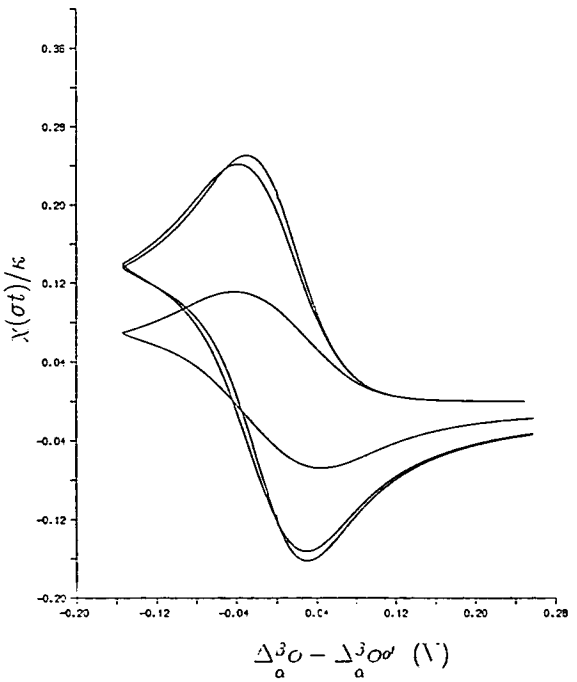

Fig. 4
Cyclic voltammograms of $\chi(\sigma t)/\kappa$, normalised dimensionless current, vs. $\Delta^{\beta}_{\alpha}\phi - \Delta^{\beta}_{\alpha}\phi^{0'}$ for α = 0.5, β = 0, with varying κ. (a) κ = 1, (b) κ = 10, (c) κ = 0.01

shows the normalised dimensionless current $\chi(\sigma t)/\kappa$ ction of the concentration ratio κ and illustrates the n from conventional behaviour when κ increases.

Conclusion

voltammetry for electron transfer reactions at liq- d interfaces yields results which differ significantly se obtained when considered only the diffusion of tant and one product to and from an interface. rticular, under pseudo first order conditions the iteria for reversibility ($\Delta E_p = 58.5$ mV and $E_{1/2} =$ apply when both the oxidation forms of the excess ecies are present. resent results also indicate that peak separations han 60 mV can be observed under reversible con- purely as a consequence of diffusion and hence ot necessarily be taken as indicative of kinetic con-

We acknowledge the S.E.R.C. for supporting this work, and for providing an Information Technology studentship to J.A.C. and a CASE award studentship in collaboration with Medisense (UK) to A.A.S.

References

[1] Z. Samec, V. Marecek, and J. Weber, J. Electroanal. Chem. *103*, 11 (1979).
[2] G. Geblewicz and D. J. Schiffrin, J. Electroanal. Chem. *244*, 27 (1988).
[3] V. Cunnane, D. J. Schiffrin, C. Beltran, G. Geblewicz, and T. Solomon, J. Electroanal. Chem. *247*, 203 (1988).
[4] S. Kihara, Z. Yoshida, M. Suzuki, K. Maeda, K. Ogura, and M. Matsui, J. Electroanal. Chem., in press.
[5] R. S. Nicholson and I. Shain, Anal. Chem. *36*, 706 (1964).
[6] H. H. Girault and D. J. Schiffrin, J. Electroanal. Chem. *244*, 15 (1988).

(Eingegangen am 9. August 1989) E 7169